NUREG/CR-4898
EGG-2503
February 1988

Results of Semiscale MOD-2C Feedwater and Steam Line Break (S-FS) Experiment Series: Bottom Main Feedwater Line Break Accident Experiments

Timothy J. Boucher

F O R M A L R E P O R T

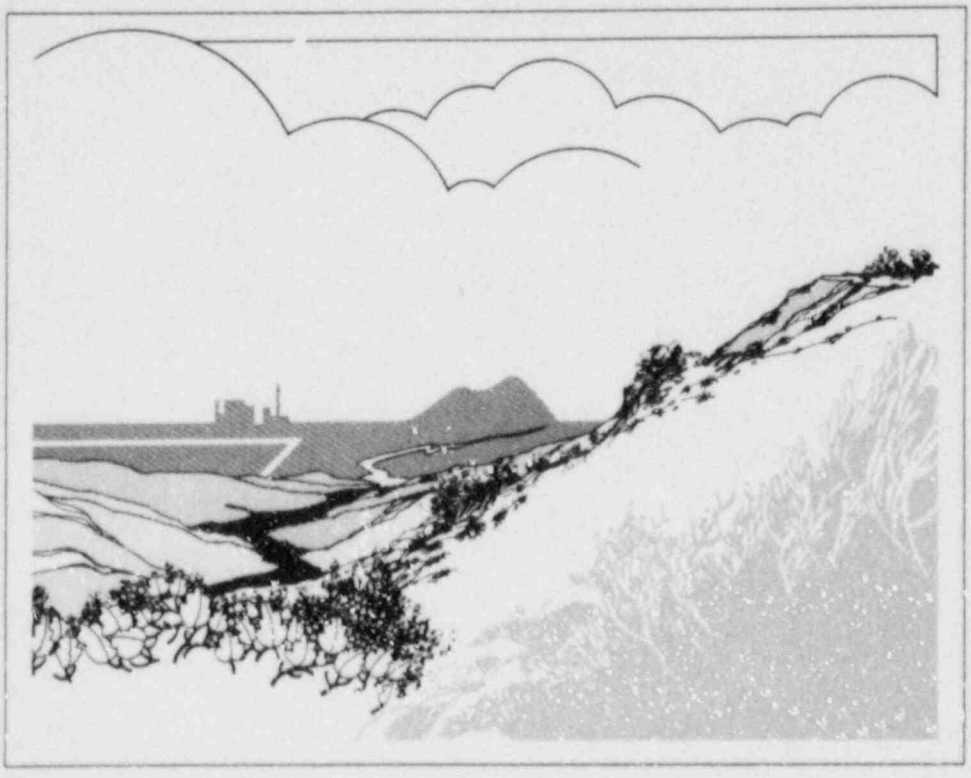

EG&G Idaho

Work performed under
DOE Contract No. DE-AC07-76ID01570

for the ***U.S. Nuclear Regulatory Commission***

Idaho National Engineering Laboratory

Managed by the U.S. Department of Energy

Available from

Superintendent of Documents
U.S. Government Printing Office
Post Office Box 37082
Washington, D.C. 20013-7982

and

National Technical Information Service
Springfield, VA 22161

NUREG/CR-4898
EGG-2503
Distribution Category: R2

RESULTS OF SEMISCALE MOD-2C FEEDWATER AND STEAM LINE BREAK (S-FS) EXPERIMENT SERIES: BOTTOM MAIN FEEDWATER LINE BREAK ACCIDENT EXPERIMENTS

Timothy J. Boucher

Published February 1988

EG&G Idaho, Inc.
Idaho Falls, Idaho 83415

Prepared for the
Division of Accident Evaluation
Office of Nuclear Regulatory Research
U.S. Nuclear Regulatory Commission
Washington, D.C. 20555
Under DOE Contract No. DE-AC07-76ID01570
FIN No. A6038

ABSTRACT

This report presents the results of four experiments simulating 100, 50, and 14.3% bottom main feedwater line break accidents performed at high pressure and temperature in the Semiscale Mod-2C facility. The primary and secondary thermal-hydraulic responses are characterized (including local secondary convective heat transfer) and the influence of the break size on the responses is discussed. A definite deficiency is identified in existing forced convection boiling heat transfer correlations and the conservatism of FSAR heat transfer degradation assumptions is shown to be questionable. The effectiveness of the recovery operations in maintaining control of the system is addressed, and the system response (including local secondary convective heat transfer) to voided secondary refill operations are discussed. Feedwater line break issues are discussed and conclusions are drawn based on the results of the analysis. Finally, recommendations are made for further utilization of the data and considerations for future code calculations.

FIN No. A6038—Semiscale Program

EXECUTIVE SUMMARY

Although ruptures of steam generator main feedwater lines are not expected to occur often in pressurized water reactor (PWR) plants, the potential for rupture of the primary pressure boundary due to overpressurization necessitates their examination. Limited existing data on present day PWR steam generators resulted in a large number of assumptions and simplifications being utilized for Final Safety Analysis Report (FSAR) calculations for a number of Combustion Engineering (C-E) System 80-type plants. The FSAR calculations predicted peak primary system pressures in excess of 110% of the system design pressure, necessitating quantification of their degree of conservatism. Concerns exist with respect to the potential for primary overpressurization, the validity and effects of combining the assumptions and simplifications, and also with the effectiveness of recovery procedures and the steam generator downcomer liquid level differential pressure measurement response effects on safety trip systems. To address these concerns, four feedwater line break experiments were performed in the Semiscale Mod-2C facility. The Mod-2C system is a small scale, nonnuclear, electrically heated, high pressure, high temperature experimental system which simulates all of the major components of a full-scale PWR. It contains a vessel and two primary coolant loops. The affected and unaffected loops simulate one loop and three loops of a four-loop PWR, respectively. Both loops contain active steam generators and pumps, with the single-loop steam generator highly instrumented for this test series. Experiments S-FS-6, S-FS-6B, S-FS-7, and S-FS-11 simulated 100, 100, 14.3 and 50% bottom main feedwater line break secondary LOCAs, respectively. Experiment S-FS-6B (a repeat of the initial phase of experiment S-FS-6) was performed to obtain local heat transfer data not obtained during experiment S-FS-6. Initial and boundary conditions were scaled from, and compounding failures and assumptions simulated, those conditions utilized for C-E System 80 FSAR calculations. Data from the experiments should be useful for quantifying the safety margin inherent in licensing assumptions, simplifications and calculations, and in providing a data base for integral system responses for assessment of computer codes and recovery procedure effectiveness.

The results of the analysis of the Semiscale Mod-2C bottom main feedwater line break data were used as a basis for addressing the principal bottom main feedwater line break issues and concerns. Items addressed include: the potential for primary overpressurization; the relative degree of conservatism inherent in FSAR assumptions and simplifications; the steam generator downcomer liquid level differential pressure measurement response effects on safety trip systems; the effects of break size; and the effectiveness of Emergency Operating Procedure (EOP)-specified recovery procedures (including vessel upper head void collapse and voided secondary refill operations).

Extrapolation of Semiscale Mod-2C measured peak pressures to those predicted for a C-E System 80 plant points out the need for further analysis. The measured peak primary system pressures for the Semiscale Mod-2C bottom main feedwater line break experiments are not a direct indicator of the peak pressures expected for a C-E System 80 plant. Therefore, a simple lumped-parameter analysis was performed which accounted for the fact that the affected steam generator represents only one-fourth of the total available heat sink in Semiscale but one-half of the total available heat sink in a C-E System 80 plant. The analysis produced estimated peak primary pressures near 110% of the design pressure limit for the C-E System 80 plant. This points out the need to perform best-estimate calculations with a thermal-hydraulic computer code that has been assessed against and verified for the results of these experiments.

Final verification of the relative degree of conservatism inherent in FSAR assumptions and simplifications will require best-estimate calculations performed with a verified computer code. However, the results of the analysis of the Semiscale Mod-2C bottom main feedwater line break data can be used as a basis for addressing the conservatism of a number of FSAR assumptions and simplifications. Assumptions which maximize the primary pressurization but do not emulate the actual response exhibited by the experimental data are considered to be conservative. The Semiscale results indicate that:

- The C-E System 80 FSAR Appendix 15B assumption of 100% heat transfer until the liquid inventory reaches 0% followed by a step change reduction to 0% heat transfer is not conservative since it emulates the actual heat transfer degradation exhibited by the experimental data
- The C-E FSAR assumptions regarding break flow severely distort the effect of the break size on the system response, provide

no real benefit to the analysis, and would preclude accurate best-estimate calculations

- The assumed main steam line check valve failure used for the C-E FSAR calculations is not conservative since the increased steam flow from the unaffected loop steam generator prior to SCRAM increases the unaffected loop primary energy removal, reducing the effect of the loss of the affected loop heat sink
- The C-E FSAR assumption regarding loss of offsite power at SCRAM is conservative since it reduces the primary cooling following SCRAM and provides limiting conditions for system recovery operations
- Configurational and fluid hydraulic response dependencies of the downcomer liquid level measurements make them suspect for conservative assumption candidates, but it is conceivable that they would produce earlier system SCRAM initiation and thus be nonconservative.

The secondary and primary thermal-hydraulic responses are relatively insensitive to the break size. The main differences observed are in the timing of events and the quantitative responses. Very slight break size sensitivities were observed in the affected loop steam generator heat transfer degradation with loss of liquid inventory and the peak primary pressures. The normalized heat transfer versus normalized liquid inventory for the affected loop steam generator shows that the normalized heat transfer remains at 100% until the normalized liquid inventory reaches almost 0% for all three break size cases. The heat transfer then rapidly decreases to 0%. A very slight break size dependency is exhibited in that the degradation in heat transfer was initiated at a slightly greater mass inventory and proceeded at a slightly slower rate for the smallest break size case. This is due to a more gradual depletion of the tube bundle liquid inventory for the smallest break size case. The measured primary pressures exhibit a very slight sensitivity to break size with peak values of 16.37, 16.41, and 16.42 MPa for the 100, 50, and 14.3% break size cases, respectively. This is due to greater unaffected-to-affected loop intersecondary flow past the failed check valve for the largest break size producing increased unaffected loop steam generator primary energy removal and reducing the net primary energy addition. While these very slight break size dependencies did exist, their effect was minimal and the basic thermal-hydraulic responses were relatively insensitive to the break size.

The automatic actions performed by the plant protective systems during the blowdown phase of the experiments left the Semiscale Mod-2C system in a quasi-stable state, but at conditions that did not ensure sufficient control of the system. The stabilization operations performed (affected loop steam generator auxiliary feedwater termination, SI termination, normal charging/letdown, pressurizer internal heater, and unaffected loop steam generator steam and feed operations) were very effective in stabilizing the system at conditions from which a controlled natural circulation cooldown and depressurization could be initiated. The guidance provided by the EOPs was both appropriate and effective in stabilizing and regaining control of the system for all of the experiments. No vessel upper head voiding occurred as the upper head fluid remained highly subcooled. The limiting criteria in regaining control of the system for all three experiments was the recovery of the unaffected loop steam generator secondary liquid level, with the smallest break size case requiring the greatest amount of time to recover the lost inventory.

The natural circulation cooldown and depressurization operations performed following system stabilization for experiment S-FS-6 (i.e., pressurizer auxiliary spray, pressurizer internal heater, normal charging/letdown, and unaffected loop steam generator steam and feed with stairstep secondary pressure reduction operations), were very effective in cooling down and depressurizing the primary fluid system in a controlled manner. The unaffected loop steam generator steam and feed operations with 0.71 MPa stairstep secondary pressure reductions were successful in cooling the primary fluid at about 25.6 K/h while maintaining satisfactory secondary inventory. Attempts to cooldown at faster rates would be limited, however, by the capability of the auxiliary feedwater flow to maintain secondary inventory. The combined operations of pressurizer auxiliary spray and internal heaters demonstrated excellent control of primary pressure and subcooled margin. No vessel upper head voiding occurred during the normal natural circulation cooldown and depressurization phase (minimum allowable primary fluid subcooled margin of 27.8 K), nor during the rapid natural circulation cooldown and depressurization phase (minimum allowable primary fluid subcooled margin of 11.1 K). However, continuous reduction in the vessel upper head fluid subcooled margin was noted for the rapid phase of the cooldown indicating that

continued operation in this mode would have resulted in eventual vessel upper head voiding.

The *fill and drain* and *pump restart* methods of vessel upper head void collapse both proved to be effective in cooling the upper head fluid and collapsing the upper head void. However, an important observation was made with respect to determining final upper head void collapse. For both methods, the pressurizer liquid level started to increase before the upper head void was completely collapsed. This points out the importance of monitoring the rate of the pressurizer liquid level increase to ensure that it matches that expected for the normal charging flow rate as a means of determining final upper head void collapse. The major differences noted for the two methods of upper head void collapse were in the rate of the void collapse and the amount of cooling provided for the upper head fluid and metal. The *fill and drain* method (normal charging/letdown and pressurizer internal heater operations) resulted in a more rapid collapse of the vessel upper head void. However, the *pump restart* method (primary coolant pump restart) resulted in more cooling of the vessel upper head fluid and metal. Therefore, it is conceivable that the cooldown and depressurization could continue at a more rapid rate using the *pump restart* method of upper head void collapse.

The voided secondary refill operations performed verified the effectiveness of the operations for maintaining stable conditions while recovering the inventory in a voided steam generator. Refilling the voided secondary provides a significant source of primary energy removal, ensures an adequate cooling source for the primary, and produces no major challenges to maintaining stable system conditions. The secondary convective heat transfer reestablishment in the affected loop steam generator exhibits the same trends in the secondary convective heat transfer coefficient with respect to the vapor-void fraction, as was observed in the full-power, steady-state, and transient data. The slower refill rate data exhibited the same phenomena but the secondary convective heat transfer coefficients were smaller in magnitude. The voided secondary refill data was obtained at conditions typical of those that occur during a loss of feedwater transient or any other situation where a steam generator's mass inventory is substantially reduced and then slowly recovered with auxiliary feedwater flow. Thus, the data would be useful for analyzing problems encountered in simulating slow secondary refill conditions with a thermal-hydraulic computer code.

Final determination of the potential for primary overpressurization and quantification of the degree of conservatism inherent in the C-E System 80 FSAR assumptions and simplifications will require the performance of best-estimate calculations with a thermal-hydraulic computer code which has been verified against this experimental data. While verification of computer codes is beyond the scope of this report, one definite code deficiency has been identified as a result of this analysis. The measured secondary convective heat transfer coefficients and vapor void fractions indicate a trend of increasing heat transfer coefficient with increasing vapor void fraction. The Chen combined boiling/vaporization convective heat transfer correlation currently used in thermal-hydraulic codes predicts exactly the opposite trend for the secondary convective heat transfer coefficient variation with the vapor void fraction. It also significantly underpredicts the magnitude of the secondary convective heat transfer coefficient. Improvements in the secondary convective heat transfer calculation methodology will be required for thermal-hydraulic computer codes to accurately calculate the actual primary-to-secondary transient heat transfer. This will require either modifications to an existing, or development of a new, boiling/vaporization convective heat transfer correlation based on the Semiscale Type III steam generator heat transfer data. The data obtained during these experiments are of sufficient detail and quality to allow verification of thermal-hydraulic computer codes for bottom main feedwater line break, system recovery, and voided secondary refill calculations. The analysis of the experiment results has provided invaluable insight into the phenomena and driving mechanisms evidenced in the experiments and is applicable to full-scale PWR plants.

ACKNOWLEDGMENTS

Acknowledgment, with thanks, is given to the following individuals who have contributed to the understanding of phenomena, the technical content, and to the production of this report. Without their assistance this report could not have been completed in its present form. In alphabetical order: T. H. Chen, D. G. Hall, W. A. Owca and M. P. Plessinger for their analysis in the Quick Look Reports for Tests S-FS-6, S-FS-11 and S-FS-7; Nello Bonicelli (DOE-ID) R. W. Shumway, Don Solberg (USNRC) and J. R. Wolf for their technical reviews of this report; C. C. McKenzie for producing the computer plots of data; S. L. Martin for help with word processing; and, S. J. Lord and S. S. Lortie for technical editing.

CONTENTS

ABSTRACT ii

EXECUTIVE SUMMARY iii

ACKNOWLEDGMENTS vi

INTRODUCTION 1

HISTORICAL BACKGROUND 3

SYSTEM DESCRIPTION AND EXPERIMENTAL PROCEDURE 5

System Description 5

Experimental Procedure 5

EXPERIMENTAL RESULTS 6

Overview of a Steam Generator Bottom Main Feedwater Line Break 6

Secondary Response to a Steam Generator Bottom Main Feedwater Line Break 8

General Secondary Response 8
Secondary Pressure Response 9
Secondary Hydraulic Response 10
Secondary Thermal Response 15

Primary Response to a Steam Generator Bottom Main Feedwater Line Break 25

General Primary Response 25
Primary Pressure Response 27
Primary Hydraulic Response 27
Primary Thermal Response 29

Influence of Bottom Main Feedwater Line Break Size on System Response 31

Effects of Break Size on Secondary Response 31

General Secondary Response Comparisons 31
Secondary Pressure Response Comparisons 31
Secondary Hydraulic Response Comparisons 33
Secondary Thermal Response Comparisons 37

Effects of Break Size on Primary Response 43

General Primary Response Comparisons 43
Primary Pressure Response Comparisons 44
Primary Hydraulic Response Comparisons 45
Primary Thermal Response Comparisons 45

System Response to Plant Stabilization Operations 49

Overall System Response to Stabilization Operations 49
System Response to Normal Charging/Letdown Operation During Stabilization 52
System Response to Pressurizer Internal Heater Operation During Stabilization 53
Comparisons of Stabilization Phase Responses 53

System Response to Plant Cooldown and Depressurization Operations (S-FS-6) 55

Overall Response to System Cooldown and Depressurization Operations 55
Effects of Unaffected Loop Steam Generator Steam and Feed Operation on the System Cooldown and Depressurization to Vessel Upper Head Fluid Saturation 58
Effects of Combined Pressurizer Auxiliary Spray and Internal Heater Operation on the System Cooldown and Depressurization to Vessel Upper Head Fluid Saturation 60

System Response to Vessel Upper Head Void Recovery Operations (S-FS-6) 60

Overall Response to Vessel Upper Head Void Collapse Operations 61
Effects of the Fill and Drain Method of Vessel Upper Head Void Collapse on the System Response 64
Effects of the Pump Restart Method of Vessel Upper Head Void Collapse on the System Response 68
Comparisons of the Fill and Drain and Pump Restart Methods of Vessel Upper Head Void Collapse 68

System Response to Voided Secondary Refill Operations 71

Overall System Response to Voided Secondary Refill Operations 72
Secondary System Response to Voided Secondary Refill Operations 72
Primary System Response to Voided Secondary Refill Operations 82
Comparisons of Voided Secondary Refill Responses 82

Relevance to Bottom Main Feedwater Line Break Issues 89

Final Safety Analysis Report Assumption Conservatisms 89
Maximum Primary Pressure 91
Emergency Operating Procedures 91

CONCLUSIONS 94

RECOMMENDATIONS 97

REFERENCES 99

APPENDIX A—DETAILED SYSTEM DESCRIPTION AND EXPERIMENTAL PROCEDURE A-1

APPENDIX B—REPEATABILITY OF RESULTS (S-FS-6/S-FS-6B COMPARISONS) B-1

APPENDIX C—STEADY-STATE RESULTS C-1

APPENDIX D—ADDITIONAL INFORMATIVE DATA D-1

FIGURES

1. Affected and unaffected loop steam generator secondary pressures and normalized secondary fluid mass inventories during the blowdown phase of a 100% FWLB experiment 7

2. Normalized affected loop steam generator energy removal, normalized net primary fluid system energy addition and pressurizer and loop cold leg pressures during the blowdown phase of a 100% FWLB experiment 9

3. Affected and unaffected loop steam generator secondary pressures during the blowdown phase of 100% FWLB experiments S-FS-6/6B (-10 to 150 s) 10

4. Measured and best-estimate break mass flow rates during the blowdown phase of 100% FWLB experiments S-FS-6/6B (-10 to 150 s) 11

5. Break fluid density during the blowdown phase of 100% FWLB experiments S-FS-6/6B (-10 to 150 s) 12

6. Affected loop steam generator upper and lower downcomer mass flow rates during the blowdown phase of 100% FWLB experiments S-FS-6/6B (-10 to 150 s) 12

7. Affected loop steam generator riser and steam mass flow rates during the blowdown phase of 100% FWLB experiments S-FS-6/6B (-10 to 150 s) 13

8. Unaffected to affected loop steam generator intersecondary mass flow rate through the crossover line during the blowdown phase of 100% FWLB experiments S-FS-6/6B (-10 to 150 s) 13

9. Affected loop steam generator overall downcomer and tube bundle uncorrected and frictional pressure drop corrected interfacial liquid levels during the blowdown phase of 100% FWLB experiments S-FS-6/6B (-10 to 50 s) 14

10. Affected loop steam generator total, downcomer and tube bundle secondary fluid mass inventories during the blowdown phase of 100% FWLB experiments S-FS-6/6B (0 to 150 s) 14

11. Affected loop steam generator tube bundle secondary fluid vapor-void fractions during the blowdown phase of 100% FWLB experiments S-FS-6/6B (-10 to 50 s) 15

12. Unaffected loop steam generator secondary fluid mass inventory, during the blowdown phase of 100% FWLB experiments S-FS-6/6B (-10 to 150 s) 16

13. Unaffected loop steam generator overall downcomer and tube bundle collapsed liquid levels and auxiliary feedwater mass flow rate during the blowdown phase of 100% FWLB experiments S-FS-6/6B (-10 to 150 s) 16

14. Affected loop steam generator average full-power, steady-state U-tube outside wall heat flux versus length along the tube (from inlet to outlet plenum) for the long and short tubes 18

15. Affected loop steam generator average full-power, steady-state U-tube outside wall integrated heat flux versus length along the tube (inlet to outlet plenum) for the long and short tubes 18

16. Affected loop steam generator average full-power, steady-state long tube hot and cold side secondary convective heat-transfer coefficients versus elevation above the top of the tube sheet 19

17. Affected loop steam generator average full-power, steady-state short tube hot and cold side secondary convective heat-transfer coefficients versus elevation above the top of the tube sheet 19

18. Affected and unaffected loop steam generator primary-to-secondary heat transfer during the blowdown phase of 100% FWLB experiments S-FS-6/6B (-10 to 150 s) 20

19. Affected loop steam generator normalized primary-to-secondary heat transfer versus normalized total liquid inventory and versus normalized tube-bundle region liquid inventory during 100% FWLB experiments S-FS-6/6B 20

20. Affected loop steam generator secondary convective heat transfer coefficients at the 61 cm elevation during the blowdown phase of 100% FWLB experiments S-FS-6/6B (-10 to 50 s) 21

21. Affected loop steam generator secondary convective heat transfer coefficients at the 99 cm elevation during the blowdown phase of 100% FWLB experiments S-FS-6/6B (-10 to 50 s) 21

22. Affected loop steam generator secondary convective heat transfer coefficients at the 137 cm elevation during the blowdown phase of 100% FWLB experiments S-FS-6/6B (-10 to 50 s) 22

23. Affected loop steam generator secondary convective heat transfer coefficients at the 213 cm elevation during the blowdown phase of 100% FWLB experiments S-FS-6/6B (-10 to 50 s) 22

24. Affected loop steam generator secondary convective heat transfer coefficients at the 404 cm elevation during the blowdown phase of 100% FWLB experiments S-FS-6/6B (-10 to 50 s) 23

25. Affected loop steam generator secondary convective heat transfer coefficients at the 556 cm elevation during the blowdown phase of 100% FWLB experiments S-FS-6/6B (-10 to 50 s) 23

26. Affected loop steam generator secondary convective heat transfer coefficients at the 709 cm elevation during the blowdown phase of 100% FWLB experiments S-FS-6/6B (-10 to 50 s) 24

27. Affected loop steam generator secondary convective heat transfer coefficient at the 886 cm elevation during the blowdown phase of 100% FWLB experiments S-FS-6/6B (-10 to 50 s) 24

28. Unaffected loop steam generator steam mass flow rate during the blowdown phase of 100% FWLB experiments S-FS-6/6B (-10 to 150 s) 26

29. Primary fluid system energy addition during the blowdown phase of 100% FWLB experiments S-FS-6/6B (-10 to 50 s) 26

30. Pressurizer and affected and unaffected loop cold leg pressures during the blowdown phase of 100% FWLB experiments S-FS-6/6B (-10 to 150 s) 28

31. Pressurizer overall collapsed liquid level during the blowdown phase of 100% FWLB experiments S-FS-6/6B (-10 to 150 s) 29

32. Core power and primary fluid system energy balance during the blowdown phase of 100% FWLB experiments S-FS-6/6B (-10 to 150 s) 30

33. Affected and unaffected loop hot and cold leg and average primary fluid system temperatures during the blowdown phase of 100% FWLB experiments S-FS-6/6B (-10 to 150 s) 30

34. Affected loop hot leg to cold leg fluid temperature measurement station loop transit time during the blowdown phase of 100% FWLB experiments S-FS-6/6B (-10 to 150 s) 32

35. Comparisons of affected and unaffected loop steam generator secondary pressures during the blowdown phases of 100, 50, and 14.3% FWLB experiments S-FS-6/6B, S-FS-11, and S-FS-7 33

36. Comparisons of measured and best estimate break mass flow rates during the blowdown phases of 100, 50, and 14.3% FWLB experiments S-FS-6/6B, S-FS-11, and S-FS-7 34

37. Comparisons of break fluid densities during the blowdown phases of 100, 50, and 14.3% FWLB experiments S-FS-6/6B, S-FS-11, and S-FS-7 35

38. Comparisons of affected loop steam generator upper downcomer mass flow rates during the blowdown phases of 100, 50, and 14.3% FWLB experiments S-FS-6/6B, S-FS-11, and S-FS-7 35

39. Comparisons of affected loop steam generator riser mass flow rates during the blowdown phases of 100, 50, and 14.3% FWLB experiments S-FS-6/6B, S-FS-11, and S-FS-7 36

40. Comparisons of affected loop steam generator lower downcomer mass flow rates during the blowdown phases of 100, 50, and 14.3% FWLB experiments S-FS-6/6B, S-FS-11, and S-FS-7 36

41. Comparisons of intersecondary mass flow rates through the crossover line during the blowdown phases of 100, 50, and 14.3% FWLB experiments S-FS-6/6B, S-FS-11, and S-FS-7 38

42. Comparisons of riser orifice frictional pressure drops during the blowdown phases of 100, 50, and 14.3% FWLB experiments S-FS-6/6B, S-FS-11, and S-FS-7 38

43. Comparisons of affected loop steam generator frictional corrected overall downcomer and tube bundle interfacial liquid levels during the blowdown phases of 100, 50, and 14.3% FWLB experiments S-FS-6/6B, S-FS-11, and S-FS-7 39

44. Comparisons of affected loop steam generator secondary fluid total, downcomer and tube bundle mass inventories during the blowdown phases of 100, 50, and 14.3% FWLB experiments S-FS-6/6B, S-FS-11, and S-FS-7 39

45. Comparisons of unaffected loop steam generator overall downcomer and tube bundle collapsed liquid levels during the blowdown phases of 100, 50, and 14.3% FWLB experiments S-FS-6/6B, S-FS-11, and S-FS-7 40

46. Comparisons of affected loop steam generator normalized heat transfer versus normalized total secondary liquid inventory and versus normalized tube-bundle region liquid inventory during the blowdown phases of 100, 50, and 14.3% FWLB experiments S-FS-6/6B, S-FS-11, and S-FS-7 41

47. Comparisons of unaffected loop steam generator primary-to-secondary heat transfer during the blowdown phases of 100, 50, and 14.3% FWLB experiments S-FS-6/6B, S-FS-11, and S-FS-7 42

48. Comparisons of primary fluid system energy addition during the blowdown phases of 100, 50 and 14.3% FWLB experiments S-FS-6/6B, S-FS-11, and S-FS-7 43

49. Comparisons of pressurizer and loop cold leg pressures during the blowdown phases of 100, 50, and 14.3% FWLB experiments S-FS-6/6B, S-FS-11, and S-FS-7 44

50. Comparisons of pressurizer overall collapsed liquid levels during the blowdown phases of 100, 50, and 14.3% FWLB experiments S-FS-6/6B, S-FS-11, and S-FS-7 46

51. Comparisons of affected loop steam generator primary energy removal and primary fluid system energy balances during the blowdown phases of 100, 50, and 14.3% FWLB experiments S-FS-6/6B, S-FS-11, and S-FS-7 47

52. Comparisons of average primary fluid temperatures during the blowdown phases of 100, 50, and 14.3% FWLB experiments S-FS-6/6B, S-FS-11, and S-FS-7 47

53. Affected and unaffected loop hot and cold leg fluid temperatures during the blowdown phase of 50% FWLB experiment S-FS-11 48

54. Affected and unaffected loop hot and cold leg fluid temperatures during the blowdown phase of 14.3% FWLB experiment S-FS-7 48

55. Unaffected loop steam generator auxiliary feedwater mass flow rate and downcomer and riser overall collapsed liquid levels during the stabilization phase of 100% FWLB experiment S-FS-6 (600 to 3800 s) 50

56. Primary hot leg and vessel upper head fluid subcooled margins and pressurizer internal heater power during the stabilization phase of 100% FWLB experiment S-FS-6 (600 to 3800 s) 50

57. Pressurizer pressure and overall collapsed liquid level during the stabilization phase of 100% FWLB experiment S-FS-6 (600 to 3800 s) 51

58. Unaffected loop steam generator secondary pressure during the stabilization phase of 100% FWLB experiment S-FS-6 (600 to 3800 s) 51

59. Affected and unaffected loop hot and cold leg and average primary fluid temperatures during the stabilization phase of 100% FWLB experiment S-FS-6 (600 to 3800 s) 52

60. Affected and unaffected loop normal charging mass flow rates during the stabilization phase of 100% FWLB experiment S-FS-6 (600 to 3800 s) 53

61. Unaffected loop hot leg, pressurizer surge line inlet and outlet, pressurizer, and pressurizer saturation fluid temperatures during the stabilization phase of 100% FWLB experiment S-FS-6 (600 to 3800 s) 54

62. Pressurizer and unaffected loop steam generator secondary pressures during the plant cooldown and depressurization phase of 100% FWLB experiment S-FS-6 (3800 to 10,600 s) 56

63. Unaffected loop hot leg fluid subcooled margin, pressurizer auxiliary spray mass flow rate, and pressurizer internal heater power during the plant cooldown and depressurization phase of 100% FWLB experiment S-FS-6 (3800 to 10,600 s) 56

64. Pressurizer overall collapsed liquid level, total normal charging and letdown mass flow rates during the plant cooldown and depressurization phase of 100% FWLB experiment S-FS-6 (3800 to 10,600 s) 57

65. Affected and unaffected loop hot and cold leg and average primary fluid temperatures during the plant cooldown and depressurization phase of 100% FWLB experiment S-FS-6 (3800 to 10,600 s) 57

66. Unaffected loop steam generator downcomer and tube bundle overall collapsed liquid levels, and auxiliary feedwater and atmospheric dump valve mass flow rates during the plant cooldown and depressurization phase of 100% FWLB experiment S-FS-6 (3800 to 10,600 s) 58

67. Average cold leg fluid, downcomer to vessel upper head bypass line fluid, vessel upper head fluid, and vessel upper head saturation temperatures during the plant cooldown and depressurization phase of 100% FWLB experiment S-FS-6 (3800 to 10,600 s) 59

68. Vessel upper head collapsed liquid level and vessel upper head fluid subcooled margin during the plant cooldown and depressurization phase of 100% FWLB experiment S-FS-6 (3800 to 10,600 s) 59

69. Unaffected loop steam generator atmospheric dump valve energy removal and core power during the plant cooldown and depressurization phase of 100% FWLB experiment S-FS-6 (3800 to 10,600 s) 60

70. Unaffected loop hot leg and vessel upper head fluid subcooled margins, pressurizer auxiliary spray mass flow rate, and pressurizer internal heater power during the vessel upper head void collapse methods investigation phase of 100% FWLB experiment S-FS-6 (10,600 to 13,900 s) 61

71. Pressurizer and unaffected loop steam generator secondary pressures during the vessel upper head void collapse methods investigation phase of 100% FWLB experiment S-FS-6 (10,600 to 13,900 s) 62

72. Pressurizer and vessel upper head collapsed liquid levels during the vessel upper head void collapse methods investigation phase of 100% FWLB experiment S-FS-6 (10,600 to 13,900 s) 62

73. Total normal charging and letdown mass flow rates during the vessel upper head void collapse methods investigation phase of 100% FWLB experiment S-FS-6 (10,600 to 13,900 s) 63

74. Affected and unaffected loop cold leg volumetric flow rates during the vessel upper head void collapse methods investigation phase of 100% FWLB experiment S-FS-6 (10,600 to 13,900 s) 64

75. Unaffected loop steam generator downcomer and tube bundle overall collapsed liquid levels during the vessel upper head void collapse methods investigation phase of 100% FWLB experiment S-FS-6 (10,600 to 13,900 s) 65

76. Pressurizer and vessel upper head collapsed liquid levels during the fill and drain vessel upper head void collapse method investigation phase of 100% FWLB experiment S-FS-6 (10,700 to 11,400 s) 65

77. Pressurizer auxiliary spray mass flow rate and internal heater power, and total normal charging mass flow rate during the fill and drain vessel upper head void collapse method investigation phase of 100% FWLB experiment S-FS-6 (10,700 to 11,400 s) 66

78. Pressurizer pressure, and unaffected loop hot leg and vessel upper head fluid subcooled margins during the fill and drain vessel upper head void collapse method investigation phase of 100% FWLB experiment S-FS-6 (10,700 to 11,400 s) 66

79. Average cold leg fluid, vessel downcomer to upper head bypass line fluid, vessel upper head fluid, and vessel upper head saturation temperatures during the fill and drain vessel upper head void collapse method investigation phase of 100% FWLB experiment S-FS-6 (10,700 to 11,400 s) 67

80. Pressurizer and vessel upper head collapsed liquid levels during the pump restart vessel upper head void collapse method investigation phase of 100% FWLB experiment S-FS-6 (11,700 to 13,200 s) 69

81. Affected and unaffected loop cold leg and vessel downcomer to upper head bypass line volumetric flow rates during the pump restart vessel upper head void collapse method investigation phase of 100% FWLB experiment S-FS-6 (11,700 to 13,200 s) 69

82. Average cold leg fluid, vessel downcomer to upper head bypass line fluid, vessel upper head fluid, and vessel upper head saturation temperatures during the pump restart vessel upper head void collapse method investigation phase of 100% FWLB experiment S-FS-6 (11,700 to 13,200 s) 70

83. Affected and unaffected loop hot and cold leg and average primary fluid temperatures during the pump restart vessel upper head void collapse method investigation phase of 100% FWLB experiment S-FS-6 (11,700 to 13,200 s) 70

84. Vessel upper head pressure, and unaffected loop hot leg and vessel upper head fluid subcooled margins during the pump restart vessel upper head void collapse method investigation phase of 100% FWLB experiment S-FS-6 (11,700 to 13,200 s) 71

85. Affected loop steam generator downcomer and tube bundle overall collapsed liquid levels and auxiliary feedwater mass flow rate during the voided secondary refill phase of 50% FWLB experiment S-FS-11 (4000 to 8000 s) 73

86. Unaffected loop steam generator downcomer and tube bundle overall collapsed liquid levels and auxiliary feedwater mass flow rate during the voided secondary refill phase of 50% FWLB experiment S-FS-11 (4000 to 8000 s) 73

87. Pressurizer pressure, and affected and unaffected loop steam generator secondary pressures, during the voided secondary refill phase of 50% FWLB experiment S-FS-11 (4000 to 8000 s) 74

88. Affected and unaffected loop pump speeds, affected and unaffected loop cold leg volumetric flow rates, and affected loop steam generator long and short tube outlet volumetric flow rates during the voided secondary refill phase of 50% FWLB experiment S-FS-11 (4000 to 8000 s) 74

89. Affected and unaffected loop hot and cold leg, and average primary fluid temperatures during the voided secondary refill phase of 50% FWLB experiment S-FS-11 (4000 to 8000 s) 75

90. Pressurizer collapsed liquid level and total normal charging mass flow rate during the voided secondary refill phase of 50% FWLB experiment S-FS-11 (4000 to 8000 s) 75

91. Unaffected loop hot leg fluid subcooled margin and pressurizer internal heater power during the voided secondary refill phase of 50% FWLB experiment S-FS-11 (4000 to 8000 s) 76

92. Affected loop steam generator secondary convective heat transfer coefficients at the 61 cm elevation during the voided secondary refill phase of 50% FWLB experiment S-FS-11 (4000 to 8000 s) 76

93. Affected loop steam generator secondary convective heat transfer coefficients at the 99 cm elevation during the voided secondary refill phase of 50% FWLB experiment S-FS-11 (4000 to 8000 s) 77

94. Affected loop steam generator secondary convective heat transfer coefficients at the 137 cm elevation during the voided secondary refill phase of 50% FWLB experiment S-FS-11 (4000 to 8000 s) 77

95. Affected loop steam generator secondary convective heat transfer coefficients at the 213 cm elevation during the voided secondary refill phase of 50% FWLB experiment S-FS-11 (4000 to 8000 s) 78

96. Affected loop steam generator secondary convective heat transfer coefficients at the 404 cm elevation during the voided secondary refill phase of 50% FWLB experiment S-FS-11 (4000 to 8000 s) 78

97. Affected loop steam generator secondary convective heat transfer coefficients at the 556 cm elevation during the voided secondary refill phase of 50% FWLB experiment S-FS-11 (4000 to 8000 s) 79

98. Affected loop steam generator secondary convective heat transfer coefficients at the 709 cm elevation during the voided secondary refill phase of 50% FWLB experiment S-FS-11 (4000 to 8000 s) 79

99. Affected loop steam generator secondary convective heat transfer coefficient at the 886 cm elevation during the voided secondary refill phase of 50% FWLB experiment S-FS-11 (4000 to 8000 s) 80

100. Affected loop steam generator tube bundle vapor-void fractions during the voided secondary refill phase of 50% FWLB experiment S-FS-11 (4000 to 8000 s) 80

101. Affected loop steam generator tube bundle mixture level, secondary convective heat transfer re-establishment level, and interfacial liquid level during the voided secondary refill phase of 50% FWLB experiment S-FS-11 (4800 to 6800 s) 81

102. Affected loop steam generator primary-to-secondary heat transfer and core power during the voided secondary refill phase of 50% FWLB experiment S-FS-11 (4000 to 8000 s) 83

103. Affected loop steam generator secondary convective heat transfer coefficients at the 61 cm elevation during the voided secondary refill phase of 14.3% FWLB experiment S-FS-7 (10,000 to 20,000 s) 83

104. Affected loop steam generator secondary convective heat transfer coefficients at the 99 cm elevation during the voided secondary refill phase of 14.3% FWLB experiment S-FS-7 (10,000 to 20,000 s) 84

105. Affected loop steam generator secondary convective heat transfer coefficients at the 137 cm elevation during the voided secondary refill phase of 14.3% FWLB experiment S-FS-7 (10,000 to 20,000 s) 84

106. Affected loop steam generator secondary convective heat transfer coefficients at the 213 cm elevation during the voided secondary refill phase of 14.3% FWLB experiment S-FS-7 (10,000 to 20,000 s) 85

107. Affected loop steam generator secondary convective heat transfer coefficients at the 404 cm elevation during the voided secondary refill phase of 14.3% FWLB experiment S-FS-7 (10,000 to 20,000 s) 85

108. Affected loop steam generator secondary convective heat transfer coefficients at the 556 cm elevation during the voided secondary refill phase of 14.3% FWLB experiment S-FS-7 (10,000 to 20,000 s) 86

109. Affected loop steam generator secondary convective heat transfer coefficients at the 709 cm elevation during the voided secondary refill phase of 14.3% FWLB experiment S-FS-7 (10,000 to 20,000 s) 86

110. Affected loop steam generator tube bundle vapor-void fractions during the voided secondary refill phase of 14.3% FWLB experiment S-FS-7 (10,000 to 20,000 s) 87

111. Affected loop steam generator tube bundle mixture level, secondary convective heat transfer re-establishment level, and interfacial liquid level during the voided secondary refill phase of 14.3% FWLB experiment S-FS-7 (12,000 to 19,500 s) 88

112. Affected loop steam generator primary-to-secondary heat transfer and core power during the voided secondary refill phase of 14.3% FWLB experiment S-FS-7 (10,000 to 20,000 s) 88

TABLE

1. Peak primary pressures predicted for C-E System 80 plant based on extrapolation of Semiscale MOD-2C data 92

RESULTS OF SEMISCALE MOD-2C FEEDWATER AND STEAM LINE BREAK (S-FS) EXPERIMENT SERIES: BOTTOM MAIN FEEDWATER LINE BREAK ACCIDENT EXPERIMENTS

INTRODUCTION

The Semiscale experimental program conducted by EG&G Idaho, Inc., is part of the overall research and development program sponsored by the U.S. Nuclear Regulatory Commission (USNRC) through the Department of Energy (DOE) to evaluate the behavior of pressurized water reactor (PWR) systems during hypothesized accident sequences. The program's primary objective is to obtain representative integral- and separate-effects thermal-hydraulic response data to provide an experimental basis for analytical model development and assessment. The subject Semiscale Mod-2C experiments,[1] S-FS-6,[2,3], S-FS-6B,[a,2,3] S-FS-7,[2,4] and S-FS-11,[5,6] were authorized and performed under this program. The experiments simulated bottom feedwater line break secondary loss of coolant accidents and were identical except for the break size (100%[b] for tests S-FS-6 and S-FS-6B, 14.3% for test S-FS-7, and 50% for test S-FS-11), and the system recovery operations simulated.

This report discusses results of the simulated bottom feedwater line break transients conducted in the Semiscale Mod-2C test facility and presents information pertinent to related safety issues. The Semiscale Mod-2C test facility is a small-scale nonnuclear model of a PWR power plant. The volume and thermal power of the test loop are 1/1705 those of the reference four-loop Westinghouse PWR (Trojan). The Semiscale Mod-2C facility is full height and contains the active components (core, pumps, steam generators, etc.) necessary to simulate all of the PWR components pertinent to transient response simulation and evaluation. The scenario in Semiscale for the initial phase of the tests was based on the scenario used for the Combustion Engineering (C-E) System 80 Final Safety Analysis Report (FSAR) Appendix 15B bottom feedwater line break calculations. Following the initial phase, plant stabilization operations were performed for tests S-FS-6, S-FS-7, and S-FS-11. Plant stabilization was followed by: plant cooldown and depressurization operations (with vessel upper head void collapse method investigations) for test S-FS-6; and affected loop steam generator break isolation and secondary refill operations for tests S-FS-7, and S-FS-11. The discussions of the responses of the primary and secondary fluid systems includes descriptions of the thermal-hydraulic response and the mechanisms that drive the response. The topics pertinent to the bottom feedwater line break transients and related safety concerns discussed include: transient identification; degradation of the affected loop steam generator primary-to-secondary heat transfer with loss of mass inventory; primary overpressurization; the effects of break size; effectiveness of plant automatic actions; effectiveness of plant stabilization operations; effectiveness of plant cooldown and depressurization operations; effectiveness of two methods of vessel upper head void collapse; and the effects of, degree of conservatism inherent in, and applicability of, FSAR assumptions. One additional topic discussed is the system response to voided secondary refill operations, which could occur in a loss of feedwater transient.

The intent of this report is to provide insight into a number of areas. First, the general appearance of the Semiscale Mod-2C bottom feedwater line break transient is presented and the main elements of the transient identified. This discussion will be helpful in gaining insight about the probable appearance of bottom feedwater line break transients in PWR plants, although the magnitude and timing of the response for specific plants must be considered separately. Next, a detailed description and analysis of a particular transient and the driving mechanisms and thermal-hydraulic response of that transient is provided. This should improve the ability to track and assess thermal-hydraulic code calculations based on the Semiscale Mod-2C bottom feedwater line break

a. Test S-FS-6B was a repeat of the initial phase of test S-FS-6 performed to obtain heat transfer data not obtained during S-FS-6.

b. Percentage of the bottom feed steam generator feedwater distribution box total outlet flow area.

transient data. The effects of the break size on the system response are presented next, with the driving mechanisms affecting the response identified. This should provide insight into the effects of break size on transient severity. Then, the system response to plant stabilization operations, plant cooldown and depressurization operations, and vessel upper head void collapse operations are discussed and the driving mechanisms affecting the response identified. This should provide insight into the effectiveness of the operations specified in Emergency Operating Procedures (EOPs) in stabilizing and recovering the plant following a bottom feedwater line break. The system response to voided secondary refill operations is discussed next, with the driving mechanisms affecting the response identified. This should provide insight into the phenomena associated with refilling voided secondaries for scenarios such as loss of feedwater transients. Finally, pertinent bottom feedwater line break issues are discussed in light of the results of these tests. Major emphasis is placed on the test results relative to FSAR assumptions, current licensing concerns, and emergency operating procedures. This should provide insight into: the relative effects, degree of conservatism inherent in, and applicability of, several bottom feedwater line break FSAR assumptions; the extent of the primary system pressurization; and the effectiveness of the EOP-specified recovery and cooldown procedures for recovering and cooling down the plant.

The overall organization of this report is as follows. Following this *Introduction*, the *Historical Background* for these tests is discussed. This is followed by a brief system description and discussion of experimental procedure. Next, the general areas outlined above are presented in the order in which they appeared above. This is followed by a discussion of the conclusions drawn based on the results of the bottom feedwater line break tests. Recommendations for additional uses of the data are provided, followed by a reference list. The appendixes contain the following information: a detailed system description and test conduct information; comparisons of S-FS-6 and S-FS-6B data to ascertain repeatability of results; characterization of the affected loop steam generator steady-state, full-power secondary thermal-hydraulics; and figures providing additional informative data from the tests.

HISTORICAL BACKGROUND

Although ruptures of steam generator main feedwater lines are not expected to occur often in pressurized water reactor (PWR) plants, the potential consequences of these events necessitates their examination. Thermal cycling has produced cracks on main feedwater lines in a number of PWR plants.[7] The cause of a feedwater line leakage event in the Maine Yankee PWR has been attributed to pipe rupture at such cracks following a water hammer event.[8] This type of failure is postulated to result in a complete pipe rupture. A recent accident at the Surry Unit No. 2 plant involved the rupture of a main feedwater line at the feedwater pump suction.[9] Although these events have not been severe, they indicate a potential for the occurrence of more severe, feedwater line rupture events. Depending on the break size and location and the response of the main feedwater system, the effects of a break in the main feedwater line can vary from a rapid heatup to a rapid cooldown of the Nuclear Steam Supply System (NSSS). Breaks downstream of feedwater line check valves have the potential to establish reverse flow from the nearest steam generator back to the break, depending on the main feedwater system operation and/or capacity. Reverse flow from the affected steam generator can cause a rapid depletion of liquid inventory, reducing the heat transfer capability and causing a rapid primary coolant system heatup and pressurization. This rapid pressurization constitutes a potential for overpressurization of PWR primary coolant systems. The associated threat to the integrity of the PWR pressure boundary necessitates examining feedwater line break events.

Due to the limited data base on present day PWR steam generators and associated systems, a large number of assumptions and simplifications are employed when performing calculations to predict system responses to main feedwater line break transients. Foremost is an assumption regarding the degradation of primary-to-secondary heat transfer with reduction of secondary inventory that was considered to be highly conservative. Such assumptions and simplifications may preclude accurate prediction of actual system response, or combine to distort overall behavior. Feedwater line break calculations performed for the Combustion Engineering (C-E) System 80,[10] St. Lucie No. 2,[11] Waterford,[12] and Palo Verde[13] Final Safety Analysis Reports (FSARs) have predicted peak primary system pressures in excess of the Standard Review Plan Section 15.2.8 pressure limit of 110% of the system design pressure.[14] Although the FSAR calculations were believed to be highly conservative, quantification of the degree of conservatism requires performing best-estimate feedwater line break calculations utilizing a computer code that has been assessed for these types of events. While significant information on integral system response was provided by three feedwater line break experiments[15,16] performed by the Semiscale Program in 1982 in the Mod-2A facility, lack of sufficient steam generator secondary side measurements made code assessment impractical. Hence, a need for experimental data required to allow assessment of computer codes for feedwater line break events was identified by the U.S. Nuclear Regulatory Commission (Reference 14). The need for experimental data on primary-to-secondary heat transfer response to secondary liquid mass inventory reductions has also been identified and included in the Westinghouse Model Boiler (MB-2)[17] and Japanese Atomic Energy Research Institute (JAERI) Rig of Safety Assessment (ROSA-IV) Large Scale Test Facility (LSTF) experimental safety research programs.[a]

With this background information in mind, the feedwater line break experiments performed during the Semiscale Mod-2C Feedwater and Steam Line Break (FS) Experiment Series were chosen to provide data within a representative range of typical PWR conditions, break sizes, and operating scenarios with appropriate conservatisms incorporated. The feedwater line break test parameters were scaled from a C-E System 80 plant. The boundary and initial conditions were consistent with those in Reference 10. Data from the experiments will be useful in quantifying the safety margin inherent in licensing assumptions, simplifications, and calculations, and in providing a data base of integral system response for assessing computer codes. The Semiscale Mod-2C integral system bottom main feedwater line break experiment heat transfer data will also be complemented by MB-2 program single component steam generator loss of feedwater experiment heat transfer data and ROSA-IV program integral system natural circulation experiment heat transfer data. The combined data from these programs will cover a wide range of scale [1/48 volume scale for ROSA-IV (LSTF); 1/159 volume scale for MB-2; 1/1705 volume scale for Semiscale Mod-2C], and should allow assessment of the affects of scale on the heat transfer phenomena observed.

In terms of reactor operation and plant behavior, major concerns regarding feedwater line break events include: recovery procedures and the effects

a. ROSA-IV Program Meeting Minutes of October 18, 1985.

thereupon due to compounding system failures; and the steam generator downcomer liquid level differential pressure measurement response to flow out of the break and the effect, thereupon, to related safety trip systems.[a] Incorrect choice of recovery procedures may lead to primary fluid system voiding and eventual core uncovery. Break location and size may also alter system behavior and transient severity. Improperly indicated steam generator downcomer liquid levels could result in delayed reactor and turbine trip, delayed main steam isolation valve closures, delayed safety injection signals, and delayed initiation of auxiliary feedwater injection. The feedwater line break experiments performed addressed the concerns and effects of the aforementioned variables.

---

a. A Memo of Conversation, J. S. Martinell to Jack Guttman (USNRC Licensing), *Feedline/Steamline Break Issues*, June 17, 1983.

SYSTEM DESCRIPTION AND EXPERIMENTAL PROCEDURE

System Description

The facility configuration required for the Feedwater and Steam Line Break (FS) Test Series is the Semiscale Mod-2C system. A more detailed description of the facility as configured and instrumented for the bottom feedwater line break tests is contained in Appendix A of this report. A greatly detailed description of the facility as configured and instrumented for the bottom feedwater line break experiments is contained in the Semiscale Mod-2C Feedwater and Steam Line Break (FS) Test Series Configuration Document.[18] Briefly, the system is scaled from a reference four-loop pressurized water reactor (PWR) system based on the core power ratio, 2(MWth)/3411(MWth).[19] Component elevations, dynamic pressure heads, and liquid distributions were maintained as similar as practical. The two-loop test configuration consisted of the vessel with a 25-rod electrically heated core and external downcomer, tube-and-shell steam generators, and associated loop piping with circulation pumps. The affected loop (in which the bottom feedwater line break occurs) is scaled to represent one loop of a four-loop PWR and the unaffected loop represents three loops of a four-loop PWR. The Mod-2C system consists of the Mod-2B system with several modifications, foremost is a new *Type III* affected loop steam generator. The Type III steam generator design incorporates a downcomer that is outside the tube bundle and riser sections. In this manner, component mass inventory and fluid property (including density/void fraction) information was obtained. The design also includes a steam dome with separator equipment which provides steam exit qualities of at least 90% during full-power, steady-state operations. Component flow areas, volumes, lengths, and pressure drops have been sized to simulate a Westinghouse Model 51 steam generator. Temperature measurements from the primary fluid, U-tube outside wall, and secondary fluid were normalized to provide heat transfer data for the tests. Measurement spool pieces in the upper and lower downcomer and the riser provided fluid hydraulics data for the tests.

Experimental Procedure

The four feedwater line break tests performed during the FS Test Series simulated transients initiated by a break in a steam generator bottom main feedwater line downstream of the check valve. The initial conditions and sequences of events were specified to simulate the initial conditions and assumptions used for the Combustion Engineering (C-E) System 80 Final Safety Analysis Report (FSAR) Appendix 15B calculations (Reference 10). A more detailed discussion of the initial conditions and sequences of events for the bottom feedwater line break tests is contained in Appendix A of this report. A greatly detailed discussion of the experimental procedure for the feedwater line break tests is contained in References 2 through 6 and 18. Briefly, with the exception of primary pressure, the initial conditions for the tests represented the full-power conditions used for the C-E System 80 FSAR calculations. The initial primary pressure represented the normal full-power operating pressure of the C-E System 80 reference plant. Many of the assumptions made for the C-E System 80 FSAR calculations were used for these tests. The assumptions simulated were: loss of all main feedwater at break initiation; failure of the check valve in the main steam line of the affected steam generator; reactor trip due to high pressurizer pressure; loss of offsite power at reactor trip; safety injection (SI) and main steam isolation valve (MSIV) closure signals generated based on low affected steam generator secondary pressure; no credit taken for the charging system; and only one train of high pressure injection (HPI) available. Compensation for environmental heat loss was provided through heat addition with trace heaters on the exterior of the pressure boundary and through augmentation of the core power.

EXPERIMENTAL RESULTS

This section presents an interpretive description of important thermal-hydraulic phenomena associated with Semiscale Mod-2C Bottom Main Feedwater Line Break Experiments S-FS-6, S-FS-6B, S-FS-7, and S-FS-11. The discussion is aimed toward aiding: code development and assessment efforts; Emergency Operating Procedure (EOP) effectiveness analysis efforts; voided secondary refill response analysis efforts; and Final Safety Analysis Report (FSAR) assumption analysis efforts. Therefore, the section concentrates on the phenomena that either is of particular challenge to code application or is pertinent to EOP effectiveness, voided secondary refill response, and/or FSAR assumption analysis efforts. Most of this section refers to S-FS-6/S-FS-6B data (the 100% break case tests). The pressure and hydraulic responses presented are from S-FS-6 data, while the local heat transfer and thermal responses presented are from S-FS-6B data. A comparison of results from tests S-FS-6 and S-FS-6B is presented in Appendix B. The excellent agreement shown in the data comparisons of Appendix B provides verification of both the repeatability of results and the validity of intermingling the data from the two tests for the experimental results discussions. Following an overview of the gross system response during the blowdown phase of a bottom feedwater line break secondary loss of coolant accident (LOCA), the secondary response during the blowdown phase is discussed along with the mechanisms driving the response. Included in the discussion on secondary response during the blowdown phase is the pressure response for both secondaries, hydraulic response for both secondaries (with the emphasis on the affected loop steam generator), and thermal response for both secondaries (with the emphasis on the affected loop steam generator and its local heat transfer response). Next, the primary response associated with the secondary response is discussed along with the mechanisms driving the response. Included in the discussion on primary response during the blowdown phase is the pressure response, hydraulic response, and thermal response. The influence of break size on the blowdown phase of a bottom feedwater line break secondary LOCA is then discussed. Included in this discussion are the secondary and primary thermal-hydraulic response comparisons and the driving mechanisms. Next, the effectiveness of plant stabilization operations is discussed for tests S-FS-6, S-FS-7, and S-FS-11. Included in this discussion are the primary and secondary pressure, temperature, and fluid inventory responses to plant stabilization operations, as taken from EOPs. The system response to plant cooldown and depressurization operations for test S-FS-6 is then discussed. Included in this discussion are the primary and secondary pressure, temperature, and fluid inventory responses to plant cooldown and depressurization operations, as taken from EOPs. Next, the system response to vessel upper head void recovery operations is discussed for test S-FS-6. Included in this discussion are the primary pressure, temperature, and fluid inventory responses for two methods of vessel upper head void collapse (the *fill and drain* and the *pump restart* methods). The system response to refilling of the voided affected loop steam generator secondary for tests S-FS-7 and S-FS-11 is then discussed. Included in this discussion is the primary and secondary pressure, temperature, and fluid inventory responses and affected loop steam generator secondary heat transfer rates (local and global) for the two tests (two different refill rates). Finally, based on the results of these tests, pertinent bottom feedwater line break issues are discussed. Major emphasis is placed on the test results relative to FSAR assumptions, current licensing concerns, and EOP-specified recovery operations.

Overview of a Steam Generator Bottom Main Feedwater Line Break

Preliminary to the detailed discussion of S-FS-6, S-FS-6B, S-FS-7, and S-FS-11 results, this section presents a qualitative overview of the gross system response to a bottom main feedwater line break secondary LOCA, with special emphasis on major events that affected the primary energy balance, and thus transient severity. System response during a bottom main feedwater line break downstream of the check valve is characterized by a secondary depressurization with total loss of the affected loop steam generator secondary fluid mass inventory and substantial loss of the unaffected loop steam generator secondary fluid mass inventory (due to the failed main steam line check valve), as shown in Figure 1. The affected loop steam generator secondary fluid mass inventory is controlled by the

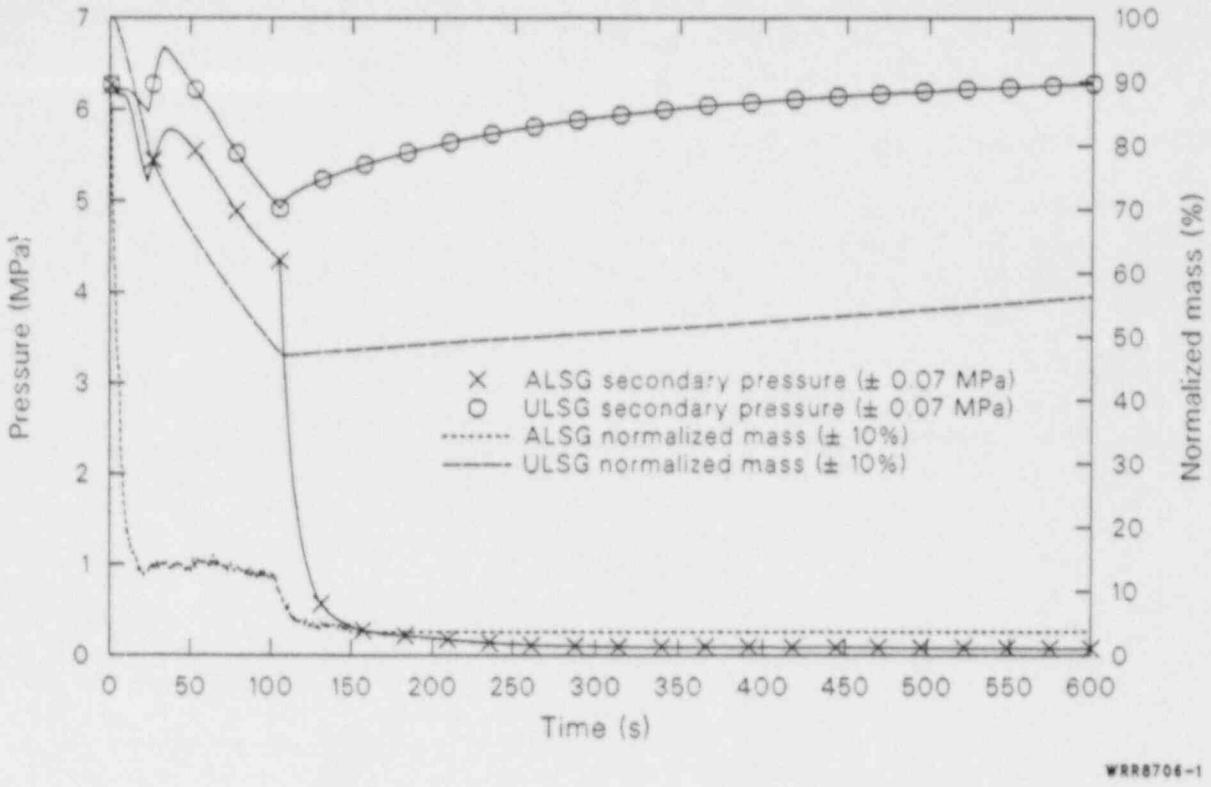

Figure 1. Affected and unaffected loop steam generator secondary pressures and normalized secondary fluid mass inventories during the blowdown phase of a 100% FWLB experiment.

fluid mass balance formed by: loss of main feedwater; flow out the break; flow out the main steam line before turbine stop valve closure; flow from the unaffected loop steam generator secondary past the failed main steam line check valve before main steam isolation valve (MSIV) closure; and auxiliary feedwater flow. The unaffected loop steam generator secondary fluid mass inventory is controlled by the fluid mass balance formed by: loss of main feedwater; flow out the main steam line before turbine stop valve closure; flow to the affected loop steam generator secondary past the failed main steam line check valve before MSIV closure; and auxiliary feedwater flow. As shown in Figure 1, the loss of mass from the secondaries initially produces only a minor step change in pressure. The pressures then hold steady as vapor generation in the secondaries continues. As the affected loop steam generator liquid inventory is depleted (normalized fluid mass of 12% is all vapor in Figure 1), the vapor generation in the affected loop steam generator is stopped. The continued loss of inventory via the break and the main steam line produces a reduction in secondary pressure. As the flow out of the affected loop steam generator main steam line decreases, the flow between the secondaries via the main steam header increases. The increased loss of inventory from the unaffected loop steam generator initiates a slow depressurization of the unaffected loop steam generator secondary. These depressurizations continue until the high pressurizer pressure reactor and turbine trip (SCRAM) set point is reached (at about 23 s in Figure 1). Due to the SCRAM signal, the turbine stop valves close causing a period of repressurization for both secondaries as the energy addition to the secondaries from the primary exceeds the energy removal via the break. This continues until the break energy removal exceeds the energy addition to the secondaries from the primary. The secondaries then enter a period of gradual depressurization under the influence of the break energy removal. The secondaries remain coupled until the affected loop steam generator secondary pressure reaches the low pressure set point (at about 101 s in Figure 1) initiating the safety injection (SI) and MSIV closure signals. The depressurization of the unaffected loop steam generator is halted when the MSIV fully closes isolating the unaffected loop steam generator and causing a slight repressurization of the secondary.

The affected loop steam generator continues to depressurize until the generator is essentially empty (at about 150 s in Figure 1). The remainder of the blowdown phase of the transient is characterized by the affected loop steam generator auxiliary feedwater entering the upper downcomer and exiting via the break while the unaffected loop steam generator auxiliary feedwater recovers the secondary inventory and provides cooling, which aides in stabilizing the unaffected loop steam generator secondary pressure and the primary system fluid temperature.

The primary fluid system response is a rapid pressurization in response to the loss of primary-to-secondary heat transfer during the bottom main feedwater line break secondary LOCA. As shown in Figure 2, the primary fluid rapidly heats up as the affected loop steam generator primary-to-secondary heat transfer reduces (beginning at about 10 s in Figure 2). This causes the primary fluid to expand and rapidly pressurizes the primary. The pressurization of the primary continues until about 4 s after the high pressurizer pressure SCRAM set point is reached (until about 27 s in Figure 2) with the peak pressure occurring in the loop cold legs. The primary system response after this point is governed primarily by automatic actions (core power decay, turbine stop valve closures, MSIV closures, and auxiliary feedwater flow) and the loop flow reductions resulting from pump coastdowns following loss of offsite power. Following SCRAM, the rapid reduction in core power combined with the slower closure time for the turbine stop valves produced a rapid depressurization of the primary fluid system. The period of rapid depressurization is followed by a period of slower depressurization due to core power decay and intersecondary flow. Finally, loop flow reduction (following loss of offsite power), MSIV closure, and auxiliary feedwater injection produce an unaffected loop steam generator energy removal rate that is close to the core decay heat level, resulting in a very slow depressurization of the primary fluid system. The primary fluid system pressure remains above the high pressure injection system (HPIS) shutoff head so that HPIS injection does not occur.

At the end of the blowdown phase of the transient, the primary and secondary systems are sufficiently stable to allow transient identification and plant stabilization and recovery operations to begin.

Secondary Response to a Steam Generator Bottom Main Feedwater Line Break

Understanding the secondary fluid system thermal-hydraulic response during a bottom main feedwater line break secondary LOCA is important, because the pressurization of the primary fluid system is controlled by the secondary response. Basically, the primary pressure response is controlled by an overall energy balance involving core power, primary-to-secondary heat transfer, and heat loss. There are several characteristic inflection points in the secondary fluid system thermal-hydraulic response to a bottom main feedwater line break secondary LOCA. The causes of these inflection points are discussed in this section. The general sequence of events affecting the secondary response are outlined first. This is followed by discussions of the pressure response, hydraulic response and thermal response for both secondaries with major emphasis on the affected loop steam generator. Because all of the bottom main feedwater line break experiments had similar basic secondary thermal-hydraulic responses, this discussion refers to S-FS-6/S-FS-6B data only. Break size effects will be discussed later.

General Secondary Response. The occurrence of a break in a steam generator bottom main feedwater line downstream of the check valve produces severe effects on the steam generator secondary. The bottom feedwater line break initiated the transient at 0 s. Secondary fluid originally at 6.26 MPa flowed from the affected loop steam generator through the break flow nozzle and into the catch tank. Compounded by the loss of all main feedwater at transient initiation, the unaffected loop steam generator also experienced a reduction in inventory under the influence of the continued steam flow before closure of the normal main steam flow control valves (turbine stop valve simulators) at SCRAM (reactor and turbine trip). Further compounded by the failure of the affected loop steam generator steam line check valve, the unaffected and affected loop steam generators remain coupled, with transfer of inventory from the unaffected loop to the affected loop steam generator and out the break, until MSIV closure. Following MSIV closure, the secondaries decouple with the

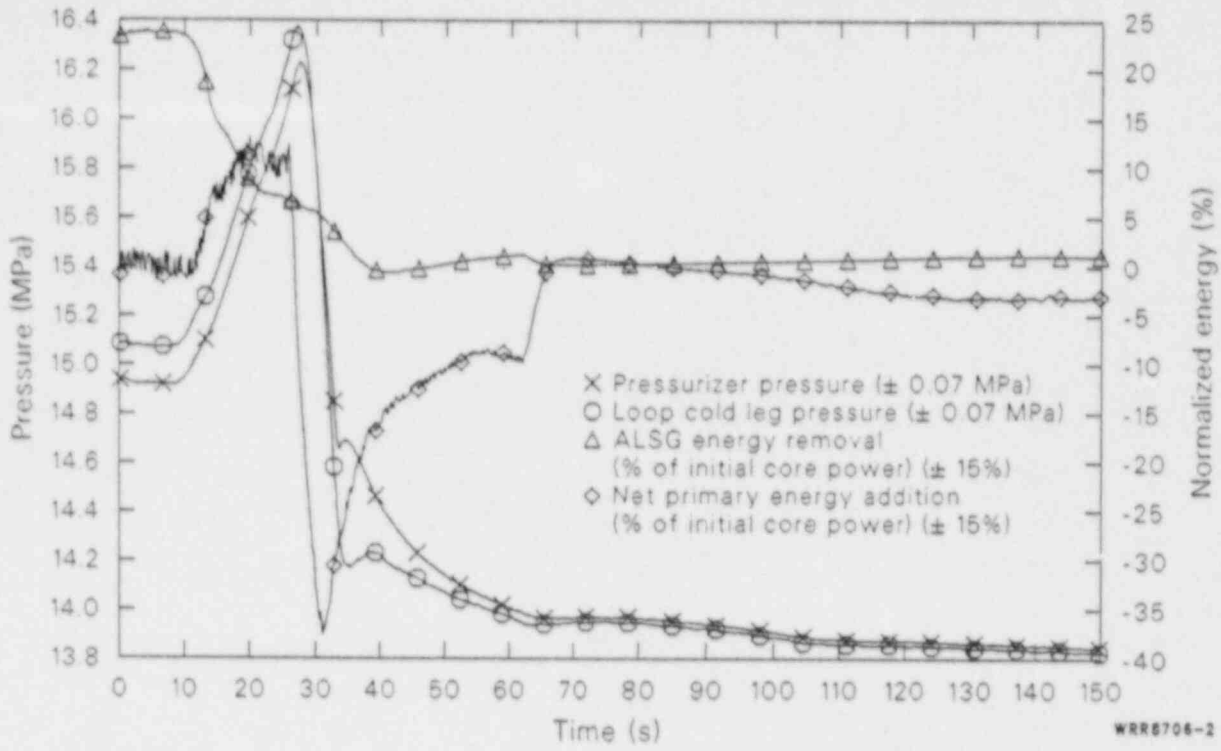

Figure 2. Normalized affected loop steam generator energy removal, normalized net primary fluid system energy addition and pressurizer and loop cold leg pressures during the blowdown phase of a 100% FWLB experiment.

affected loop steam generator emptying and decoupling from the primary and the unaffected loop steam generator slowly refilling with auxiliary feedwater and slowly repressurizing.

Secondary Pressure Response. The secondary pressure responses are characterized by a number of inflection points associated with changes in the mass and energy balances. As shown in Figure 3, the loss of mass from the secondaries initially produced only a minor step change in pressure at about 2 s. The pressures were then held steady as vapor generation in the secondaries, due to the primary-to-secondary heat transfer, continued. After the loss of liquid inventory at about 13 s, the vapor generation in the affected loop steam generator was stopped with the secondary fluid inventory consisting solely of vapor. The continued loss of inventory via the break and the main steam line produced a reduction in secondary pressure. As the flow out of the affected loop main steam line decreased, the flow between the secondaries via the crossover line increased. This increased the loss of inventory from the unaffected loop steam generator and initiated a slow depressurization of the unaffected loop secondary. The depressurization of the secondaries continued until the normal steam flow control valves (turbine stop valve simulators) closed at SCRAM (at about 23 s). The secondaries then experienced a period of repressurization as the energy addition to the secondaries from the primary exceeded the energy removed via the break. This continued until about 35 s when the break energy removal exceeded the energy addition to the secondaries from the primary. The secondaries then entered a period of gradual depressurization under the influence of the break energy removal. The affected loop steam generator secondary reached the low pressure set point of 4.47 MPa at about 101 s. This initiated the SI and MSIV closure signals. The depressurization of the unaffected loop steam generator was halted when the MSIV fully closed at about 104 s. Following MSIV closure, the unaffected loop steam generator experienced a slight repressurization due to energy addition from the primary fluid system in the absence of secondary feeding and steaming. The affected loop steam generator continued to depressurize until the generator was essentially empty at about 150 s. The affected loop steam generator became essentially decoupled from the primary fluid system for the remainder of the transient. The

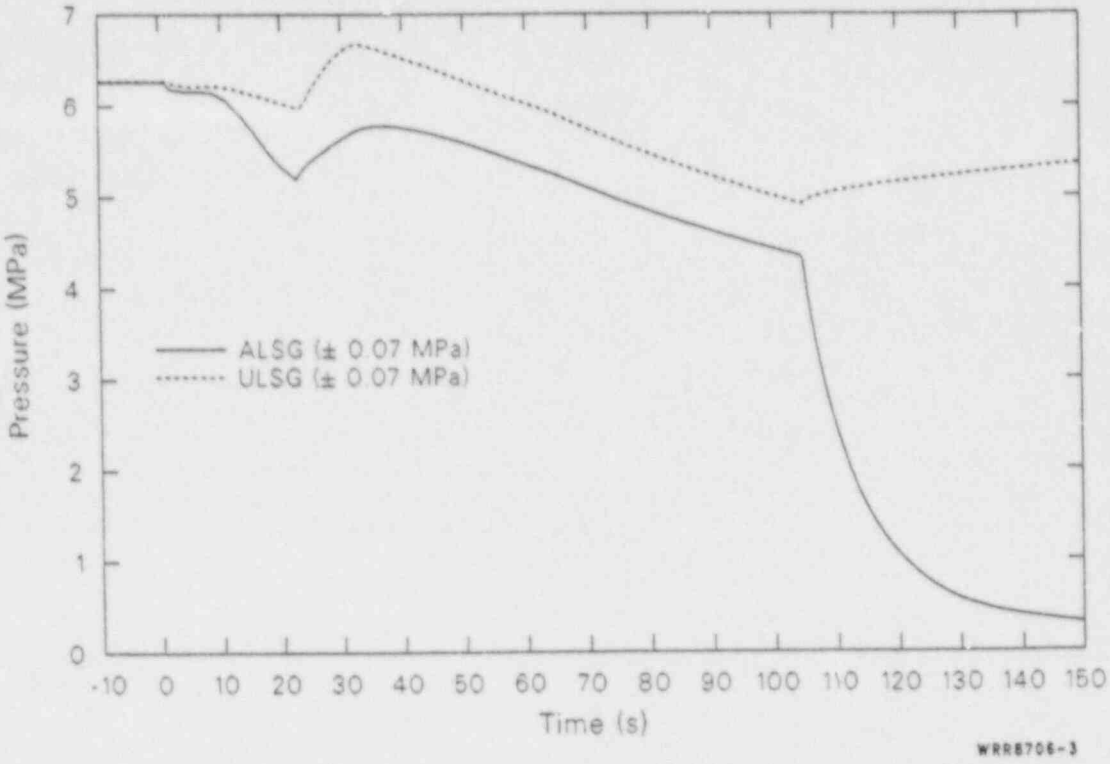

Figure 3. Affected and unaffected loop steam generator secondary pressures during the blowdown phase of 100% FWLB experiments S-FS-6/6B (-10 to 150 s).

unaffected loop steam generator secondary pressure continued to experience a very gradual increase due to the primary energy addition exceeding the auxiliary feedwater energy removal. At the end of the blowdown phase of the transient, the secondary pressures were fairly stable.

Secondary Hydraulic Response. Understanding and calculating the affected loop steam generator secondary fluid system hydraulic response to a bottom feedwater line break requires consideration of the intercomponent as well as the break flow responses. The transient hydraulic response may be better understood after considering the hydraulic conditions that exist in the secondary fluid system at steady-state, full-power conditions. The steady-state secondary fluid hydraulic characteristics can be gleaned from the included figures for times before transient initiation (time = 0 s), or from the discussion in Appendix C. Briefly, the secondary fluid hydraulics at steady-state, full-power conditions consist of a two-phase natural circulation flow condition. The flow is driven by the liquid head difference between the downcomer and the tube bundle, boiling in the tube-bundle region, addition of subcooled liquid in the lower downcomer, and extraction of steam in the steam dome. The intercomponent flow consists of two-phase flow in the tube-bundle region with separated steam exiting the steam dome and liquid being recirculated down the downcomer. Subcooled liquid is added in the lower downcomer to replace the mass of steam removed in the steam dome. The downcomer downflow, tube bundle upflow, and steam and feedwater flows result in a mass balance for all of the secondary components.

The affected loop steam generator secondary fluid hydraulic characteristics are substantially altered during a bottom main feedwater line break secondary LOCA. The simulated bottom main feedwater line rupture initiated the loss of inventory and the resulting changes in the fluid hydraulic conditions at time 0. As shown in Figure 4, the break flow peaked at about 1 s as subcooled liquid critical flow was established. The subcooled liquid break flow exceeded the measurement capacity of the drag screen assembly for a short period of time. However, a best-estimate break flow was obtained, which provides good indication of the subcooled liquid and single-phase vapor break flow for the transient. The break flow transited the full range of possible fluid flow states (i.e., subcooled liquid,

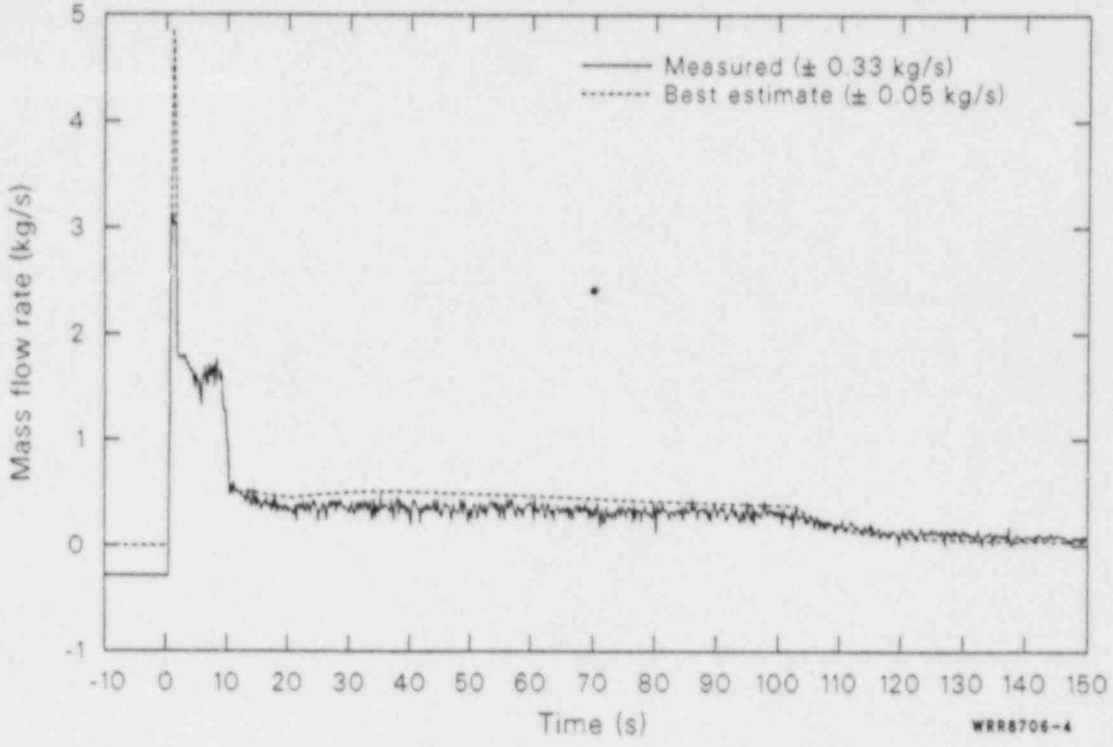

Figure 4. Measured and best-estimate break mass flow rates during the blowdown phase of 100% FWLB experiments S-FS-6/6B (-10 to 150 s).

saturated liquid, two-phase fluid, and single-phase vapor) as the secondary fluid mass inventory was depleted (Figure 5). The break flow was of sufficient magnitude to cause the flow in the affected loop steam generator upper downcomer to increase, while the flow in the lower downcomer between the break and the tube-bundle section reversed (Figure 6). However, because of the continued boiling in the tube-bundle region and the continued normal steam flow, the flow at the top of the affected loop steam generator riser did not reverse, but merely decreased in magnitude (Figure 7). These flow conditions existed until about 10 s into the transient when the secondary liquid inventory was nearly depleted. Thus, a flow split existed in the tube-bundle region until the secondary liquid inventory was nearly depleted. After the secondary liquid inventory was depleted, a new mass balance was achieved in the secondary. Steam entered the steam dome from the crossover line (Figure 8). The flow then split, with approximately half of the steam flowing down the downcomer to the break, and the other half flowing down the tube bundle to the break.

It is important to note that the transient induced intercomponent mass flow rate imbalances resulted in nonuniform rates of inventory reduction for the downcomer and tube-bundle regions, as shown in Figures 9 and 10. The initial reduction in total secondary mass inventory involved a more rapid rate of reduction in the tube bundle mass inventory than in the downcomer mass inventory. The reduction in the tube bundle flow rate and inventory, combined with the continued energy addition from the primary, drove the initially stratified two-phase tube bundle fluid to a uniform two-phase condition with a void fraction of about 0.9 (Figure 11) at about 5 s. The entire tube-bundle region secondary fluid inventory then transitioned to an all-vapor condition (void fraction of 1.0) as the tube bundle liquid inventory was finally depleted. This had a severe effect on the primary-to-secondary heat transfer, as will be discussed presently, because the transient heat transfer is almost totally dependent upon the tube bundle secondary fluid hydraulics. Thus, accurate modeling of the entire secondary fluid system flow areas, volumes, and hydraulic resistances and accurate calculation of the intercomponent as well as the break mass flow rates is necessary to ensure accurate prediction of the heat transfer response during a bottom feedwater line break transient.

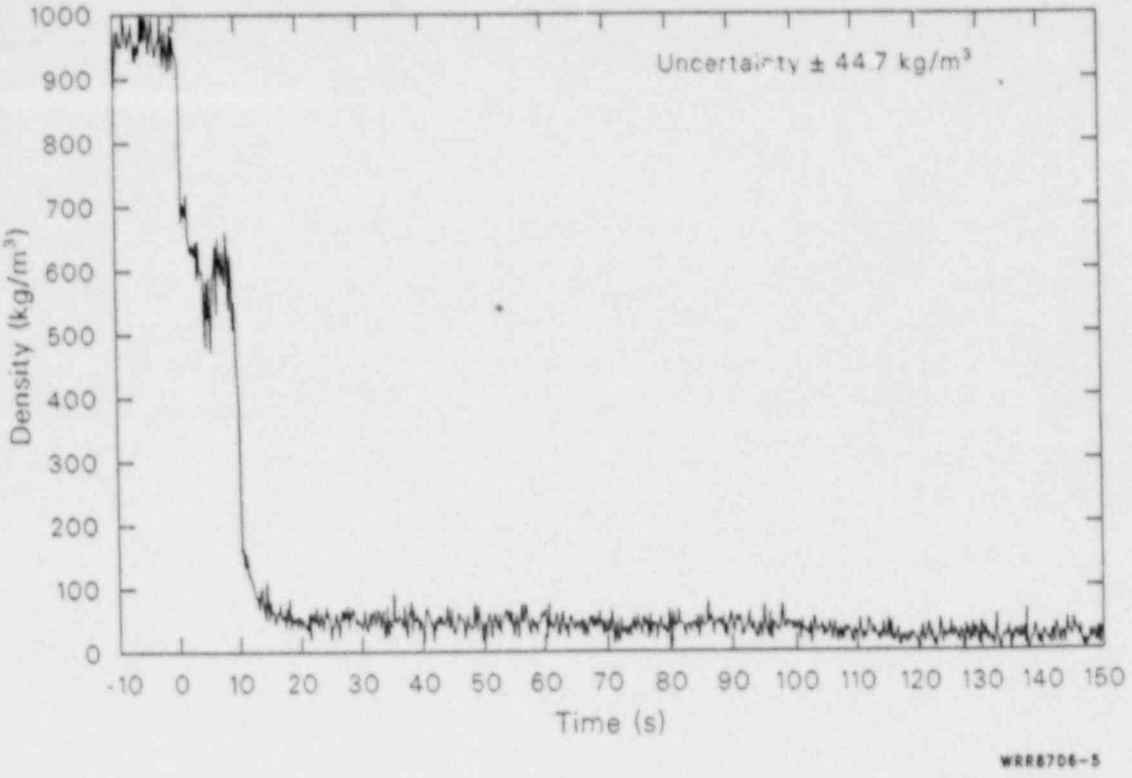

Figure 5. Break fluid density during the blowdown phase of 100% FWLB experiments S-FS-6/6B (-10 to 150 s).

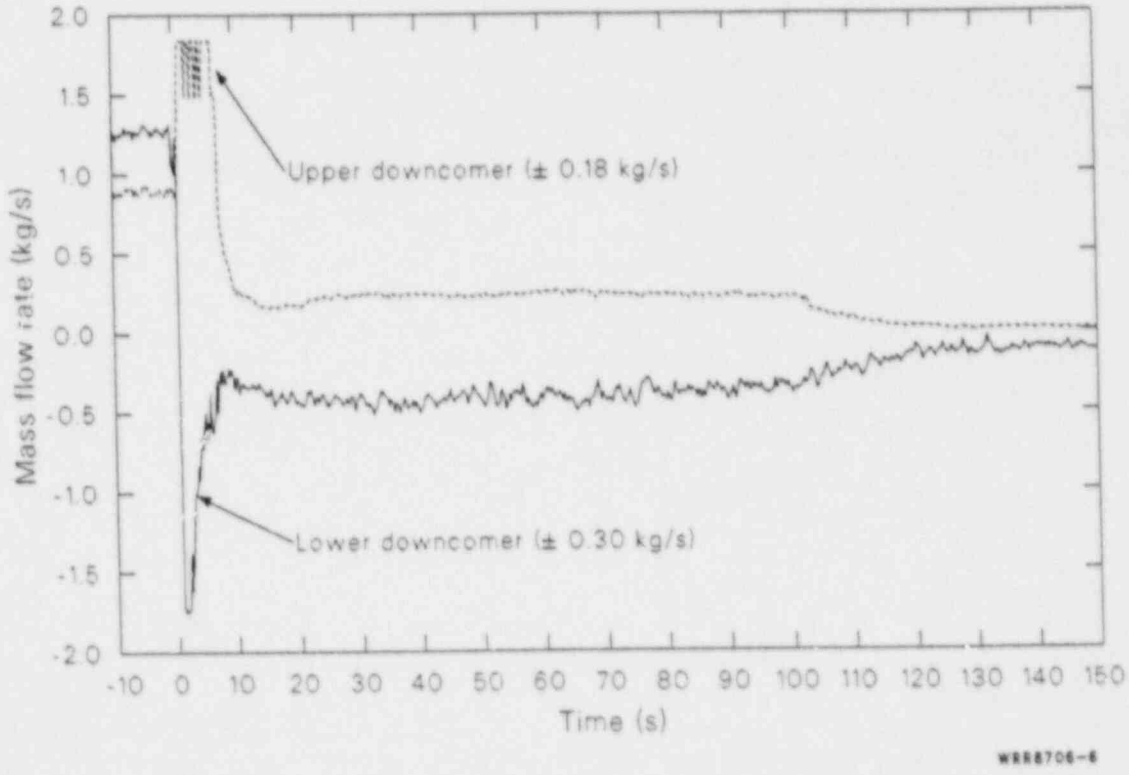

Figure 6. Affected loop steam generator upper and lower downcomer mass flow rates during the blowdown phase of 100% FWLB experiments S-FS-6/6B (-10 to 150 s).

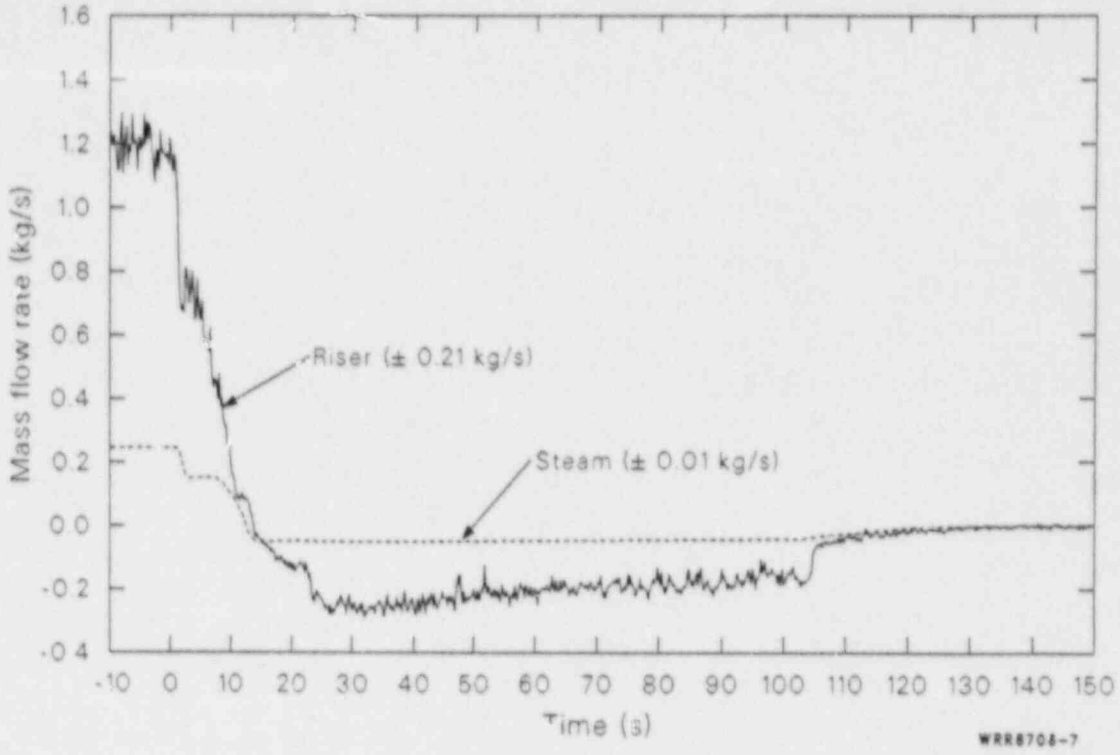

Figure 7. Affected loop steam generator riser and steam mass flow rates during the blowdown phase of 100% FWLB experiments S-FS-6/6B (-10 to 150 s).

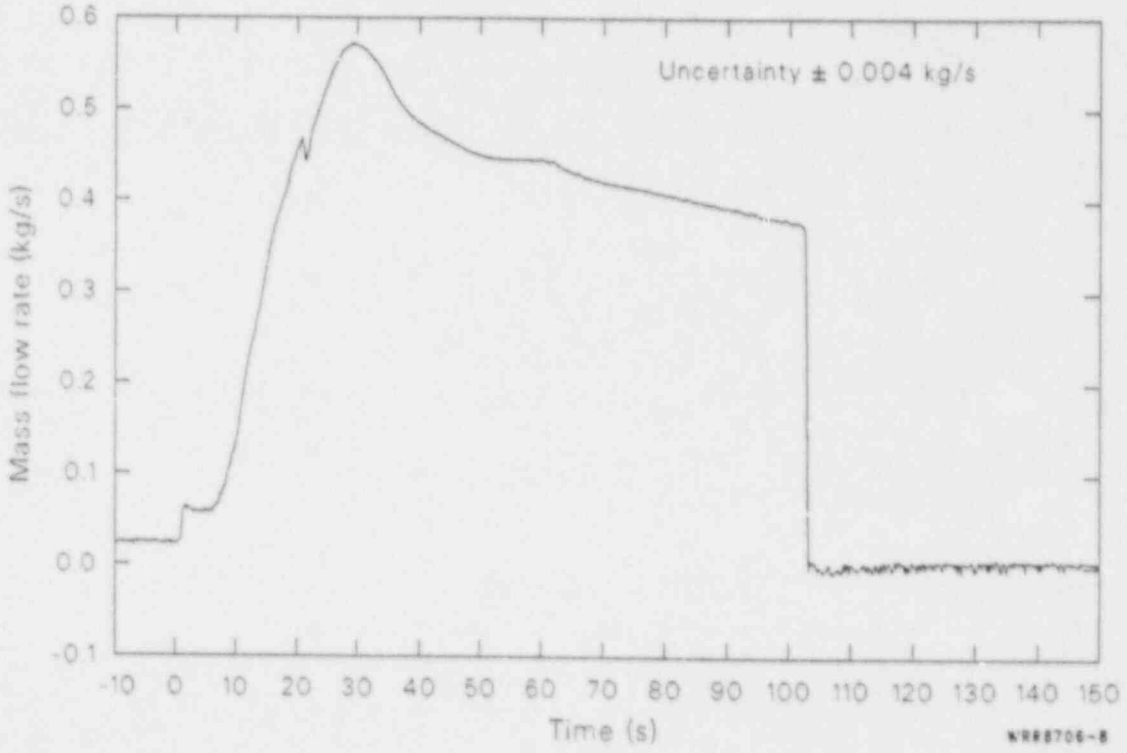

Figure 8. Unaffected to affected loop steam generator intersecondary mass flow rate through the crossover line during the blowdown phase of 100% FWLB experiments S-FS-6/6B (-10 to 150 s).

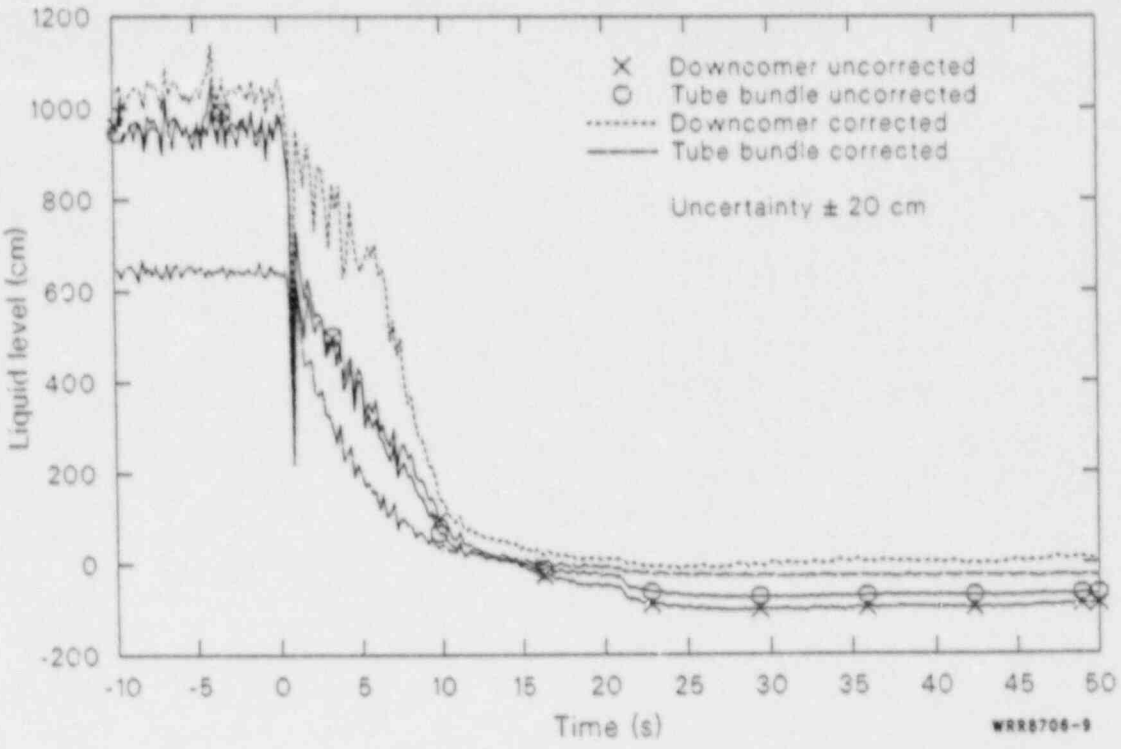

Figure 9. Affected loop steam generator overall downcomer and tube bundle uncorrected and frictional pressure drop corrected interfacial liquid levels during the blowdown phase of 100% FWLB experiments S-FS-6/6B (-10 to 50 s).

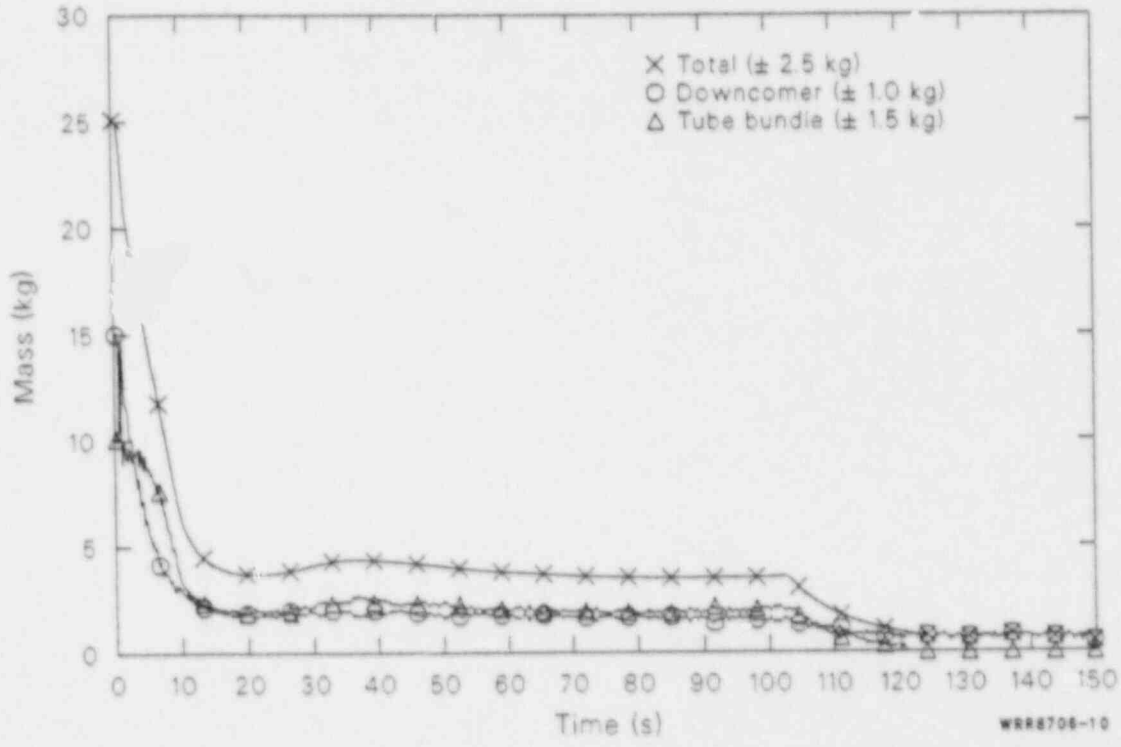

Figure 10. Affected loop steam generator total, downcomer and tube bundle secondary fluid mass inventories during the blowdown phase of 100% FWLB experiments S-FS-6/6B (0 to 150 s).

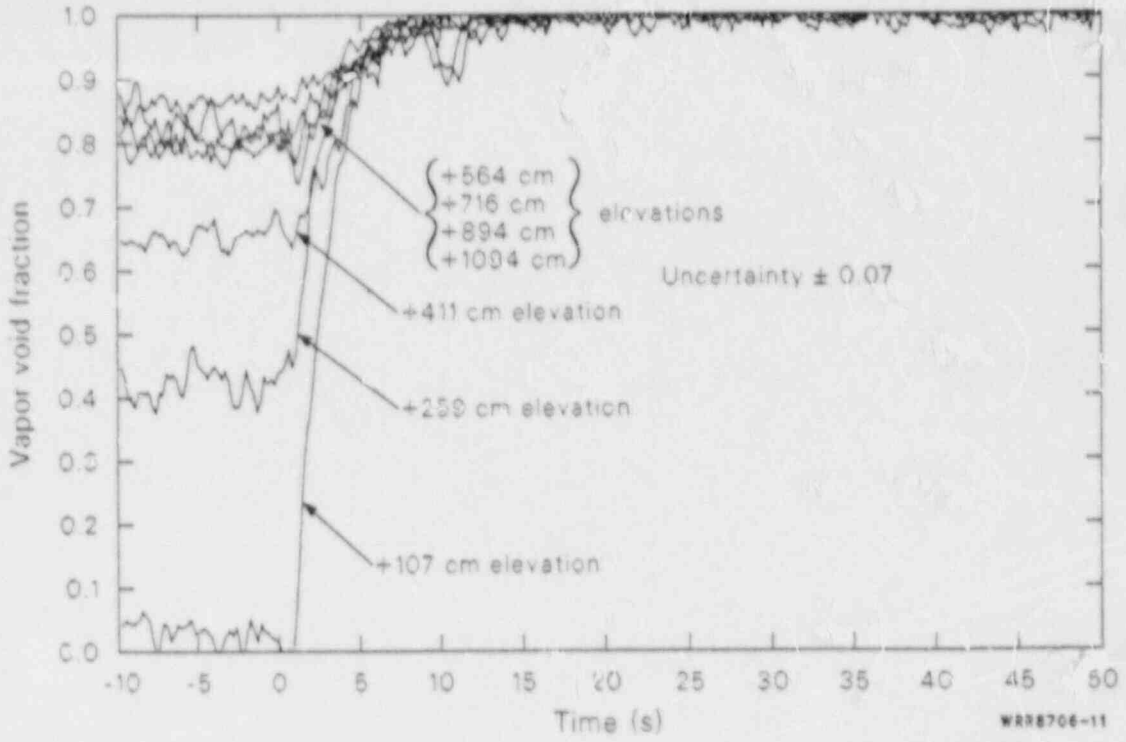

Figure 11. Affected loop steam generator tube bundle secondary fluid vapor-void fractions during the blowdown phase of 100% FWLB experiments S-FS-6/6B (-10 to 50 s).

The secondary fluid hydraulic response of the unaffected loop steam generator was effected by the mass balance for the secondary. The mass balance was effected by the feedwater and steam flows and the intersecondary flow. The loss of all feedwater at break initiation caused the initial mass imbalance for the unaffected loop steam generator secondary fluid system. Continued steaming at full-power conditions without feedwater addition initiated the loss of secondary inventory, as shown in Figure 12. The situation was aggravated further when the intersecondary flow (Figure 8) increased as the affected loop steam generator secondary fluid inventory was depleted. Following SCRAM, the closure of the normal steam flow control valves (turbine stop valve simulators) reduced the rate of inventory loss with the inventory at about 78% of the initial mass. However, the intersecondary flow continued to reduce the secondary inventory to a minimum value of about 45% of the initial mass at MSIV closure. Recovery of the secondary inventory was then initiated by auxiliary feedwater injection, as indicated by the liquid level response (Figure 13). At the end of the blowdown phase of the test, the secondary inventory had recovered to about 51% of the initial mass.

Secondary Thermal Response. Understanding and calculating the affected loop steam generator secondary fluid system thermal response to a bottom feedwater line break requires consideration of the tube-bundle region secondary fluid thermal-hydraulic response. The transient thermal response may be better understood after considering the thermal conditions that exist in the secondary fluid system at steady-state, full-power conditions. The steady-state secondary fluid thermal characteristics can be gleaned from the included figures for times before transient initiation (time = 0 s), or from the discussion in Appendix C. Briefly the secondary fluid thermal characteristics at steady-state, full-power conditions consist of: feedwater entering the lower downcomer and producing slightly subcooled liquid at the entrance to the tube bundle; combined forced convection nucleate boiling and forced convection vaporization heat transfer in the tube-bundle region; two-phase fluid mixture exiting the tube bundle; and vapor generated in the tube-bundle region exiting the steam generator as high quality steam. The energy addition from the primary fluid system, removal of the feedwater subcooling, boiling in the tube bundle, and high quality steam flow out of the secondary result in an energy balance for the secondary fluid system.

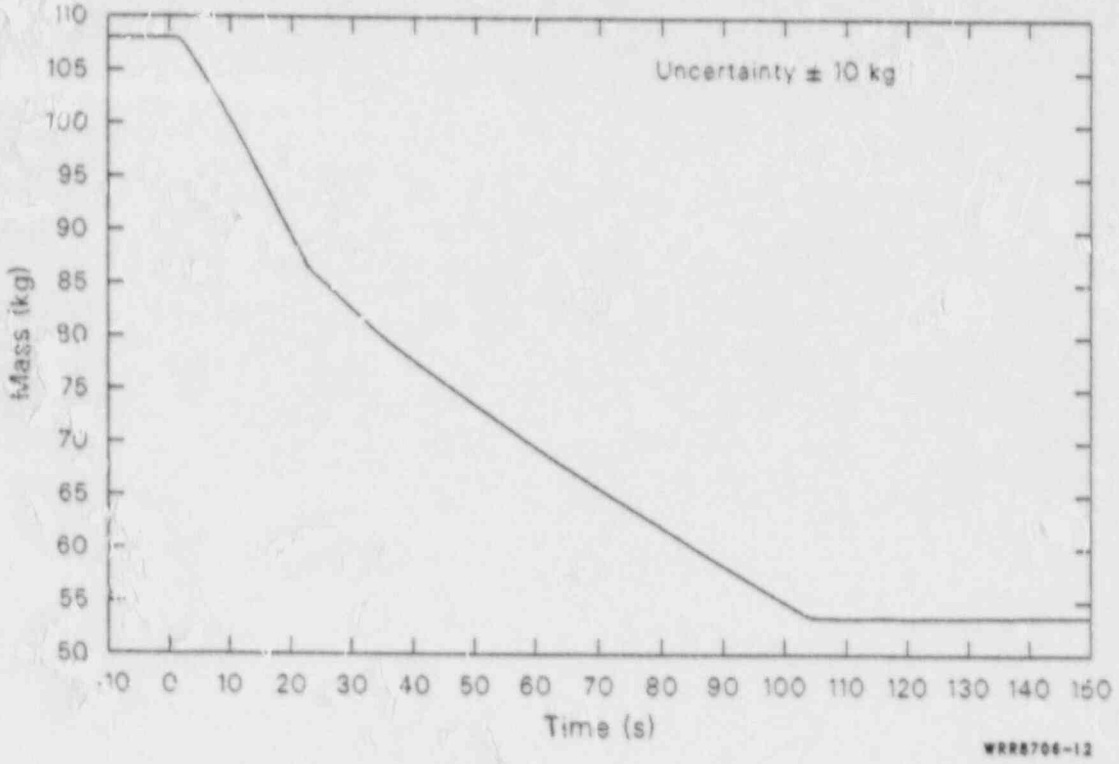

Figure 12. Unaffected loop steam generator secondary fluid mass inventory, during the blowdown phase of 100% FWLB experiments S-FS-6/6B (-10 to 150 s).

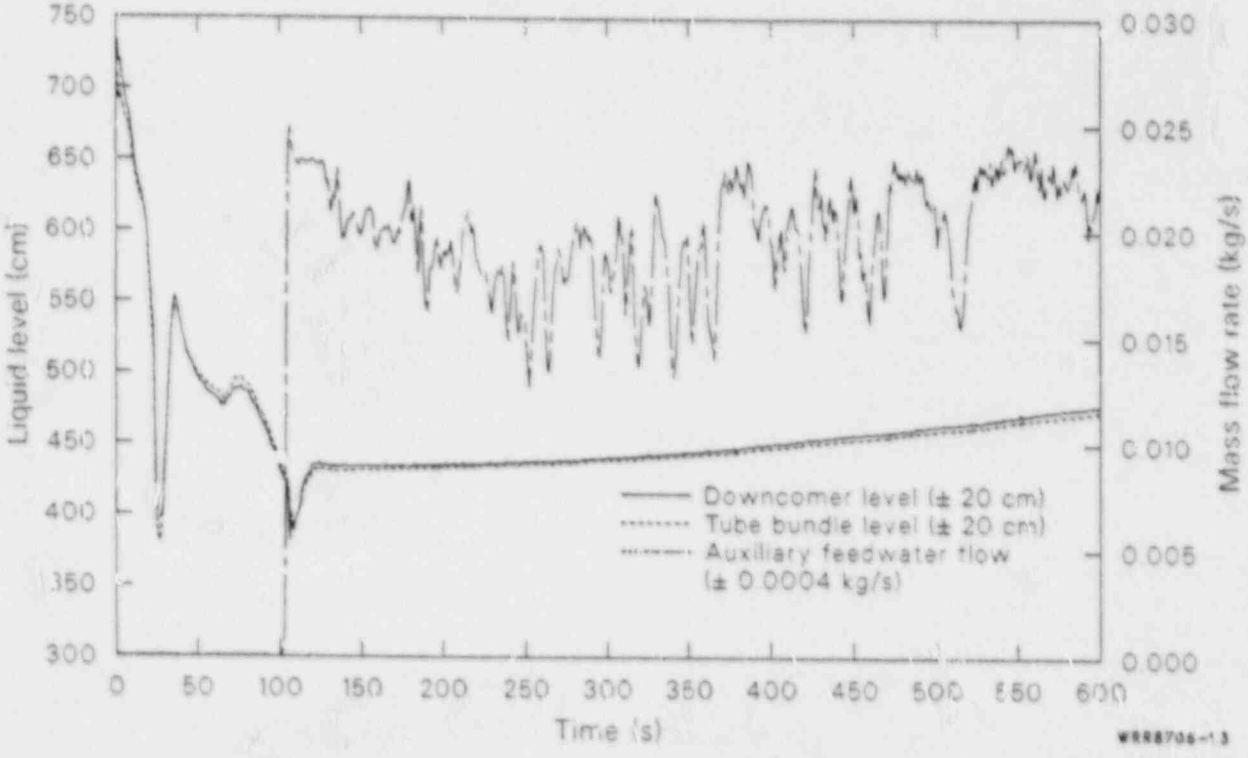

Figure 13. Unaffected loop steam generator overall downcomer and tube bundle collapsed liquid levels and auxiliary feedwater mass flow rate during the blowdown phase of 100% FWLB experiments S-FS-6/6B (-10 to 150 s).

Consideration of the steady-state local heat transfer parameters provides invaluable insight into understanding the transient primary-to-secondary heat transfer response. Briefly, the local heat transfer parameters were obtained from: the normalized primary fluid, U-tube outside wall and secondary fluid temperature measurements, (the normalized temperature triplet measurements); the primary fluid pressure measurements; the U-tube volumetric flow rate measurements; and iterating using the Colburn correlation to determine the U-tube inside wall primary fluid convective heat transfer coefficient and the U-tube inside wall metal temperature. The measurements and correlation were utilized in the solution of the energy equation to determine the local heat flux and the local secondary fluid convective heat transfer coefficient. The procedure is discussed in greater detail in Appendix C. The U-tube outside wall heat flux distribution (Figure 14) shows a large variation in the local heat flux versus length along the tube for both tubes. The majority of the primary energy removal (approximately 75%) occurs in the upflow side of the tubes, as evidenced by the integrated local heat flux versus length along the tube (Figure 15). This is due primarily to the larger primary fluid-to-secondary fluid temperature difference on the upflow side. The measured secondary fluid convective heat transfer coefficient distribution also shows a large variation with elevation above the top of the tube sheet and upflow to downflow side locations (Figures 16 and 17). Thus, the measured secondary convective heat transfer coefficient increases with increasing vapor-void fraction (Figures 16, 17 and C-5) and decreases with decreasing wall-to-fluid temperature difference (Figures 16, 17 and C-8 through C-11). This measured trend in the secondary convective heat transfer coefficient provides a major clue to the measured transient response.

Existing correlations for forced convection boiling heat transfer will not provide accurate calculations of transient heat transfer response. As shown in Appendix C, forced convection correlations, such as Jens-Lottes[20] and Thom[21] predict the correct trend of decreasing convective heat transfer coefficients with decreasing wall-to-fluid temperature difference, but do not include a void fraction dependency. Also, the predicted values are, for the most part, significantly smaller than the measured values. Forced convection vaporization heat transfer correlations such as Dengler and Addoms[22] and Bennett,[23] and combined nucleate boiling/vaporization heat transfer correlations, such as Chen[24] also predict the correct trend of decreasing convective heat transfer coefficients with decreasing wall-to-fluid temperature difference. However, the Chen correlation predicts the wrong trend for the heat transfer coefficient variation with void fraction (decreasing heat transfer coefficients with increasing void fraction). Here too, the predicted values for the Dengler and Addoms, Bennett and Chen correlations are, for the most part, significantly smaller than the measured. A slightly modified version of the Chen correlation is used in current thermal-hydraulic computer codes.[25,26] Reasonable calculations of the steady-state primary-to-secondary heat transfer can be obtained using this correlation because the steady-state heat transfer is controlled by the conduction through the U-tube wall. As long as the calculated secondary convective heat transfer coefficient is of large enough magnitude to remove the energy conducted through the wall, the steady-state heat transfer will be satisfactorily calculated. However, during a transient involving the loss of secondary inventory, the primary-to-secondary heat transfer is eventually limited by the convection heat transfer to the secondary fluid. Because existing correlations do not predict the proper void fraction dependency for the convective heat transfer coefficient, the calculated transient heat transfer response will not be accurate.

While the affected loop steam generator secondary fluid thermal characteristics are altered significantly during a bottom main feedwater line break secondary LOCA, the total primary-to-secondary heat transfer is not altered substantially until the tube bundle liquid inventory is depleted. As shown in Figure 18, the affected loop steam generator total primary-to-secondary heat transfer remained at the initial condition value until the secondary liquid inventory was depleted at about 13 s. The primary-to-secondary heat transfer then decreased rapidly. Plotting the normalized heat transfer versus normalized total and tube-bundle region liquid inventory versus the normalized tube-bundle region liquid inventory for the affected loop steam generator (Figure 19) shows that the normalized heat transfer remained at 100% until the normalized total and tube-bundle region liquid masses reached almost 0%. The heat transfer then decreased rapidly to 0%. This close relationship between the heat transfer and the liquid inventory is due to the strong dependency of the secondary convective heat transfer coefficient upon the vapor-void fraction. As shown in Figures 20 through 27, the local secondary convective heat transfer coefficients increase in

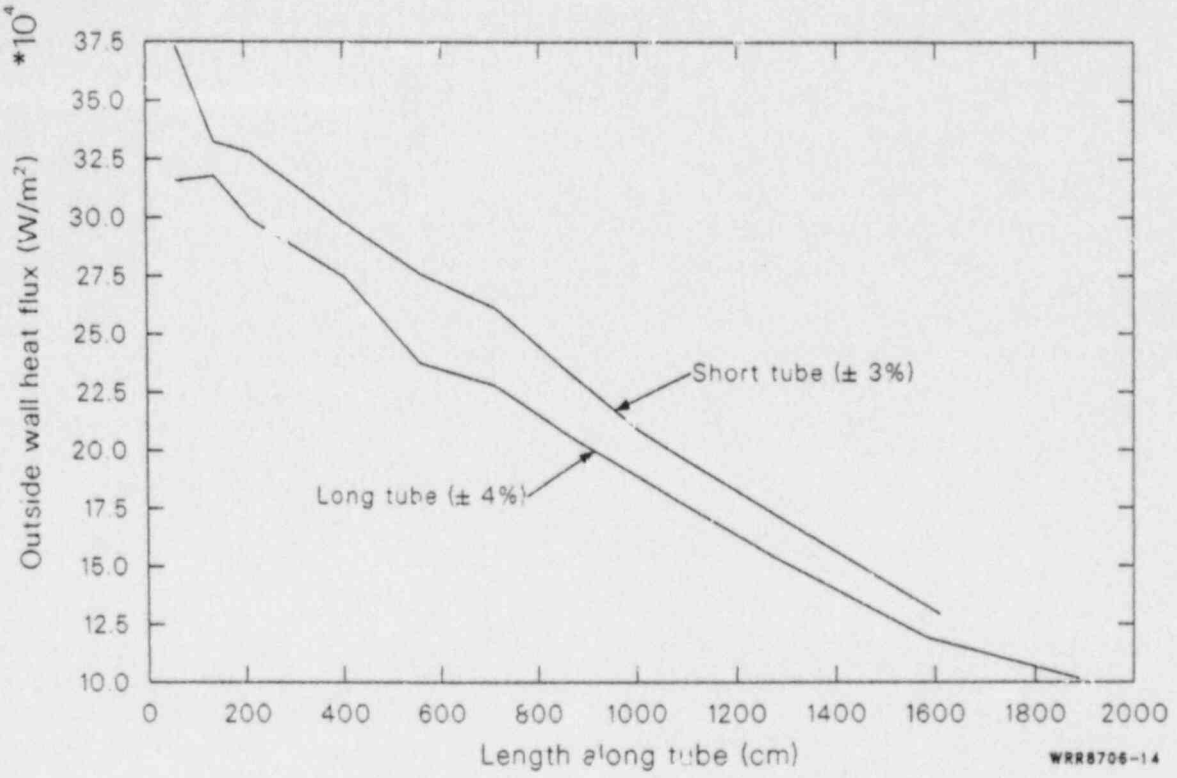

Figure 14. Affected loop steam generator average full-power, steady-state U-tube outside wall heat flux versus length along the tube (from inlet to outlet plenum) for the long and short tubes.

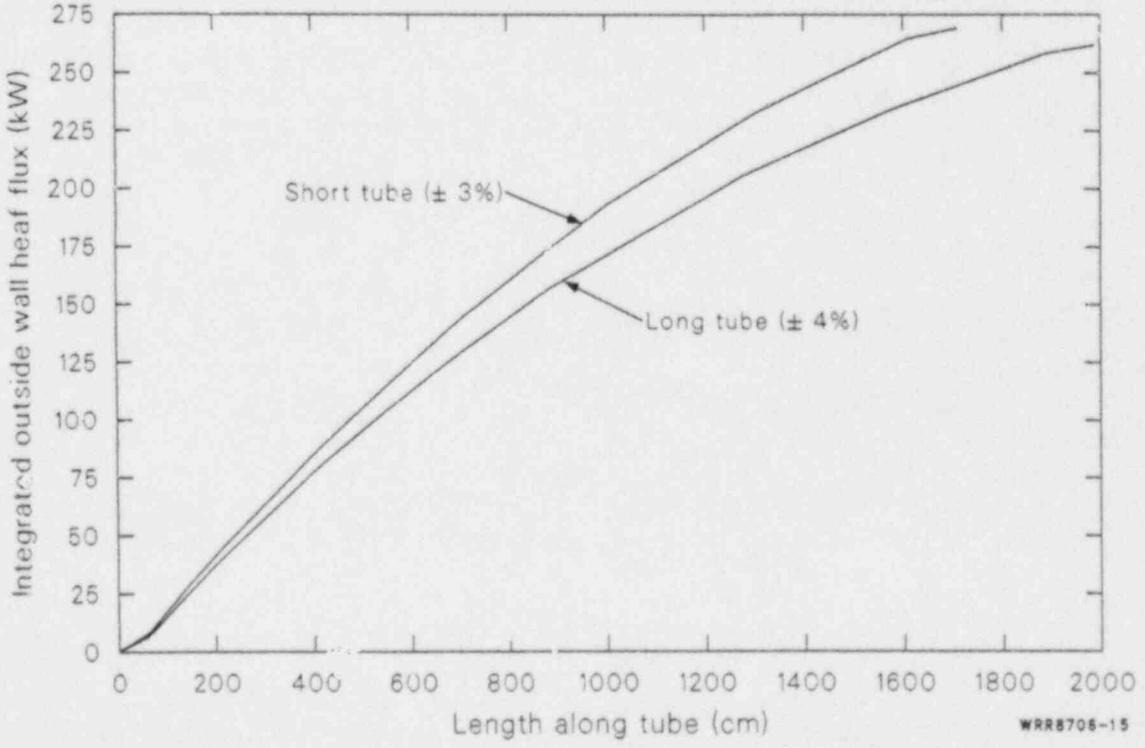

Figure 15. Affected loop steam generator average full-power, steady-state U-tube outside wall integrated heat flux versus length along the tube (inlet to outlet plenum) for the long and short tubes.

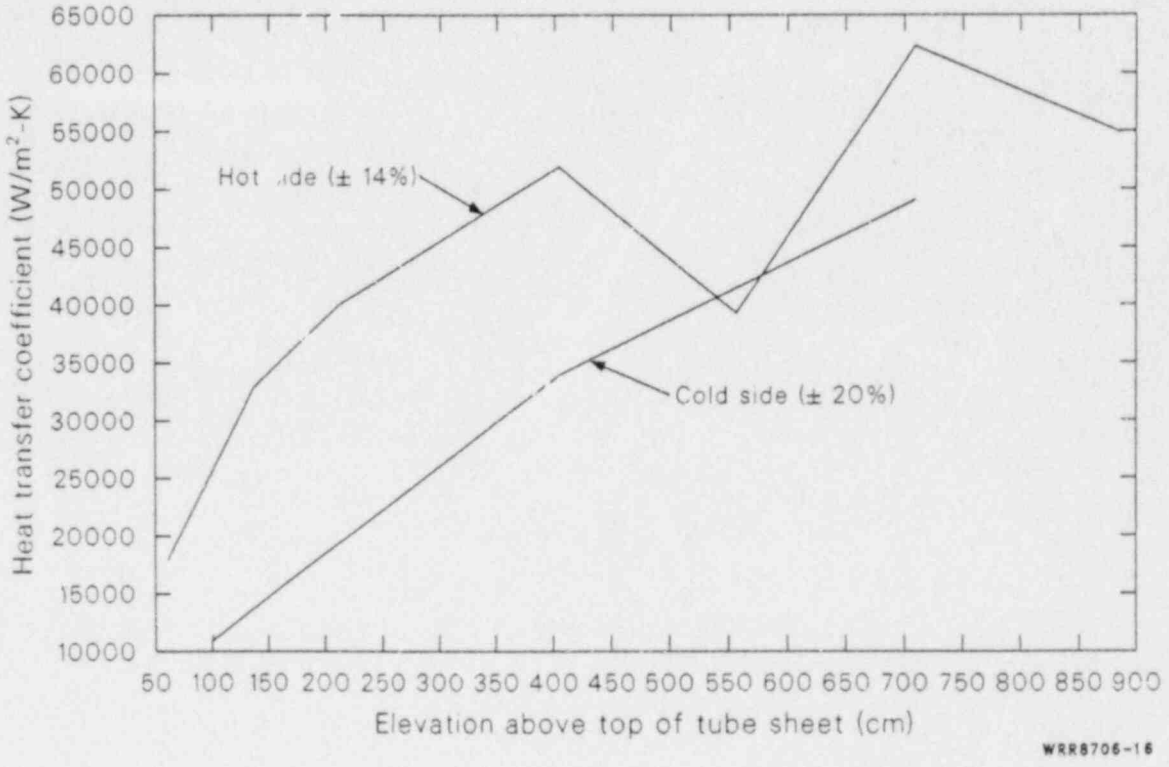

Figure 16. Affected loop steam generator average full-power, steady-state long tube hot and cold side secondary convective heat transfer coefficients versus elevation above the top of the tube sheet.

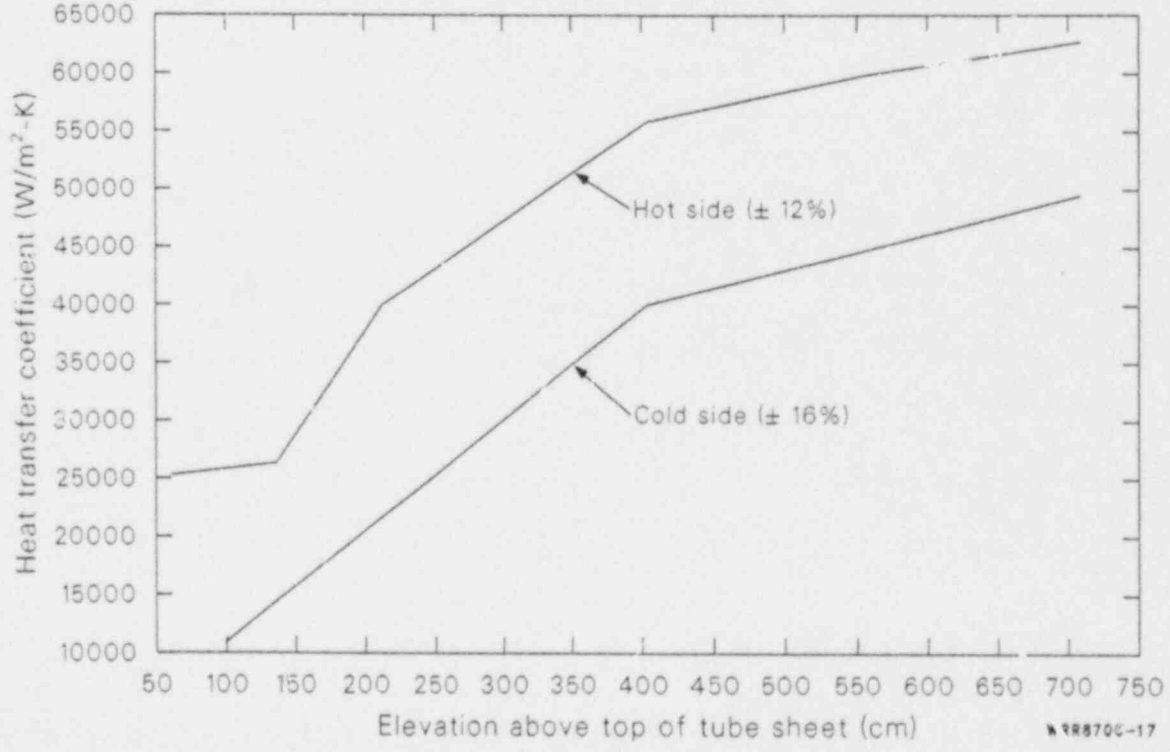

Figure 17. Affected loop steam generator average full-power, steady-state short tube hot and cold side secondary convective heat transfer coefficients versus elevation above the top of the tube sheet.

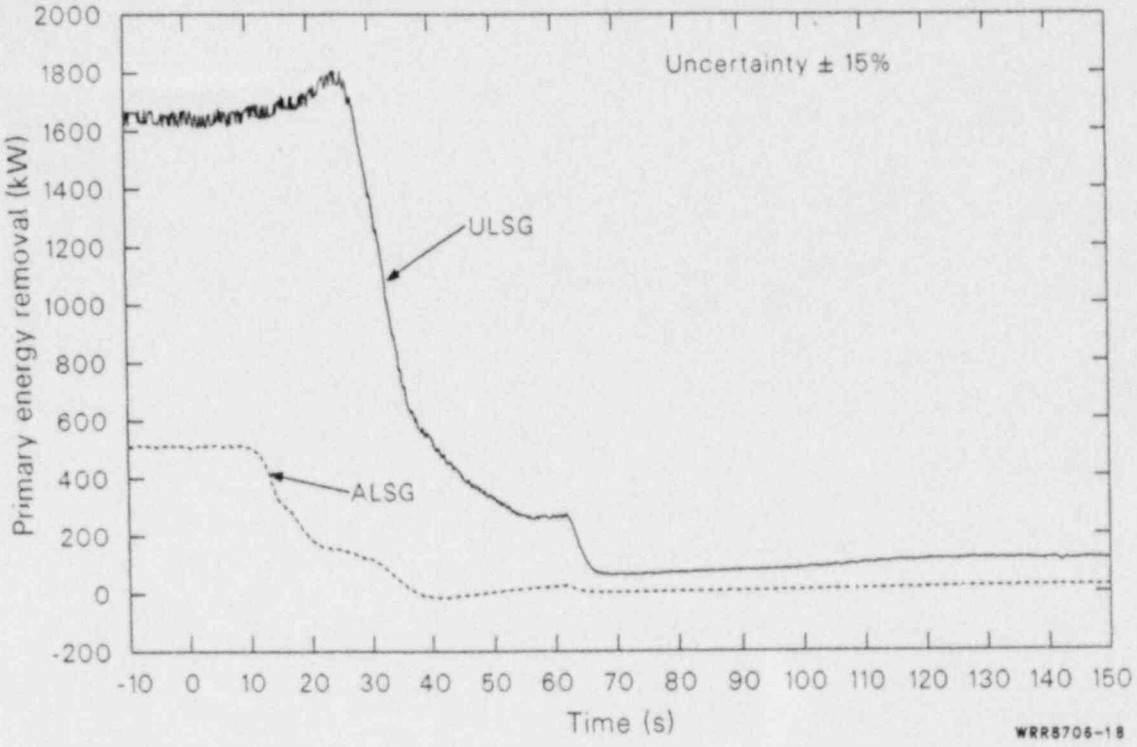

Figure 18. Affected and unaffected loop steam generator primary-to-secondary heat transfer during the blowdown phase of 100% FWLB experiments S-FS-6/6B (-10 to 150 s).

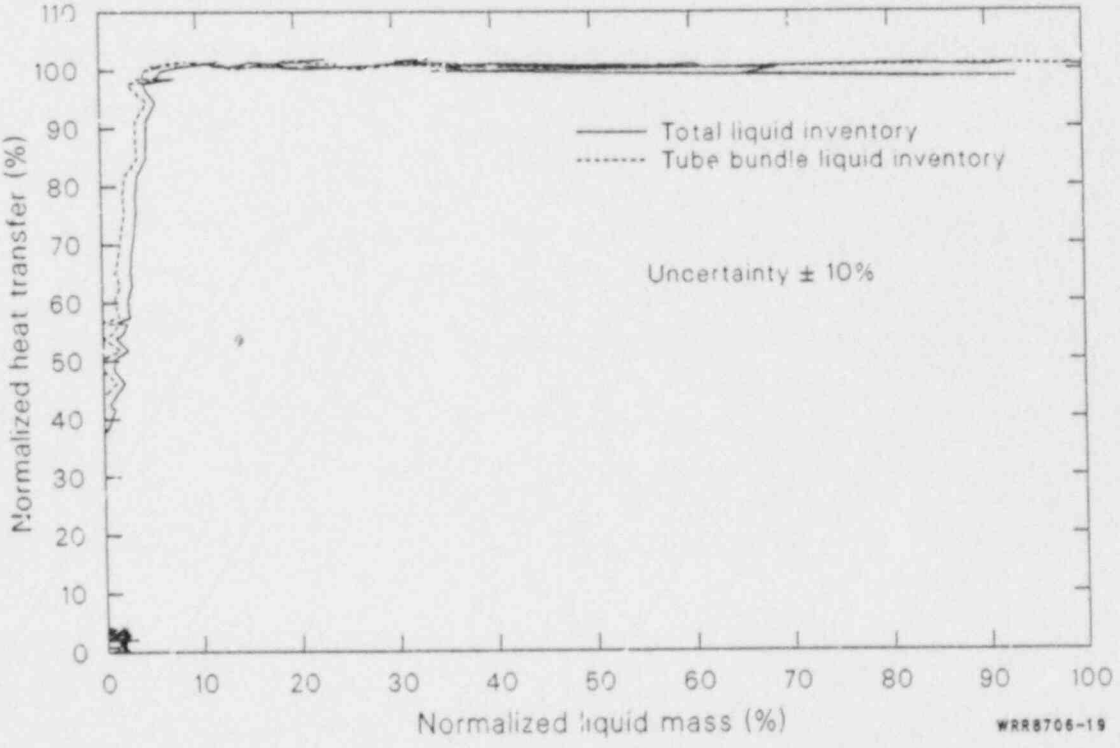

Figure 19. Affected loop steam generator normalized primary-to-secondary heat transfer versus normalized total liquid inventory and versus normalized tube-bundle region liquid inventory during 100% FWLB experiments S-FS-6/6B.

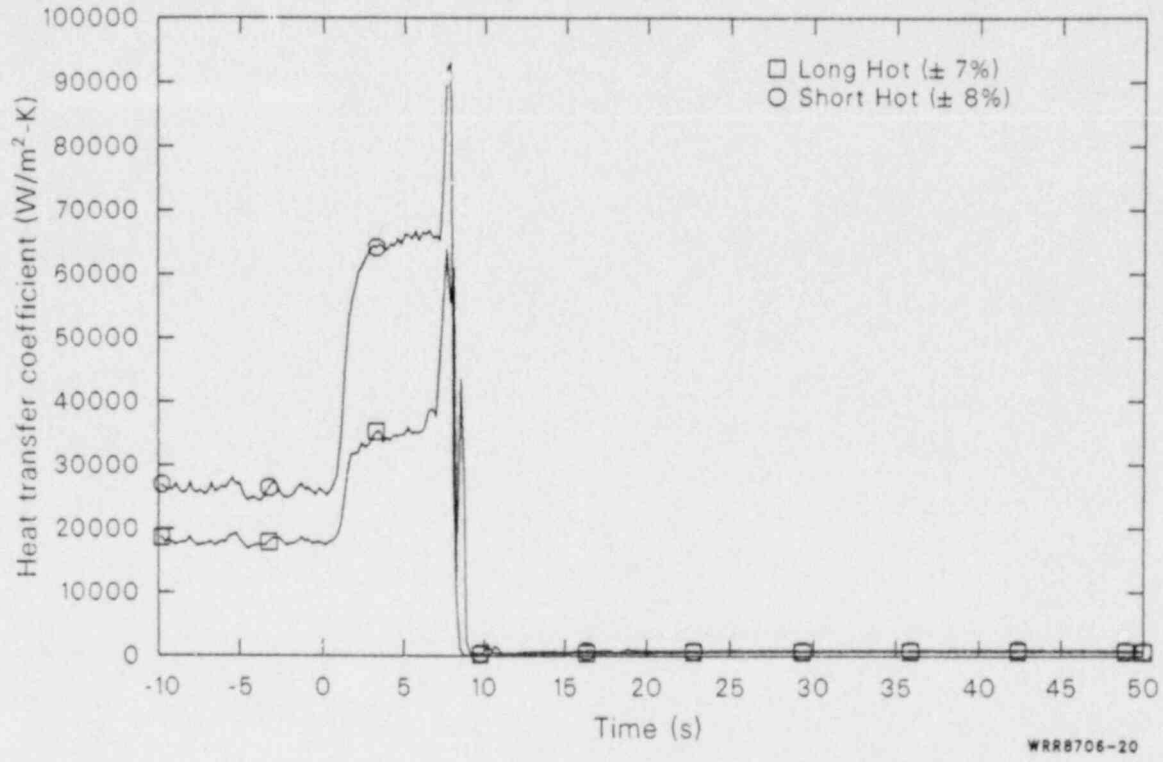

Figure 20. Affected loop steam generator secondary convective heat transfer coefficients at the 61 cm elevation during the blowdown phase of 100% FWLB experiments S-FS-6/6B (-10 to 50 s).

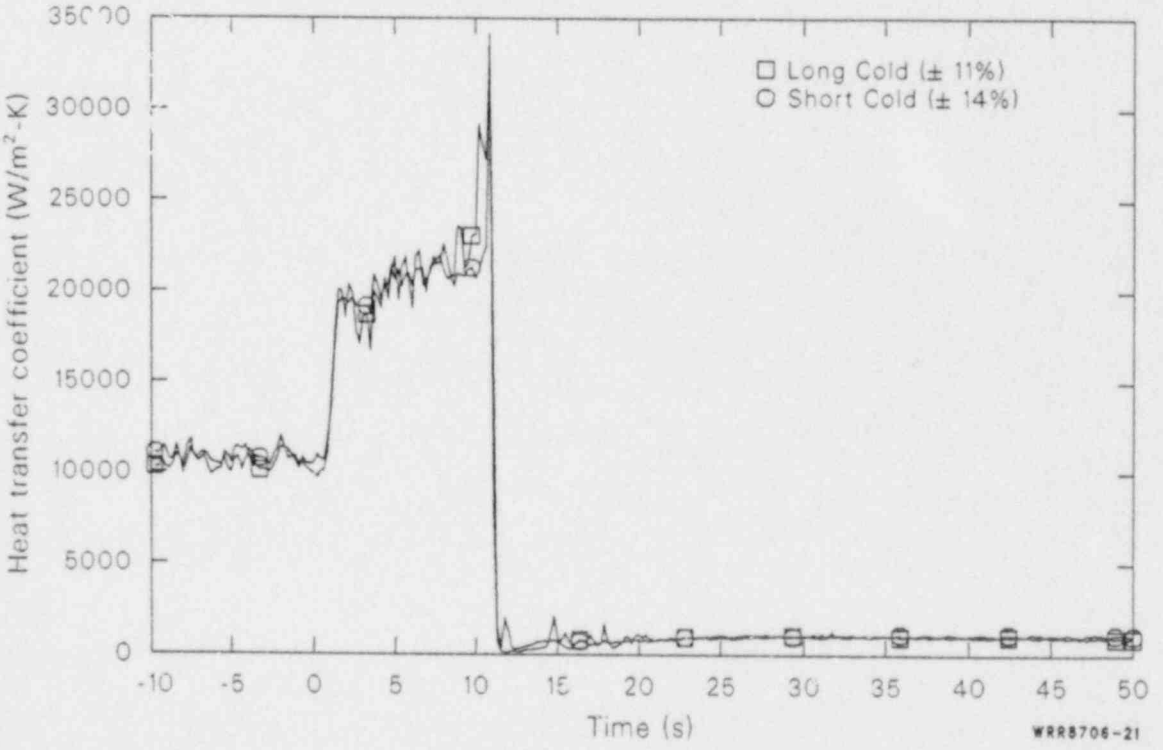

Figure 21. Affected loop steam generator secondary convective heat transfer coefficients at the 99 cm elevation during the blowdown phase of 100% FWLB experiments S-FS-6/6B (-10 to 50 s).

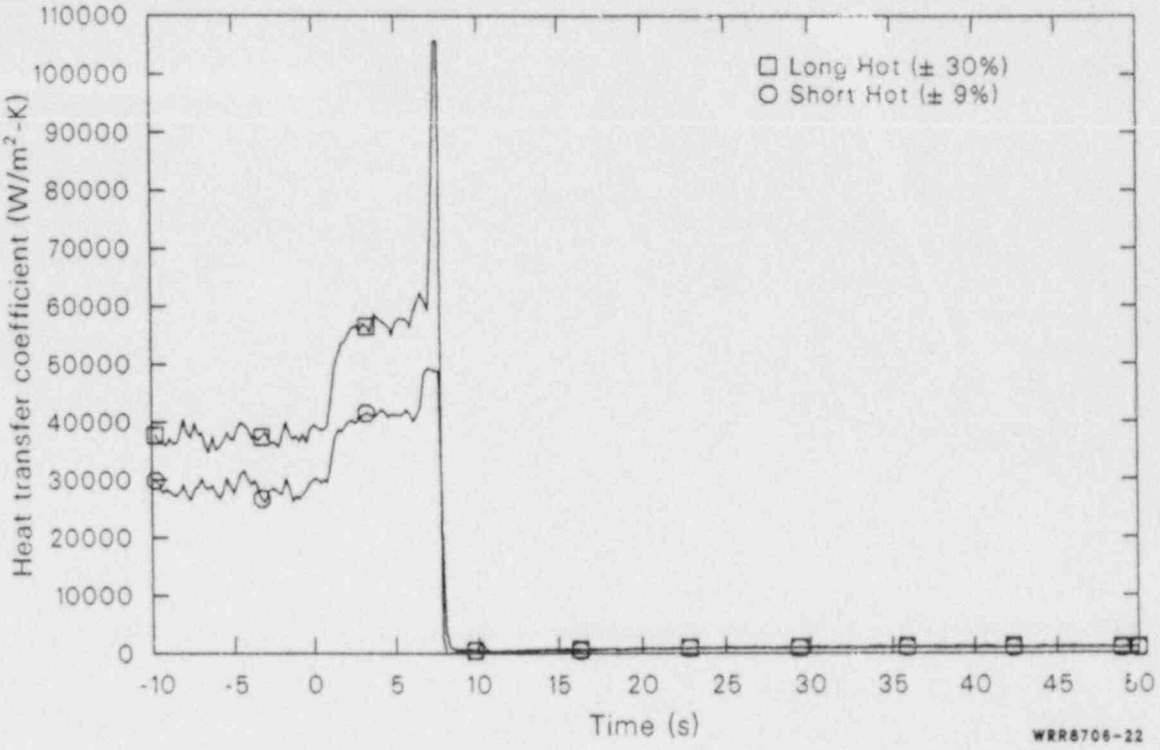

Figure 22. Affected loop steam generator secondary convective heat transfer coefficients at the 137 cm elevation during the blowdown phase of 100% FWLB experiments S-FS-6/6B (-10 to 50 s).

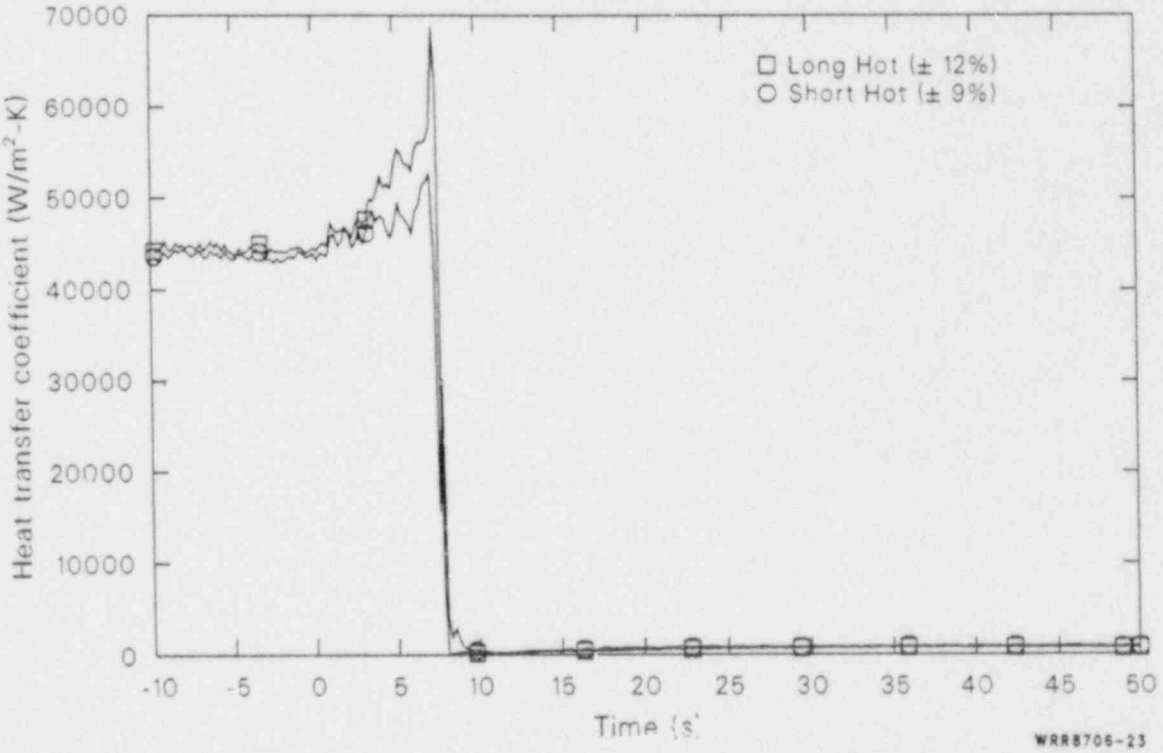

Figure 23. Affected loop steam generator secondary convective heat transfer coefficients at the 213 cm elevation during the blowdown phase of 100% FWLB experiments S-FS-6/6B (-10 to 50 s).

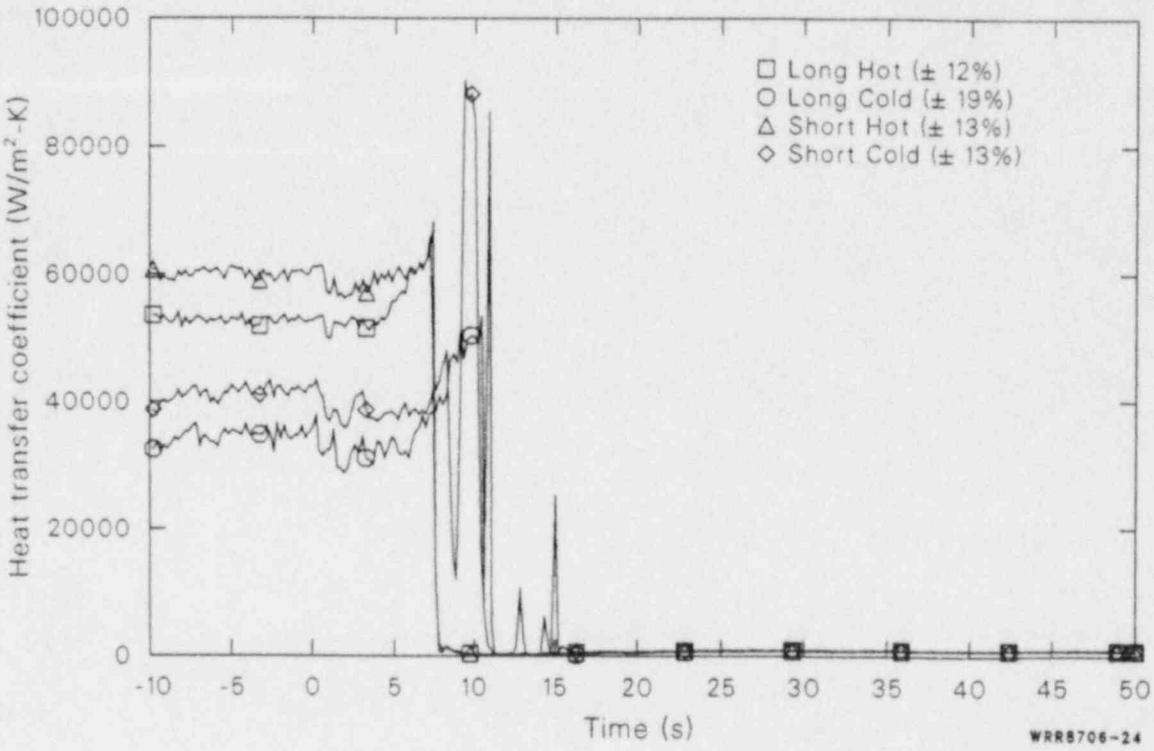

Figure 24. Affected loop steam generator secondary convective heat transfer coefficients at the 404 cm elevation during the blowdown phase of 100% FWLB experiments S-FS-6/6B (-10 to 50 s).

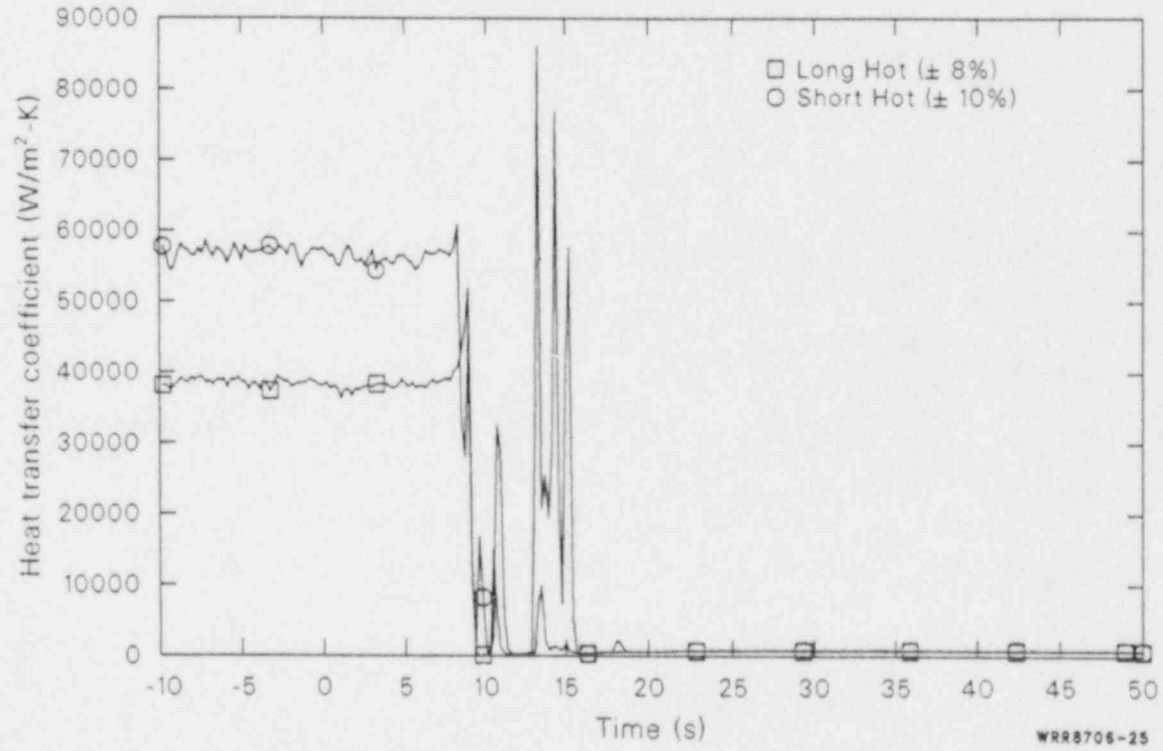

Figure 25. Affected loop steam generator secondary convective heat transfer coefficients at the 556 cm elevation during the blowdown phase of 100% FWLB experiments S-FS-6/6B (-10 to 50 s).

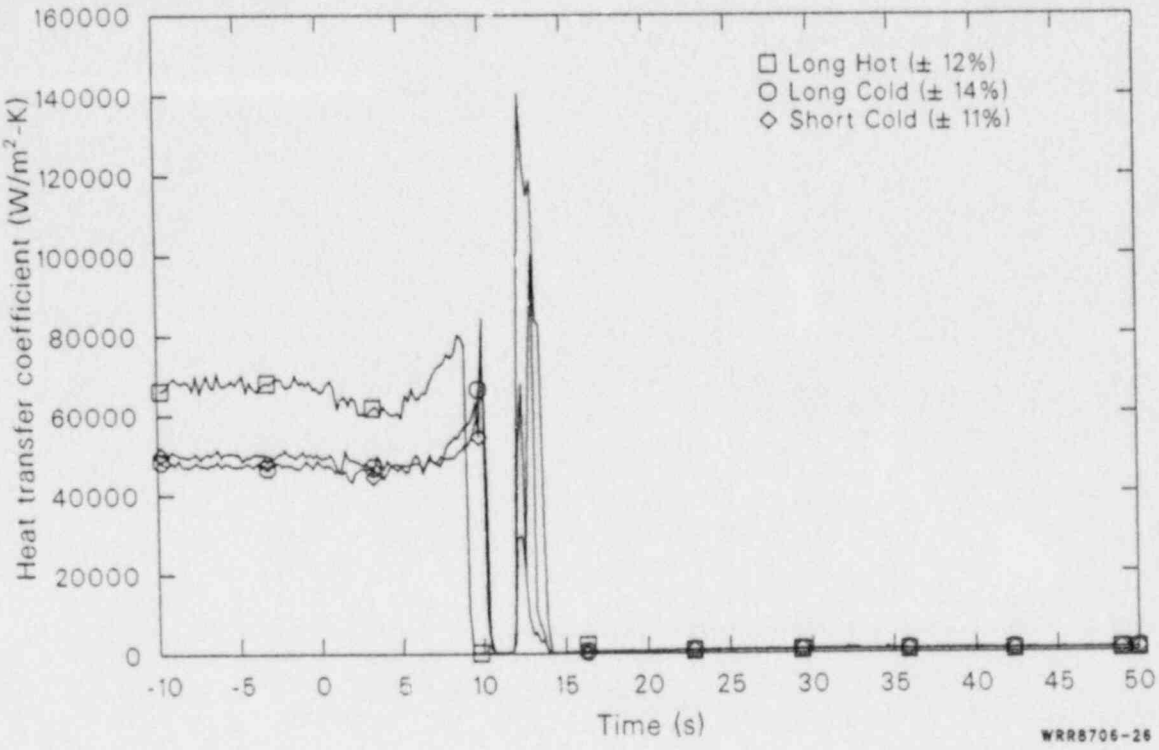

Figure 26. Affected loop steam generator secondary convective heat transfer coefficients at the 709 cm elevation during the blowdown phase of 100% FWLB experiments S-FS-6/6B (-10 to 50 s).

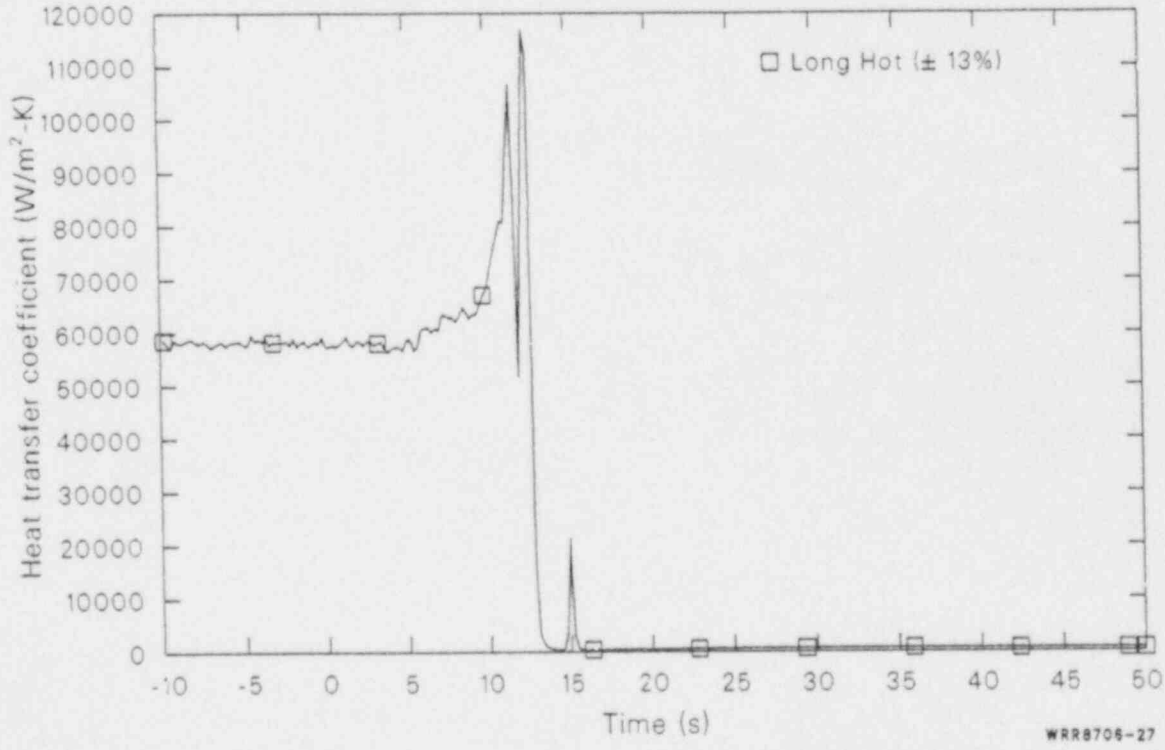

Figure 27. Affected loop steam generator secondary convective heat transfer coefficient at the 886 cm elevation during the blowdown phase of 100% FWLB experiments S-FS-6/6B (-10 to 50 s).

a manner directly proportional to the local vapor-void fractions (Figure 11). This continues until a liquid-deficient condition exists (the local vapor-void fractions reach a value of 1.0), causing the local heat transfer coefficient to rapidly decrease to zero. Thus, the total primary-to-secondary heat transfer remains high until the tube-bundle region is devoid of liquid. The heat transfer then degrades rapidly to zero due to the liquid-deficient conditions. This indicates that the assumption made for the C-E System 80 FSAR Appendix 15B calculations regarding the reduction of heat transfer with liquid inventory (i.e., 100% heat transfer until the liquid inventory is depleted followed by a step change reduction in the heat transfer to 0%) is not conservative, but closely emulates the measured secondary convective heat transfer response to the loss of liquid inventory.

The secondary fluid thermal response of the unaffected loop steam generator was affected by the energy balance for the secondary. The energy balance was affected by the feedwater and steam flows, intersecondary flow, primary loop flow reductions, and auxiliary feedwater injection. The loss of energy removal capacity associated with the loss of all feedwater at break initiation was initially offset by the increased normal steam flow (Figure 28). This allowed the total primary-to-secondary heat transfer (Figure 18) to remain at the initial condition value. The continued normal steam flow before SCRAM, combined with the increased intersecondary flow, increased the unaffected loop steam generator total primary-to-secondary heat transfer before SCRAM. Following SCRAM, the loss of offsite power induced the primary coolant pump trips and associated loop flow reductions. The decreased unaffected loop flow caused a decrease in the unaffected loop steam generator total primary-to-secondary heat transfer as the loop transitioned to the natural circulation mode of heat transfer. The natural circulation heat transfer was enhanced by the removal of energy from the secondary via the intersecondary flow before MSIV closure. Following MSIV closure and SI signal generation, the secondary energy removal was provided by the injection of auxiliary feedwater into the unaffected loop steam generator secondary starting at about 104 s. The auxiliary feedwater provided secondary energy removal for the remainder of the test.

The increased unaffected loop steam generator total primary-to-secondary heat transfer produced by the intersecondary flow caused the overall primary energy removal deficit (Figure 29) to be less than the amount associated with the loss of the affected loop steam generator heat sink (nominally 500 kW). Thus, the failure of the affected steam generator main steam line check valve resulted in increased unaffected loop steam generator primary-to-secondary and limited the net primary energy addition to only about one-half of that associated with loss of the affected loop steam generator heat sink. This reduced the rate of the primary fluid expansion and lessened the amount of primary fluid system pressurization, as will be discussed next.

Primary Response to a Steam Generator Bottom Main Feedwater Line Break

Understanding the primary fluid system thermal-hydraulic response during a bottom main feedwater line break secondary LOCA is important, because the degree of pressurization of the primary fluid system depends upon the thermal-hydraulic response to the loss of the heat sink. The primary pressure response is determined by the primary energy balance and the pressurizer surge line hydraulic resistance. There are several characteristic inflection points in the primary fluid system thermal-hydraulic response to a bottom feedwater line break secondary LOCA. The causes of these inflection points are discussed in this section. The general sequence of events affecting the primary response are outlined first. This is followed by discussions of the pressure response, hydraulic response, and thermal response for the primary fluid system. Because all of the bottom main feedwater line break experiments had similar basic primary thermal-hydraulic responses, this discussion refers to S-FS-6/S-FS-6B data only. As with the secondary response discussion, break size effects will be discussed later.

General Primary Response. The occurrence of a break in a steam generator bottom main feedwater line downstream of the check valve produces severe effects on the primary fluid system. The bottom main feedwater line break initiated the transient at 0 s. The primary fluid system exhibits a rapid pressurization in response to the net loss of primary-to-secondary heat transfer during the secondary LOCA. The primary fluid rapidly heats up as the affected loop steam generator primary-to-secondary heat transfer reduces. This causes the primary fluid to expand and rapidly pressurizes the

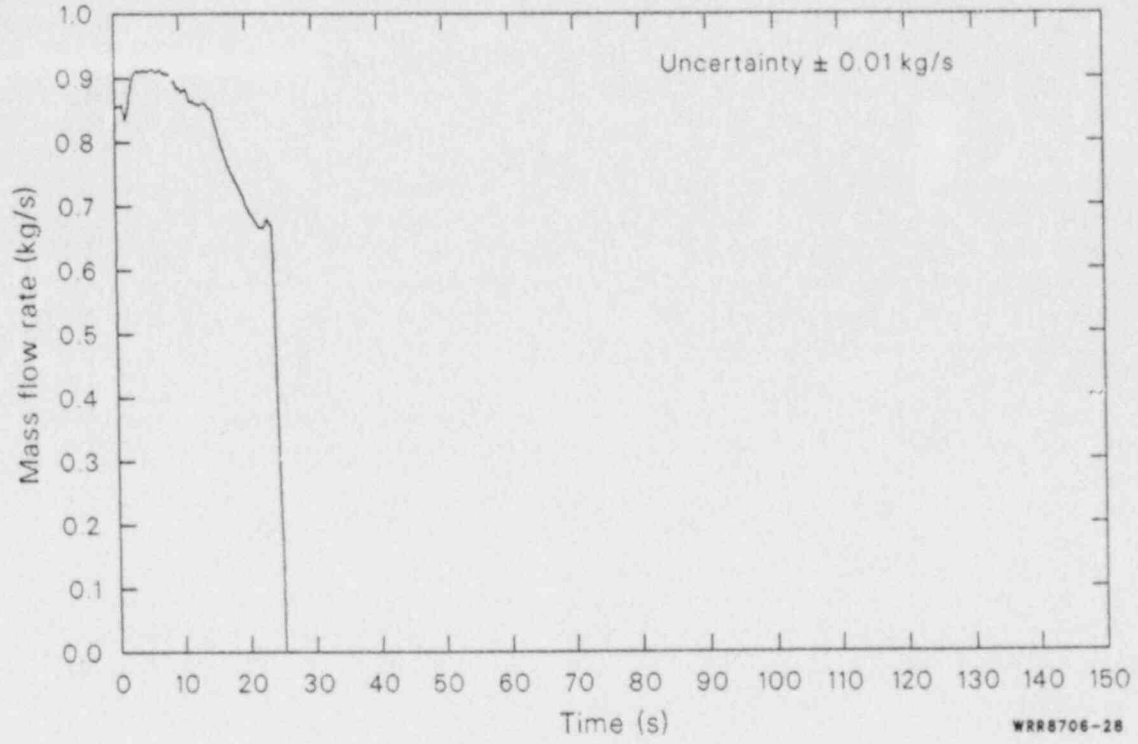

Figure 28. Unaffected loop steam generator steam mass flow rate during the blowdown phase of 100% FWLB experiments S-FS-6/6B (-10 to 150 s).

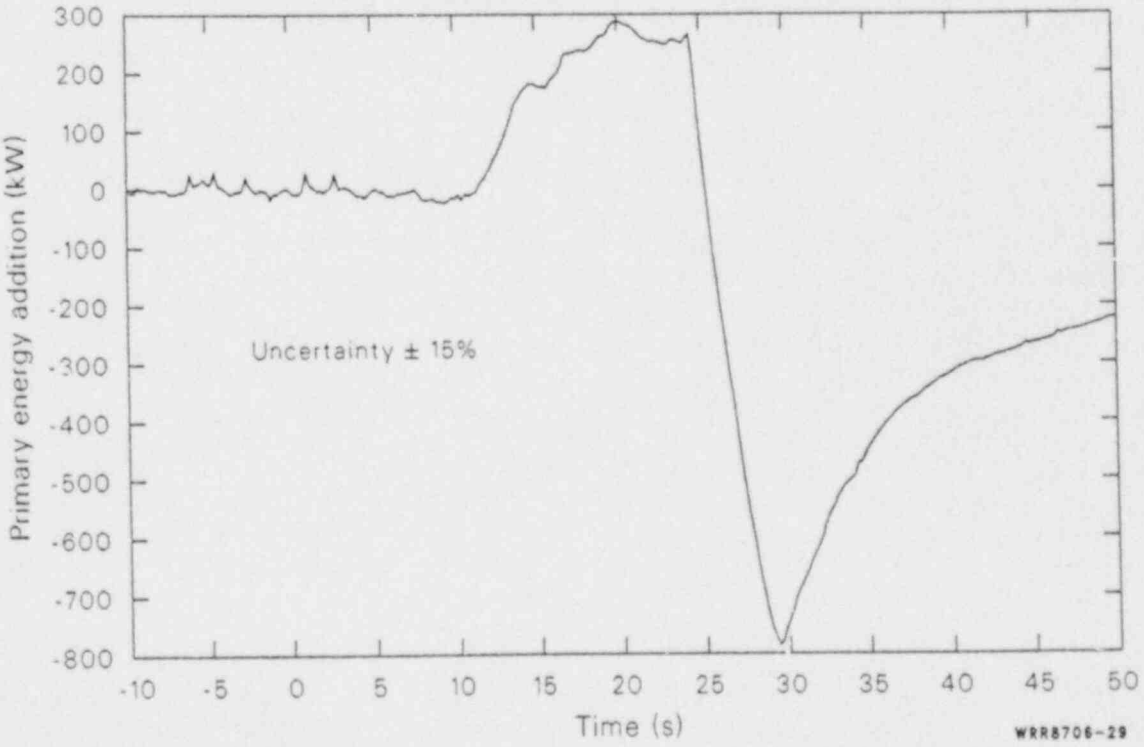

Figure 29. Primary fluid system energy addition during the blowdown phase of 100% FWLB experiments S-FS-6/6B (-10 to 50 s).

primary. The pressurization of the primary continues until about 4 s after the high pressurizer pressure SCRAM set point is reached with the peak pressure occurring in the loop cold legs. Following SCRAM, the rapid reduction in core power combined with the slower closure time for the normal steam flow control valves (turbine stop valve simulators) produced a rapid cooldown and depressurization of the primary fluid system. The period of rapid cooling is followed by a period of slower cooling and depressurization due to core power decay and intersecondary flow. Loop flow reductions (following loss of offsite power) degrade the unaffected loop steam generator energy removal resulting in a short period of primary fluid heating and pressurization until natural circulation flow was established in the unaffected loop. Gradual cooling and depressurization of the primary fluid was then provided by the continued intersecondary flow. Following the low affected loop steam generator secondary pressure SI signal, MSIV closure and auxiliary feedwater injection resulted in an unaffected loop steam generator energy removal rate that was close to the core decay heat level. This resulted in a very slow cooldown and depressurization of the primary fluid system. The primary fluid system pressure remained above the HPIS shutoff head so that HPIS injection did not occur. Also, no voiding of the primary fluid system was observed during the blowdown phase of the transient.

Primary Pressure Response. The primary pressure response is characterized by a number of inflection points associated with changes in the energy balance. As shown in Figure 30, the bottom main feedwater line break secondary LOCA initially produced no effect on the primary fluid system pressure. The primary energy balance was maintained until the affected loop steam generator primary-to-secondary heat transfer started to degrade at about 13 s. The resulting loss of a portion of the primary fluid system heat sink created an energy imbalance, which resulted in rapid pressurization of the primary fluid system. The pressurization of the primary fluid system continued until about 3 to 4 s after SCRAM (until about 1 s after the core power decay was initiated). The peak pressurizer pressure was 16.2 MPa, which was equal to the specified pressurizer code safety relief valve (SRV) simulator opening set point. However, the SRV did not open because the actual set point was slightly higher but within the specified tolerance of the specified set point. The peak primary pressure of 16.37 MPa occurred at about 27 s in the loop cold legs (Figure 30). This represents a difference of about 0.51 MPa between the high pressurizer pressure trip set point (15.86 MPa) and the peak system pressure. This pressure difference would have been even greater had the unaffected loop steam generator primary-to-secondary heat transfer not increased due to the substantial intersecondary flow, as discussed in the secondary response section. The increased unaffected loop steam generator primary energy removal reduced the net primary energy balance deficit associated with losing the affected loop steam generator primary energy removal. The net result was that the primary energy addition was only about one-half of that associated with the loss of the affected loop steam generator heat sink. This reduced the rate of primary fluid heating and expansion and lessened the amount of primary pressurization. The core power decay, moderated slightly by the normal steam flow control valve (turbine stop valve simulators) closures, initiated a rapid cooldown and depressurization of the primary fluid system at about 4 s after SCRAM. This rapid depressurization continued until loop flow reductions occurred in response to the loss of offsite power at SCRAM. The loop flow reductions initiated a reduction in the unaffected loop steam generator primary-to-secondary heat transfer, which reduced the rate of primary cooling during the initial core power decay. This continued until the pump coastdowns were completed at about 66 s. The unaffected loop steam generator primary energy removal rate was then reduced as natural circulation flow was being established. This produced a period of slight heating of the primary fluid system, which continued until the natural circulation flow was finally established at about 80 s. During this period, the primary pressure increased slightly in response to the slight heating. Following the establishment of natural circulation flow, the primary energy removal via the unaffected loop steam generator recovered to the level of the core power, aided by the continued intersecondary flow. This resulted in a period of gradual primary fluid cooling and depressurization, which was moderated following MSIV closure at about 109 s (due to the low affected loop steam generator secondary pressure) by terminating the intersecondary flow. The primary fluid system then entered a stage of very gradual cooling and depressurization under the influence of the unaffected loop steam generator auxiliary feedwater injection energy removal, and the slight system leakage.

Primary Hydraulic Response. The hydraulic response of the primary fluid system during a bottom feedwater line break secondary LOCA is characterized by a rapid expansion of liquid into the pressurizer. As the affected loop heat sink rapidly degrades, the primary liquid heats up and expands into the pressurizer,

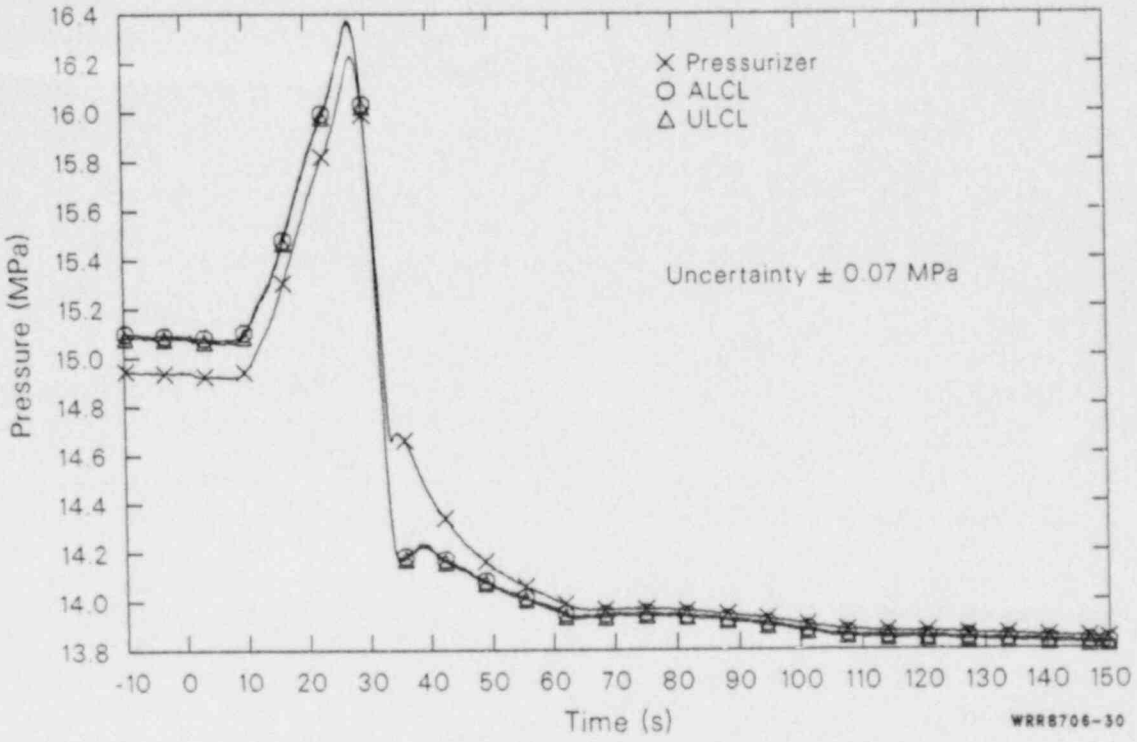

Figure 30. Pressurizer and affected and unaffected loop cold leg pressures during the blowdown phase of 100% FWLB experiments S-FS-6/6B (-10 to 150 s).

as shown in Figure 31. The rate of the expansion was determined by the initial primary pressure and temperature, the initial pressurizer vapor volume, the energy balance, and the pressurizer surge line hydraulic resistance. The initial primary pressure and temperature determine the initial energy content of the primary fluid system. The amount of the primary liquid expansion (increase in the liquid specific volume) was determined by the integrated energy addition to the primary fluid and the initial energy content of the primary liquid. The rate of the primary liquid expansion was determined primarily by the rate of the energy addition (the impetus for the expansion), and the resistance to flow through the pressurizer surge line and work required to compress the vapor volume in the pressurizer (the resistances to the expansion). It was also determined to some extent by the initial energy content of the primary fluid system, as will be discussed in the next section. The basic mechanism involves the primary liquid energy content increasing due to the net energy addition. The increased energy content produces an increased liquid specific volume and liquid pressure, which causes a pressure gradient between the primary loop hot leg and the pressurizer. The primary liquid then flows into the pressurizer, at a rate determined by the pressure difference, liquid specific volume, and surge line hydraulic resistance. As the liquid flows into the pressurizer, the increasing liquid volume compresses the vapor volume, decreasing the vapor specific volume, and pressurizing the pressurizer. During the rapid expansion of liquid into the pressurizer, the predominant factors determining the pressure differential between the primary loop and the pressurizer are the rate of energy addition to the primary system liquid and the surge line hydraulic resistance. For a given surge line hydraulic resistance, the greater the rate of primary energy addition, the greater the pressure difference developed due to the greater volumetric rate of liquid expansion through the surge line into the pressurizer. Similarly, for a given rate of energy addition, the greater the surge line hydraulic resistance, the greater the pressure difference required to accommodate the volumetric rate of liquid expansion through the surge line into the pressurizer. The expansion continues until about 3 to 4 s after SCRAM, when the core power decay produces a net energy removal from the primary fluid system. The liquid then contracts as the primary system cools and the liquid specific volume decreases. For the remainder of the blowdown phase of the transient, the primary liquid flows out of the pressurizer and into the loop hot leg under the influence of the continued cooling provided by the unaffected loop

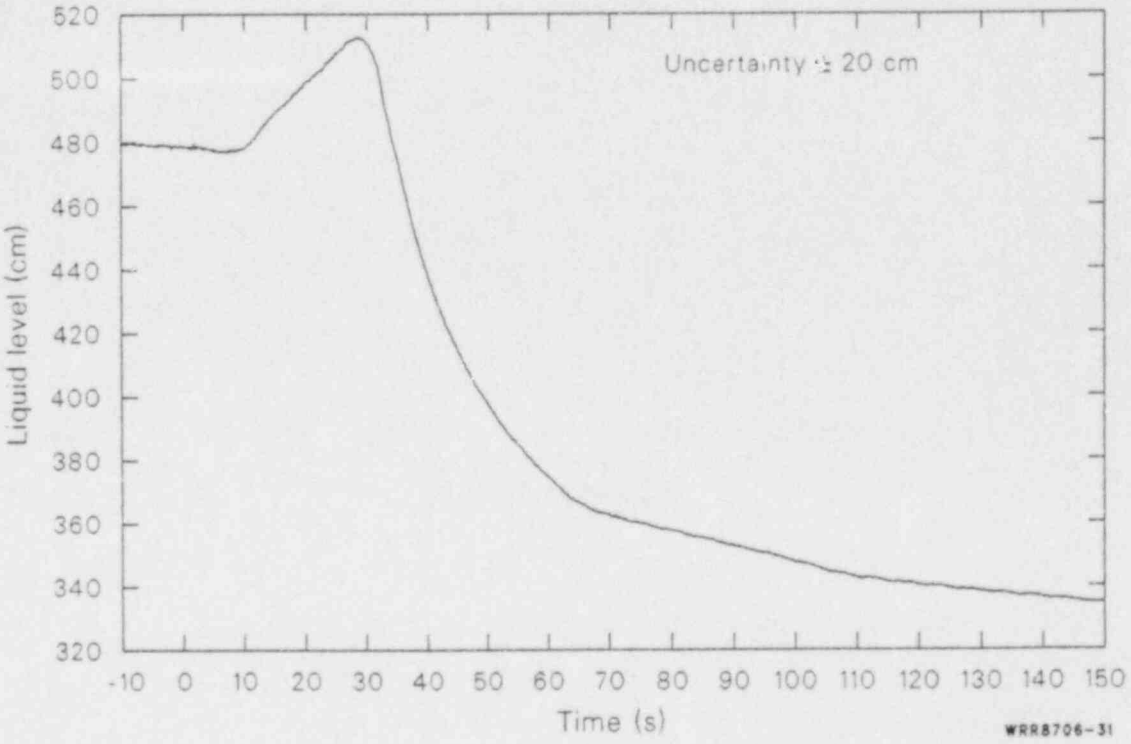

Figure 31. Pressurizer overall collapsed liquid level during the blowdown phase of 100% FWLB experiments S-FS-6/6B (-10 to 150 s).

steam generator and slight primary fluid system leakage.

Primary Thermal Response. The thermal response of the primary fluid system during a bottom main feedwater line break secondary LOCA is characterized as a rapid heatup of primary fluid. As shown in Figure 32, before the degradation in the affected loop steam generator primary-to-secondary heat transfer (before about 13 s in Figure 32), the primary energy balance is maintained by the continued normal steam flow, intersecondary flow, and break flow for the secondaries. As the affected loop heat sink rapidly degrades, the primary energy balance is lost and energy is added to the primary fluid causing the fluid to rapidly heat up. This continues until about 3 to 4 s after SCRAM, when the core power decays to a level below the unaffected loop steam generator primary energy removal rate.

During the period of primary heatup, the primary fluid average temperature (Figure 33) increased at an average rate of about 0.46 K/s. This represents an average primary energy addition rate of about 350 kW, which is in good agreement with the measured primary energy balance shown in Figure 33. The primary fluid average temperature increased by about 4.5 K due to the energy imbalance. This represents a total primary energy addition during the heatup of about 2800 kJ. As discussed in the secondary thermal response section, the intersecondary flow from the unaffected loop steam generator increased its primary energy removal substantially and reduced the net primary energy addition rate to a value less than that associated with the loss of the affected loop heat sink. If this had not occurred, the average primary energy addition rate would have been about 500 kW. Assuming that the net energy addition required to reach the SCRAM pressure set point would be the same and that the time between SCRAM and the core power decay reaching the unaffected loop secondary energy removal rate would be about the same, this would have produced a total primary energy addition during the heatup of about 3250 kJ, which would have produced a peak pressure of 16.42 MPa.

The loop hot and cold leg fluid temperature responses (Figure 33) show a characteristic response that indicates the affected loop cold leg fluid temperature exceeds the hot leg fluid temperature following the loss of the affected loop heat sink. While this would indicate reverse heat transfer

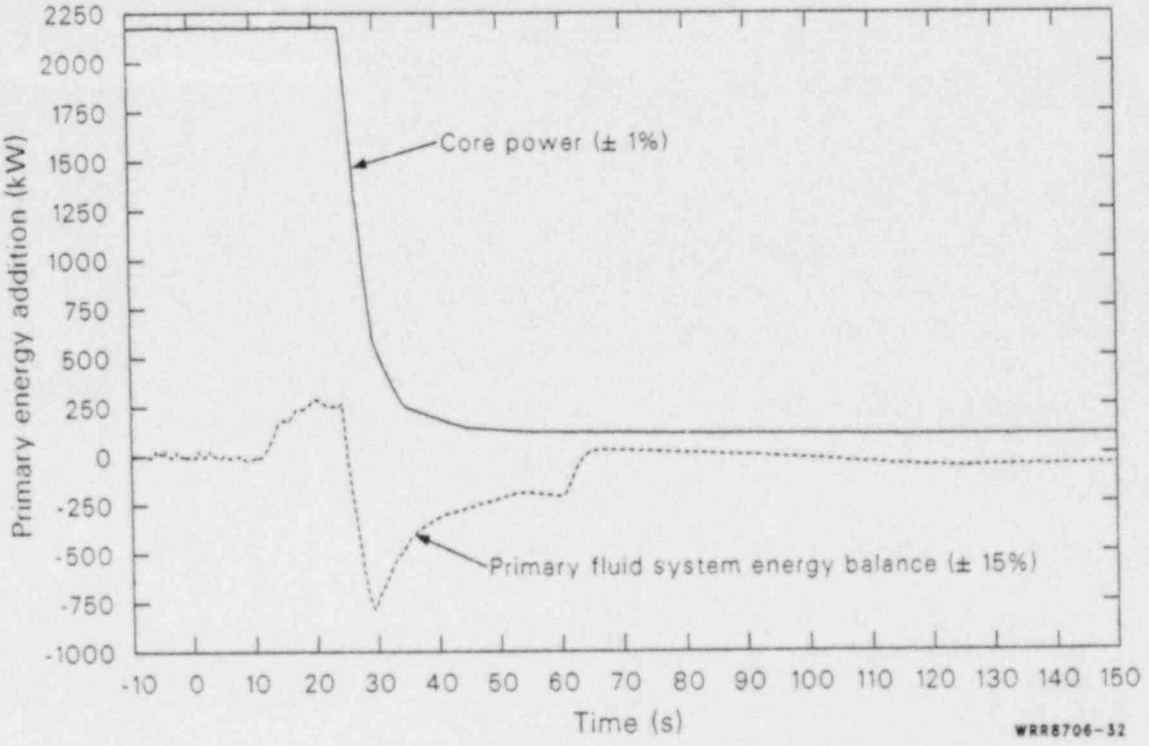

Figure 32. Core power and primary fluid system energy balance during the blowdown phase of 100% FWLB experiments S-FS-6/6B (-10 to 150 s).

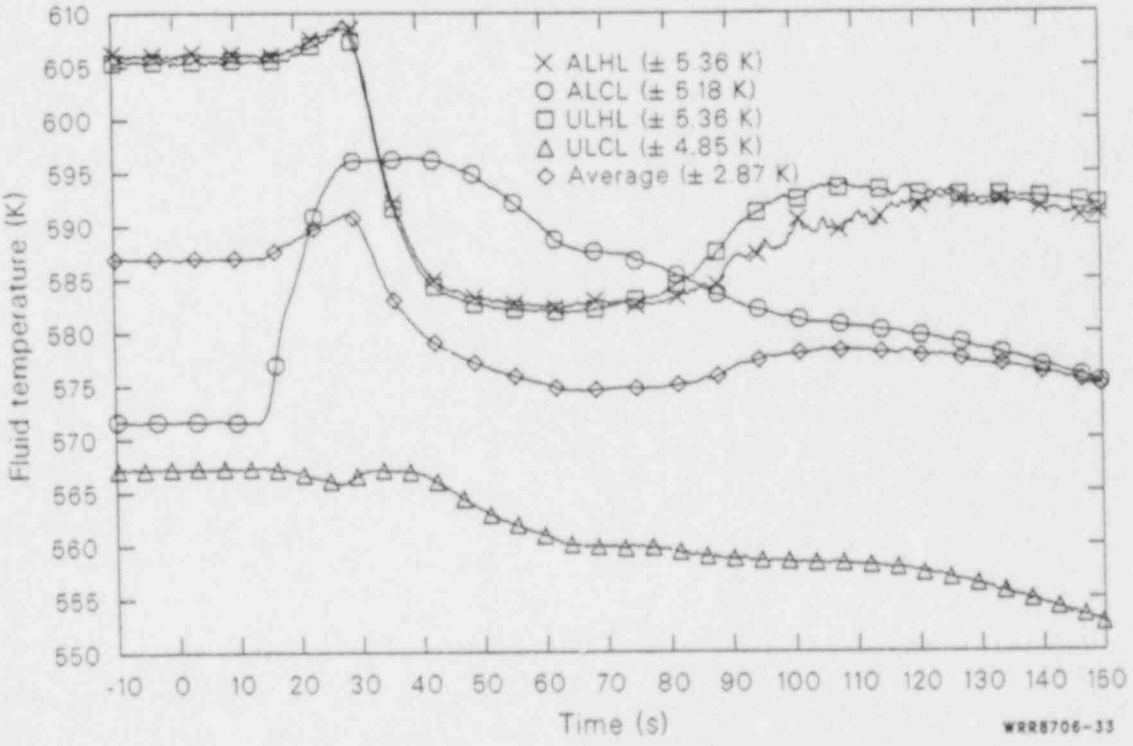

Figure 33. Affected and unaffected loop hot and cold leg and average primary fluid system temperatures during the blowdown phase of 100% FWLB experiments S-FS-6/6B (-10 to 150 s).

in the affected loop steam generator, in actuality, it is a result of the loss of the affected loop heat sink and the increased loop transit time (Figure 34) due to the reduced loop flows following loss of offsite power. The cold leg fluid temperature measurement station is simply measuring the temperature of the fluid that had been at the hot leg fluid temperature measurement station earlier in the transient. The loop flow reduction substantially increased the time required for the fluid to flow from the hot leg to cold leg temperature measurement stations (the loop transit time). This combined with the rapid loss of the affected loop steam generator heat sink and the decreasing vessel outlet temperatures to produce the observed temperature responses.

The primary fluid system thermal response moderated following the loop flow reductions as the system transitioned to a natural circulation mode of heat transfer. As the natural circulation flow was being established, the primary fluid was gradually heating as evidenced by the average fluid temperature increase. Once the natural circulation flow was established, as evidenced by the unaffected loop hot leg to cold leg temperature difference reaching a maximum, the system entered a phase of gradual cooling until MSIV closure. Following MSIV closure, the energy removal provided by the steam flow from the unaffected loop steam generator to the affected loop steam generator was lost leaving the unaffected loop steam generator auxiliary feedwater as the only source of energy removal. This caused the primary fluid thermal response to moderate even further, exhibiting a very gradual cooling through the end of the blowdown phase.

Influence of Bottom Main Feedwater Line Break Size on System Response

Concerns exist with respect to the effects of the break size on the primary and secondary system responses to a bottom main feedwater line break secondary LOCA. Parametric variation studies performed for the C-E System 80 FSAR Appendix 15B bottom main feedwater line break calculations showed a definite sensitivity of the calculated primary pressurization to the break size. In this section, the effects of the break size on the transient severity are addressed by comparing first the secondary and then the primary fluid system thermal-hydraulic responses for break sizes equivalent to 100% (tests S-FS-6/S-FS-6B), 50% (test S-FS-11), and 14.3% (test S-FS-7) of the bottom feedwater distribution box total outlet flow area. The discussion is organized into two subsections with one subsection covering the secondary fluid system response and the other subsection covering the primary fluid system response.

Effects of Break Size on Secondary Response

As discussed earlier, the pressurization of the primary fluid system is controlled by the secondary response to the bottom main feedwater line break secondary LOCA. Therefore, it is important to understand the effects of the feedwater line break size on the secondary thermal-hydraulic response in order to understand the relative severity of the resulting primary pressurization. All of the bottom main feedwater line break experiments had similar basic thermal-hydraulic responses. However, several differences in the responses are worthy of note. Comparisons of the general secondary system responses to the general sequences of events are discussed first. This is followed by comparisons of the secondary pressure responses, hydraulic responses, and thermal responses for both secondaries with major emphasis on the affected loop steam generator.

General Secondary Response Comparisons. The general secondary responses for the bottom main feedwater line break experiments were qualitatively the same. The major differences observed are in the timing of events and the quantitative responses. For all three break sizes, the occurrence of the break produced severe effects on the steam generator secondary. In all three cases, the unaffected loop steam generator also experiences a reduction in inventory due to the loss of all main feedwater at break initiation and the continued steam flow before closure of the normal steam flow control valves (turbine stop valve simulators) at SCRAM. The unaffected and affected loop steam generators remain coupled during all three experiments, with transfer of inventory from the unaffected loop to the affected loop steam generator and out the break, until MSIV closure. Following MSIV closure, the secondaries decouple with the affected loop steam generator emptying and decoupling from the primary, and the unaffected steam generator slowly refilling with auxiliary feedwater and slowly repressurizing.

Secondary Pressure Response Comparisons. The secondary pressure responses exhibited the

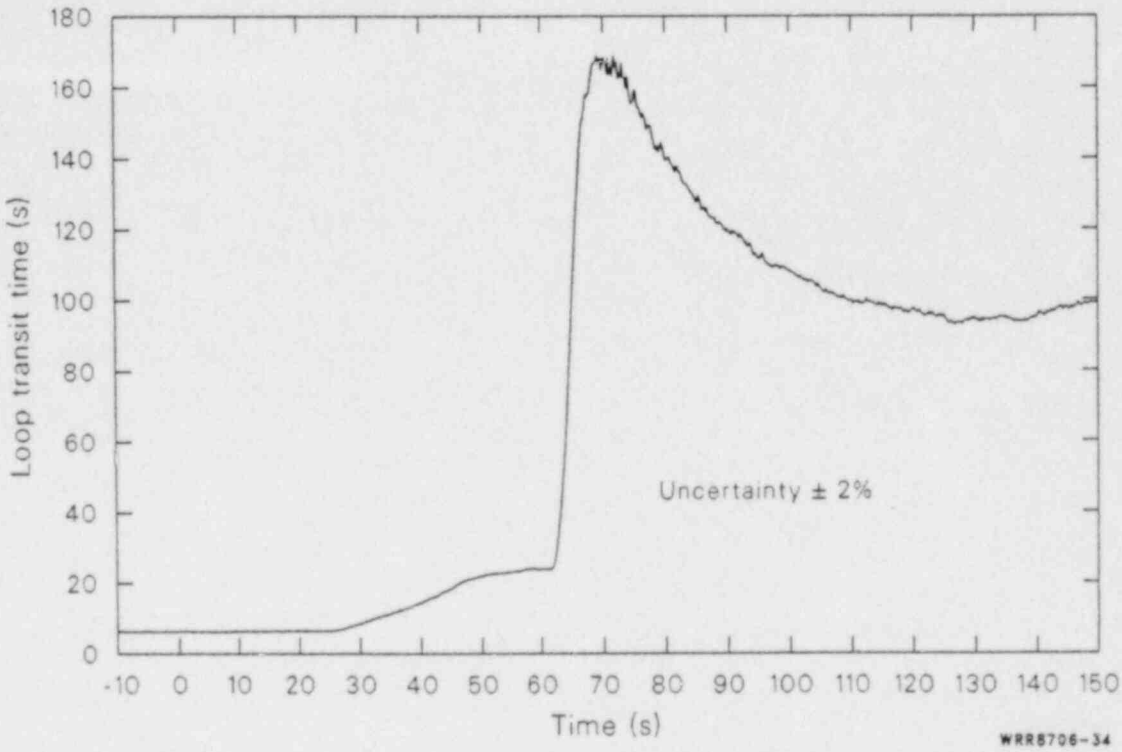

Figure 34. Affected loop hot leg to cold leg fluid temperature measurement station loop transit time during the blowdown phase of 100% FWLB experiments S-FS-6/6B (-10 to 150 s).

same basic trends for all three break sizes. In all three cases, the secondary pressure responses are characterized by a number of inflection points associated with changes in the mass and energy balances. As shown in Figure 35, the loss of mass from the secondaries initially produced only minor changes in the secondary pressures, with the smallest break size test showing the largest variation from the steady-state values (a slight pressurization). In all three cases, the transient condition does not become apparent in the secondary pressure responses until after the affected loop steam generator secondary liquid inventory is depleted, stopping the vapor generation in the steam generator. The transient condition is then reflected in the affected loop steam generator secondary depressurization before the closure of the normal steam flow control valves (turbine stop valve simulators) at SCRAM, with the largest break case exhibiting the greatest amount of depressurization. Following SCRAM, the net energy addition to the secondaries caused both secondaries to repressurize for all three break sizes, with the smallest break case exhibiting the greatest amount of repressurization. These repressurization/depressurization break size sensitivities are a result of the break flow secondary energy removal capacities. Larger break sizes produce greater break flow, and hence greater secondary energy removal rates.

The relative break size is also reflected in the developing pressure difference between the secondaries during the period of repressurization, relative pressure differential maintained during the ensuing depressurization to the MSIV closure set point pressure, and rate of the secondary depressurizations before MSIV closure. The secondary pressure difference is governed by the main steam line piping hydraulic resistance and the intersecondary mass flow rate. Following the depletion of the affected loop steam generator liquid inventory, the break mass flow rate controls the intersecondary mass flow rate. Thus, the larger break sizes produce greater break flow rates and greater intersecondary flow rates. This produces greater secondary pressure differences because the main steam line piping hydraulic resistance remains essentially constant.

The secondary pressure responses following MSIV closure also exhibit the same basic trends, with the break size reflected in the rate of the affected loop steam generator depressurization and the pressure at which the unaffected loop steam generator secondary stabilizes. The rate of the

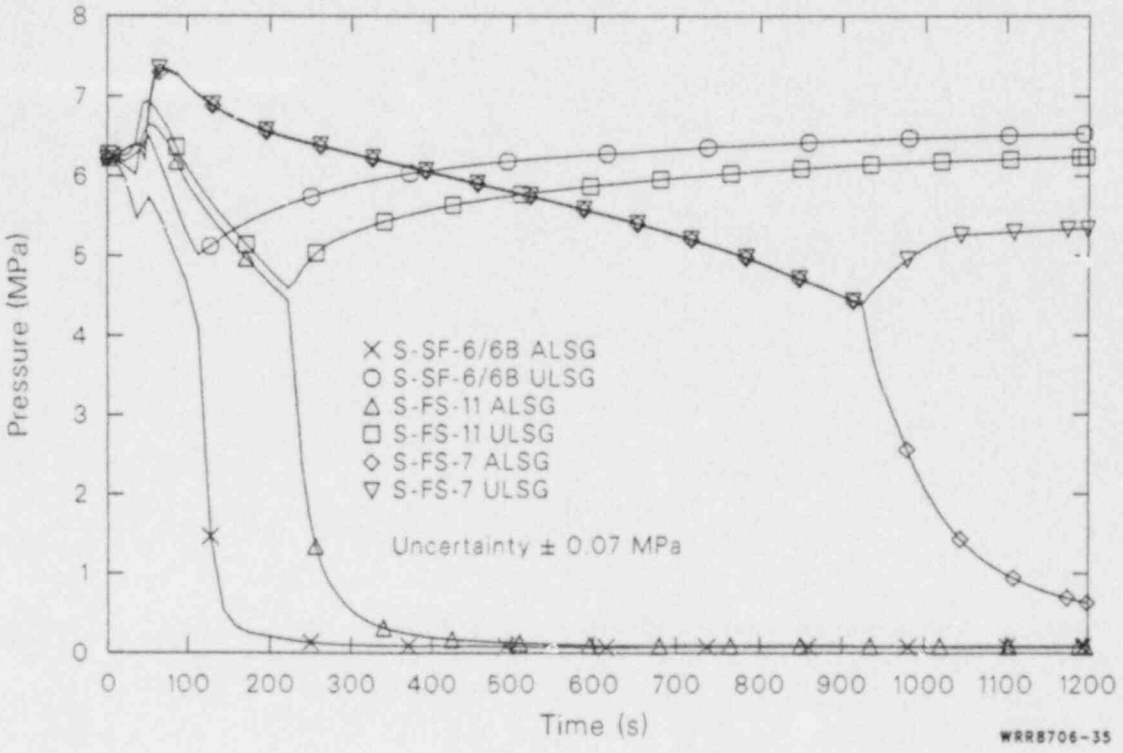

Figure 35. Comparisons of affected and unaffected loop steam generator secondary pressures during the blowdown phases of 100, 50, and 14.3% FWLB experiments S-FS-6/6B, S-FS-11, and S-FS-7.

affected loop steam generator depressurization is directly proportional to the break flow energy removal, and hence the break size. The larger break sizes result in earlier MSIV closure. This causes the unaffected loop steam generator isolation to occur earlier in the transient with the core decay heat at a higher level and greater unaffected loop steam generator secondary mass inventory. This causes the unaffected loop steam generator secondary pressure to stabilize at a higher level because of greater vapor generation and less steam volume. For all three cases, following MSIV closure, the affected loop steam generator decouples from the primary, while the unaffected loop steam generator gradually pressurizes. At the end of the blowdown phase of the transients, the secondary pressures were fairly stable.

Secondary Hydraulic Response Comparisons. The secondary hydraulic responses exhibited the same basic trends for all three break sizes. The affected loop steam generator secondary fluid hydraulic characteristics were substantially altered from the steady-state, full-power conditions (Appendix C) during all three break size cases. The simulated bottom main feedwater line rupture initiated the loss of inventory and the resulting changes in the fluid hydraulic conditions at time zero (t = 0 s) for all three cases. As shown in Figure 36, the break flow peaked at about 1 s in all three cases as subcooled liquid critical flow was established. The break flow drag screen measurement device indicated a substantial period of negative break flow for the 14.3% break test (S-FS-7). However, reverse break flow is physically impossible because the secondary pressure is substantially greater than the pressure downstream of the break. It is believed that the drag screen experienced the force of a shock wave created by the opening of the blowdown valve. The force of the shock wave lifted the drag screen, indicating negative flow, with a magnitude sufficient to produce an electronic signal that *saturated* the drag measurement electronic components. A finite amount of time was required for the electronic components to recover from being *saturated* and indicate the true measured force electronic signal. This produced the measured response. The best-estimate break flow provides a better indication of the true flow rate during this period and for periods of 100% vapor break flow conditions. The relative magnitudes of the initial peaks in the subcooled liquid break flows are in

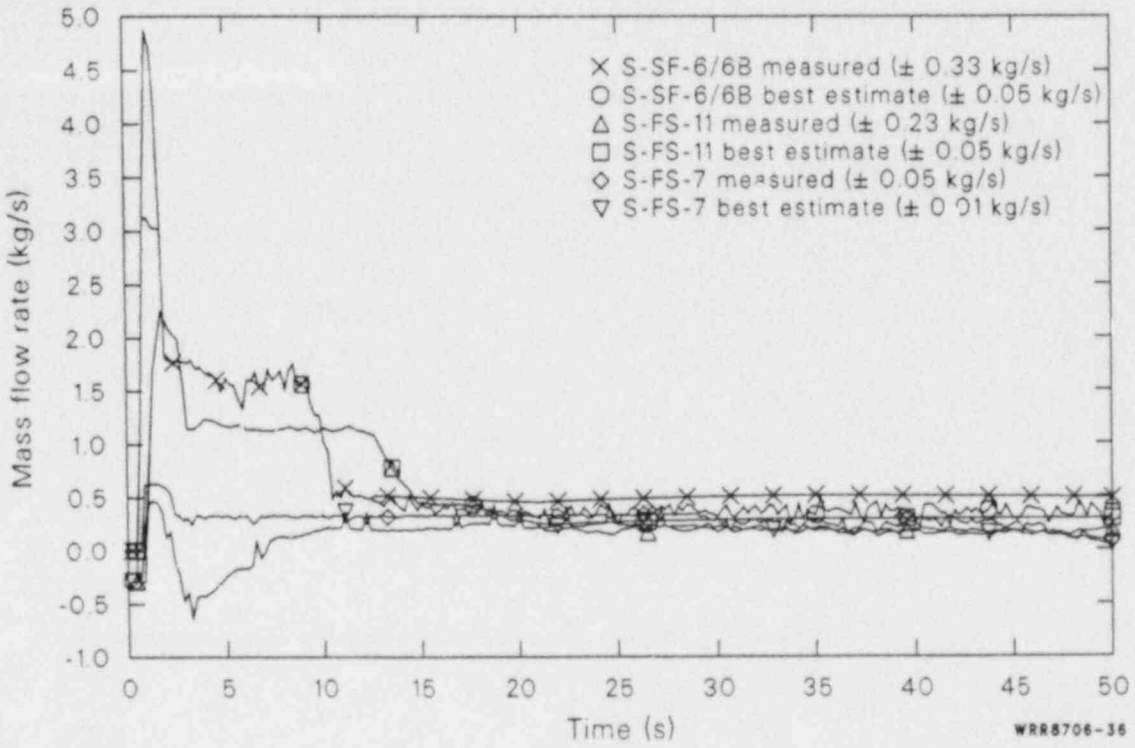

Figure 36. Comparisons of measured and best estimate break mass flow rates during the blowdown phases of 100, 50, and 14.3% FWLB experiments S-FS-6/6B, S-FS-11, and S-FS-7.

good agreement with the relative break sizes (i.e., the peak flow for the 100% break case is about twice as large as the peak flow for the 50% break case and about seven times larger than the peak flow for the 14.3% break case). This is because the initial subcooled break flow conditions produced the same initial mass flux at the break nozzle for all three cases.

The break flows transited the full range of possible fluid flow states (i.e., subcooled liquid, saturated liquid, two-phase fluid, and single-phase vapor) as the secondary fluid mass inventory was depleted in all three break size cases (Figure 37). The break flow was of sufficient magnitude in all three cases to cause the flow in the affected loop steam generator upper downcomer to increase (Figure 38). Also, because of the continued boiling in the tube-bundle region and the continued normal steam flow, the flow at the top of the affected loop steam generator tube bundle riser did not reverse, but merely decreased in magnitude for all three break size cases (Figure 39). The effect of the break size was more strongly reflected by the flow in the lower downcomer between the break and the tube-bundle section (Figure 40). The 100% break case exhibited immediate, continued flow reversal, while the 50% break case exhibited immediate flow reversal initially, followed by a period of normal flow and eventual flow reversal as the liquid inventory was depleted. The 14.3% break case did not exhibit the initial flow reversal exhibited in the other cases, but did exhibit the eventual flow reversal as the liquid inventory was depleted. These flow conditions existed for all three break size cases until the secondary liquid inventory was depleted.

The effect of the break size on the secondary hydraulic response can be characterized in a manner similar to the characterizations made for primary LOCA vessel hydraulic response break size effects.[27] The large break hydraulic response is characterized by a flow split in the tube-bundle region caused by the break flow momentum driven flow reversal between the lower downcomer feedwater inlet location and the tube-bundle region. The flow split persists as the tube bundle liquid inventory is rapidly depleted. In contrast, the small break hydraulic response is characterized by a reduction in the flow between the lower downcomer feedwater inlet location and the tube-bundle region (as a portion of the recirculated downcomer flow is lost to the break), while the flow out of the tube-bundle region is maintained by the boiling in the

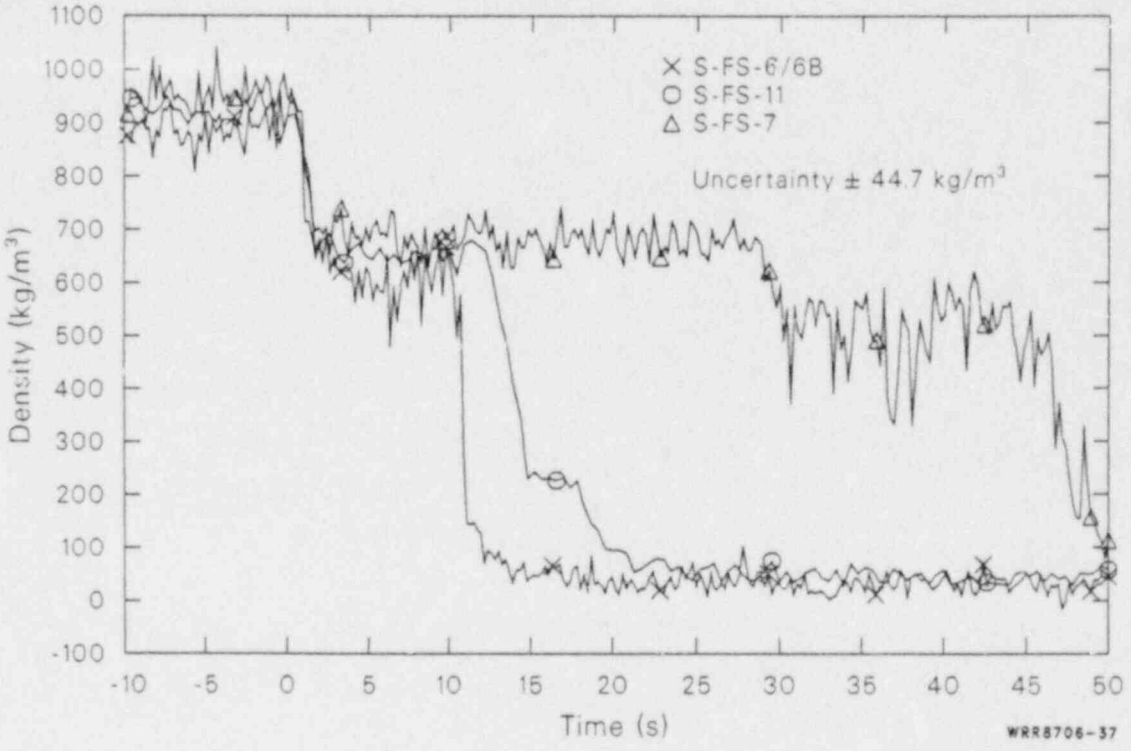

Figure 37. Comparisons of break fluid densities during the blowdown phases of 100, 50, and 14.3% FWLB experiments S-FS-6/6B, S-FS-11, and S-FS-7.

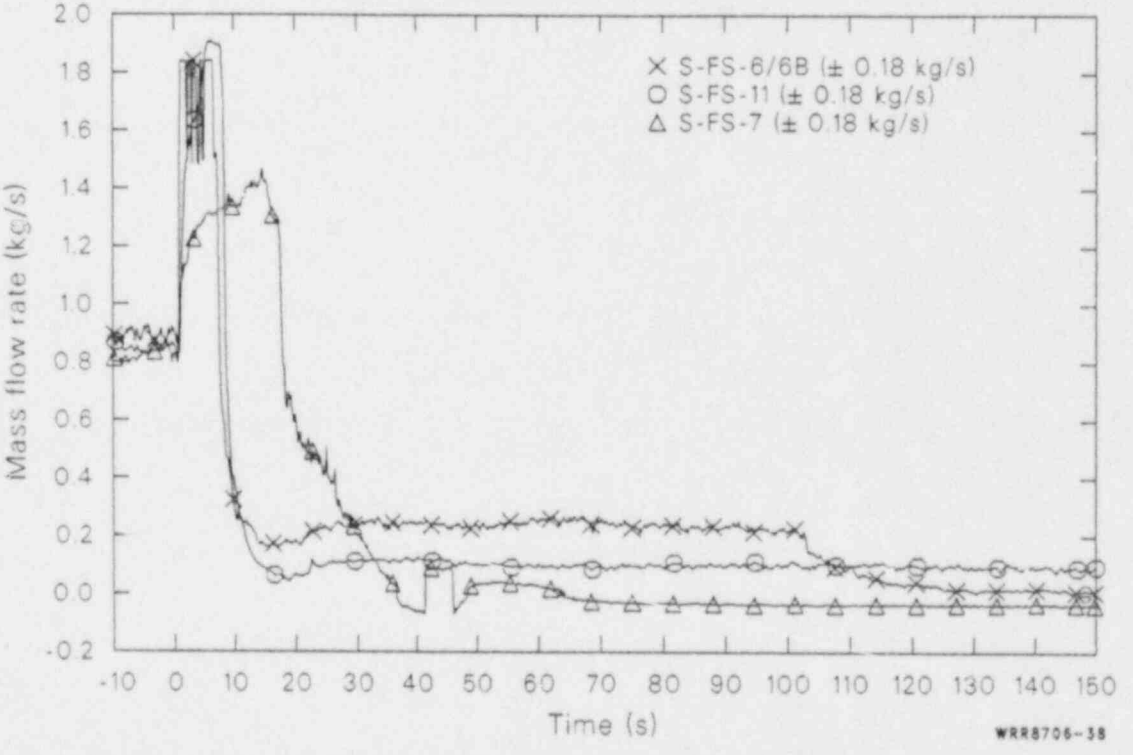

Figure 38. Comparisons of affected loop steam generator upper downcomer mass flow rates during the blowdown phases of 100, 50, and 14.3% FWLB experiments S-FS-6/6B, S-FS-11, and S-FS-7.

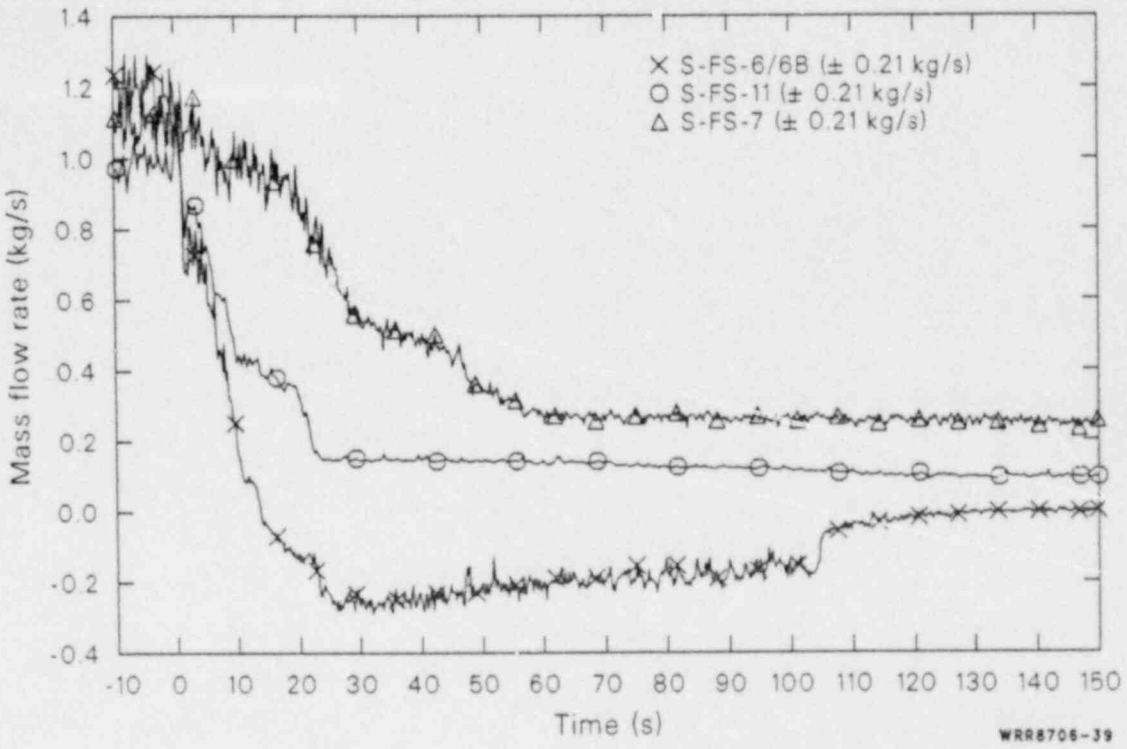

Figure 39. Comparisons of affected loop steam generator riser mass flow rates during the blowdown phases of 100, 50, and 14.3% FWLB experiments S-FS-6/6B, S-FS-11, and S-FS-7.

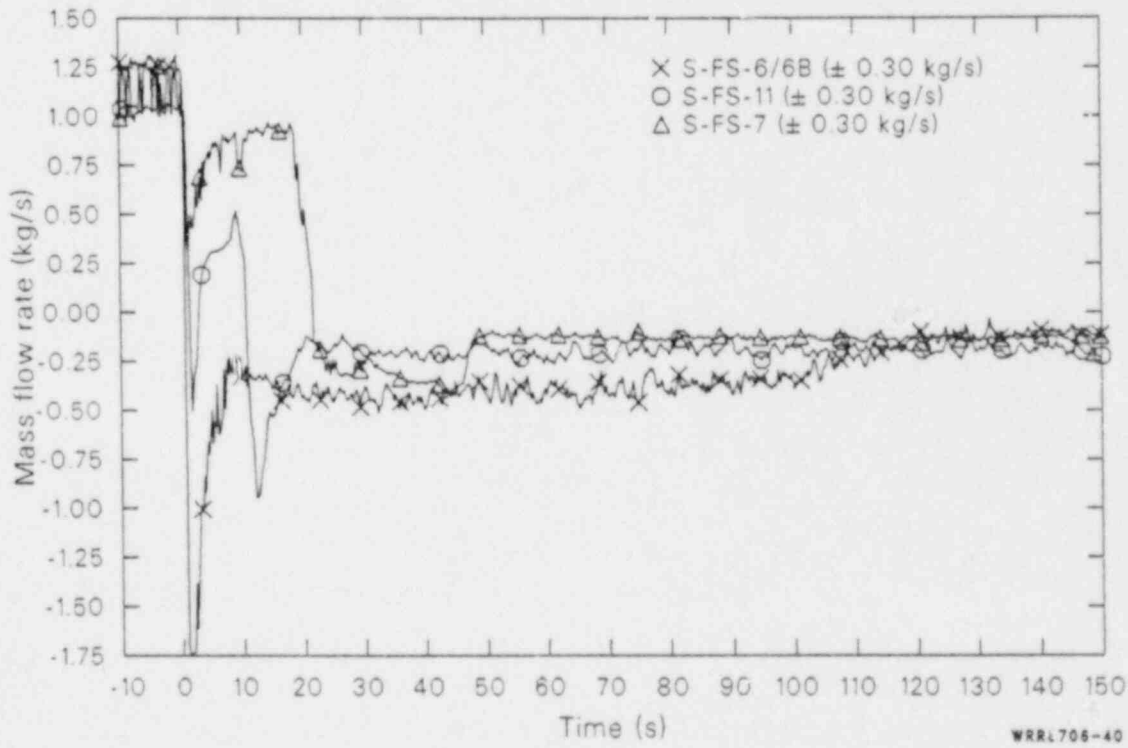

Figure 40. Comparisons of affected loop steam generator lower downcomer mass flow rates during the blowdown phases of 100, 50, and 14.3% FWLB experiments S-FS-6/6B, S-FS-11, and S-FS-7.

tube bundle. This produces a more gradual depletion of the tube bundle liquid inventory than occurs during the large break case. Intermediate break sizes produce periods of rapid inventory depletion due to brief tube bundle flow split followed by periods of more gradual draining due to reduced tube bundle inlet flows.

After the secondary liquid inventory was depleted, a new mass balance was achieved in the secondary for all three break size cases. Steam entered the steam dome from the crossover line (Figure 41). The flow then split with approximately one-half of the steam flowing down the downcomer (Figure 38) to the break and the other half flowing down the tube bundle to the break. While tube bundle flow reversal was necessary to satisfy the steam dome mass balance, the reversed tube bundle flow was below the measurement range of the drag screen measurement assembly and, therefore, was not reflected in the riser mass flow rate measurement for tests S-FS-6B, S-FS-7, or S-FS-11. However, the tube bundle flow reversal was evident in the negative frictional pressure drop across the riser orifice (Figure 42). An overall mass balance was maintained for the affected loop steam generator as the steam flow entering the secondary from the crossover line was matched by the steam flow exiting the secondary via the break. Following the depletion of the secondary inventory, the break flow controlled the intersecondary flow for all three break size cases. The break flow caused the affected loop secondary to depressurize relative to the unaffected loop secondary until the developed intersecondary pressure difference was of sufficient magnitude to overcome the crossover line hydraulic resistance and produce an intersecondary flow that matched the break flow. In addition, the rate of the secondary depressurizations was controlled by the break flow, energy addition to the unaffected loop steam generator, and total steam volume associated with both secondaries and their main steam line piping. This shows the need to accurately simulate the single-phase steam break flow, unaffected loop steam generator energy addition, main steam line piping hydraulic resistance, and main steam line piping volume in order to accurately calculate the secondary response during this phase of the tests.

It is important to note that nonuniform rates of inventory reduction for the downcomer and the tube-bundle regions occurred for all three break size cases (Figures 43 and 44). This was due to the transient induced intercomponent mass flow rate imbalances. In all three break size cases, the initial reduction in total secondary mass inventory involved a more rapid rate of reduction in the tube bundle mass inventory than in the downcomer mass inventory. While the general trend of the inventory reductions was similar, differences occurred in the response of the two-phase fluid in the tube-bundle region for the different break size cases (Figures 11, and D.1 and D.2 in Appendix D). The largest break size produced a uniform two-phase condition in the tube-bundle region before the depletion of the liquid inventory. The smallest break size did not exhibit this uniform two-phase condition. However, in all three break size cases, the tube-bundle region exhibited a rapid transition to a uniform liquid-deficient condition (all vapor condition as evidenced by the vapor-void fraction reaching a value of 1.0). This rapid transition to a liquid-deficient condition produced severe effects on the primary-to-secondary heat transfer, as will be discussed presently, because the transient heat transfer is almost totally dependant upon the tube bundle secondary fluid hydraulics.

The secondary fluid hydraulic response of the unaffected loop steam generator was similar for all three break size cases, with the major differences occurring in the magnitudes of the parameters and the timing of events. The major difference observed was in the rate of secondary inventory reductions following the depletion of the affected loop secondary inventory (Figure 45). This was due to the different intersecondary flows and timing of events for the tests. The longer time required for SCRAM for the smaller break sizes produced greater reductions in the secondary inventory before SCRAM. While the intersecondary flow rate was smaller for the smaller break size cases, the MSIV closure occurred much later resulting in substantially greater loss of secondary inventory before MSIV closure. (At MSIV closure the unaffected loop secondary inventory was reduced to about 45, 35, and 15% of the initial inventory for the 100, 50, and 14.3% break cases, respectively.) It is important to note the substantial loss of inventory for the smallest break size case. Because the unaffected loop steam generator is the only remaining source for primary energy removal, some concern for the effect of this substantial loss of inventory on the energy removal capability of the secondary is warranted. However, the length of time required for the inventory reduction to occur was substantial, and it is quite likely that the operators would identify the transient and isolate the secondary before the automatic MSIV closure.

Secondary Thermal Response Comparisons. The measured secondary thermal responses for the three different break size cases are very similar when

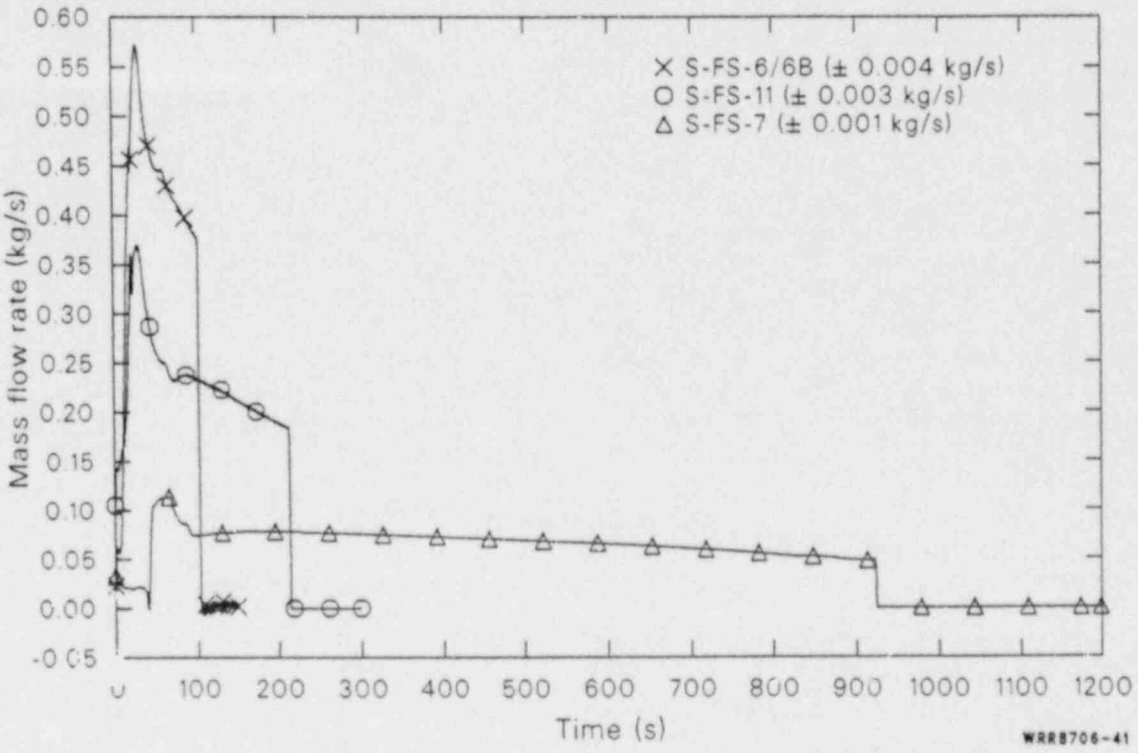

Figure 41. Comparisons of intersecondary mass flow rates through the crossover line during the blowdown phases of 100, 50, and 14.3% FWLB experiments S-FS-6/6B, S-FS-11, and S-FS-7.

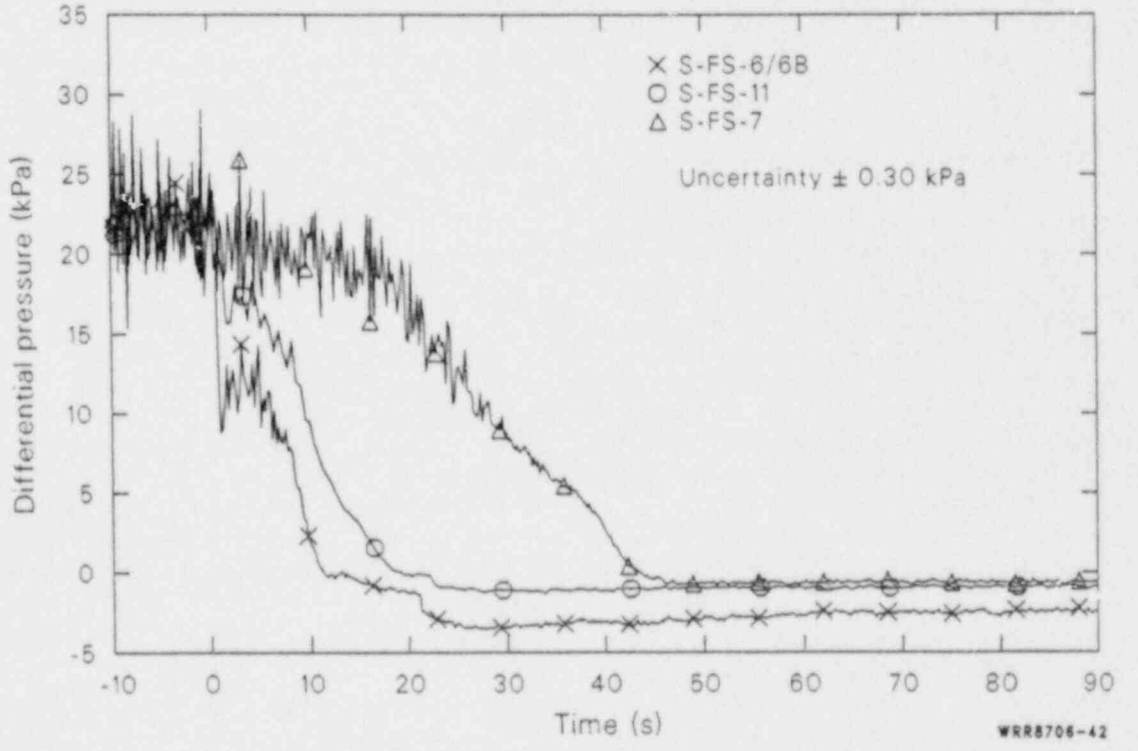

Figure 42. Comparisons of riser orifice frictional pressure drops during the blowdown phases of 100, 50, and 14.3% FWLB experiments S-FS-6/6B, S-FS-11, and S-FS-7.

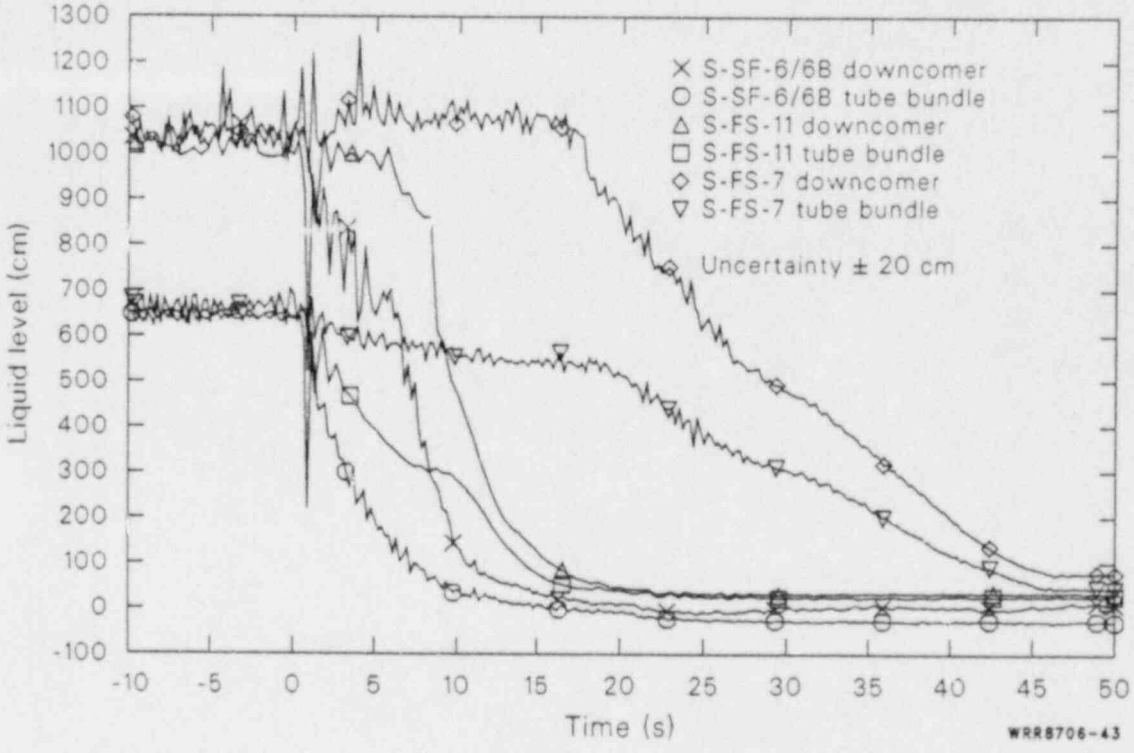

Figure 43. Comparisons of affected loop steam generator frictional corrected overall downcomer and tube bundle interfacial liquid levels during the blowdown phases of 100, 50, and 14.3% FWLB experiments S-FS-6/6B, S-FS-11, and S-FS-7.

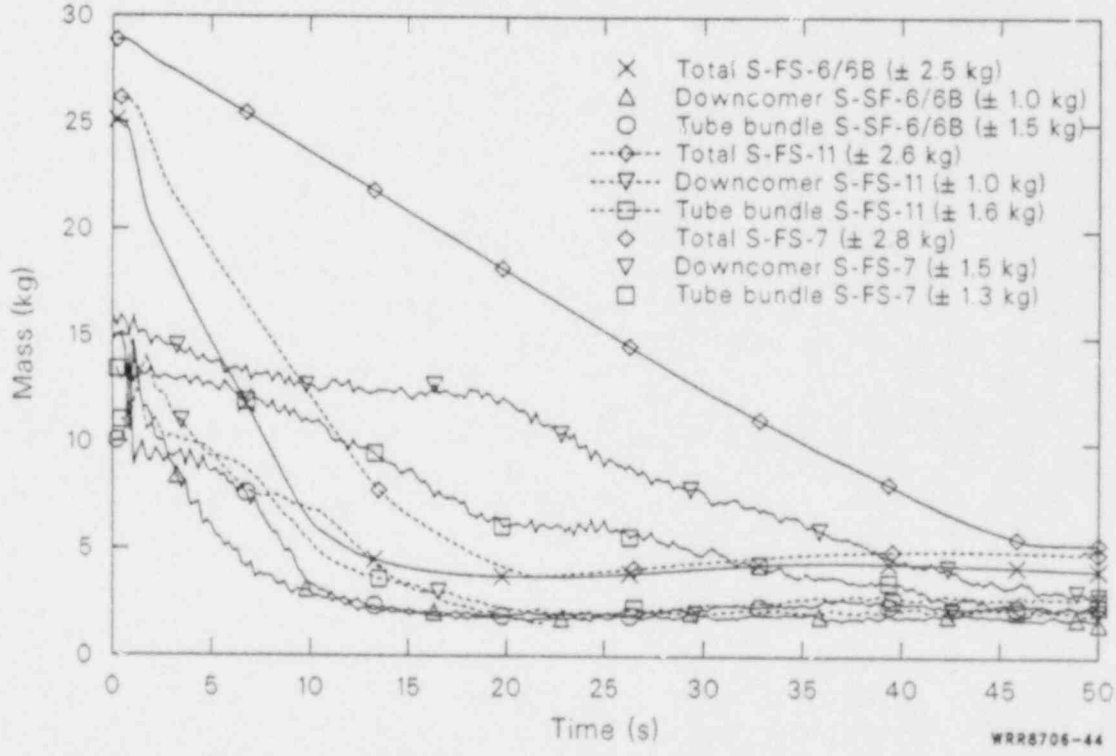

Figure 44. Comparisons of affected loop steam generator secondary fluid total, downcomer and tube bundle mass inventories during the blowdown phases of 100, 50, and 14.3% FWLB experiments S-FS-6/6B, S-FS-11, and S-FS-7.

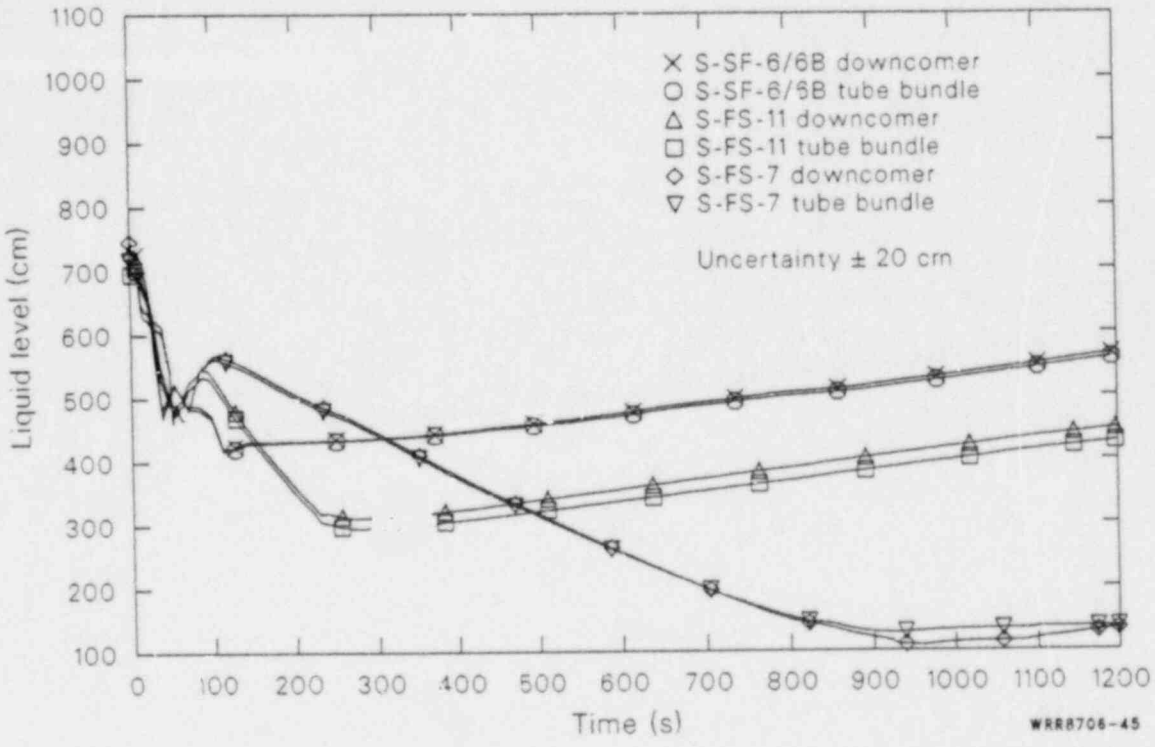

Figure 45. Comparisons of unaffected loop steam generator overall downcomer and tube bundle collapsed liquid levels during the blowdown phases of 100, 50, and 14.3% FWLB experiments S-FS-6/6B, S-FS-11, and S-FS-7.

normalized to the mass inventory. The affected loop steam generator secondary thermal response is relatively insensitive to the break size. The minor differences noted were due to the different rates of secondary inventory reduction. The unaffected loop steam generator secondary thermal response exhibited some sensitivity to break size associated with the energy removal provided by the intersecondary flow. Here again, clearer understanding of the transient thermal response for these tests may be achieved by considering the steady-state, full-power thermal conditions. The steady-state secondary fluid thermal characteristics may be gleaned from the included figures for times before transient initiation, from the discussion in Appendix C, or from the discussion in the *Secondary Thermal Response* subsection of the *Secondary Response to a Steam Generator Bottom Main Feedwater Line Break* section. The major result of the steady-state analyses was the characterization of the secondary convective heat transfer coefficient. The measured heat transfer coefficient increases with increasing vapor-void fraction and decreases with decreasing wall-to-fluid temperature difference. This measured trend in the secondary convective heat transfer coefficient was observed for all three break size cases, and provides a major clue to the measured transient response.

While the affected loop steam generator secondary fluid thermal characteristics for all three break size cases were altered significantly, the total primary-to-secondary heat transfer was not altered substantially until the tube bundle liquid inventory was depleted. The affected loop steam generator total primary-to-secondary heat transfer remained at the initial condition value until the secondary inventory was depleted. The primary-to-secondary heat transfer then decreased rapidly. Plotting the normalized heat transfer versus normalized total liquid inventory and versus the normalized tube-bundle region liquid inventory for the affected loop steam generator for all three break size cases (Figure 46) shows that the normalized heat transfer remained at 100% until the normalized total and tube-bundle region liquid masses reached almost 0%. The heat transfer then decreased rapidly to 0%. A very slight break size dependency was exhibited in that the degradation in heat transfer was initiated at a slightly greater mass inventory and proceeded at a slightly slower rate for the smallest break size case.

The close relationship between the heat transfer and the liquid inventory for all three break size cases was

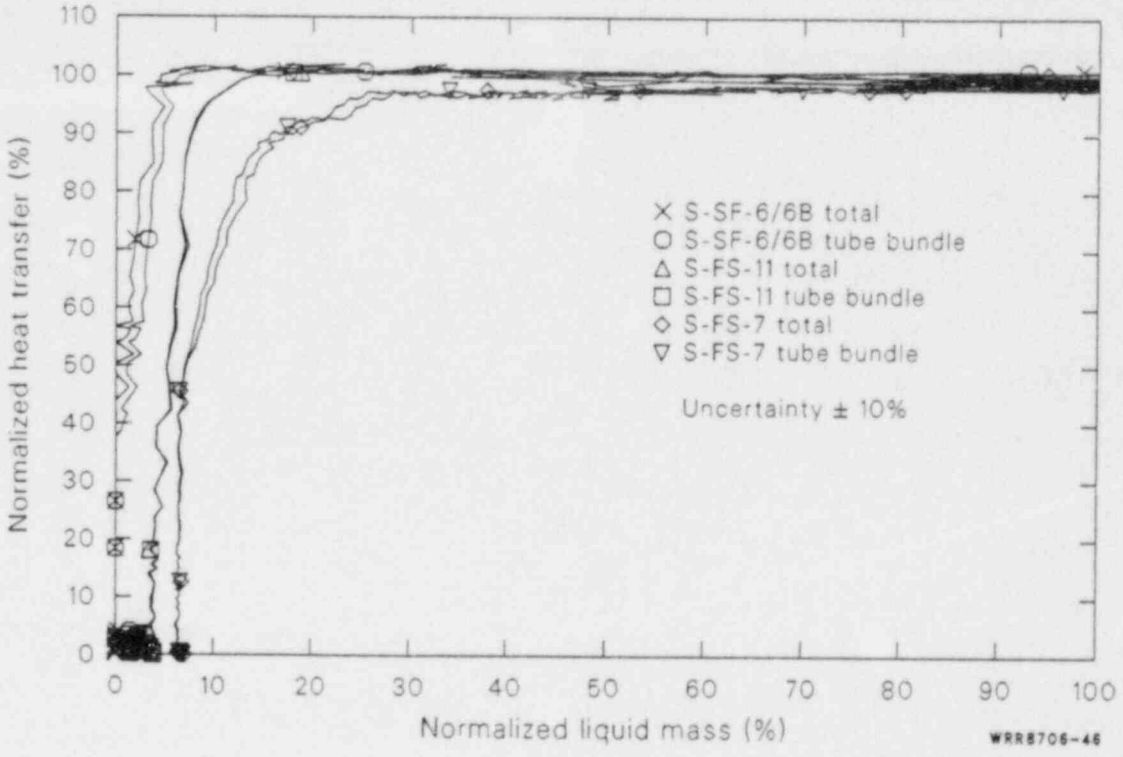

Figure 46. Comparisons of affected loop steam generator normalized heat transfer versus normalized total secondary liquid inventory and versus normalized tube-bundle region liquid inventory during the blowdown phases of 100, 50, and 14.3% FWLB experiments S-FS-6/6B, S-FS-11, and S-FS-7.

due to the strong dependency of the secondary convective heat transfer coefficient upon the vapor-void fraction. As shown in Figures 20 through 27 (and D-3 through D-18 in Appendix D), the local secondary convective heat transfer coefficients increase in a manner directly proportional to the local vapor-void fractions (Figures 11, and D.1 and D.2 of Appendix D). This continues for all three break size cases until a local liquid-deficient condition exists (the local vapor-void fractions reach a value of 1.0), causing the local heat transfer coefficient to rapidly decrease to zero. Thus, the primary-to-secondary heat transfer remains high until the tube-bundle region is devoid of liquid. The heat transfer then degrades rapidly to zero due to the liquid-deficient conditions. For the smallest break size case, the tube-bundle region liquid inventory was depleted more gradually. This decreased the rate of progression of local liquid deficiencies in the tube-bundle region and caused a reduction in local heat transfer in part of the tube bundle, while a portion of the tube bundle still contained some liquid. The net result was that the normalized heat transfer began to decrease at a slightly greater normalized mass and decreased at a slightly slower rate for the smallest break size case. Although the observed responses show a slight difference, the basic phenomena were the same for all three break size cases. The results indicate that the assumption made for the C-E System 80 FSAR Appendix 15B calculations regarding the reduction of heat transfer with liquid inventory (i.e., 100% heat transfer until the liquid inventory is depleted followed by a step change reduction in the heat transfer to 0%) is not conservative, but closely emulates the measured secondary convective heat transfer response to the loss of liquid inventory.

The unaffected loop steam generator secondary thermal response exhibited some sensitivity to break size. The thermal response was affected by the energy balance for the secondary. The energy balance was affected by the feedwater and steam flows, intersecondary flow, primary loop flow reduction, and auxiliary feedwater injection. The loss of energy removal capacity associated with the loss of all feedwater at break initiation was initially offset by the increased normal steam flow for all three break size cases. This allowed the primary-to-secondary heat transfer (Figure 47) to remain at the initial condition value. For the smaller break size cases (50 and 14.3% break cases), the continued normal steam flow before SCRAM, combined with the increased intersecondary flow, maintained the unaffected loop steam generator primary-to-secondary heat transfer at the initial condition value until the

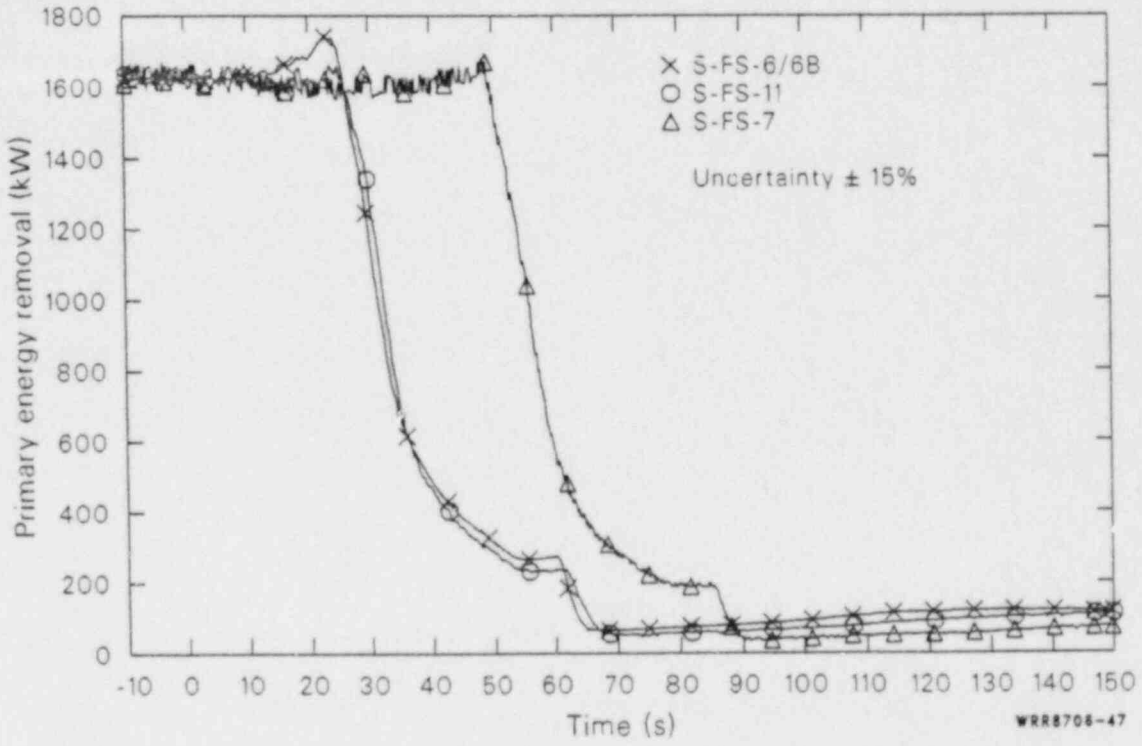

Figure 47. Comparisons of unaffected loop steam generator primary-to-secondary heat transfer during the blowdown phases of 100, 50, and 14.3% FWLB experiments S-FS-6/6B, S-FS-11, and S-FS-7.

normal steam flow control valves (turbine stop valve simulators) were closed following SCRAM. However, for the largest break size case (100% break case), the intersecondary flow increased sufficiently to increase the unaffected loop steam generator primary-to-secondary heat transfer before SCRAM.

The thermal response of the unaffected loop steam generator secondary fluid following SCRAM was similar for all three break size cases. Following SCRAM, the loss of offsite power induced the primary coolant pump trips and associated loop flow reductions. The decreased unaffected loop flow caused a decrease in the unaffected loop steam generator primary-to-secondary heat transfer as the loop transitioned to the natural circulation mode of heat transfer. The natural circulation heat transfer was enhanced by the intersecondary flow before MSIV closure. Following MSIV closure and SI signal generation, the secondary energy removal was provided by injecting auxiliary feedwater into the unaffected loop steam generator secondary. The auxiliary feedwater provided secondary energy removal for the remainder of the test.

The increased unaffected loop steam generator primary-to-secondary heat transfer for the largest break size case caused the overall primary energy removal deficit before SCRAM (Figure 48) to be smaller than for the other two break size cases. The measured deficit for the other two break size cases was approximately equal to the amount associated with the loss of the affected loop steam generator heat sink (nominally 500 kW). Thus, the failure of the affected steam generator main steam line check valve resulted in increased unaffected loop steam generator primary-to-secondary heat transfer for the largest break size case and constant heat transfer for the other two break size cases. For the largest break size case, the net primary energy addition was limited to only about one-half of that associated with the loss of the affected loop steam generator heat sink. For the other two break size cases, the net primary energy addition was limited to the amount associated with the loss of the affected loop steam generator heat sink. The rate of primary fluid expansion was, therefore, significantly reduced for the largest break size case and somewhat reduced for the other two break size cases. Thus, the primary fluid system pressurization was reduced due to the intersecondary flow for all three break size cases, as will be discussed next.

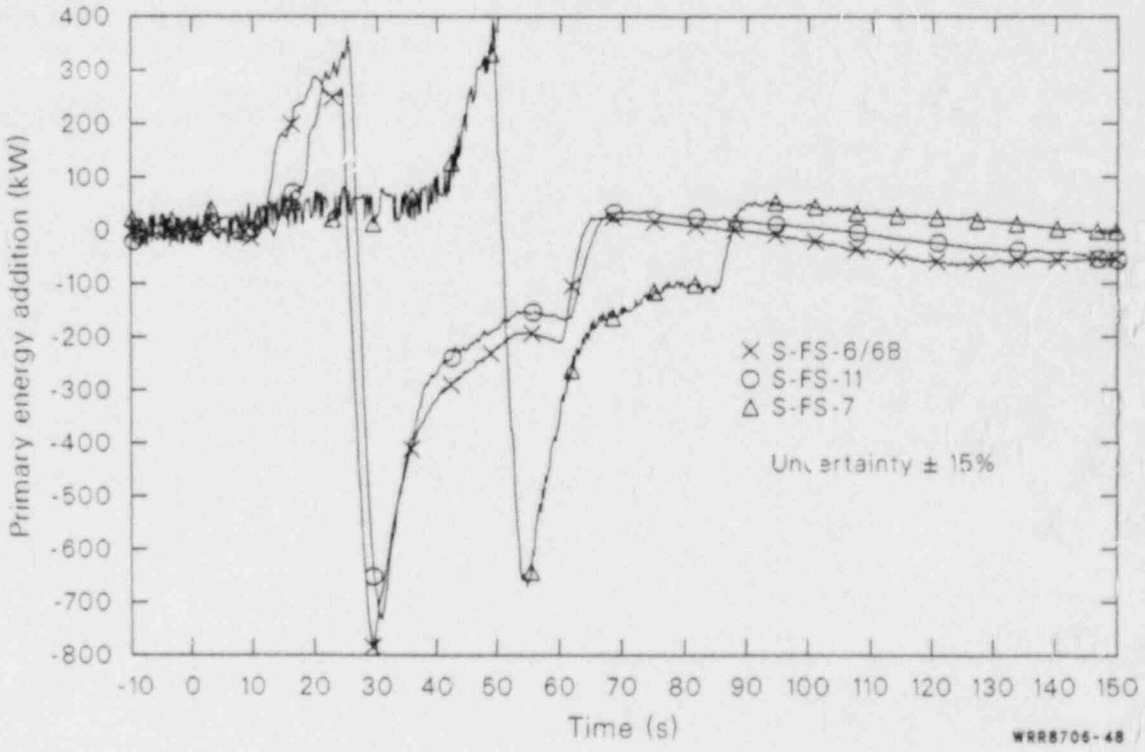

Figure 48. Comparisons of primary fluid system energy addition during the blowdown phases of 100, 50 and 14.3% FWLB experiments S-FS-6/6B, S-FS-11, and S-FS-7.

Effects of Break Size on Primary Response

The degree of pressurization of the primary fluid system depends upon the thermal-hydraulic response to the loss of the heat sink. Therefore, it is important to understand the effects of the feedwater line break size on the primary thermal-hydraulic response in order to understand the relative severity of the resulting primary pressurization. All of the bottom main feedwater line break experiments had similar basic thermal-hydraulic responses. However, several differences in the responses are worthy of note. Comparisons of the general primary system responses to the general sequences of events are discussed first. This is followed by comparisons of the primary pressure responses, hydraulic responses, and thermal responses.

General Primary Response Comparisons. The general primary responses for the bottom main feedwater line break experiments were similar. The minor differences observed were in the timing of events and the quantitative responses. For all three break sizes, the occurrence of the break produced severe effects on the primary fluid system. In all three cases, the primary fluid system exhibited a rapid pressurization in response to the loss of primary-to-secondary heat transfer during the secondary LOCA. The pressurization of the primary continued until about 4 s after the high pressurizer pressure SCRAM set point was reached for all three break size cases, with the peak pressure occurring in the loop cold legs. Following SCRAM, the rapid reduction in the core power combined with the slower closure time for the normal steam flow control valves (turbine stop valve simulators) produced a rapid cooldown and depressurization of the primary fluid system for all three cases. Similarly, the period of rapid cooling was followed by a period of slower cooling and depressurization due to core power decay and intersecondary flows for all three cases. Loop flow reductions (following loss of offsite power) degraded the unaffected loop steam generator energy removal resulting in a short period of primary fluid heating and pressurization until natural circulation flow was established in the unaffected loop. Gradual cooling and depressurization of the primary fluid was then provided in all three cases by the continued intersecondary flow, with the rate of the cooling and depressurization varying in a manner directly proportional to the intersecondary flow rate. For all three cases, following the low affected loop steam generator secondary pressure SI signal, MSIV closure, and

auxiliary feedwater injection resulted in an unaffected loop steam generator energy removal rate that was close to the core decay heat level. This resulted in a very slow cooldown and depressurization of the primary fluid system. The primary fluid system pressure remained above the HPIS shutoff heat so that HPIS injection did not occur in any of the experiments. Also, no voiding of the primary fluid system was observed during the blowdown phase of any of the transients.

Primary Pressure Response Comparisons. The primary pressure responses exhibited the same basic trends for all three break sizes. In all three cases, the primary pressure responses are characterized by a number of inflection points associated with changes in the energy balance. As shown in Figure 49, the bottom main feedwater line break secondary LOCA initially produced no effect on the primary fluid system pressures. The primary energy balances were maintained until the affected loop steam generator primary-to-secondary heat transfer started to degrade. The resulting loss of a portion of the primary fluid system heat sink created an energy imbalance, which resulted in rapid pressurization of the primary fluid system for all three break size cases. The pressurization of the primary fluid system continued until about 3 to 4 s after SCRAM (until about 1 s after the core power decay was initiated). The double spike in the pressurizer pressure for the 50 and 14.3% break cases was due to the cycling of the pressurizer simulated SRV. The peak pressurizer pressure was 16.2 MPa for the 100% break test, which was equal to the specified pressurizer SRV simulator opening set point. However, the SRV did not open because the actual set point was slightly higher but within the specified tolerance of the specified set point.

The peak primary pressure for all three break size cases occurred at about 4 s after SCRAM in the loop cold legs (Figure 49). The measured pressures exhibit a very slight sensitivity to break size with peak values of 16.37, 16.41, and 16.42 MPa for the 100, 50, and 14.3% break size cases, respectively. These pressures represent differences of about 0.51, 0.65, and 0.66 MPa between the high pressurizer pressure trip set point (15.86 MPa) and the peak system pressure. These pressure differences would have been even greater if the unaffected loop steam generator primary-to-secondary heat transfer had not been enhanced due to the substantial intersecondary flow, as discussed in the secondary response section. Particularly for the 100% break case where the intersecondary flow increased the unaffected loop steam generator primary

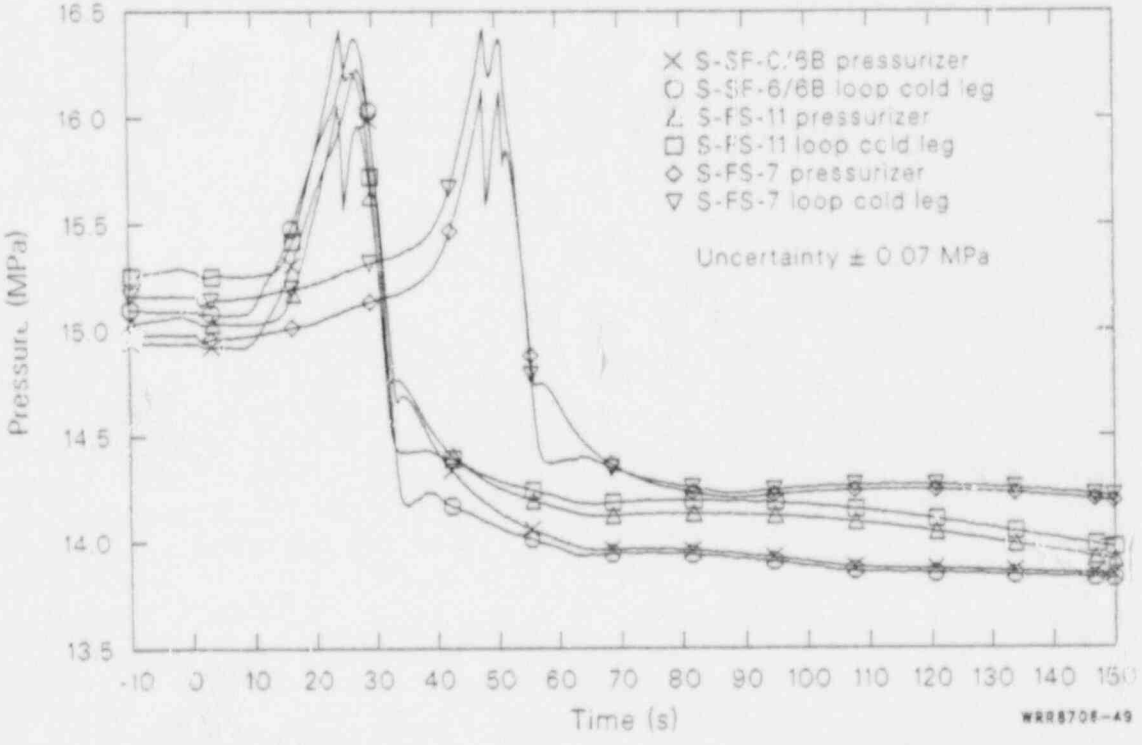

Figure 49. Comparisons of pressurizer and loop cold leg pressures during the blowdown phases of 100, 50, and 14.3% FWLB experiments S-FS-6/6B, S-FS-11, and S-FS-7.

energy removal, reducing the net primary energy balance deficit associated with losing the affected loop steam generator primary energy removal. As pointed out in the *Primary Pressure Response* subsection, had the net energy deficit equaled the amount associated with the affected loop steam generator heat sink, an integrated energy addition analysis predicts a peak primary pressure of 16.42 MPa for the loop cold leg. This is very close to the measured peak pressure for the other two break size cases. Without the intersecondary flow resulting from the failed check valve, it is conceivable that the unaffected loop secondary primary energy removal could decrease somewhat before SCRAM producing an even larger primary energy deficit. Thus, the failed check valve assumption may not be a conservative assumption.

The pressure responses for the remainder of the transients were qualitatively similar with only some minor differences in the timing of events and magnitude of the pressure. The trends were, however, identical. The core power decay, moderated slightly by the normal steam flow control valve (turbine stop valve simulators) closures, initiated a rapid cooldown and depressurization of the primary fluid system at about 4 s after SCRAM for all three break size cases. This rapid depressurization continued until loop flow reductions occurred in response to the loss of offsite power at SCRAM. The loop flow reductions initiated a reduction in the unaffected loop steam generator primary-to-secondary heat transfer, which reduced the rate of primary cooling during the initial core power decay. This continued until the pump coastdowns were completed at about 41 s after SCRAM. The unaffected loop steam generator primary energy removal rate was then reduced as natural circulation flow was being established. This produced a period of slight heating of the primary fluid system, which continued until the natural circulation flow was finally established about 15 s later. During this period, the primary pressure increased slightly in response to the slight heating. Following the establishment of natural circulation flow, the primary energy removal via the unaffected loop steam generator recovered to the level of the core power, aided by the continued intersecondary flow. This resulted in a period of gradual primary fluid cooling and depressurization, with rates varying in a manner directly proportional to the intersecondary flow rates. The rates of cooling and depressurization were moderated following MSIV closure by terminating the intersecondary flow. For all three break size cases, the primary fluid system then entered a stage of very gradual cooling and depressurization under the influence of the unaffected loop steam generator auxiliary feedwater injection energy removal, and the slight system leakage.

Primary Hydraulic Response Comparisons. The primary hydraulic response exhibited the same basic trends for all three break sizes. The hydraulic response of the primary fluid system during all three cases is characterized by a rapid expansion of liquid into the pressurizer. As the affected loop heat sink rapidly degrades, the primary liquid heats up and expands into the pressurizer, as shown in Figure 50. For all three cases, the rate of the expansion was determined by the initial primary pressure and temperature, initial pressurizer vapor volume, energy balance, and pressurizer surge line hydraulic resistance. The initial primary pressure and temperature determine the initial energy content of the primary fluid system. The amount of the primary liquid expansion (increase in the liquid specific volume) was determined by the integrated energy addition to the primary liquid and the initial energy content of the primary liquid. The rate of the primary liquid expansion was determined primarily by the rate of the energy addition (the impetus for the expansion), and the resistance to flow through the pressurizer surge line and work required to compress the vapor volume in the pressurizer (the resistances to the expansion). It was also determined to some extent by the initial energy content of the primary fluid system, as will be discussed in the next section. As discussed in the *Primary Hydraulic Response* subsection, during the rapid expansion of liquid into the pressurizer, the predominant factors determining the pressure differential between the primary loop and the pressurizer are the rate of energy addition to the primary system fluid and the surge line hydraulic resistance. The greater rate of primary energy addition for the 50 and 14.3% break size cases caused a greater pressure difference to be developed across the surge line due to the greater volumetric rate of liquid expansion through the surge line into the pressurizer. For all three break size cases, the primary liquid expansion continued until about 3 to 4 s after SCRAM, when the core power decay produced a net energy removal from the primary fluid system. The liquid then contracted as the primary system cooled and the liquid specific volume decreased. For the remainder of the blowdown phase of all three transients, the primary liquid flowed out of the pressurizer and into the loop hot leg under the influence of the continued cooling provided by the unaffected loop steam generator and slight primary fluid system leakage.

Primary Thermal Response Comparisons. The measured primary thermal responses for the three

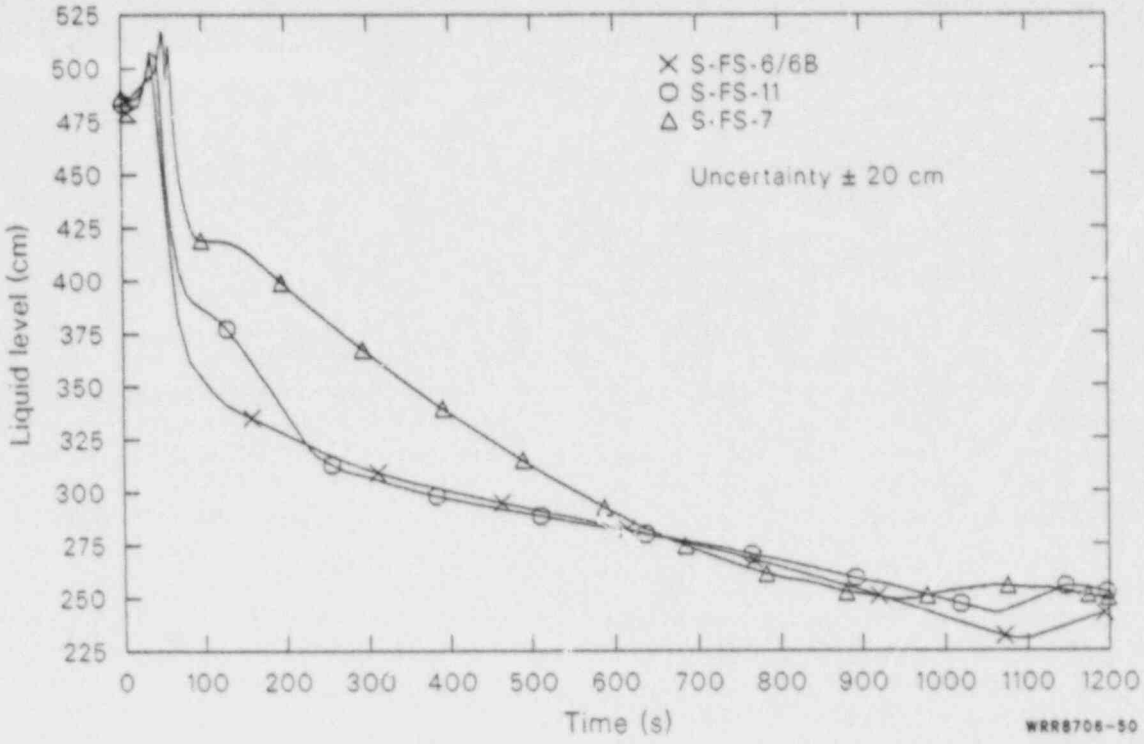

Figure 50. Comparisons of pressurizer overall collapsed liquid levels during the blowdown phases of 100, 50, and 14.3% FWLB experiments S-FS-6/6B, S-FS-11, and S-FS-7.

different break size cases are very similar. The differences noted were in the timing of events and thermal response to the different unaffected loop steam generator energy removal characteristics for the largest break size case. The thermal response of the primary fluid system during all three bottom main feedwater line break secondary LOCAs was characterized by a rapid heatup of primary liquid. As shown in Figure 51, before the degradation in the affected loop steam generator primary-to-secondary heat transfer, the primary energy balance is maintained by the continued normal steam flow, intersecondary flow, and break flow for the secondaries. As the affected loop heat sink rapidly degrades, the primary energy balance is lost and energy is added to the primary liquid causing the liquid to rapidly heat up. This continues until about 3 to 4 s after SCRAM, when the core power decays to a level below the unaffected loop steam generator primary energy removal rate.

The primary pressure response was controlled primarily by the primary energy balance for all three break size cases because the pressurizer to primary hot leg pressure difference did not increase significantly during the insurge. During the period of primary heatup, the primary fluid average temperature (Figure 52) increased by about 4.5 K for all three break size cases. This represents a the total primary energy addition during the heatup of about 2800 kJ for the 100% break case, and about 3150 kJ for the 50 and 14.3% break cases. The smaller total energy addition for the 100% break case is a result of the increased unaffected loop steam generator primary-to-secondary heat transfer that was caused by the increased intersecondary flow.

For the C-E System 80 plant, the affected loop steam generator comprises one-half of the total available heat sink versus one-fourth for the Semiscale Mod-2C Type III affected loop steam generator. The rate of primary energy addition would, therefore, be approximately twice as great for the C-E System 80 plant, which would produce a substantially greater pressurizer insurge rate and a substantially greater pressure drop through the surge line. Thus, the pressure drop through the surge line would have a much greater effect on the primary pressure response than observed in the Semiscale Mod-2C data.

The loop hot and cold leg fluid temperature responses (Figures 33, 53, and 54) show the same characteristic responses for all three break size cases. In all three cases, the affected loop cold leg

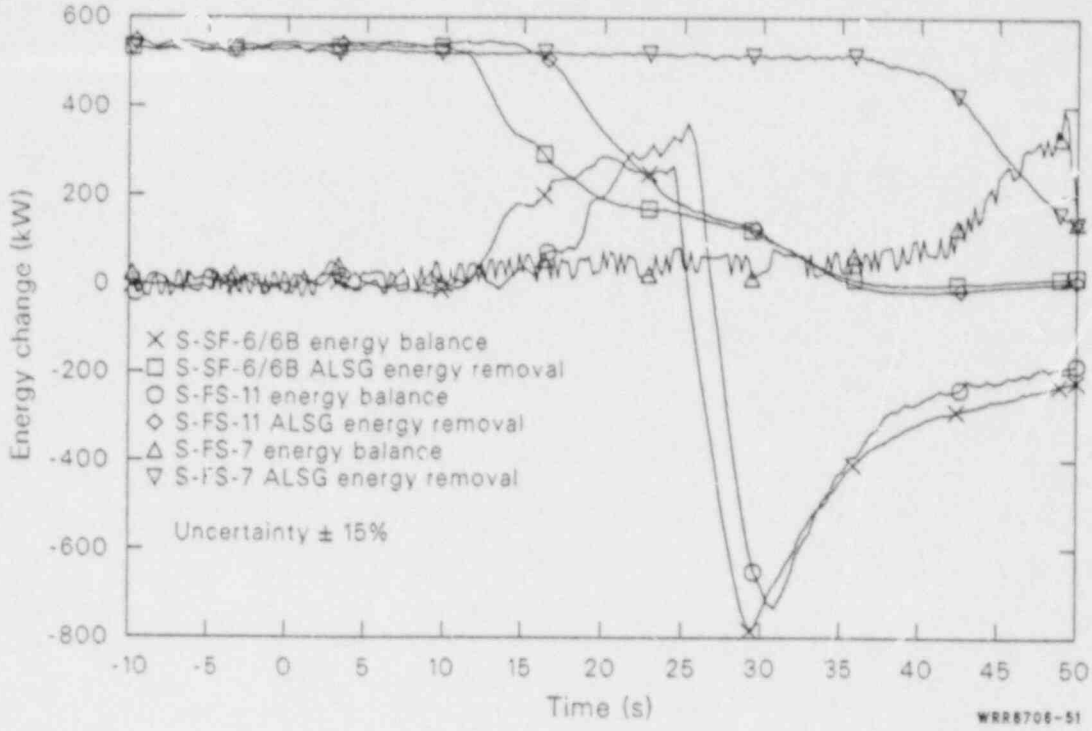

Figure 51. Comparisons of affected loop steam generator primary energy removal and primary fluid system energy balances during the blowdown phases of 100, 50, and 14.3% FWLB experiments S-FS-6/6B, S-FS-11, and S-FS-7.

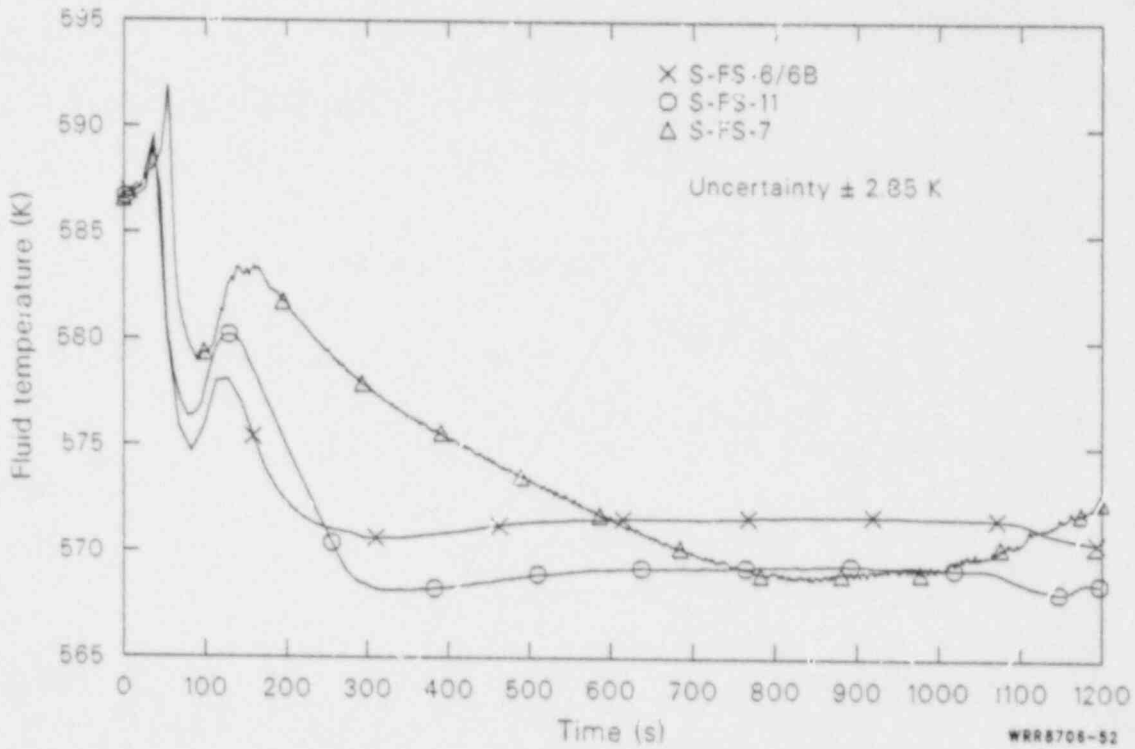

Figure 52. Comparisons of average primary fluid temperatures during the blowdown phases of 100, 50, and 14.3% FWLB experiments S-FS-6/6B, S-FS-11, and S-FS-7.

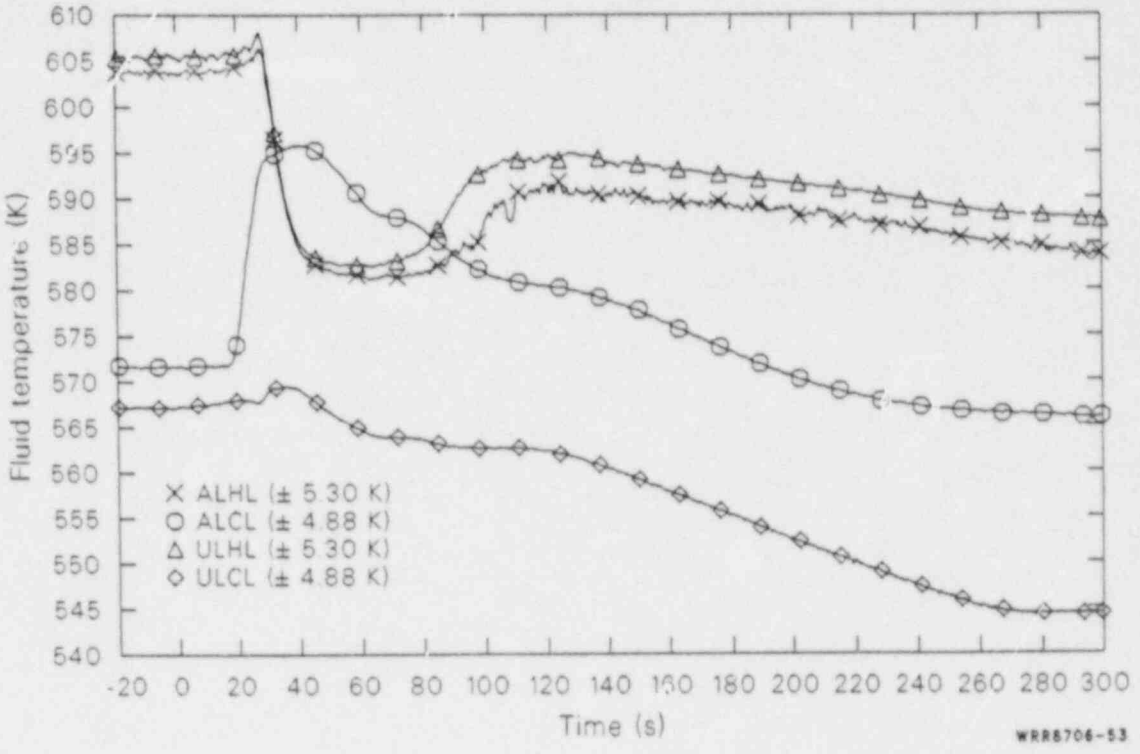

Figure 53. Affected and unaffected loop hot and cold leg fluid temperatures during the blowdown phase of 50% FWLB experiment S-FS-11.

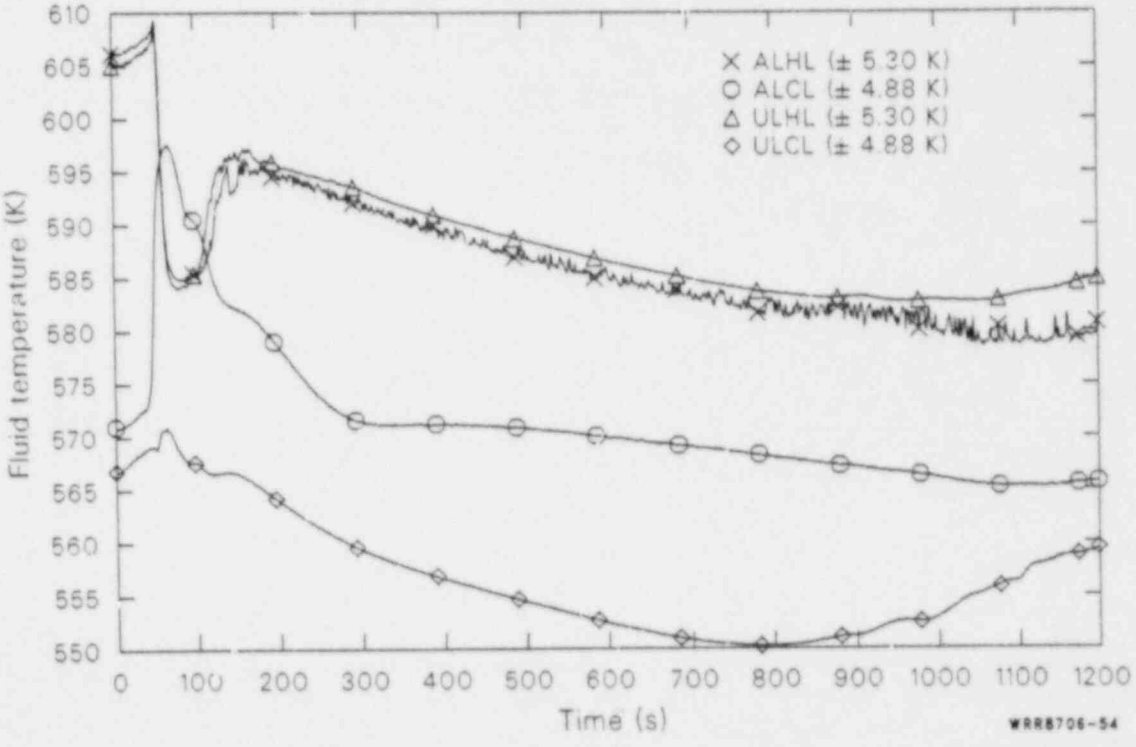

Figure 54. Affected and unaffected loop hot and cold leg fluid temperatures during the blowdown phase of 14.3% FWLB experiment S-FS-7.

fluid temperature exceeds the hot leg fluid temperature following the loss of the affected loop heat sink. As discussed in the *Primary Thermal Response* subsection, this observed response is a result of the loss of the affected loop heat sink and the increased loop transit time due to the reduced loop flows following loss of offsite power.

For all three break size cases, the primary fluid system thermal response moderated following the loop flow reductions as the system transitioned to a natural circulation mode of heat transfer. As the natural circulation flow was being established, the primary fluid was gradually heating as evidenced by the average fluid temperature increase. Once the natural circulation flow was established, as evidenced by the unaffected loop hot leg to cold leg temperature difference reaching a maximum, the system entered a phase of gradual cooling until MSIV closure. Following MSIV closure, the energy removal provided by the steam flow from the unaffected loop steam generator to the affected loop steam generator was lost leaving the unaffected loop steam generator auxiliary feedwater as the only source of energy removal. This caused the primary fluid thermal response to moderate even further, exhibiting a very gradual cooling through the end of the blowdown phase for all three break size cases.

System Response to Plant Stabilization Operations

The system stabilization phase of tests S-FS-6, S-FS-7, and S-FS-11 was performed, for the most part, in accordance with the guidance provided in the Waterford Unit No. 3 (a C-E System 80 plant) EOPs[12,28] for recovery from a secondary transient. The system stabilization for the tests involved affected loop steam generator auxiliary feedwater termination, SI (HPIS) termination, pressurizer internal heater operation, normal charging/letdown operation, and an unaffected loop steam generator steam and feed operation. Stable in this sense meant maintaining: (a) the pressurizer liquid level[a] at 245 ± 10 cm; (b) the unaffected loop steam generator liquid level[a] between 910 and 1000 cm; (c) the unaffected loop steam generator secondary pressure ≤6.98 MPa; and (d) the unaffected loop hot leg subcooled margin ≥27.8 K.

a. Collapsed liquid level referenced to the zero reference.

Examination of the Semiscale Mod-2C system response to the plant stabilization operations provides invaluable insight into both the effectiveness of the EOP-specified operations in stabilizing the plant, and the characteristic response to the stabilization operations. The characteristic response to the stabilization operations was very similar for all three tests. Therefore, the detailed discussion of the characteristic system response to the stabilization operations will be limited to the test S-FS-6 results. The overall system response for test S-FS-6 will be discussed first. This will be followed by discussions of the system response to normal charging/letdown operations and pressurizer internal heater operations. A brief comparison to the results for tests S-FS-7 and S-FS-11 will be made at the end of this section.

Overall System Response to Stabilization Operations. The stabilization operations were specified to be initiated at the end of the blowdown phase of the test when operator identification of the transient and operator intervention would be expected to occur. For Test S-FS-6, the stabilization operations were initiated at 600 s because MSIV closure had already occurred. At 600 s, the affected loop steam generator auxiliary feedwater flow (Figure 55) was terminated. Because the primary (unaffected loop hot leg) subcooled margin was below 27.8 K (Figure 56), the SI (HPIS) flow could not be terminated at 600 s. The pressurizer internal heaters (Figure 56) were turned on at 720 s to recover the primary subcooled margin. At 900 s, the subcooled margin reached 27.8 K while the pressurizer collapsed liquid level (Figure 57) was at 250 cm. Because this satisfied the SI termination criteria, the SI (HPIS) flow was terminated. At that time, the pressurizer pressure (Figure 57) was 14.5 MPa, unaffected loop steam generator liquid level (Figure 58) was at 510 cm; unaffected loop steam generator secondary pressure (Figure 58) was 6.42 MPa, and the average primary fluid temperature (Figure 59) was 572 K. Because the primary pressure remained above the HPIS shutoff head (12.324 MPa), no HPIS injection occurred. Once the pressurizer internal heaters had recovered the subcooled margin to within the specified tolerances (see Reference 2 for the specified tolerances), they were turned off (at about 1054 s). At this point, the pressurizer liquid level was below the specified range for letdown operations; therefore, letdown was not used.

The limiting criteria in achieving stable conditions was the recovery of the unaffected loop steam

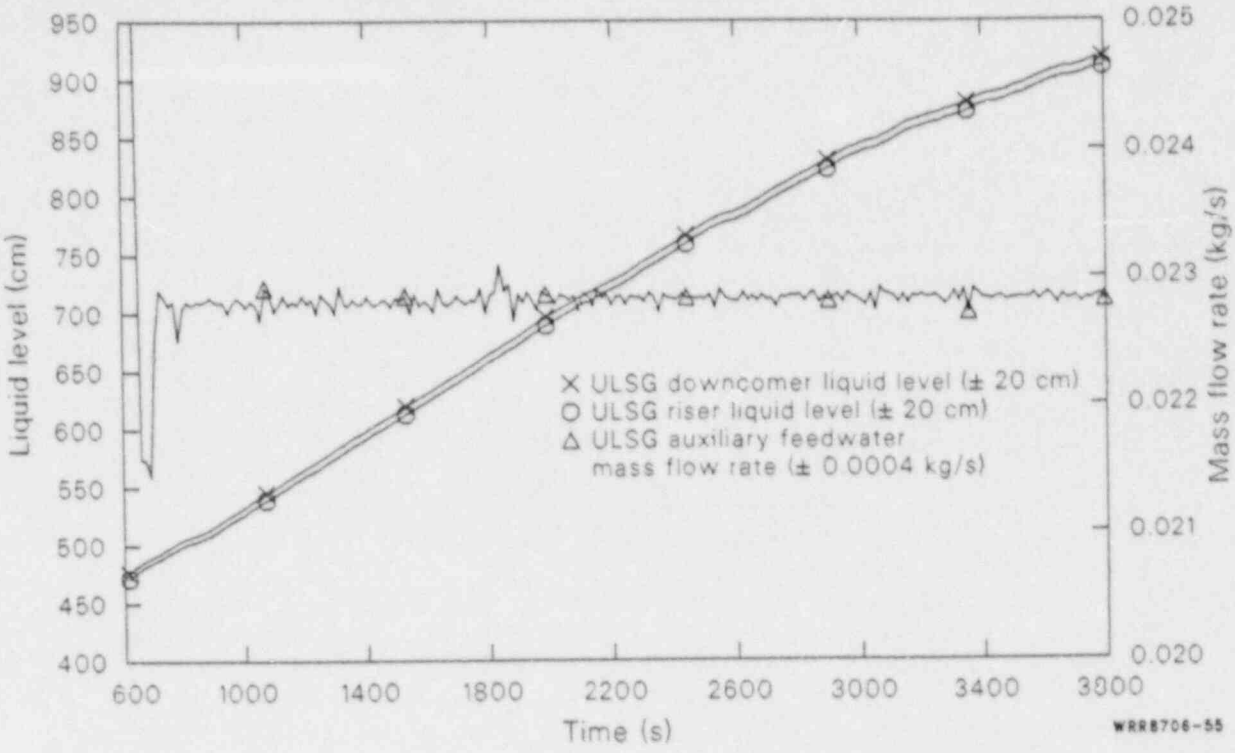

Figure 55. Unaffected loop steam generator auxiliary feedwater mass flow rate and downcomer and riser overall collapsed liquid levels during the stabilization phase of 100% FWLB experiment S-FS-6 (600 to 3800 s).

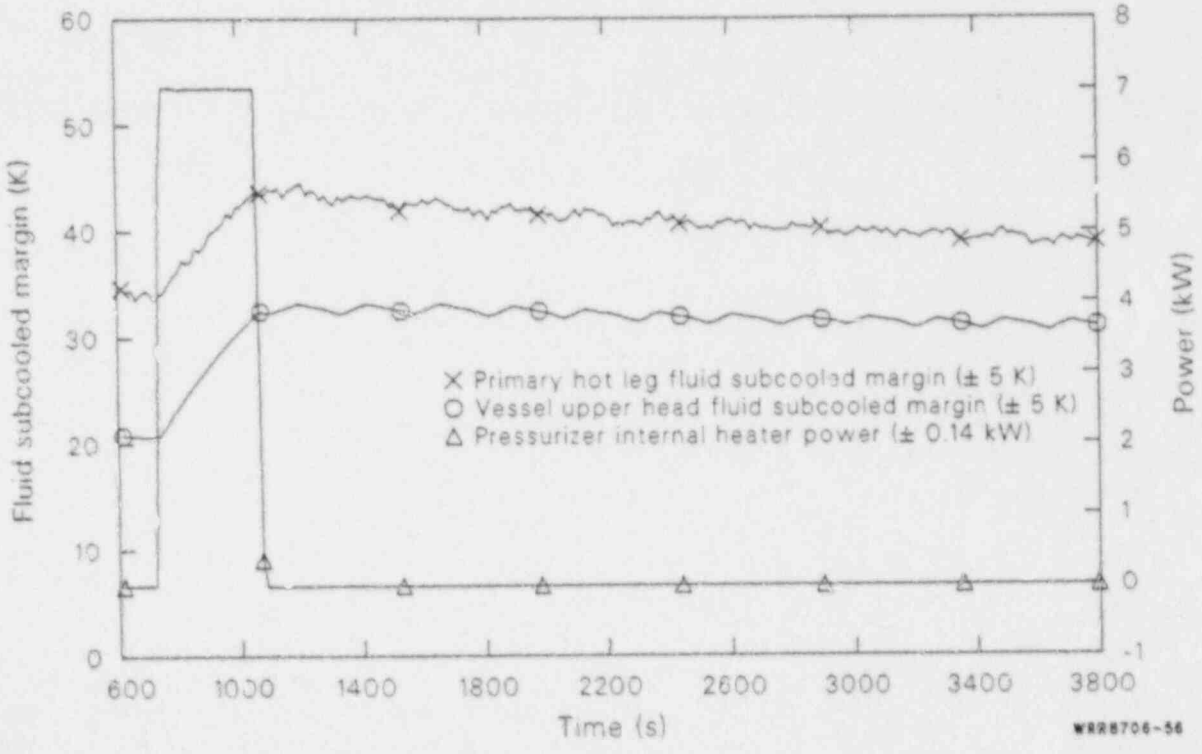

Figure 56. Primary hot leg and vessel upper head fluid subcooled margins and pressurizer internal heater power during the stabilization phase of 100% FWLB experiment S-FS-6 (600 to 3800 s).

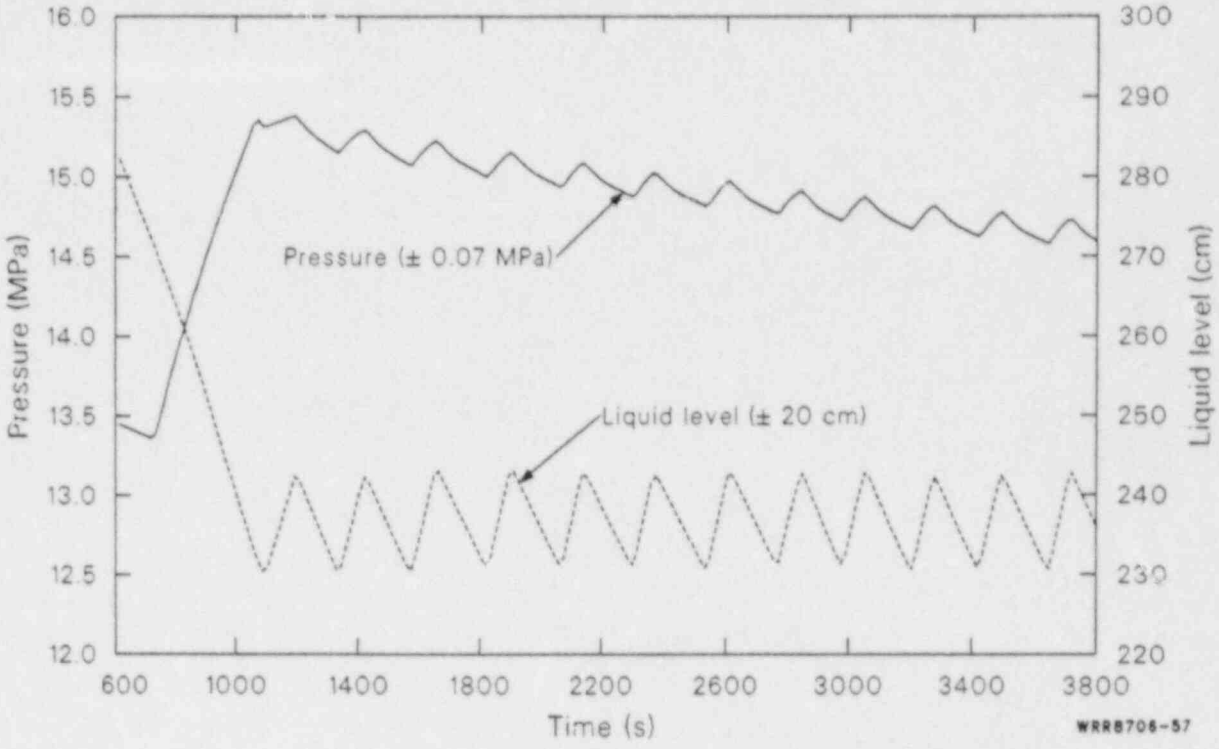

Figure 57. Pressurizer pressure and overall collapsed liquid level during the stabilization phase of 100% FWLB experiment S-FS-6 (600 to 3800 s).

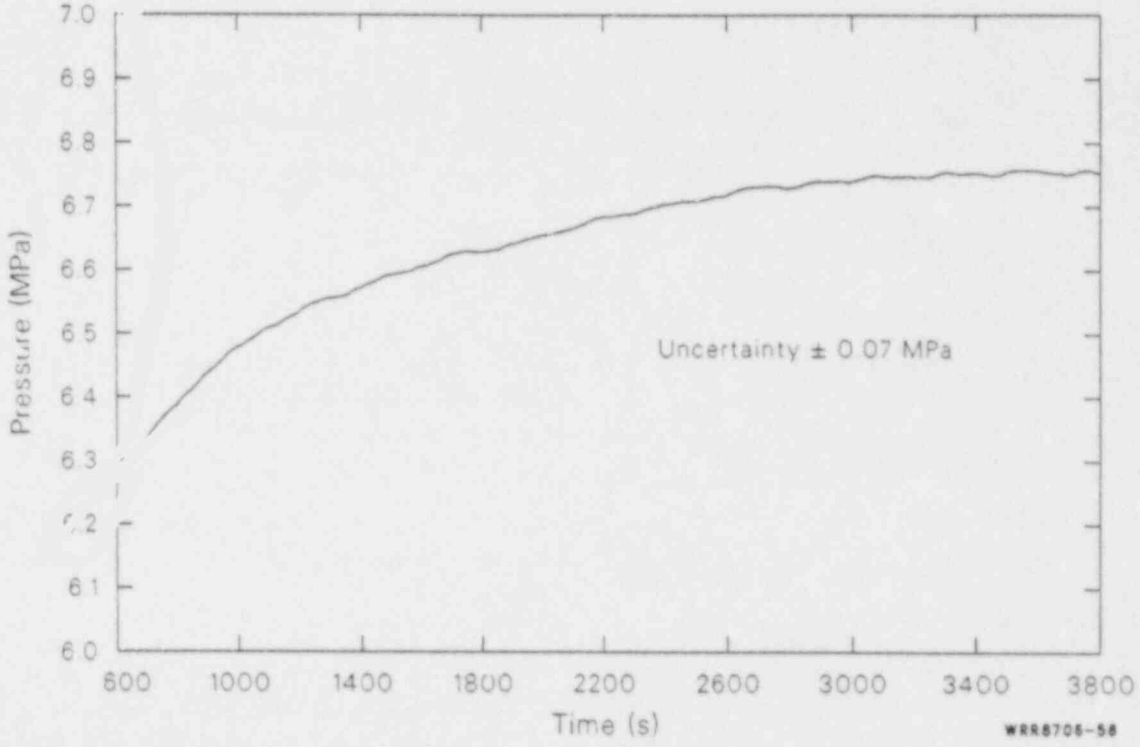

Figure 58. Unaffected loop steam generator secondary pressure during the stabilization phase of 100% FWLB experiment S-FS-6 (600 to 3800 s).

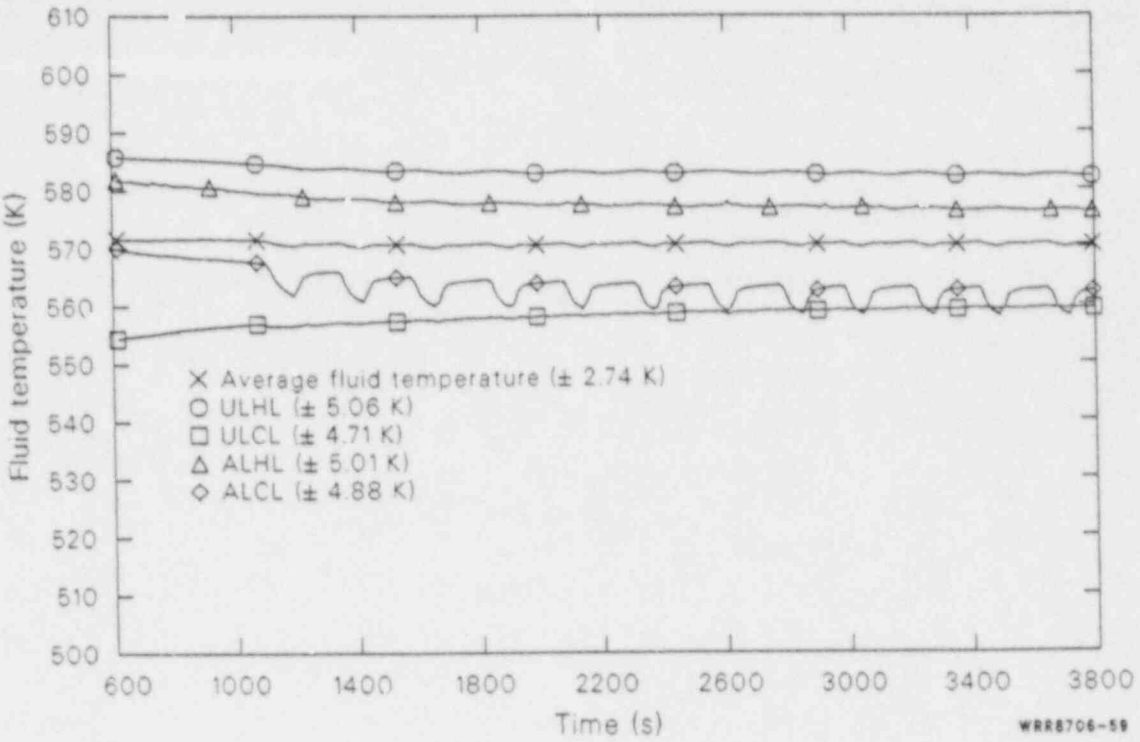

Figure 59. Affected and unaffected loop hot and cold leg and average primary fluid temperatures during the stabilization phase of 100% FWLB experiment S-FS-6 (600 to 3800 s).

generator liquid level. To reach the specified stable conditions, it was necessary to maintain the above conditions in the specified tolerances while the unaffected loop steam generator liquid level was recovered by auxiliary feedwater flow (Figure 55). Normal charging (Figure 60) was cycled 12 times, starting at 1081 s, to maintain the pressurizer liquid level within the specified conditions. The primary subcooled margin remained above 27.8 K for the remainder of the stabilization phase so that no further pressurizer internal heater operations were required. The unaffected loop steam generator secondary pressure increased very gradually as the subcooled auxiliary feedwater was heated by the primary system. However, because the pressure remained below 6.98 MPa, it was not necessary to cycle the atmospheric dump valve (ADV). The auxiliary feedwater continued to refill the unaffected loop steam generator and recovered the liquid level to 910 cm at about 3800 s. Because all of the other system stabilization criteria were also satisfied, the system was considered to be stabilized at 3800 s.

The automatic actions performed by the safety systems during the blowdown phase of the test left the Semiscale Mod-2C system in a quasi-stable state, but at conditions that did not ensure sufficient control of the system. The stabilization operations performed were very effective in stabilizing the Semiscale Mod-2C system at conditions that ensured sufficient control of the system. The guidance provided by the EOPs was both appropriate and effective in stabilizing and regaining control of the system. No upper head voiding occurred as the upper head fluid remained highly subcooled (Figure 56); the limiting criteria in regaining control of the system was the recovery of the unaffected loop steam generator secondary liquid level.

The effectiveness of the stabilization operations in stabilizing the plant may be better understood by considering the system response to the various operations performed. The next subsections discuss the system response to the normal charging/letdown operations and the pressurizer internal heater operations.

System Response to Normal Charging/Letdown Operation During Stabilization. Normal charging/letdown were used during the stabilization phase to establish and maintain the pressurizer collapsed liquid level within the specified tolerance. Letdown was not used. Normal charging flow was approximately 0.0134 kg/s for

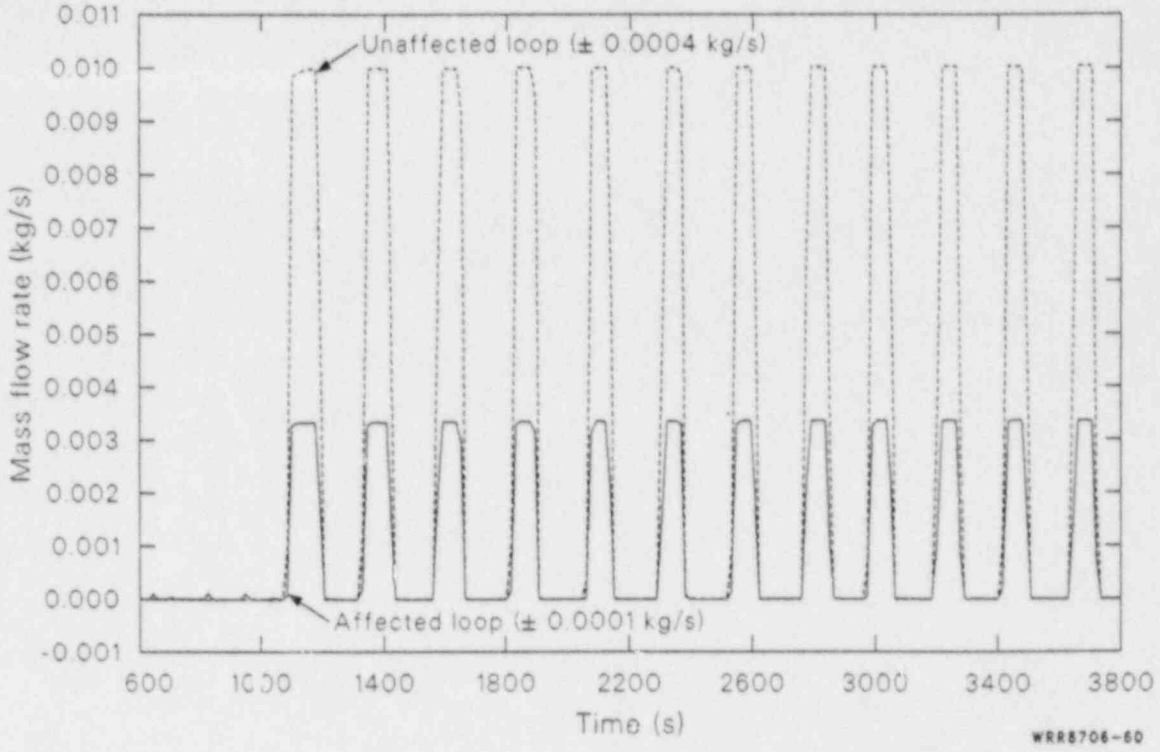

Figure 60. Affected and unaffected loop normal charging mass flow rates during the stabilization phase of 100% FWLB experiment S-FS-6 (600 to 3800 s).

the entire range of stabilization pressures. This flow rate adequately controlled the pressurizer level. The injection of cold water and the low loop flow produced the oscillations observed in the affected loop cold leg temperature (Figure 59); the only noticeable effect. However, one result of the system leakage and normal charging makeup was a net loss of energy from the system, which was most noticeable in the pressurizer pressure response (Figure 57). As the system leakage caused the pressurizer to lose inventory, the resulting expansion of the steam volume caused a slight reduction in pressure. As the normal charging flow recovered the pressurizer inventory, the repressurization of the pressurizer due to compression of the steam volume was not as large as the preceding reduction. This was caused by subcooled liquid entering the pressurizer from the unaffected loop hot leg and surge line and removing sufficient energy to condense some of the steam from the steam space. Because the steam volume was preserved (because the liquid level was preserved), the reduction in steam mass caused the reduction in pressurizer pressure. The situation was aggravated by the additional cooling of the insurge fluid due to the surge line heat loss (Figure 61). The net effect was a gradual reduction in the pressurizer pressure.

System Response to Pressurizer Internal Heater Operation During Stabilization. Pressurizer internal heaters were used to maintain the primary system subcooled margin by maintaining primary pressure control in the pressurizer. Because the pressurizer fluid was at saturation when the internal heaters were operated, the energy addition provided by the heaters generated steam which: decreased the pressurizer vapor specific volume (because the volume occupied by the steam was constant); and raised the saturation temperature of the pressurizer liquid. The net result was an increase in the pressurizer saturation pressure. The pressurizer internal heater operations were very effective in controlling the primary pressure during the stabilization phase of the transient.

Comparisons of Stabilization Phase Responses. The system stabilization phase of tests S-FS-6, S-FS-7, and S-FS-11 involved the same recovery operations and stabilization criteria. The basic response of the system

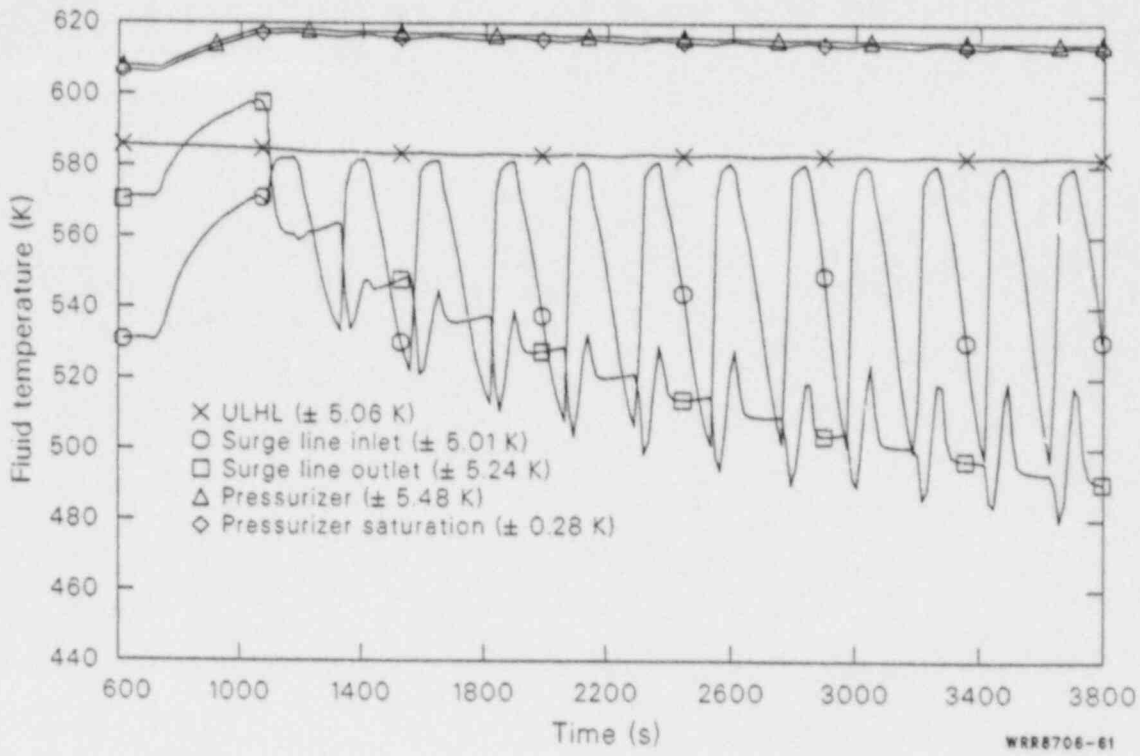

Figure 61. Unaffected loop hot leg, pressurizer surge line inlet and outlet, pressurizer, and pressurizer saturation fluid temperatures during the stabilization phase of 100% FWLB experiment S-FS-6 (600 to 3800 s).

to the stabilization operations was the same for all three tests with differences primarily in the timing of events. Figures containing the pertinent parameters (the same parameters as those presented for test S-FS-6), for tests S-FS-7 and S-FS-11 may be found in Appendix D (Figures D-19 through D-32).

The stabilization operations were specified to be initiated at the end of the blowdown phase of the test when operator identification of the transient and operator intervention would be expected to occur. For the 100% and 50% break size cases (tests S-FS-6 and S-FS-11), the stabilization operations were initiated at 600 s because MSIV closure had already occurred. For the 14.3% break size case (test S-FS-7), the initiation of stabilization operations was delayed until 923 s due to the later MSIV closure timing. For all three tests, the first operation performed was terminating the affected loop steam generator auxiliary feedwater flow. Similarly, for all three tests, pressurizer internal heater operations were required to increase the primary subcooled margin and allow SI termination. The primary pressure remained above the HPIS shutoff head (12.324 MPa) for all three tests, so that no HPIS injection occurred. Letdown operations were not required for any of the tests.

The limiting criteria in achieving stable conditions for all three tests was the recovery of the unaffected loop steam generator liquid level. The smaller break sizes caused later MSIV closure timing, allowing greater unaffected loop steam generator inventory loss during the blowdown. Therefore, the time required to recover the unaffected loop steam generator secondary inventory was greater for the smaller break size cases. This was the major difference observed in the stabilization phase of the tests. The longer unaffected loop secondary refill time required that more normal charging operations be performed for tests S-FS-7 and S-FS-11 than for test S-FS-6. It also required that one additional pressurizer internal heater operation be performed for test S-FS-7. However, for all three tests, the unaffected loop secondary pressure remained below 6.98 MPa, so it was not necessary to utilize the ADV to limit the secondary pressure. The stabilization criteria were satisfied and the system stabilization phase was considered to be completed when the unaffected loop steam generator liquid level reached 910 cm (3800 s for test S-FS-6, 4055 s for test S-FS-11, and 5943 s for test S-FS-7).

The system response to the normal charging/letdown operations and the pressurizer internal

heater operations were the same for the three tests with the only differences occurring in the timing of events. For all three tests, the automatic actions performed by the safety systems left the system in a quasi-stable condition and the EOP-specified recovery operations were very effective in stabilizing the Semiscale Mod-2C system.

System Response to Plant Cooldown and Depressurization Operations (S-FS-6)

The objective of the cooldown and depressurization phase was to reduce the average fluid temperature and system pressure such that, in the course of the cooldown and depressurization, the vessel upper head subcooled margin reduced to ≤2 K. After the upper head subcooled margin reached ≤2 K, the system was monitored for upper head void formation. Because upper head void formation did not occur within 600 s, the system was depressurized to force a void formation. The first upper head void was then collapsed using the *fill and drain* method of upper head void collapse. A second void was then forced and was collapsed using the *pump restart* method. Following collapse of the second void, the system was shown to be in a controlled *forced flow* cooldown and depressurization, and the test was terminated. During the cooldown and depressurization, in the absence of an upper head void, the cooldown continued while maintaining: the pressurizer liquid level at 245 ± 10 cm; subcooled margin between 11.1 and 13.9 K; and the unaffected loop steam generator collapsed liquid level ≥700 cm. This was accomplished using combined operations of pressurizer internal heaters, normal charging/letdown, pressurizer auxiliary spray, and an unaffected loop steam generator steam and feed operation. This section discusses the thermal-hydraulic response of the system during the cooldown and depressurization to the point in time where the vessel upper head fluid subcooled margin had reached ≤2 K for 600 s (3800 to 10,600 s). The system response to vessel upper head void collapse operations will be discussed following this section.

This portion of the cooldown and depressurization was performed, for the most part, in accordance with the guidance provided in the St. Lucie Unit No. 2 (a C-E System 80 plant) EOPs (References 11, 29) for a natural circulation cooldown. With exception of the rate of depressurization, the EOP guidelines were followed to the extent possible. The primary depressurization was within the EOP guidelines up until about 4900 s, when the primary system pressure dropped below the specified minimum pressure for that time into the cooldown. This deviation from the EOP guidance was taken in light of limited test time (the EOP-guided cooldown would require 100,000 s to finish) and the desire to investigate vessel upper head void formation and collapse. The overall system response to the cooldown and depressurization operations will be discussed first. This will be followed by discussions of the effects of unaffected loop steam generator steam and feed operations and combined pressurizer auxiliary spray and internal heater operations on the system response.

Overall Response to System Cooldown and Depressurization Operations. The system stabilization criteria were met and cooldown and depressurization operations commenced 3800 s after transient initiation. At 3815 s, the controlled unaffected loop steam generator secondary depressurization was initiated by opening the ADV. Figure 62 shows the secondary pressure and illustrates the stairstep secondary depressurization at the specified rate of 0.71 MPa per decrement. The secondary pressure was maintained at the lower pressure for at least 600 s after each stairstep. At 3827 s, the controlled primary depressurization (Figure 62) was initiated by turning on the pressurizer auxiliary spray (Figure 63). The decreasing pressurizer pressure produced a corresponding primary subcooled margin reduction (Figure 63) to 11.1 K. Normal charging (Figure 64) was cycled on and off throughout this period to make up for the loss of pressurizer inventory due to small system leakage and primary shrinkage. Letdown (Figure 64) was also cycled on and off throughout this period to make up for the increase in pressurizer inventory due to pressurizer auxiliary spray mass addition. Pressurizer internal heaters (Figure 63) were cycled on and off to maintain the minimum primary subcooled margin at 11.1 K.

The unaffected loop steam generator secondary depressurization resulted in a primary system cooldown (Figure 65). The primary cooled down initially at a rate of approximately 25.6 K/h. Throughout the early cooldown period, the unaffected loop steam generator liquid level continued to decrease as ADV flow exceeded auxiliary feedwater flow (Figure 66). The rate of level decrease slowed as the ADV flow reduced, due to the secondary pressure reduction, to the range of the auxiliary feedwater flow. The auxiliary feedwater flow adequately controlled the secondary level since it did not decrease to 700 cm.

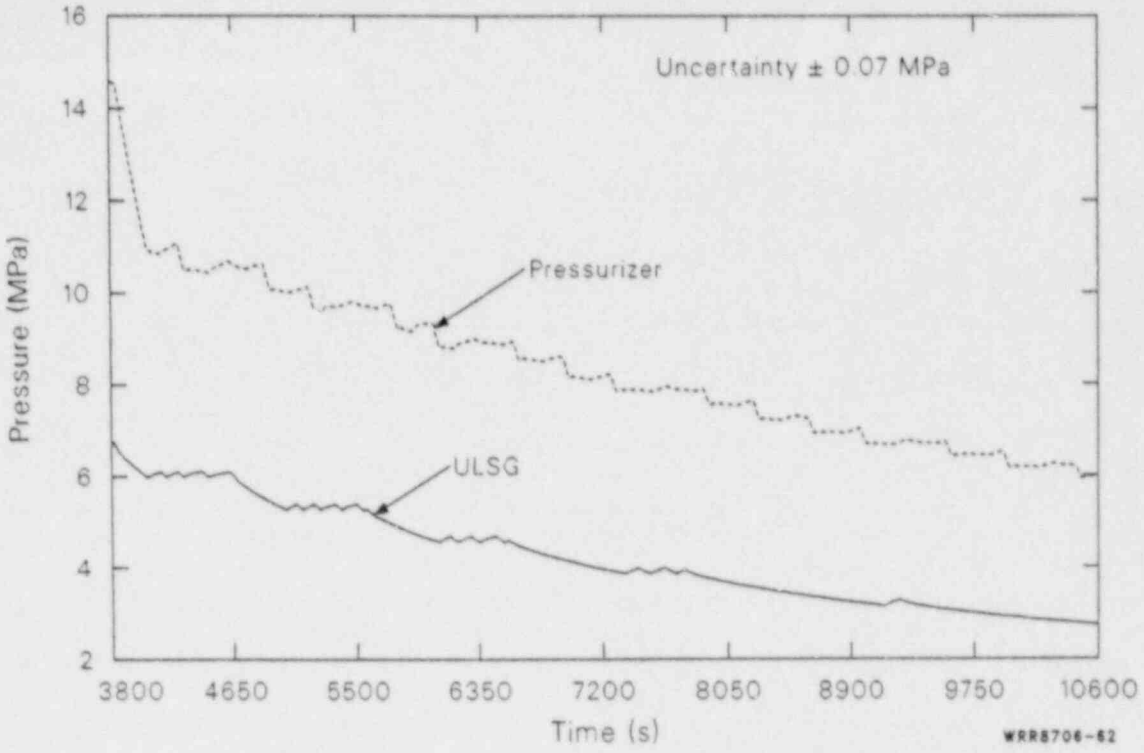

Figure 62. Pressurizer and unaffected loop steam generator secondary pressures during the plant cooldown and depressurization phase of 100% FWLB experiment S-FS-6 (3800 to 10,600 s).

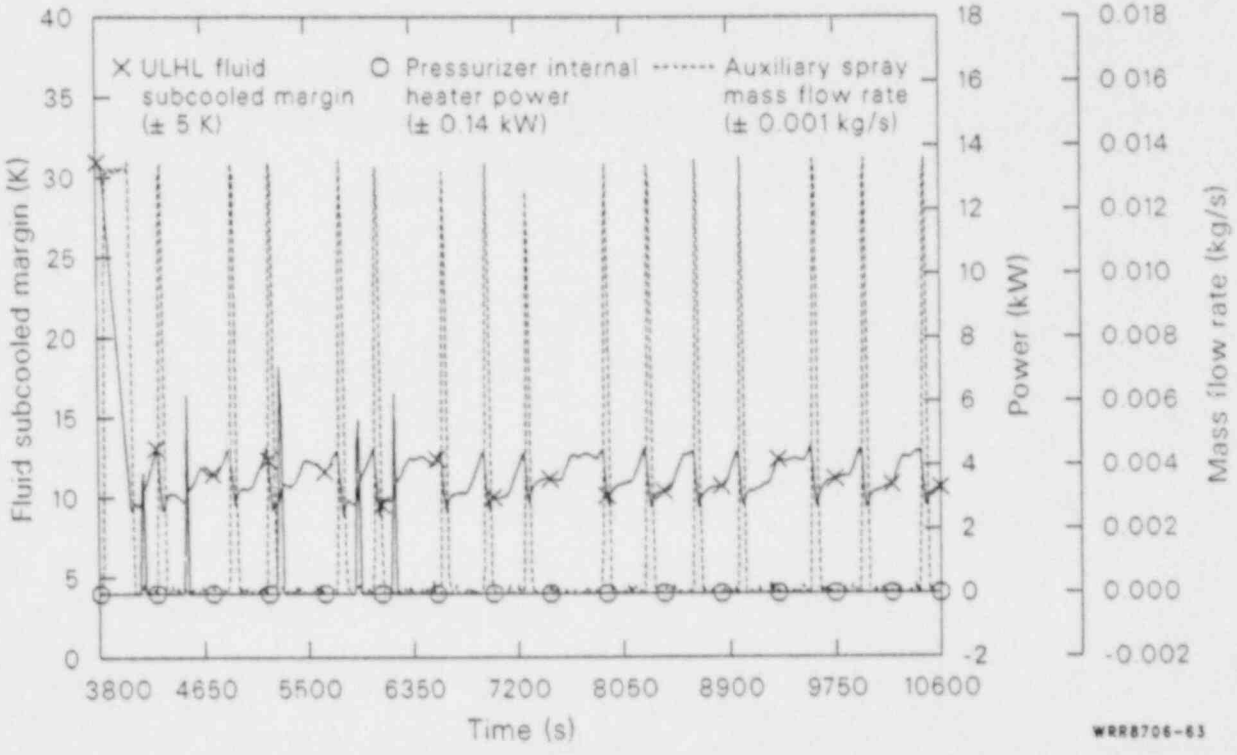

Figure 63. Unaffected loop hot leg fluid subcooled margin, pressurizer auxiliary spray mass flow rate, and pressurizer internal heater power during the plant cooldown and depressurization phase of 100% FWLB experiment S-FS-6 (3800 to 10,600 s).

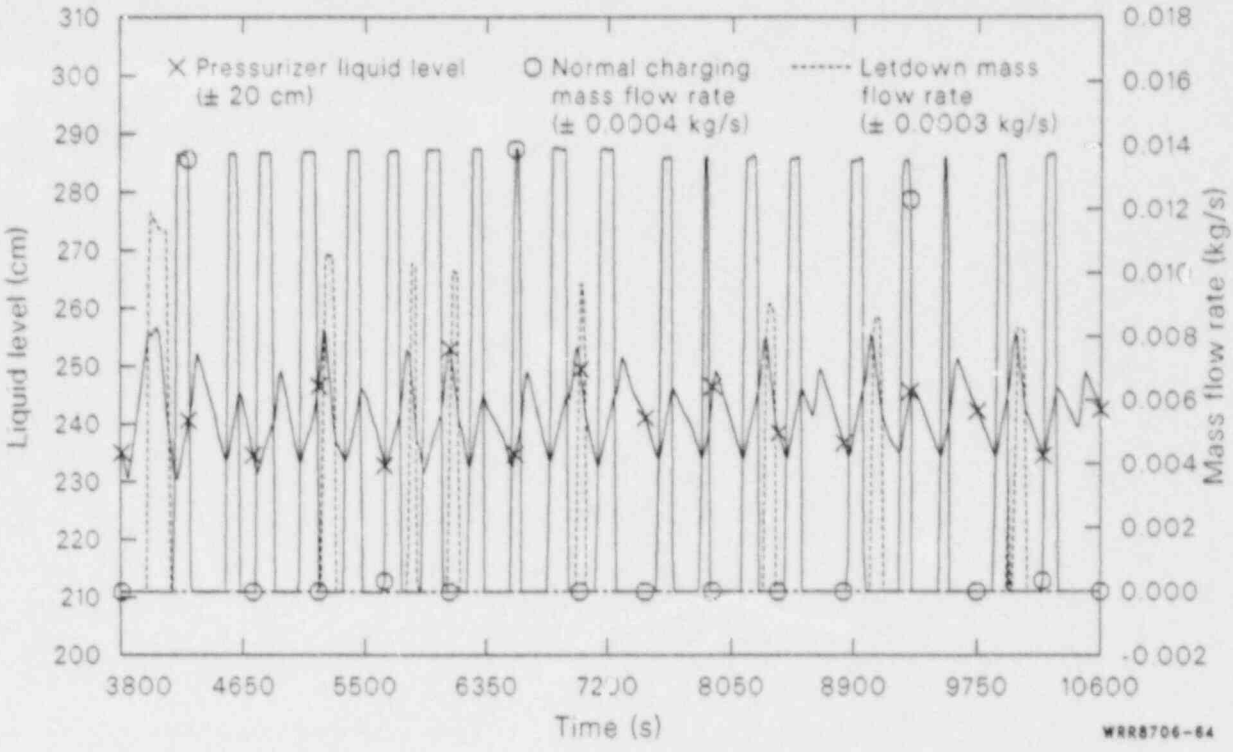

Figure 64. Pressurizer overall collapsed liquid level, total normal charging and letdown mass flow rates during the plant cooldown and depressurization phase of 100% FWLB experiment S-FS-6 (3800 to 10,600 s).

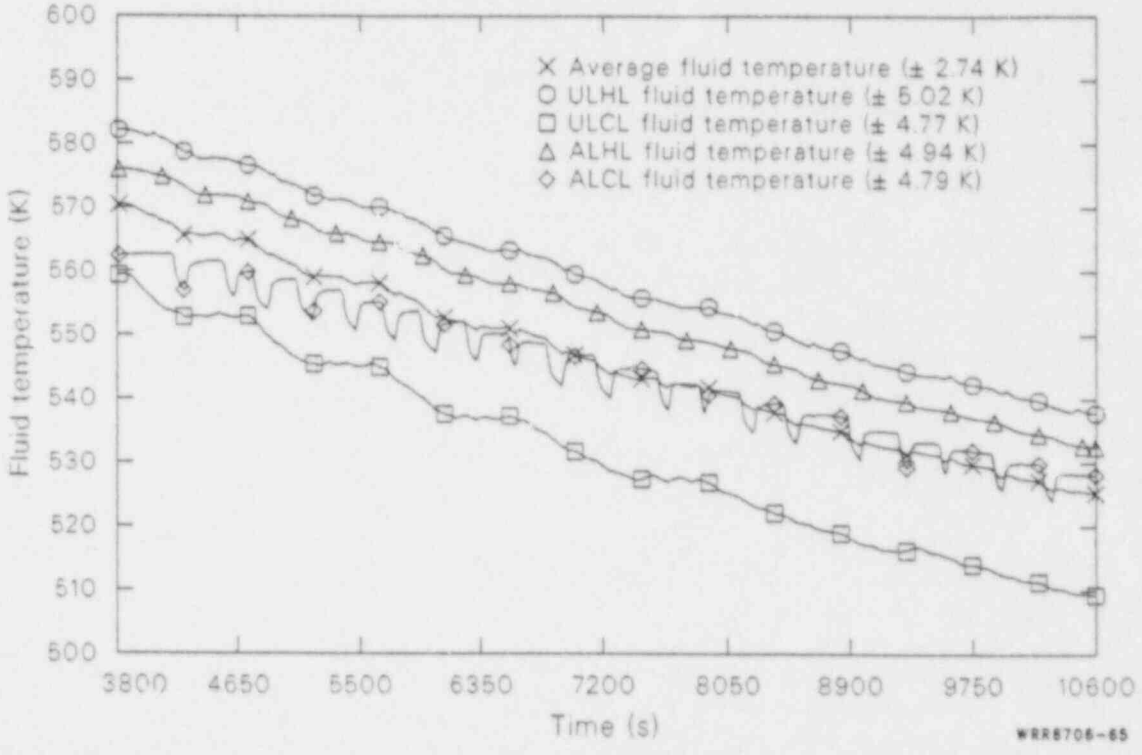

Figure 65. Affected and unaffected loop hot and cold leg and average primary fluid temperatures during the plant cooldown and depressurization phase of 100% FWLB experiment S-FS-6 (3800 to 10,600 s).

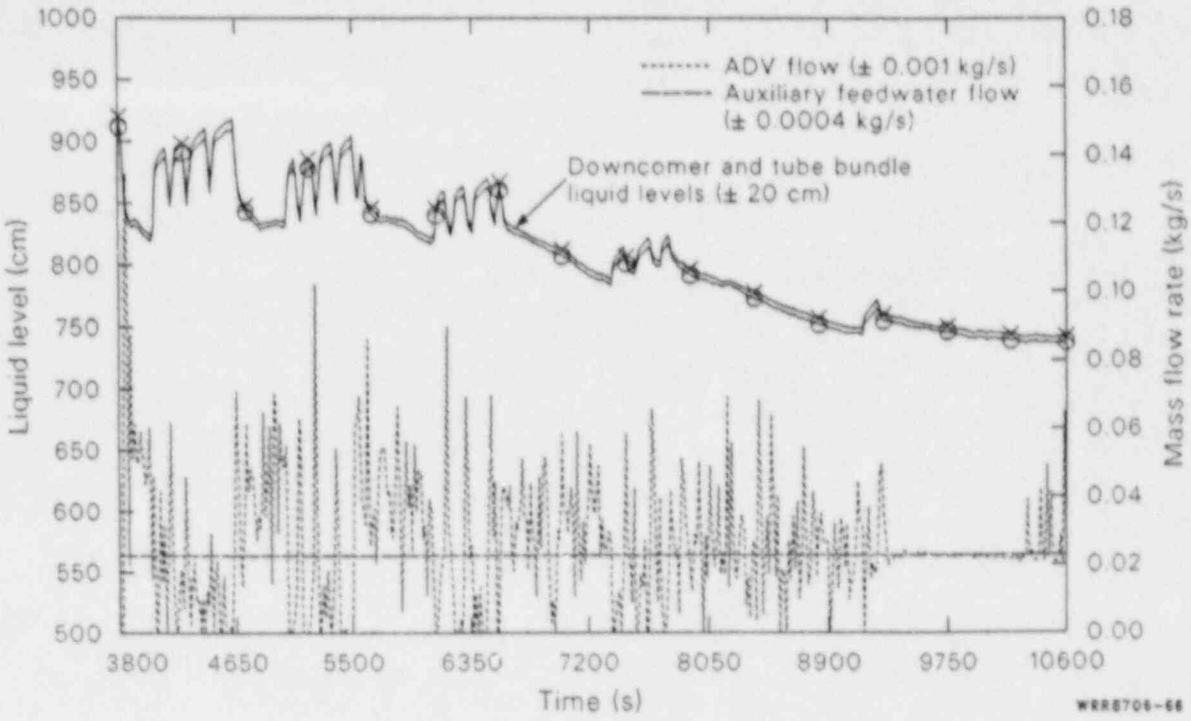

Figure 66. Unaffected loop steam generator downcomer and tube bundle overall collapsed liquid levels, and auxiliary feedwater and atmospheric dump valve mass flow rates during the plant cooldown and depressurization phase of 100% FWLB experiment S-FS-6 (3800 to 10,600 s).

The primary depressurization resulted in a reduction in the primary system subcooled margin (Figure 63). The pressurizer auxiliary spray was cycled 16 times during this portion of the test to reduce the primary pressure and maintain a maximum primary subcooled margin of 13.9 K above the cooling unaffected loop hot leg temperature (Figure 65). The lack of flow through the vessel upper head limited the cooling of the upper head fluid (Figure 67) so that, due to the continuous depressurization, the upper head subcooled margin (Figure 68) decreased continuously during this portion of the test. The pressurizer internal heaters (Figure 63) were cycled on and off five times during this portion of the test to increase the primary pressure and maintain a minimum primary subcooled margin of 11.1 K above the cooling unaffected loop hot leg temperature. Both operations were effective in maintaining a controlled primary depressurization. Normal charging was cycled 20 times and letdown was cycled 9 times to maintain the pressurizer liquid level within the specified conditions of 245 ± 10 cm (Figure 64).

The vessel upper head subcooled margin (Figure 68) reached 2 K at about 10,000 s. However, no upper head voiding was indicated during the 600-s observation period (between 10,000 and 10,600 s). This portion of the cooldown and depressurization was then considered to be complete and vessel upper head void recovery investigations were then initiated.

Effects of Unaffected Loop Steam Generator Steam and Feed Operation on the System Cooldown and Depressurization to Vessel Upper Head Fluid Saturation. The unaffected loop steam generator steam and feed operation consisted of steaming through the ADV and feeding with auxiliary feedwater. The intention of the stairstep secondary depressurization was to reduce the secondary saturation temperature resulting in a controlled primary system cooldown. The 0.71 MPa stairstep decrements shown in Figure 62 produced an average primary fluid temperature decrease of approximately 25.6 K/h between 3800 and 9200 s. The cooldown rate decreased slightly between 9200 and 10,600 s as the choked ADV mass flow rate and steam enthalpy decreased due to the decreased secondary pressure. This combination greatly reduced the energy removal capacity of the secondary ADV (Figure 69), and reduced the rate of primary cool down.

The unaffected loop steam generator steam and feed operations were successful in cooling down the

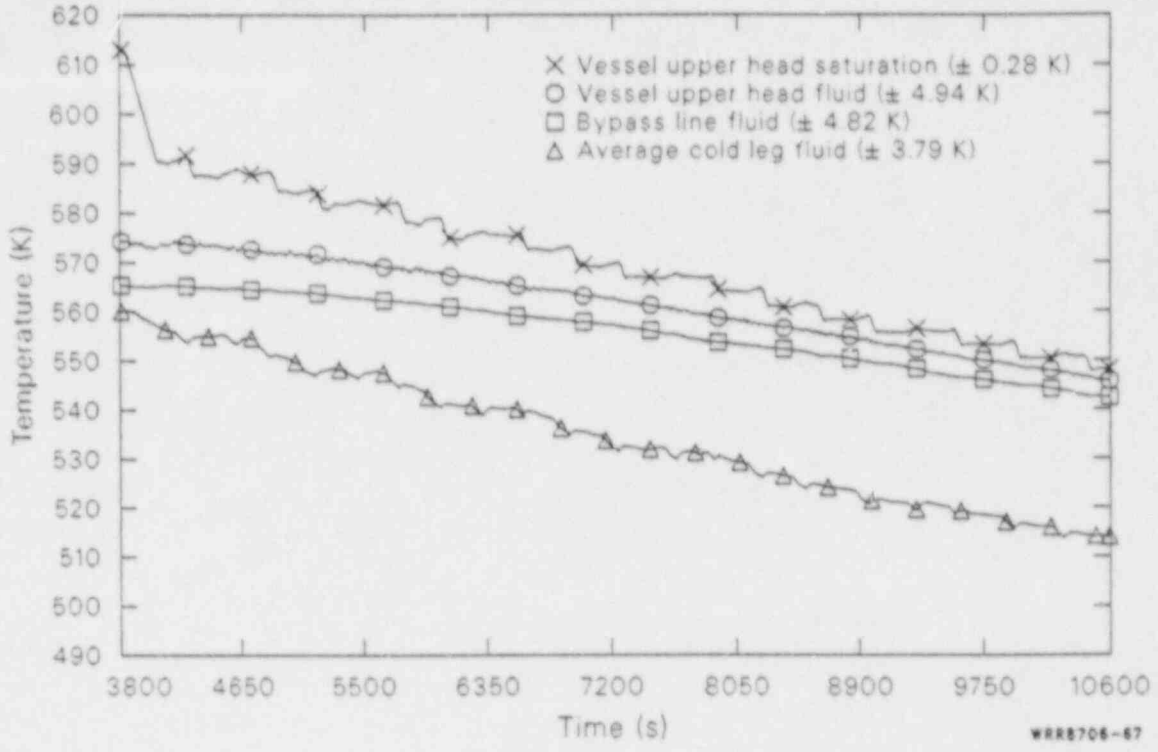

Figure 67. Average cold leg fluid, downcomer to vessel upper head bypass line fluid, vessel upper head fluid, and vessel upper head saturation temperatures during the plant cooldown and depressurization phase of 100% FWLB experiment S-FS-6 (3800 to 10,600 s).

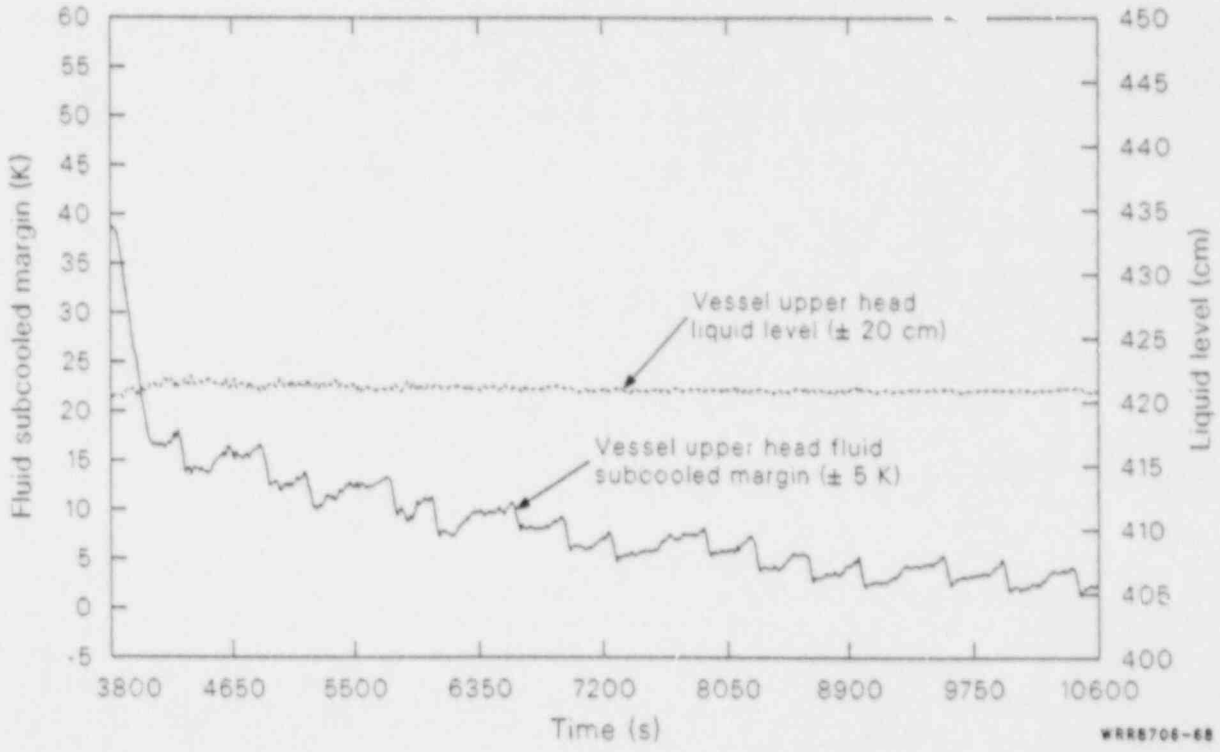

Figure 68. Vessel upper head collapsed liquid level and vessel upper head fluid subcooled margin during the plant cooldown and depressurization phase of 100% FWLB experiment S-FS-6 (3800 to 10,600 s).

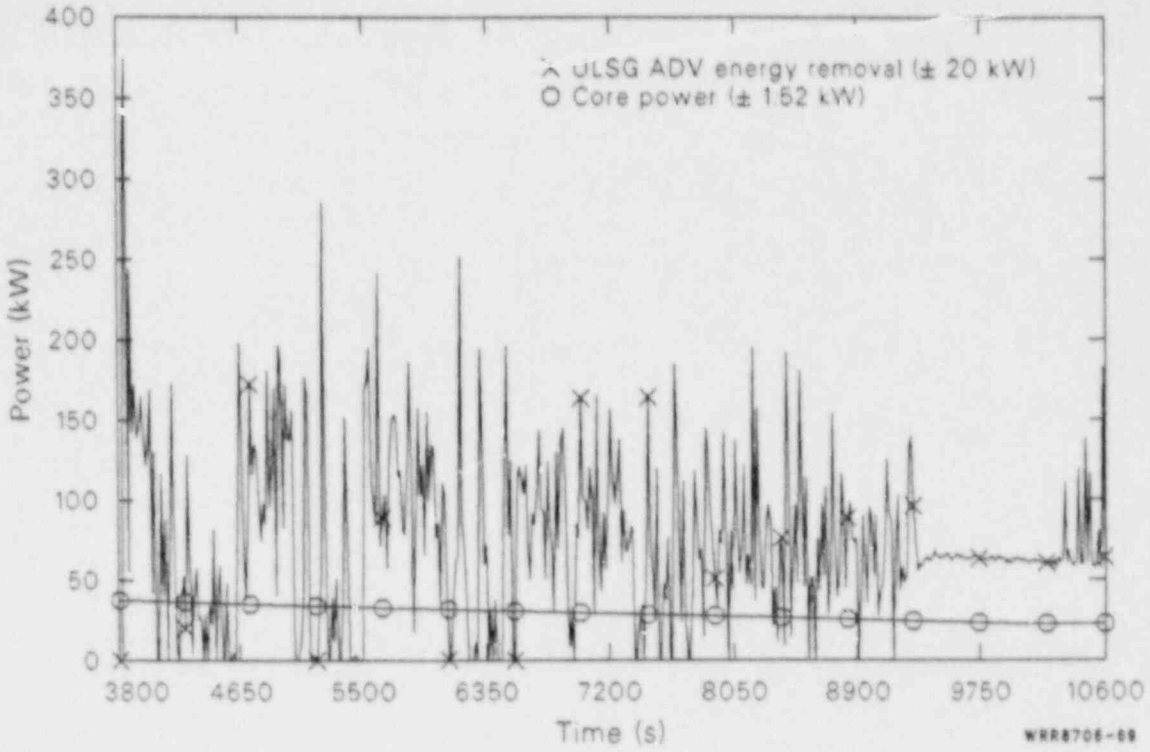

Figure 69. Unaffected loop steam generator atmospheric dump valve energy removal and core power during the plant cooldown and depressurization phase of 100% FWLB experiment S-FS-6 (3800 to 10,600 s).

primary fluid system while maintaining satisfactory secondary inventory. Attempts to cool down at faster rates would be limited, however, by the capability of the auxiliary feedwater flow to maintain the secondary inventory.

Effects of Combined Pressurizer Auxiliary Spray and Internal Heater Operation on the System Cooldown and Depressurization to Vessel Upper Head Fluid Saturation. During this portion of the test, the pressurizer auxiliary spray was cycled 20 times to maintain a maximum primary subcooled margin of 13.9 K. The intent was to reduce the primary system pressure at the maximum rate permitted by the primary system cooldown. The depressurization rate produced by using auxiliary spray was 0.0166 MPa/s, during the initial total pressure drop of approximately 3.70 MPa (Figure 62). The average depressurization rate produced by using auxiliary spray was 0.0122 MPa/s, during subsequent average total pressure drops of approximately 0.55 MPa. The subcooled margin was reduced to approximately 9.5 K during each spray cycle (Figure 63).

The pressurizer internal heaters were cycled five times to maintain a minimum primary subcooled margin of 11.1 K. This was intended to maintain control of the primary system, as guided by the EOPs. The pressurization rate using pressurizer internal heaters at 6.99 kW was approximately 0.0048 MPa/s during an average total pressure increase of 0.15 MPa (Figure 63).

The combined operations of pressurizer auxiliary spray and internal heaters demonstrated excellent control of primary pressure and subcooled margin during the primary cooldown and depressurization to vessel upper head fluid saturation.

System Response to Vessel Upper Head Void Recovery Operations (S-FS-6)

This portion of Test S-FS-6 was performed in accordance with the guidance provided in the St. Lucie Unit No. 2 EOPs for a rapid natural circulation cooldown and depressurization with upper head void formation. The EOP guidelines were followed to the extent possible. After forcing upper head void formations, two methods of upper head void collapse methods were investigated. The first method, the *fill and drain* method, involved using normal charging, aided by pressurizer internal heaters, to fill the vessel upper

head with cooler fluid and collapse the upper head void. The second method, the *pump restart* method, involved restarting the primary coolant pumps in each loop at one-half their initial condition flow. This method, aided by normal charging to maintain system inventory, forces more flow through the upper head resulting in mixing of the cooler cold leg fluid with the upper head fluid and collapse of the upper head void. The overall system response to the upper head void collapse operations will be discussed first. This will be followed by discussions of the effects of the *fill and drain* method of void collapse and the *pump restart* method of void collapse on the system response.

Overall Response to Vessel Upper Head Void Collapse Operations. At 10,600 s after transient initiation, the vessel upper head fluid had been within approximately 2 K of saturation for 600 s. However, no upper head voiding had occurred. At 10,736 s, the depressurization of the primary system was initiated by starting the pressurizer auxiliary spray (Figure 70). The reduction in primary pressure (Figure 71) produced a corresponding reduction in the primary hot leg and vessel upper head subcooled margins (Figure 70). The formation of the first upper head void was indicated by the pressurizer and upper head liquid level responses (Figure 72) at approximately 10,795 s. The vessel upper head liquid level reached 356 cm and the upper head external heaters were turned off at approximately 10,854 s. The pressurizer liquid level reached 365 cm and the pressurizer auxiliary spray, letdown (Figure 73), and the cooldown were stopped at approximately 10,865 s. Normal charging flow (Figure 73) and pressurizer internal heater (Figure 70) operations were initiated at approximately 10,886 s. However, the pressurizer liquid level rapidly increased beyond the 380 cm and 395 cm pressurizer internal heater initiation and normal charging termination set points. Normal charging flow was then terminated at approximately 10,904 s. As the pressurizer internal heaters started to mitigate the voiding, the pressurizer and vessel upper head liquid levels reached their maximum and minimum values of approximately 418 cm and 262 cm, respectively. The upper head void reduction was initiated at about 10,950 s, recovering the vessel upper head level and reducing the pressurizer level. The normal charging flow was re-initiated at about 11,045 s, when the pressurizer level decreased to 395 cm. This caused the slight increase in the rate of upper head void collapse

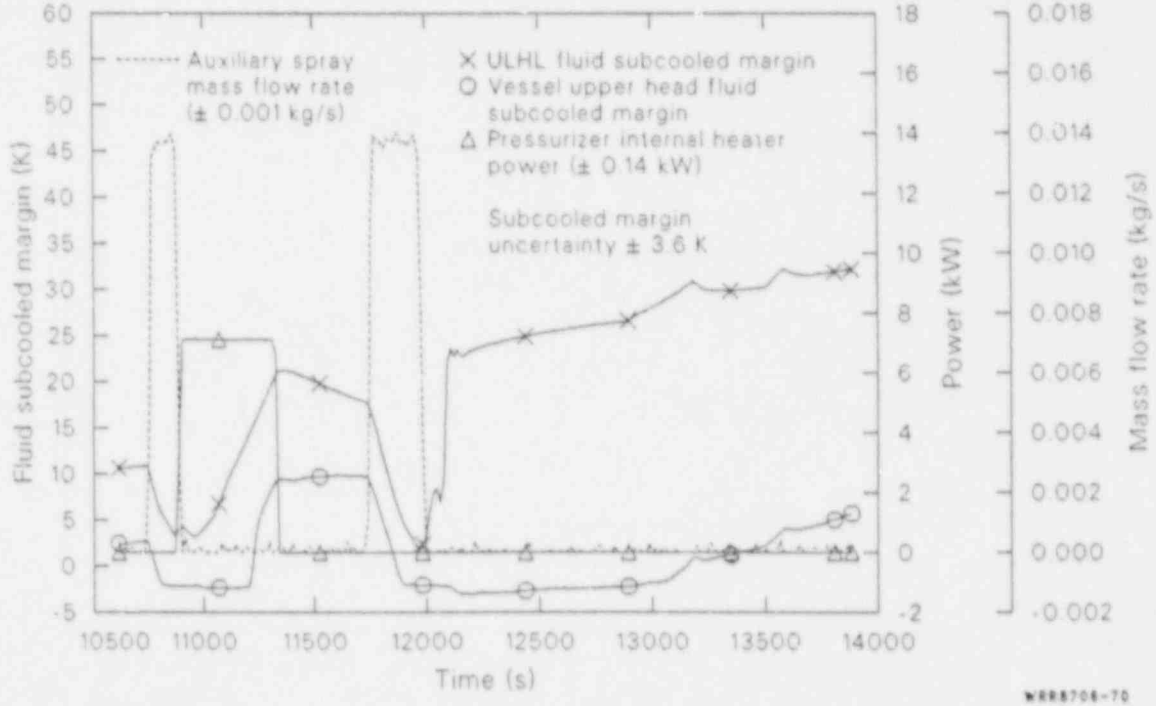

Figure 70. Unaffected loop hot leg and vessel upper head fluid subcooled margins, pressurizer auxiliary spray mass flow rate, and pressurizer internal heater power during the vessel upper head void collapse methods investigation phase of 100% FWLB experiment S-FS-6 (10,600 to 13,900 s).

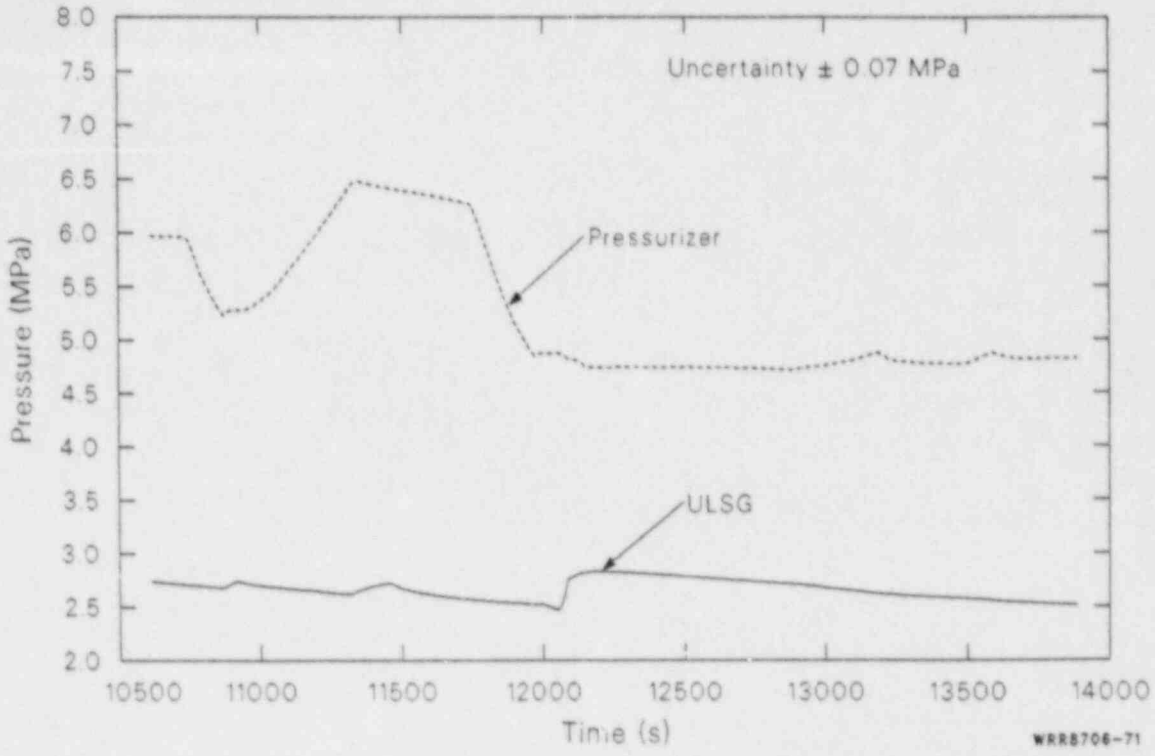

Figure 71. Pressurizer and unaffected loop steam generator secondary pressures during the vessel upper head void collapse methods investigation phase of 100% FWLB experiment S-FS-6 (10,600 to 13,900 s).

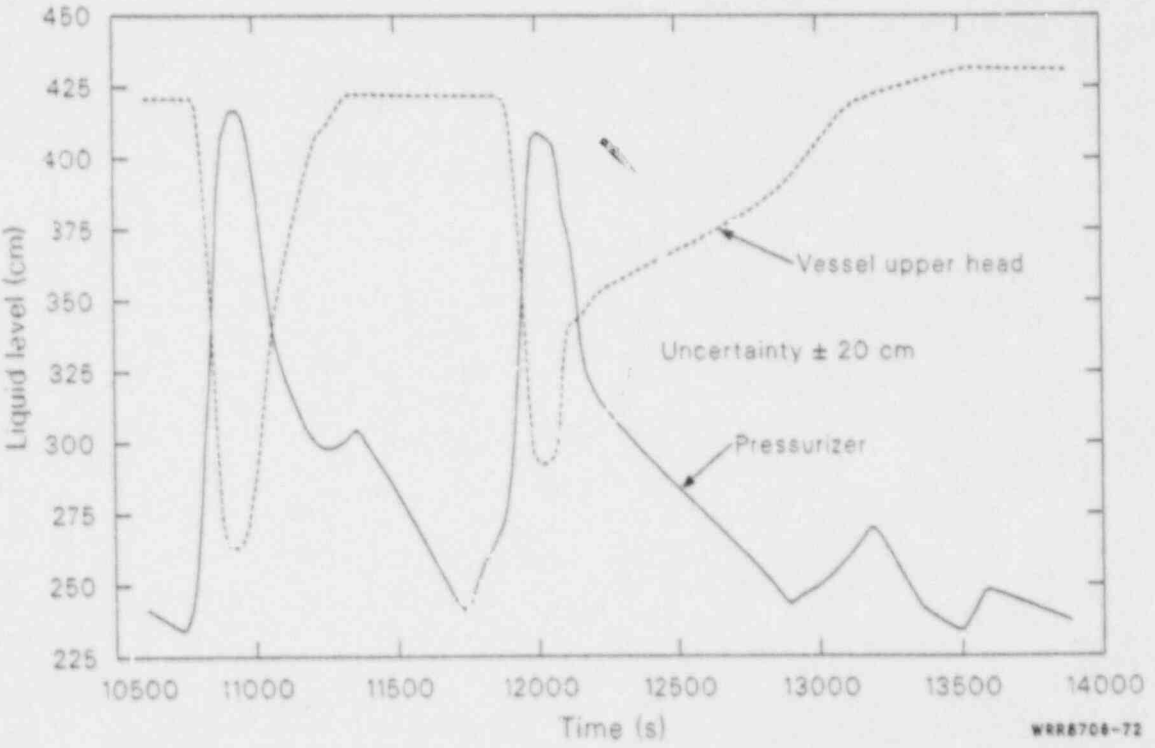

Figure 72. Pressurizer and vessel upper head collapsed liquid levels during the vessel upper head void collapse methods investigation phase of 100% FWLB experiment S-FS-6 (10,600 to 13,900 s).

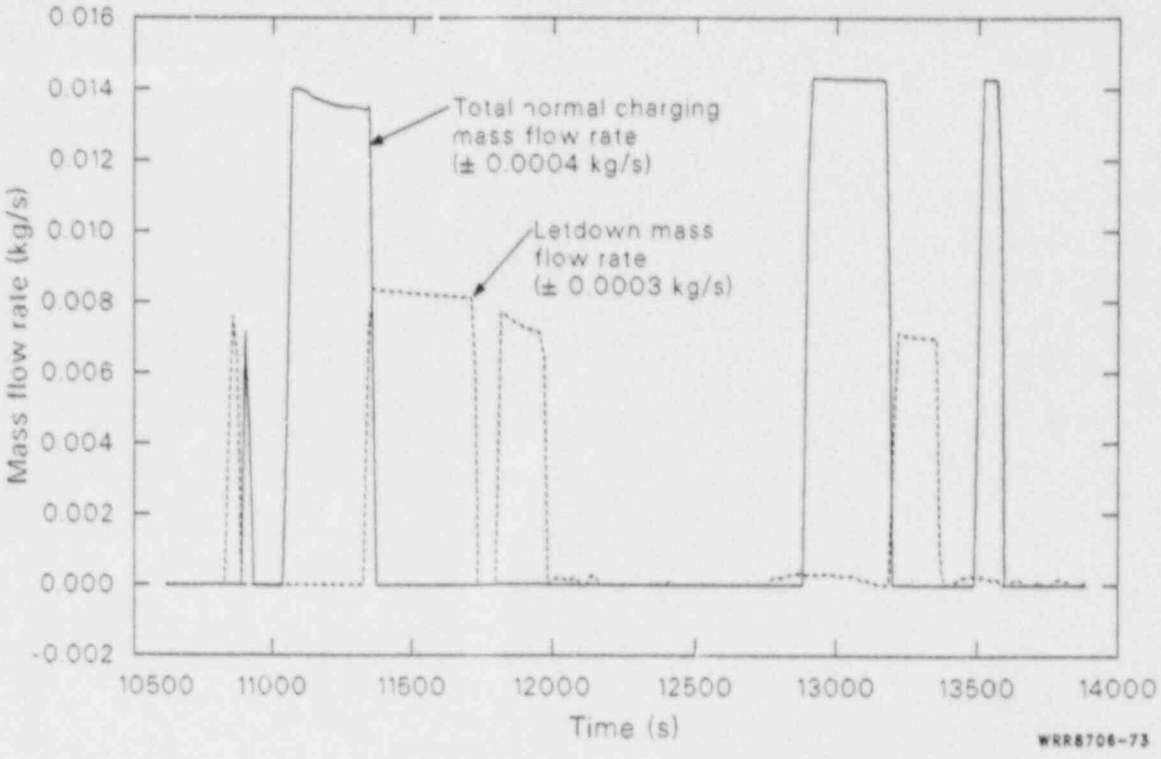

Figure 73. Total normal charging and letdown mass flow rates during the vessel upper head void collapse methods investigation phase of 100% FWLB experiment S-FS-6 (10,600 to 13,900 s).

shown in Figure 72. The on/off cycling of the vessel upper head external heaters was re-initiated at about 11,104 s, when the vessel upper head level increased to 356 cm. The void reduction continued with final collapse of the void indicated at approximately 11,325 s, when the upper head level reached 421 cm and the pressurizer level started to increase. Normal charging flow and pressurizer internal heater operations were then terminated and letdown operations were initiated to return the pressurizer level to 245 ± 10 cm. Letdown flow was terminated at 11,715 s with the pressurizer liquid level at 245 cm.

At 11,715 s after transient initiation, the first vessel upper head void had been collapsed and all other parameters were within the specified range of conditions. At 11,730 s, the depressurization of the primary system was re-initiated by starting the pressurizer auxiliary spray. The resulting reduction in primary pressure and primary hot leg and vessel upper head subcooled margins can be seen in Figures 70 and 71. The formation of the second upper head void was indicated by the pressurizer and upper head liquid level responses (Figure 72) at approximately 11,896 s. The vessel upper head liquid level reached 356 cm and the upper head external heaters were turned off at approximately 11,930 s. The pressurizer liquid level reached 365 cm and the pressurizer auxiliary spray, letdown, and cooldown were stopped at approximately 11,960 s. The affected and unaffected loop primary coolant pumps were then restarted with the affected loop pump starting at approximately 11,965 s; the unaffected loop pump starting at approximately 12,057 s. The pumps were adjusted to bring the loop flows (Figure 74) to 5.5 L/s and 1.8 L/s for the unaffected and affected loop, respectively. As the forced flow increased the flow through the vessel upper head, the voiding was halted. The pressurizer and vessel upper head liquid levels reached their maximum and minimum values of approximately 410 cm and 292 cm, respectively. The upper head void reduction was initiated at about 12,060 s, recovering the vessel upper head level and reducing the pressurizer level. The on/off cycling of the vessel upper head external heaters was re-initiated at about 12,265 s, when the vessel upper head level increased to 356 cm. The normal charging flow was re-initiated at about 12,882 s, when the pressurizer level decreased to 245 cm. This caused the slight increase in the rate of upper head void collapse, shown in Figure 72.

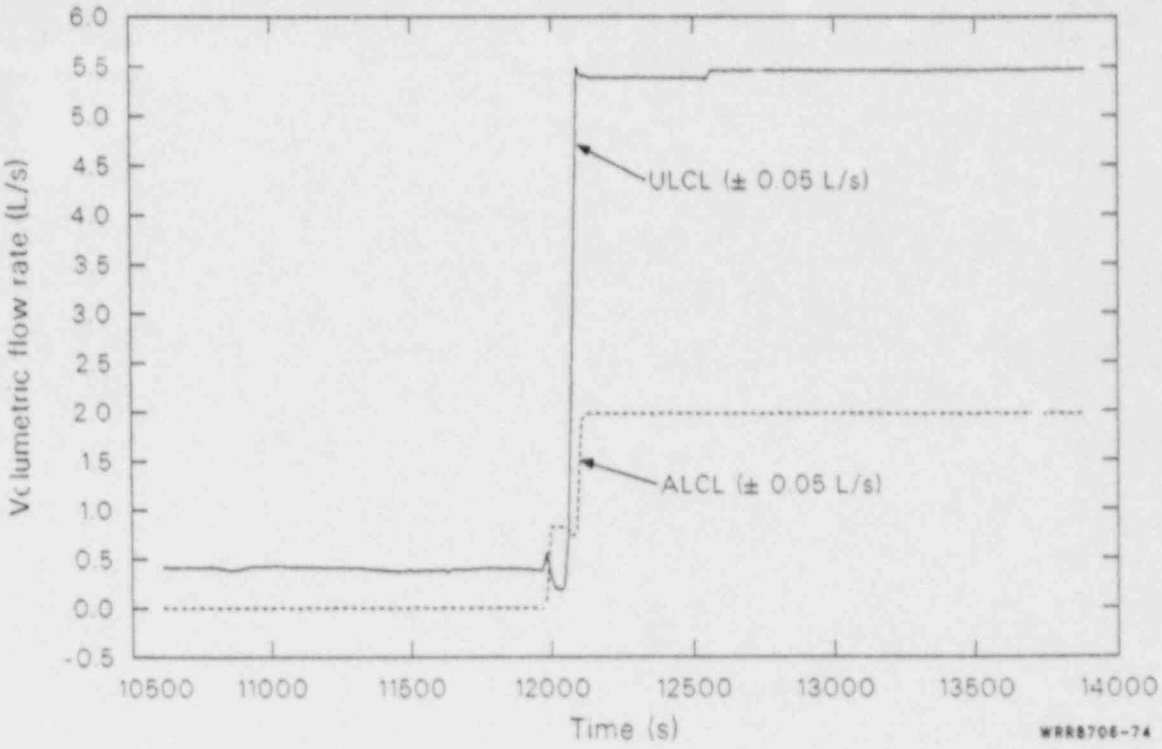

Figure 74. Affected and unaffected loop cold leg volumetric flow rates during the vessel upper head void collapse methods investigation phase of 100% FWLB experiment S-FS-6 (10,600 to 13,900 s).

The void reduction continued with final collapse, of the void indicated at approximately 13,176 s, when the upper head level reached 421 cm and the rate of pressurizer level rise started to increase. Normal charging flow was then terminated and letdown operations were initiated at 11,193 s, to return the pressurizer level to 245 ± 10 cm. The pressurizer level reached 255 cm at approximately 13,300 s. At this point, all parameters were within the specified tolerances. Letdown was terminated at 13,349 s with the pressurizer level at 245 cm, all other parameters meeting specification, and the forced flow cooldown continuing.

At 13,900 s, the pressurizer level was at 238 cm and had been between 235 and 255 cm; unaffected loop steam generator liquid level (Figure 75) was at 770 cm and was increasing; subcooled margin was at 32.0 K; and the average primary fluid temperature was at 503 K, and had been decreasing for more than 600 s. This satisfied the test termination criteria. The test was then terminated at 13,900 s.

Effects of the Fill and Drain Method of Vessel Upper Head Void Collapse on the System Response. The *fill and drain* method of vessel upper head void collapse, as outlined in the St. Lucie Unit No. 2 EOPs, consists of filling the system with normal charging and utilizing pressurizer internal heaters to return the steam bubble to the pressurizer.

After initial indication of voiding at approximately 10,795 s, the vessel upper head level decreased at an average rate of approximately 2 cm/s between 10,825 and 10,885 s, while the pressurizer level increased at an average rate of approximately 1.8 cm/s over the same time period (Figure 76). The rate of void formation decreased rapidly following auxiliary spray termination and pressurizer internal heater and normal charging flow initiation (Figure 77). The maximum voiding occurred at approximately 10,935 s, as the internal heaters pressurized the pressurizer (Figure 78) and started to force fluid out of the pressurizer and into the upper head. The subcooled cold leg fluid entered the upper head through the vessel downcomer to upper head bypass line and cooled the liquid in the upper head (Figure 79), which in turn started to condense the steam in the upper head. The upper head level increased initially at an average rate of approximately 0.9 cm/s over the range of 280 to 336 cm. Over this same time span, the pressurizer level also decreased at an average rate of

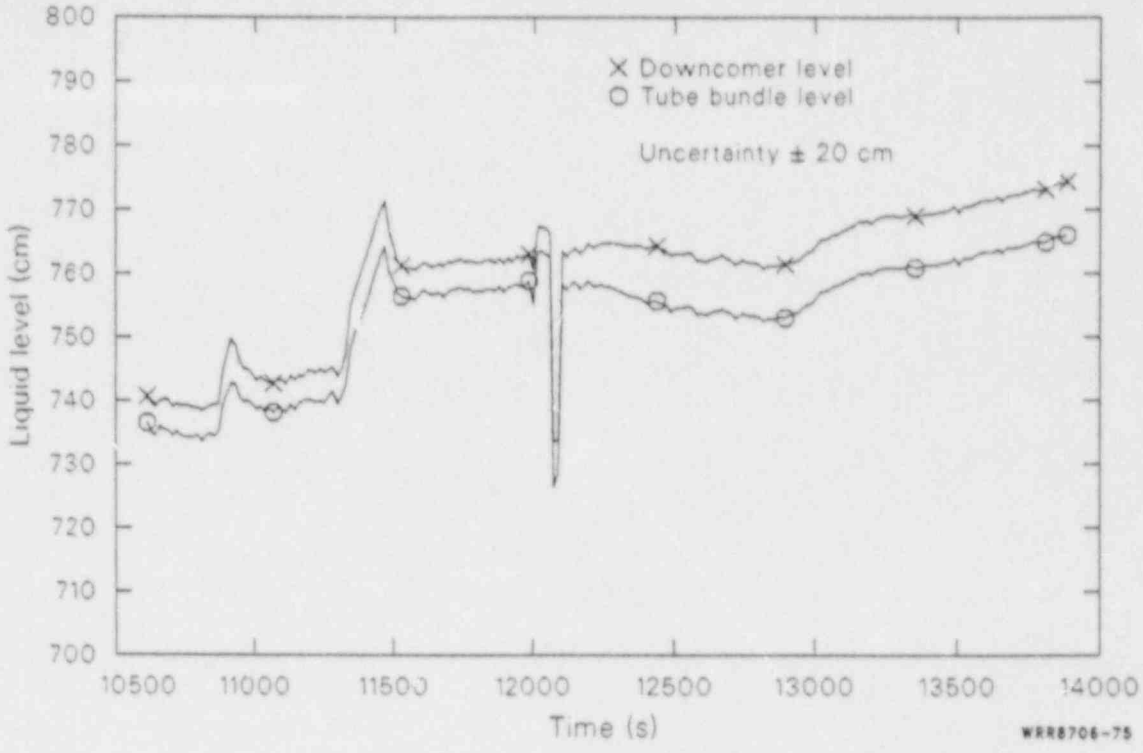

Figure 75. Unaffected loop steam generator downcomer and tube bundle overall collapsed liquid levels during the vessel upper head void collapse methods investigation phase of 100% FWLB experiment S-FS-6 (10,600 to 13,900 s).

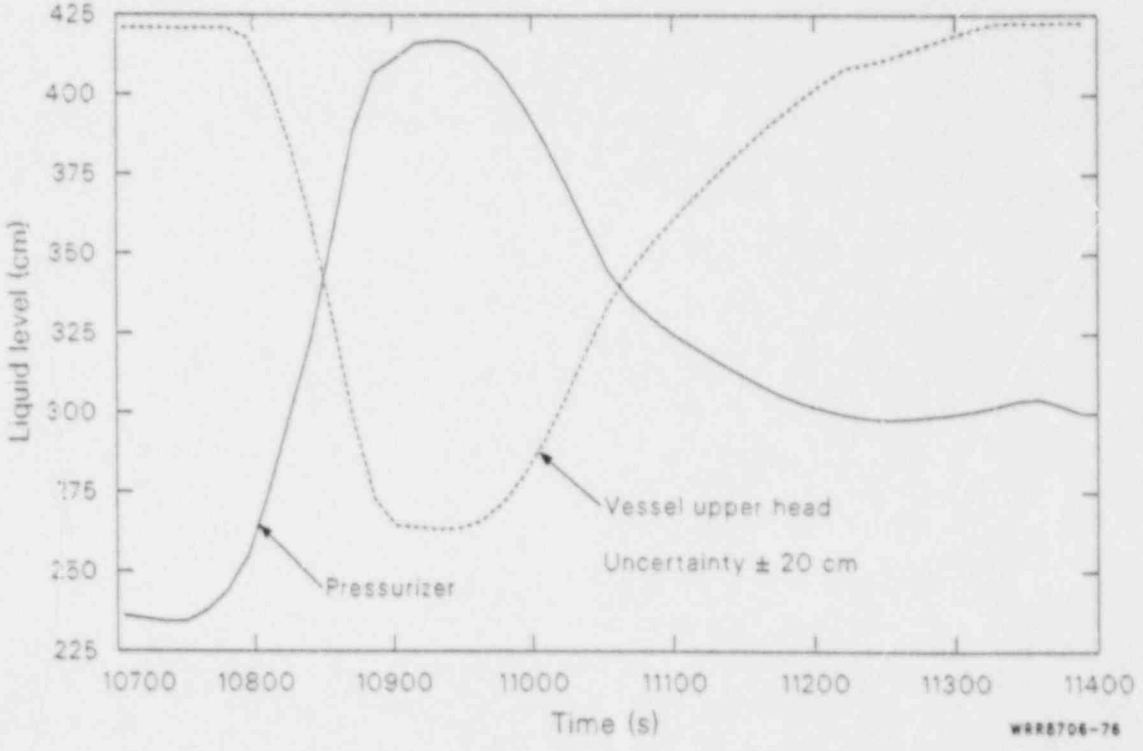

Figure 76. Pressurizer and vessel upper head collapsed liquid levels during the fill and drain vessel upper head void collapse method investigation phase of 100% FWLB experiment S-FS-6 (10,700 to 11,400 s).

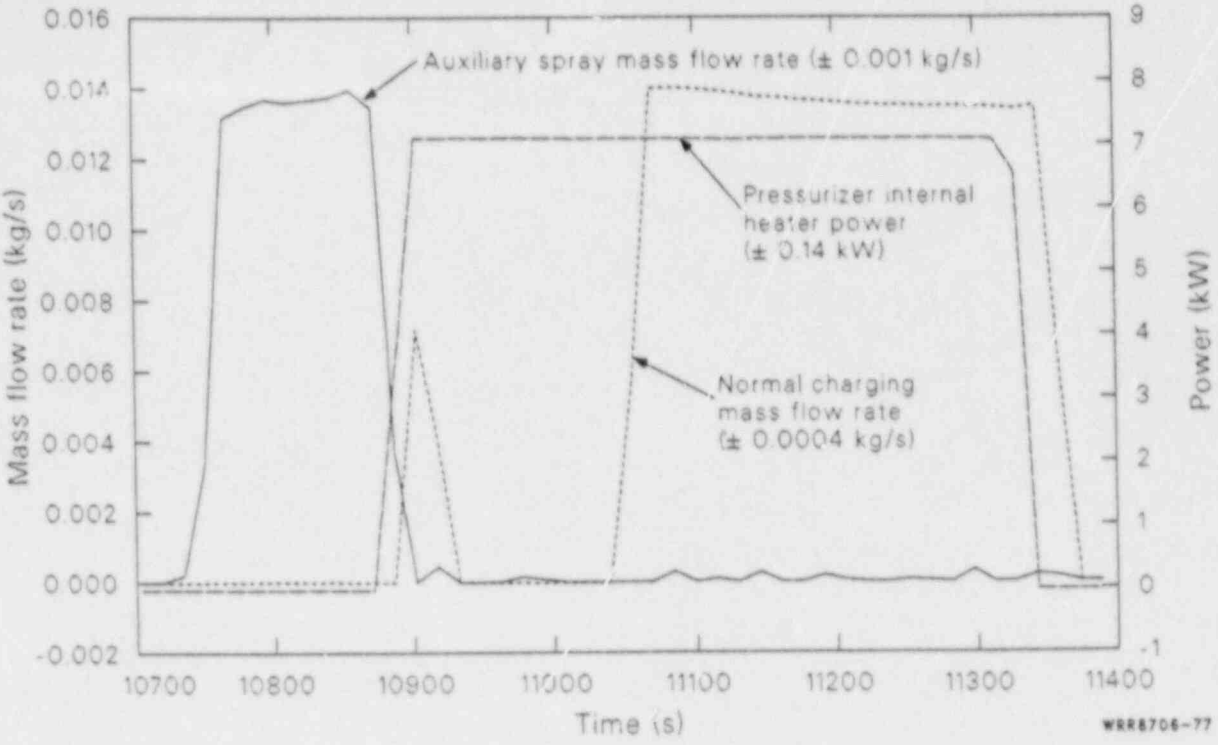

Figure 77. Pressurizer auxiliary spray mass flow rate and internal heater power, and total normal charging mass flow rate during the fill and drain vessel upper head void collapse method investigation phase of 100% FWLB experiment S-FS-6 (10,700 to 11,400 s).

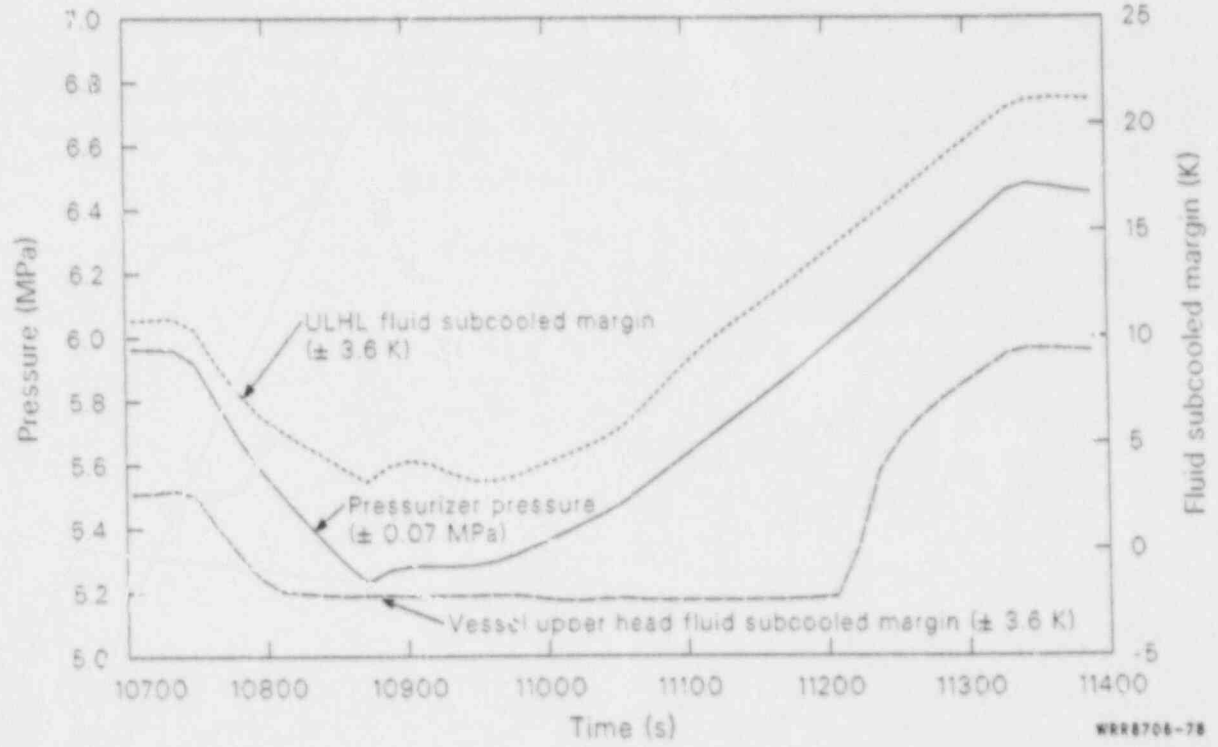

Figure 78. Pressurizer pressure, and unaffected loop hot leg and vessel upper head fluid subcooled margins during the fill and drain vessel upper head void collapse method investigation phase of 100% FWLB experiment S-FS-6 (10,700 to 11,400 s).

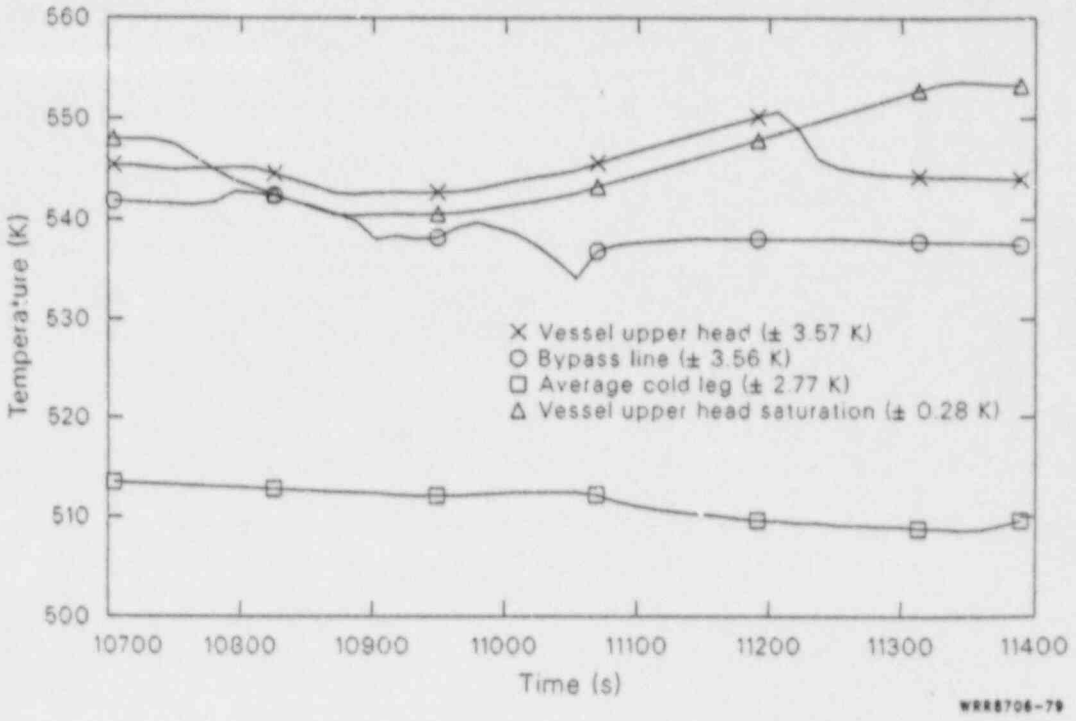

Figure 79. Average cold leg fluid, vessel downcomer to upper head bypass line fluid, vessel upper head fluid, and vessel upper head saturation temperatures during the fill and drain vessel upper head void collapse method investigation phase of 100% FWLB experiment S-FS-6 (10,700 to 11,400 s).

approximately 0.9 cm/s. This similarity in the rate of level change is due to the pressurizer area being only slightly larger than the vessel upper head area, difference in the pressurizer and upper head fluid densities, and the slight system leakage.

When the upper head liquid level reached approximately 335 cm, the average rate of level increase reduced to approximately 0.5 cm/s. This is due in part to the fluid reaching the level of the top of the guide tube (335.8 cm) in the upper head resulting in an increase in the upper head area. However, the major reason for this reduction in the rate of level increase is the continual reduction in the upper head fluid density as the upper head fluid cools, and the increase in the upper head pressure due to compression of the steam bubble. The re-initiation of normal charging at 11,045 s aided in cooling the upper head fluid, as shown in Figure 79. Subcooled liquid reached the 402 cm elevation in the upper head at approximately 11,210 s. This is evident in the fluid thermocouple response (Figure 79), and the upper head subcooled margin (~9 K) obtained from the thermocouple data (Figure 78). Final collapse of the upper head void occurred at approximately 11,325 s. This is evident in both the pressurizer and upper head liquid level responses. However, special note should be made of the fact that the pressurizer level started to increase before the upper head void was fully collapsed. Care should be taken to ensure that the rate of pressurizer level increase agrees with that expected due to the normal charging flow.

The *fill and drain* method is an effective method of vessel upper head void collapse. The total time required for void collapse following void identification was approximately 530 s. The normal charging flow increased the rate of the cooling of the upper head. However, based on these results, and past experience in Semiscale,[30] normal charging alone may not be sufficient to collapse the upper head void. Charging flow may enter and fill the pressurizer rather than the vessel upper head. Using pressurizer internal heaters proved to be very beneficial in collapsing the upper head void, as they pressurized the pressurizer and forced more cold fluid into the upper head. Hence, the combined use of normal charging and pressurizer internal heater operations appears to be effective in both cooling the vessel upper head and collapsing the upper head void.

Effects of the Pump Restart Method of Vessel Upper Head Void Collapse on the System Response. The *pump restart* method of vessel upper head void collapse, as outlined in the St. Lucie Unit No. 2 EOPs, consists of restarting one pump in each loop (a C-E System 80 plant has a two loop, two pump per loop, configuration). This increases the flow through the loops to about one-half of the full flow value. The flow of fluid bypassing the core to the vessel upper head is also increased, resulting in cooling of the upper head fluid.

After initial indication of voiding at approximately 11,896 s, the vessel upper head level decreased at an average rate of approximately 1.7 cm/s between 11,910 and 11,977 s, while the pressurizer level increased at an average rate of approximately 1.5 cm/s over the same time period (Figure 80). The voiding halted abruptly at approximately 11,995 s as the loop and vessel downcomer to upper head bypass line flows increased (Figure 81). The subcooled cold leg fluid entered the upper head through the vessel downcomer to upper head bypass line and cooled the liquid in the upper head (Figure 82), which in turn started to condense the steam in the upper head. The upper head level increased initially at an average rate of approximately 1.2 cm/s over the range of 300 to 340 cm. Over this same time span, the pressurizer level decreased at an average rate of approximately 0.7 cm/s.

During the period of loop flow increase (12,000 to 12,100 s), the effects on the primary response were quite pronounced. The increased flow through the core reduced the temperature increase of the primary fluid while the increased flow through the unaffected loop steam generator reduced the temperature decrease of the primary fluid. This resulted in a substantial decrease in the unaffected loop hot leg fluid temperature (22 K), affected loop hot leg fluid temperature (16 K), affected loop cold leg fluid temperature (10 K), and a slight increase in the unaffected loop cold leg fluid temperature (4 K) (Figure 83). The net effect was a reduction in the average fluid temperature of approximately 10 K, and an increase in the primary subcooled margin (Figure 84) of about 22 K.

When the upper head liquid level reached approximately 340 cm, the average rate of level increase reduced to approximately 0.05 cm/s. This is due in part to the fluid reaching the level of the top of the guide tube (335.8 cm) in the upper head, resulting in an increase in the upper head area. However, the major reason for this reduction in the rate of level increase is the reduction in the upper head fluid density as highly subcooled (30 K) liquid entered the upper head through the bypass line (Figure 82). During this period, the vessel upper head pressure remained essentially constant (Figure 84). This indicates that the energy removal from the steam through condensation and heat loss matched the work performed on the steam as the steam was compressed. In other words, the mass rate of steam condensation and the rate of steam volume reduction were matched such that the specific volume of the steam remained essentially constant.

At approximately 12,882 s, the pressurizer liquid level reached 245 cm and normal charging flow was reinitiated. The charging flow provided added cooling to the primary system, including the upper head. The charging flow also increased the rate of level increase in the upper head to an average of approximately 0.12 cm/s, while it started to increase the level in the pressurizer at an average rate of approximately 0.09 cm/s. This indicates that approximately one-half of the charging flow minus leakage was entering the upper head with the other one-half entering the pressurizer. Subcooled liquid reached the 402 cm elevation in the upper head at approximately 13,070 s. This is evident in the fluid thermocouple response (Figure 82). Final collapse of the upper head void was indicated at approximately 13,176 s, when the upper head liquid level reached 421 cm and the pressurizer liquid level started to increase more rapidly. Here again, special note should be made of the fact that the pressurizer level started to increase before the upper head void was collapsed. Care should be taken to ensure that the rate of pressurizer level increase agrees with that expected due to the normal charging flow.

The *pump restart* method is an effective method of vessel upper head void collapse. The total time required for void collapse following void identification was approximately 1280 s. The forced flow through the vessel upper head provided significant cooling of the upper head and recoupled the upper head fluid and metal with the rest of the primary system. Before the initiation of normal charging flow, the rate of void collapse appeared to be controlled by the rate of condensation in the upper head. The normal charging flow increased the rate of void collapse but did not significantly affect the degree of upper head fluid and metal cooling.

Comparisons of the Fill and Drain and Pump Restart Methods of Vessel Upper Head Void Collapse. Both the *fill and drain* and the *pump restart* method proved to be effective in cooling the vessel upper head fluid and collapsing the vessel upper head void. Two major differences were noted. The *fill and drain* method collapsed the vessel upper head void more rapidly that the *pump restart* method (530 s versus 1280 s). However, the pump restart method cooled

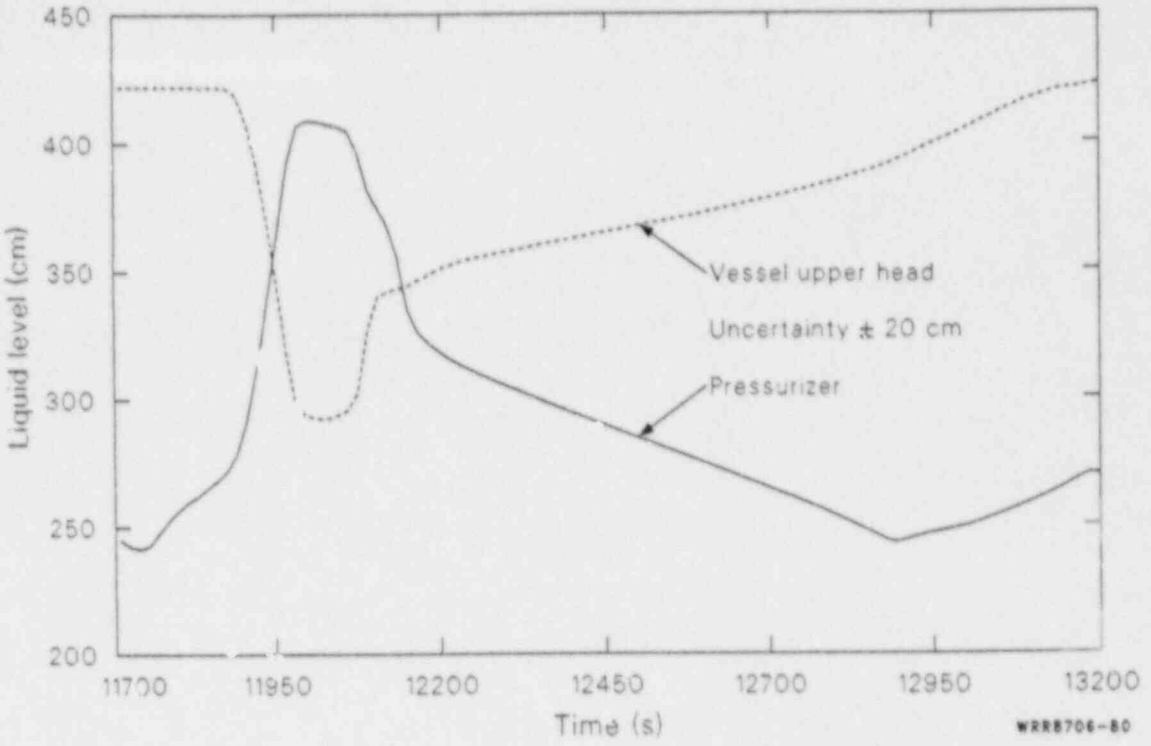

Figure 80. Pressurizer and vessel upper head collapsed liquid levels during the pump restart vessel upper head void collapse method investigation phase of 100% FWLB experiment S-FS-6 (11,700 to 13,200 s).

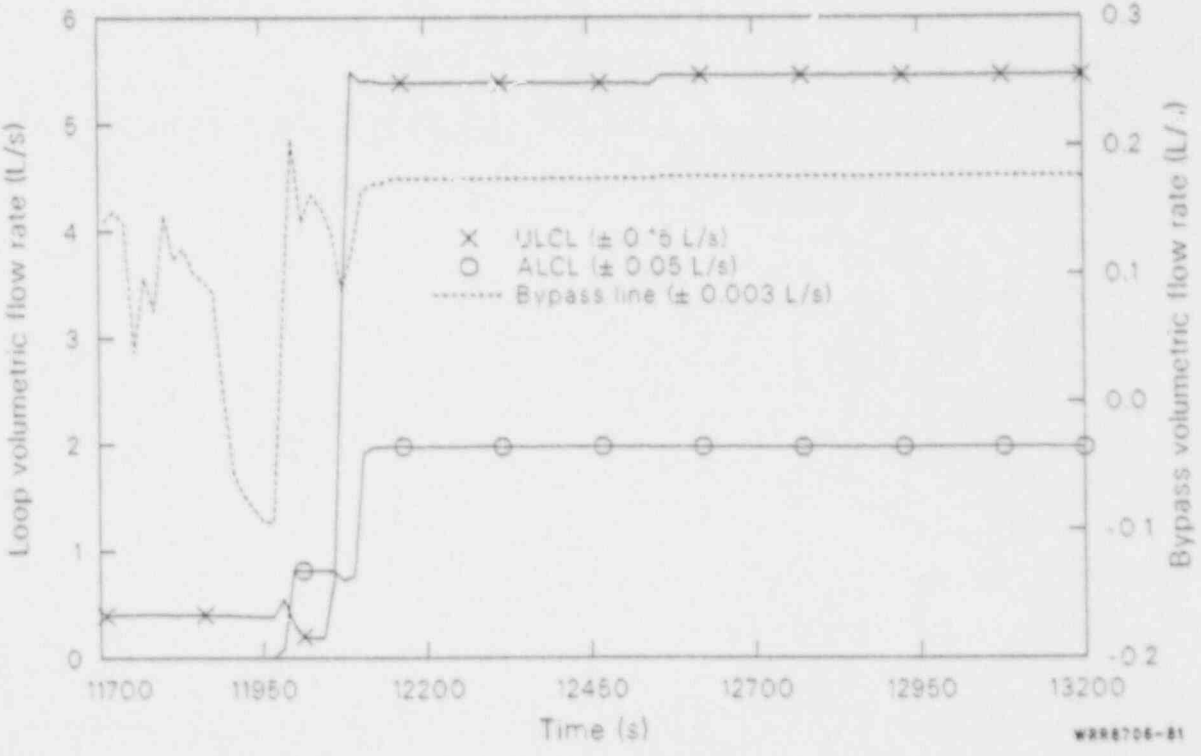

Figure 81. Affected and unaffected loop cold leg and vessel downcomer to upper head bypass line volumetric flow rates during the pump restart vessel upper head void collapse method investigation phase of 100% FWLB experiment S-FS-6 (11,700 to 13,200 s).

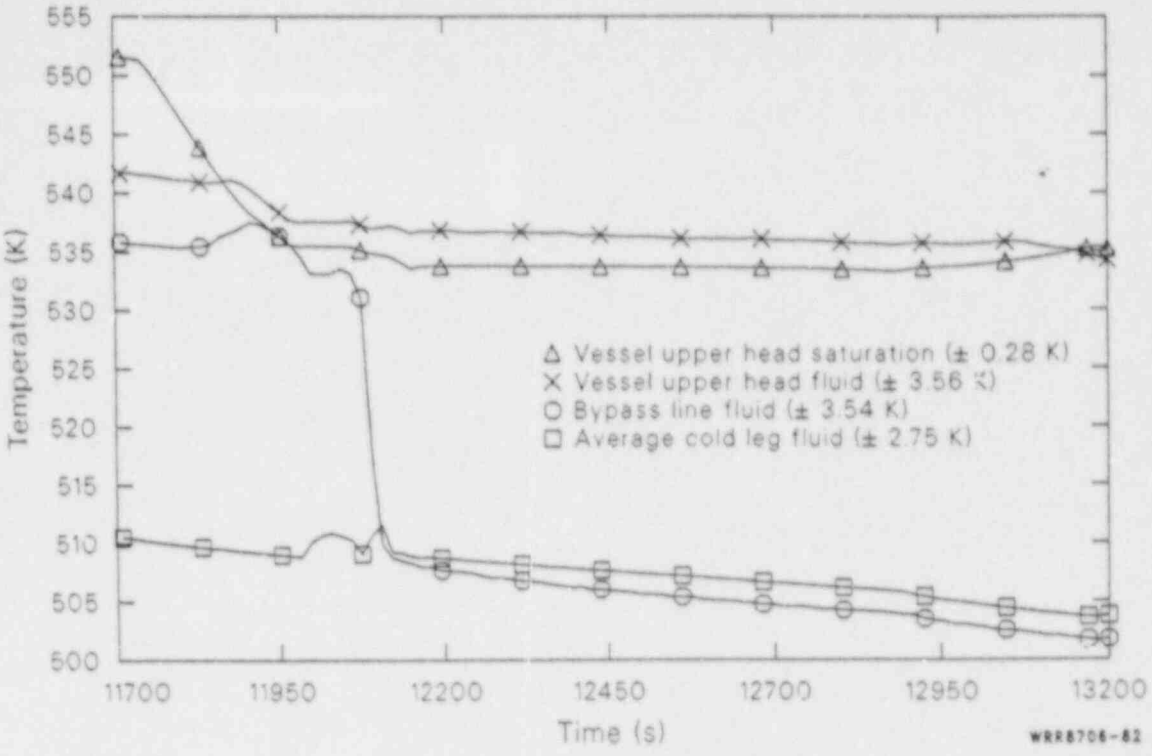

Figure 82. Average cold leg fluid, vessel downcomer to upper head bypass line fluid, vessel upper head fluid, and vessel upper head saturation temperatures during the pump restart vessel upper head void collapse method investigation phase of 100% FWLB experiment S-FS-6 (11,700 to 13,200 s).

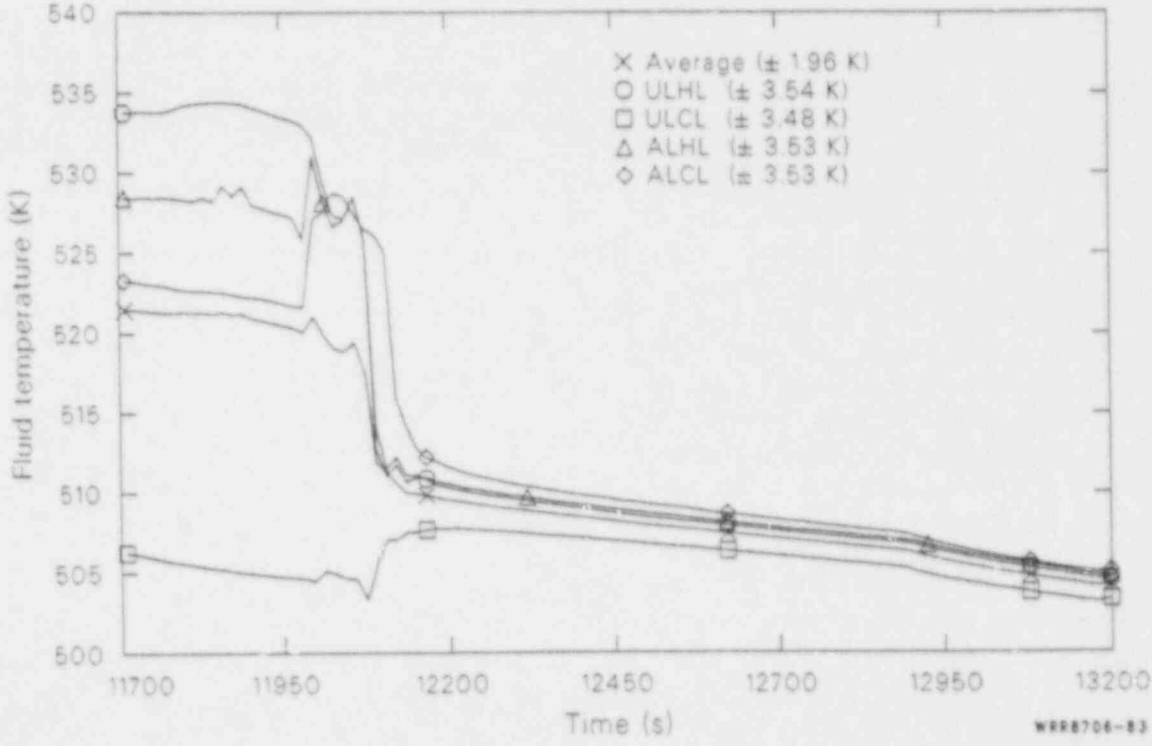

Figure 83. Affected and unaffected loop hot and cold leg and average primary fluid temperatures during the pump restart vessel upper head void collapse method investigation phase of 100% FWLB experiment S-FS-6 (11,700 to 13,200 s).

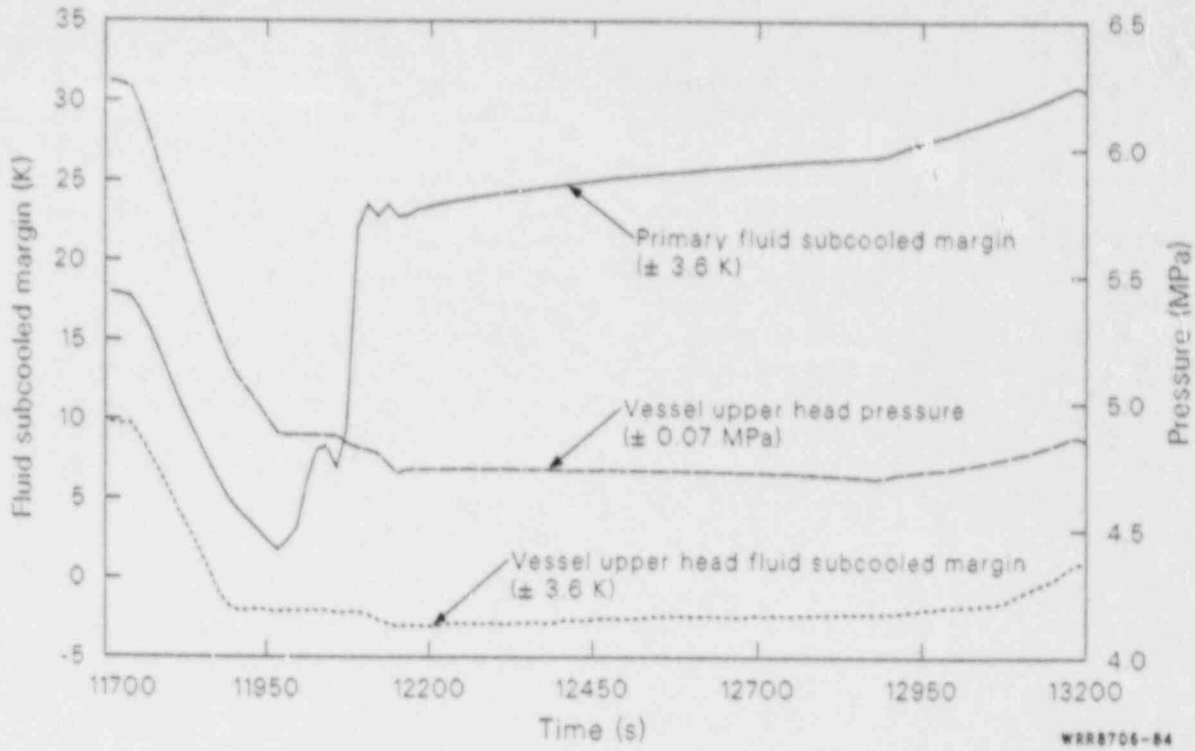

Figure 84. Vessel upper head pressure, and unaffected loop hot leg and vessel upper head fluid subcooled margins during the pump restart vessel upper head void collapse method investigation phase of 100% FWLB experiment S-FS-6 (11,700 to 13,200 s).

the vessel upper head fluid and metal much more than the *fill and drain* method (a maximum of 40 K for the *pump restart* method versus a maximum of 8 K for the *fill and drain* method).

The results for both methods of vessel upper head void collapse indicate the need to carefully monitor the rate of pressurizer liquid level increase in determining final collapse of the upper head void. For both methods, the pressurizer liquid level started to increase before the upper head void was collapsed. Thus, determining final collapse of the upper head void cannot be based solely on an increasing pressurizer liquid level. The rate of the pressurizer level increase should be monitored to ensure that it agrees with that expected due to the normal charging flow.

System Response to Voided Secondary Refill Operations

The voided secondary refill operations performed for tests S-FS-7 and S-FS-11 are not normal recovery operations for a bottom feedwater line break transient. However, the data obtained during this phase of the experiments provides needed information on primary-to-secondary heat transfer during secondary refill conditions such as could occur during a loss of feedwater transient. The data also provides invaluable insight into the primary-to-secondary heat transfer mechanisms that existed in the unaffected loop steam generator as it refilled following MSIV closure during these experiments.

The voided secondary refill phase of the experiments was commenced after the completion of the plant stabilization phase. The refill operations consisted of: break isolation; affected loop steam generator auxiliary feedwater re-initiation (at 0.004 g/s for S-FS-7 and 0.016 kg/s for S-FS-11); maintaining the stable conditions achieved during the plant stabilization phase, (pressurizer liquid level between 235 and 255 cm, subcooled margin $\geq$ 27.8 K, unaffected loop steam generator downcomer liquid level between 910 and 1000 cm, and unaffected loop steam generator secondary pressure $\leq$ 6.98 MPa); and restarting the primary coolant pumps at their minimum speed, if necessary, to provide a measurable primary fluid flow rate. The refill was specified to be terminated upon achieving an affected loop steam generator secondary liquid level of 1036 cm.

Examination of the Semiscale Mod-2C system response to the voided secondary refill operations provides invaluable insight into both the effectiveness of

the refill operation in maintaining stable conditions and the nature of the primary-to-secondary heat transfer mechanism. The characteristic response to the voided secondary refill operations was very similar for both tests. Therefore, the detailed discussion of the characteristic system response to the voided secondary refill operations will be limited to test S-FS-11 results. The overall system response for test S-FS-11 will be discussed first, followed by discussions of the secondary responses to the voided secondary refill operations for test S-FS-11. The response of the primary system to the voided secondary refill operations for test S-FS-11 will be discussed next. Finally a comparison of the results for tests S-FS-11 and S-FS-7 is made to provide insight into the effects of different refill rates on the voided secondary refill system response.

Overall System Response to Voided Secondary Refill Operations. The overall response of the system is characterized as maintaining stable system conditions while re-establishing the affected loop steam generator secondary inventory and primary-to-secondary heat transfer. The predominant factors governing the system response were the rate of the affected loop steam generator secondary inventory recovery and the affected loop steam generator primary-to-secondary heat transfer.

The voided secondary refill phase of test S-FS-11 was initiated at 4100 s by closing the affected loop steam generator bottom main feedwater line break valve (isolating the break) and re-initiating the affected loop steam generator auxiliary feedwater flow at the scaled typical flow rate (0.016 kg/s). The characteristic response of the primary and secondary systems is graphically depicted in Figures 85 through 91. The auxiliary feedwater started recovering the affected loop steam generator secondary liquid level, after refilling the break assembly and main feedwater line piping, at about 4300 s. As the secondary inventory started to increase, liquid supplied to the tube-bundle region was heated, generating steam and re-initiating the primary-to-secondary heat transfer. The energy addition from the primary and the compression of the secondary steam volume caused a pressurization of the affected loop steam generator secondary. The re-initiation of the affected loop steam generator primary energy removal caused a reduction in the unaffected loop steam generator primary energy removal rate, thereby causing a reduction in the unaffected loop steam generator secondary pressure. The unaffected loop steam generator auxiliary feedwater flow was terminated when the secondary liquid level reached 1000 cm. The liquid level remained above 910 cm for the remainder of the transient, precluding the need to re-initiate the auxiliary feedwater flow. The unaffected loop steam generator secondary pressure remained below 6.98 MPa, precluding the need to cycle the ADV. The natural circulation flow developed in the affected loop was below the measurement range of the U-tube outlet turbo-probes. Therefore, the primary coolant pumps were restarted at their minimum speed to provide a measurable primary fluid flow rate. Problems encountered in restarting the unaffected loop pump precluded operating the pump. However, the flow provided by the affected loop pump was sufficient to provide a measurable primary fluid flow rate. The primary fluid system exhibited a gradual depressurization under the influence of the secondary energy removal and the slight system leakage. The primary system average fluid temperature exhibited a marked decrease when the affected loop steam generator secondary inventory started to increase and its primary-to-secondary heat transfer was re-initiated. The average fluid temperature then leveled off as the energy addition due to core power was offset by the energy removal via the secondaries. Pressurizer inventory was maintained by normal charging flow and the primary subcooled margin remained above 27.8 K.

Secondary System Response to Voided Secondary Refill Operations. The principal objective of the voided secondary refill phase of these experiments was to obtain steam generator primary-to-secondary heat transfer data under refill conditions. The secondary pressure and inventory responses for both secondaries were outlined in the overall system response subsection. The mechanisms driving their responses consist simply of energy and mass balances for the secondaries and require no further elaboration. Therefore, this discussion will be limited primarily to the measured affected loop steam generator primary-to-secondary heat transfer data and the phenomena related to that data.

The response of the secondary convective heat transfer coefficient (Figures 92 through 99) to the voided secondary refill is characterized as a step change increase as saturated steam contacts the U-tube wall outside surface followed by a gradual reduction as the local vapor-void fraction (Figure 100) decreases. As shown in Figure 101, re-initiation of the local secondary convective heat transfer at each elevation does not occur until the tube bundle mixture level (the level determined

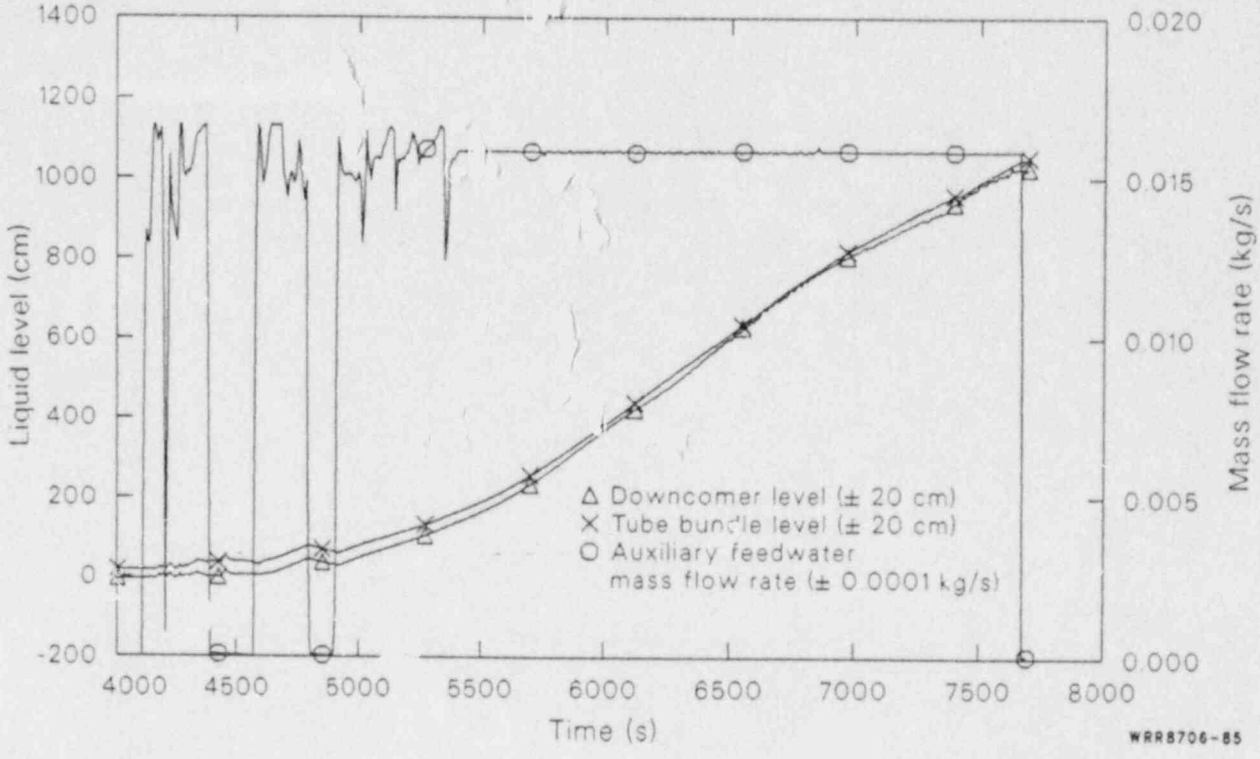

Figure 85. Affected loop steam generator downcomer and tube bundle overall collapsed liquid levels and auxiliary feedwater mass flow rate during the voided secondary refill phase of 50% FWLB experiment S-FS-11 (4000 to 8000 s).

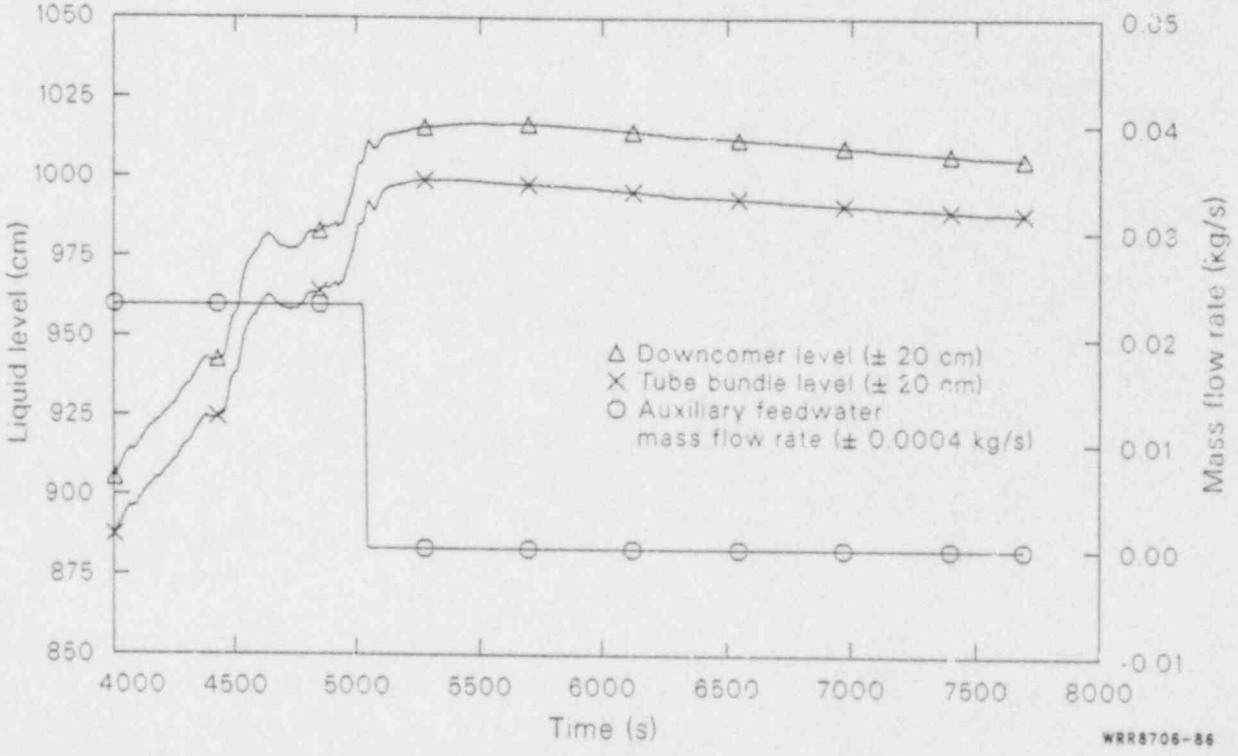

Figure 86. Unaffected loop steam generator downcomer and tube bundle overall collapsed liquid levels and auxiliary feedwater mass flow rate during the voided secondary refill phase of 50% FWLB experiment S-FS-11 (4000 to 8000 s).

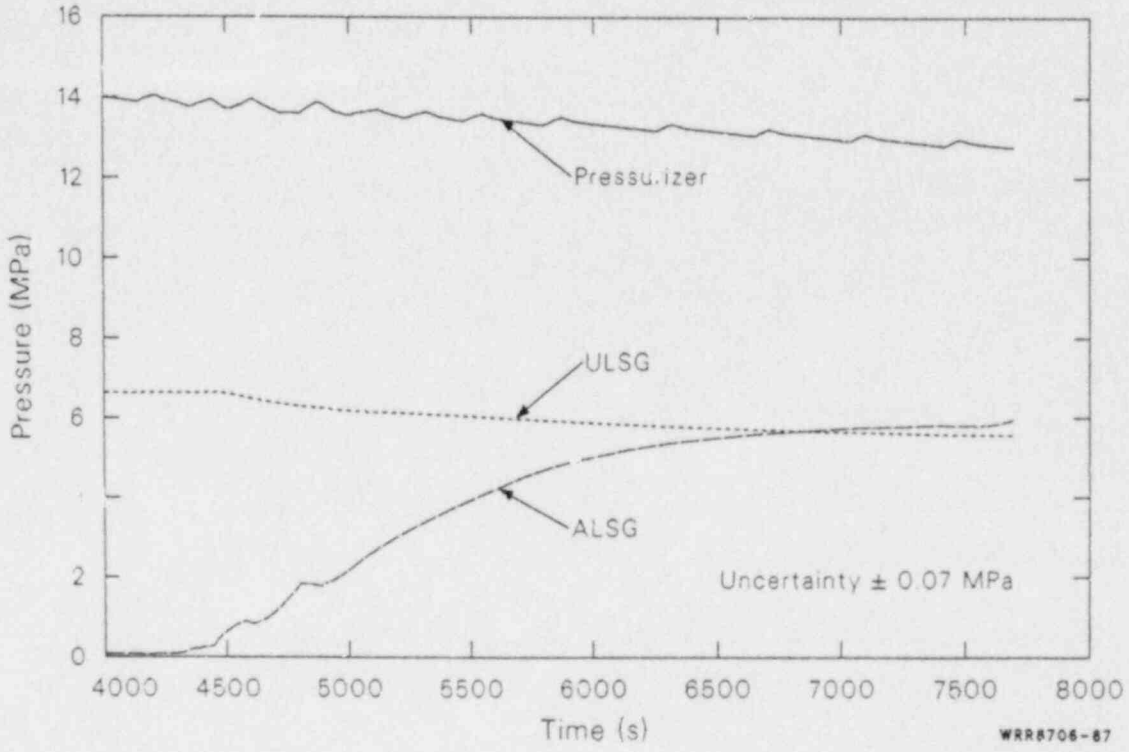

Figure 87. Pressurizer pressure, and affected and unaffected loop steam generator secondary pressures during the voided secondary refill phase of 50% FWLB experiment S-FS-11 (4000 to 8000 s).

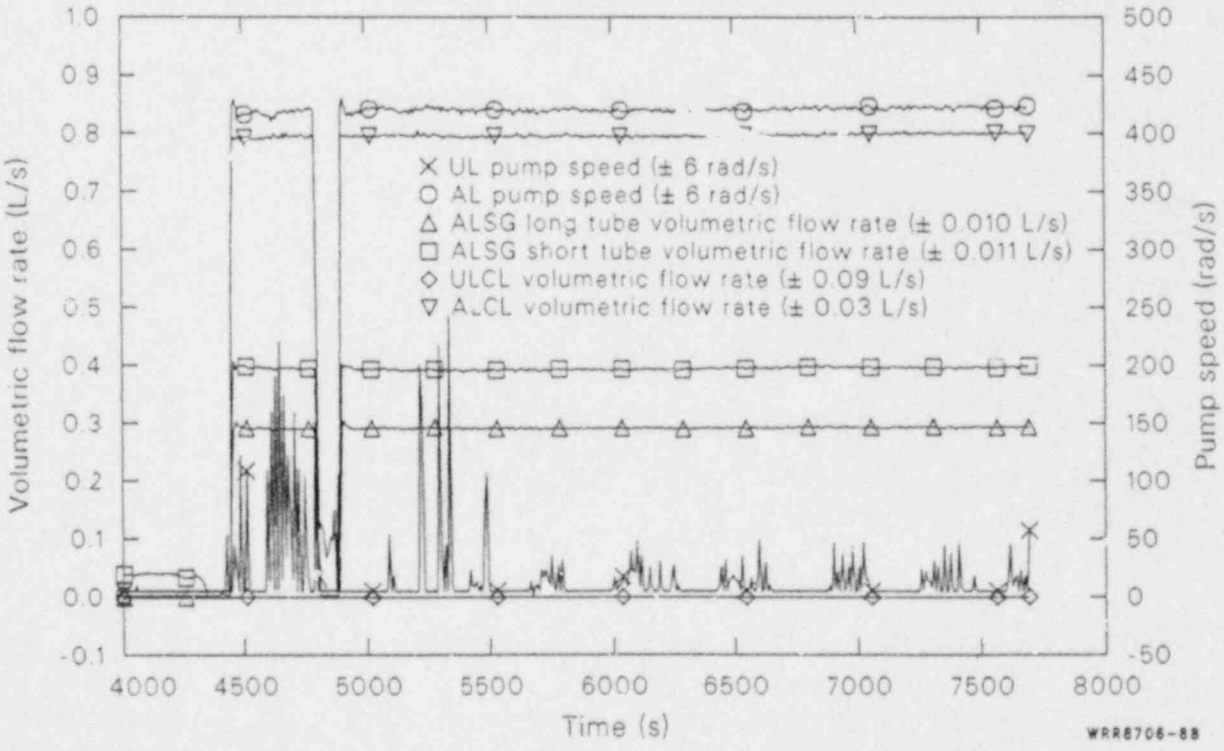

Figure 88. Affected and unaffected loop pump speeds, affected and unaffected loop cold leg volumetric flow rates, and affected loop steam generator long and short tube outlet volumetric flow rates during the voided secondary refill phase of 50% FWLB experiment S-FS-11 (4000 to 8000 s).

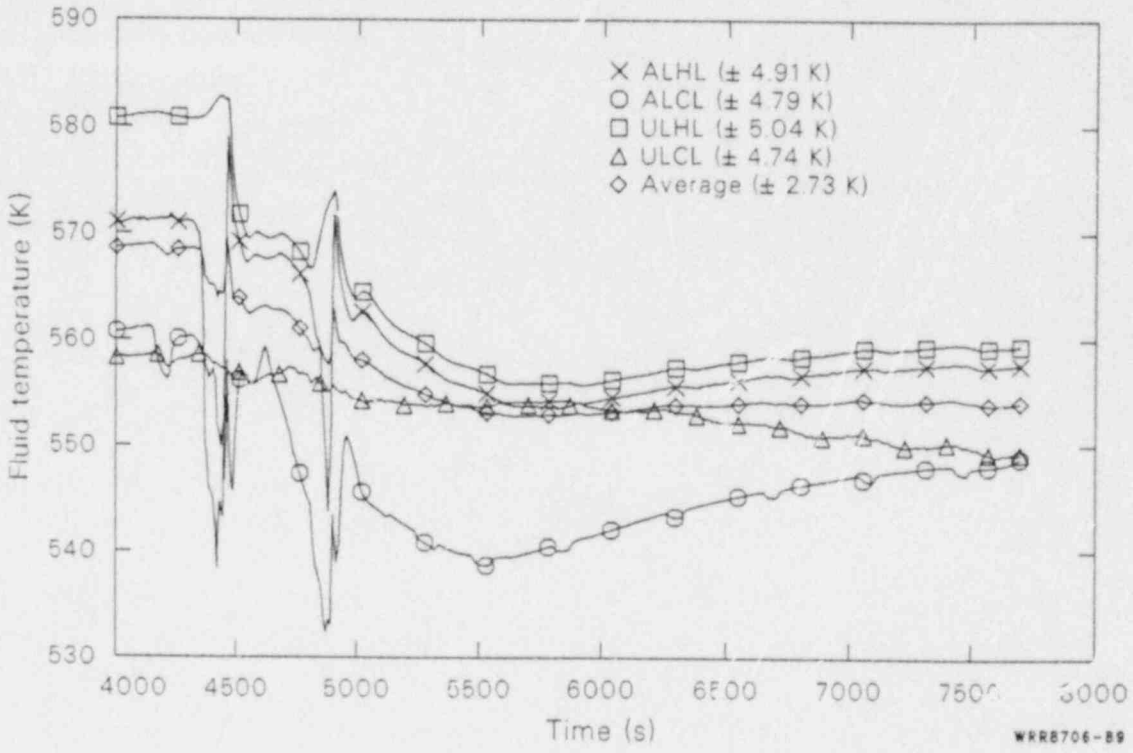

Figure 89. Affected and unaffected loop hot and cold leg, and average primary fluid temperatures during the voided secondary refill phase of 50% FWLB experiment S-FS-11 (4000 to 8000 s).

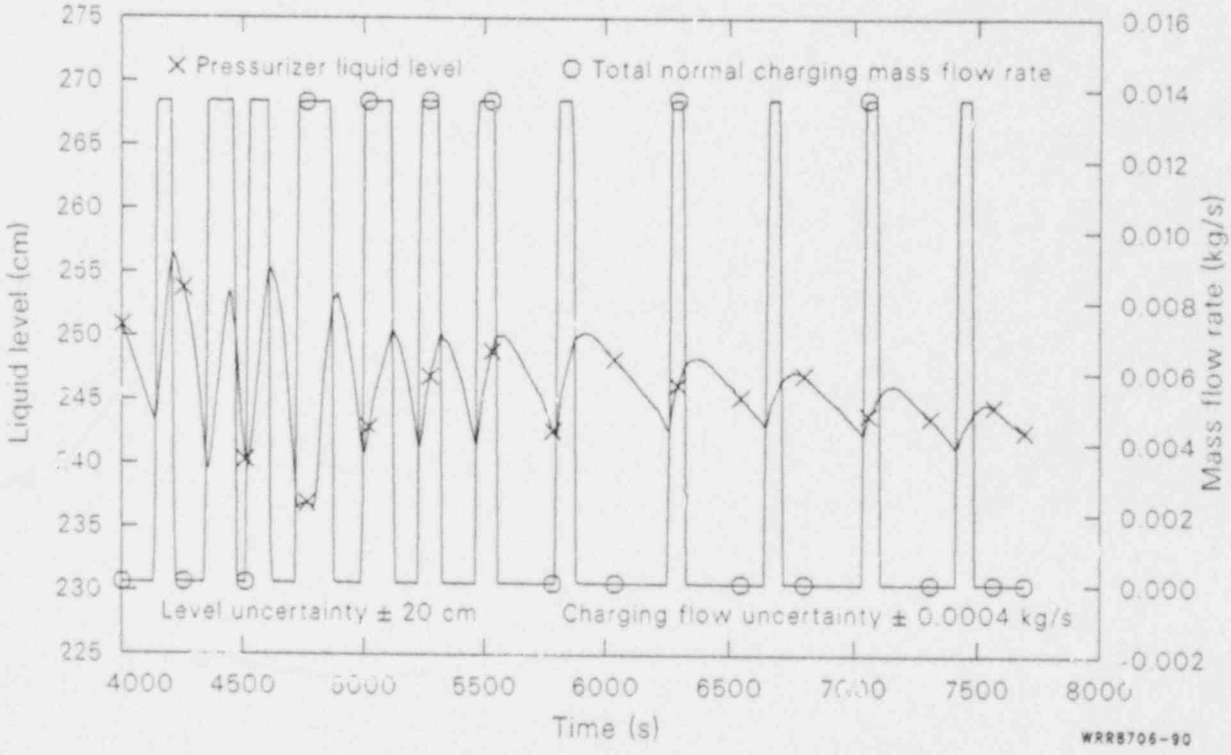

Figure 90. Pressurizer collapsed liquid level and total normal charging mass flow rate during the voided secondary refill phase of 50% FWLB experiment S-FS-11 (4000 to 8000 s).

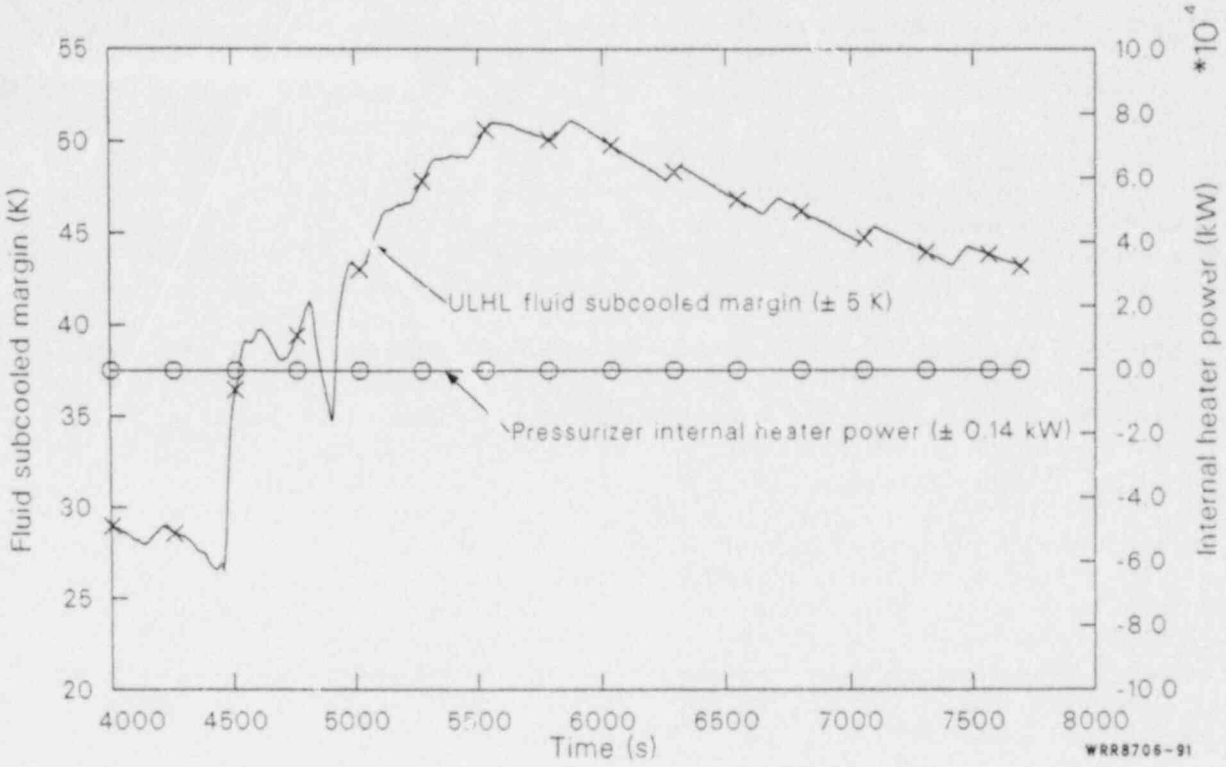

Figure 91. Unaffected loop hot leg fluid subcooled margin and pressurizer internal heater power during the voided secondary refill phase of 50% FWLB experiment S-FS-11 (4000 to 8000 s).

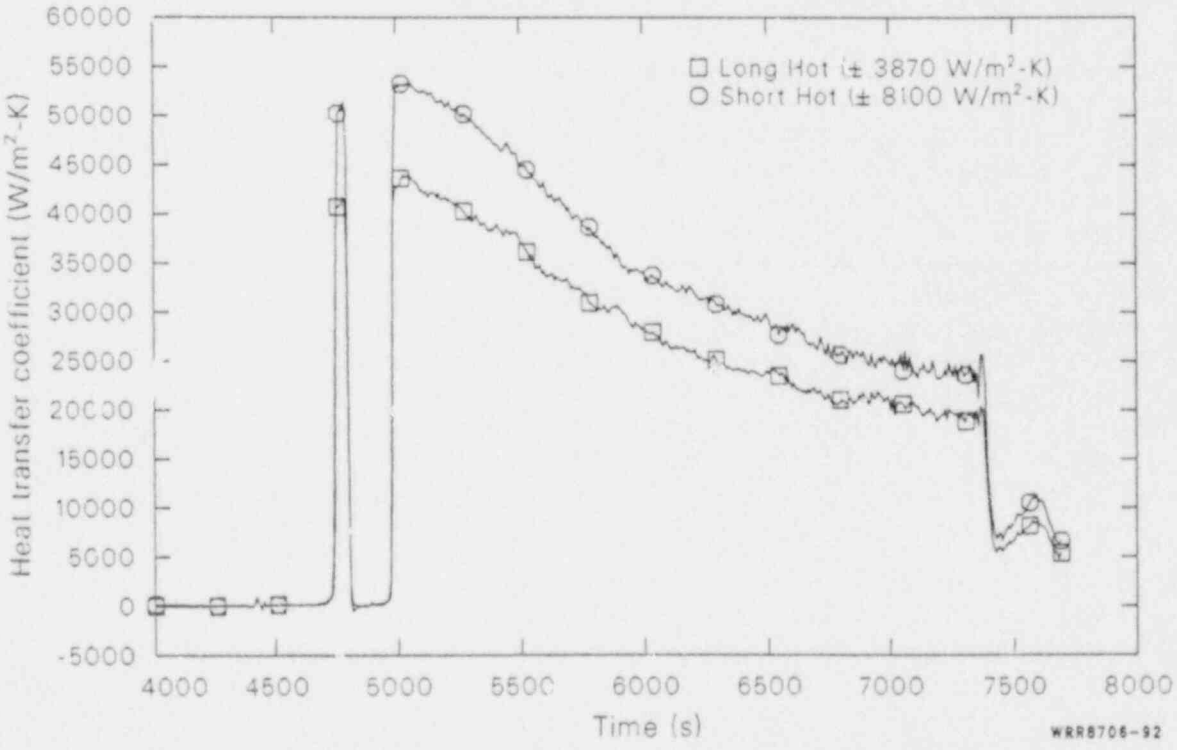

Figure 92. Affected loop steam generator secondary convective heat transfer coefficients at the 61 cm elevation during the voided secondary refill phase of 50% FWLB experiment S-FS-11 (4000 to 8000 s).

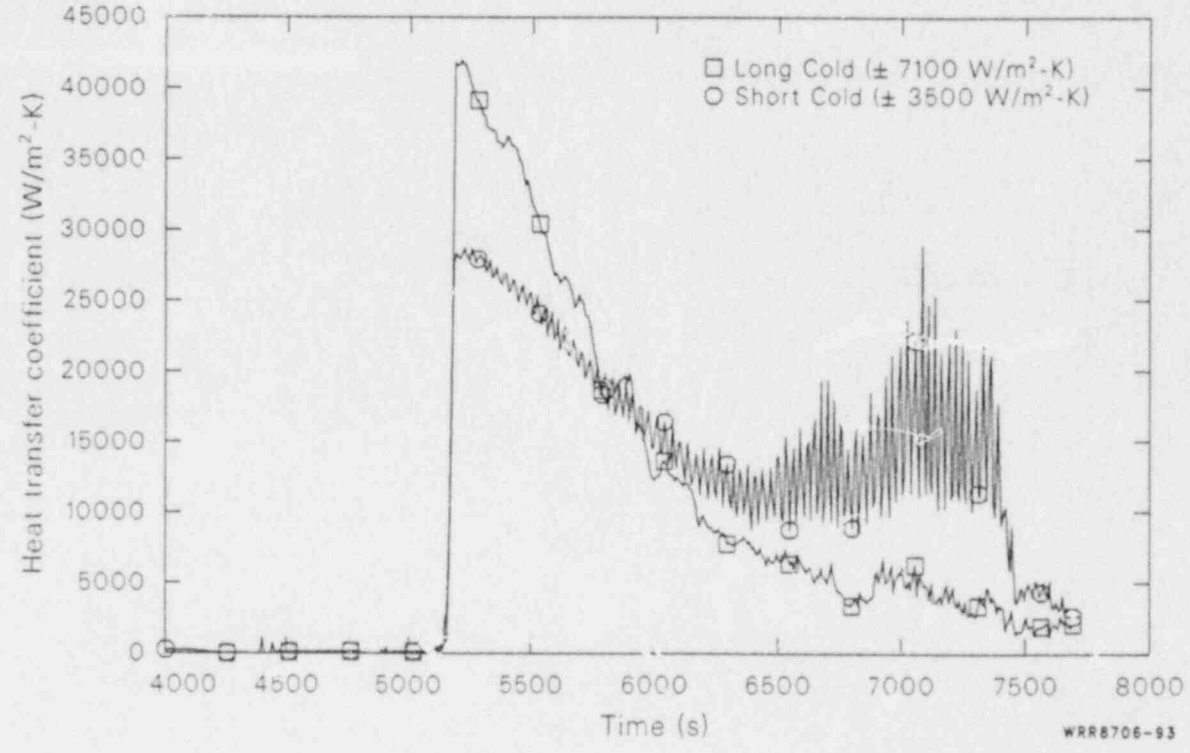

Figure 93. Affected loop steam generator secondary convective heat transfer coefficients at the 99 cm elevation during the voided secondary refill phase of 50% FWLB experiment S-FS-11 (4000 to 8000 s).

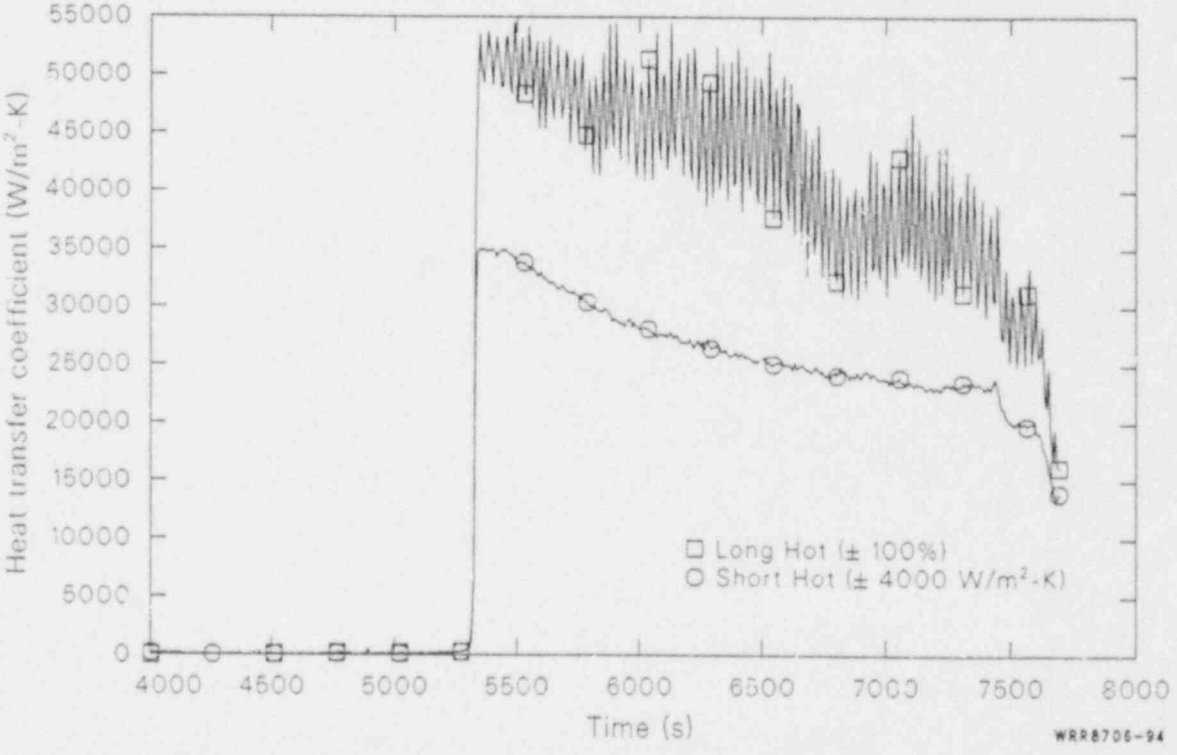

Figure 94. Affected loop steam generator secondary convective heat transfer coefficients at the 137 cm elevation during the voided secondary refill phase of 50% FWLB experiment S-FS-11 (4000 to 8000 s).

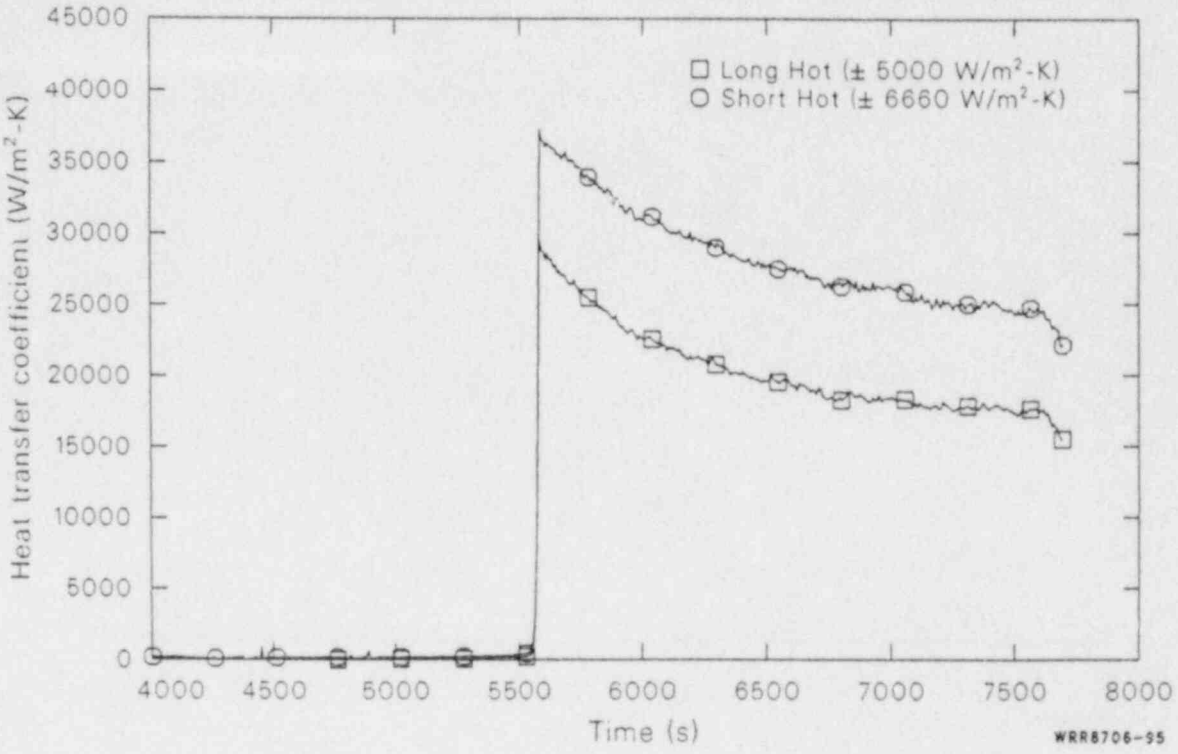

Figure 95. Affected loop steam generator secondary convective heat transfer coefficients at the 213 cm elevation during the voided secondary refill phase of 50% FWLB experiment S-FS-11 (4000 to 8000 s).

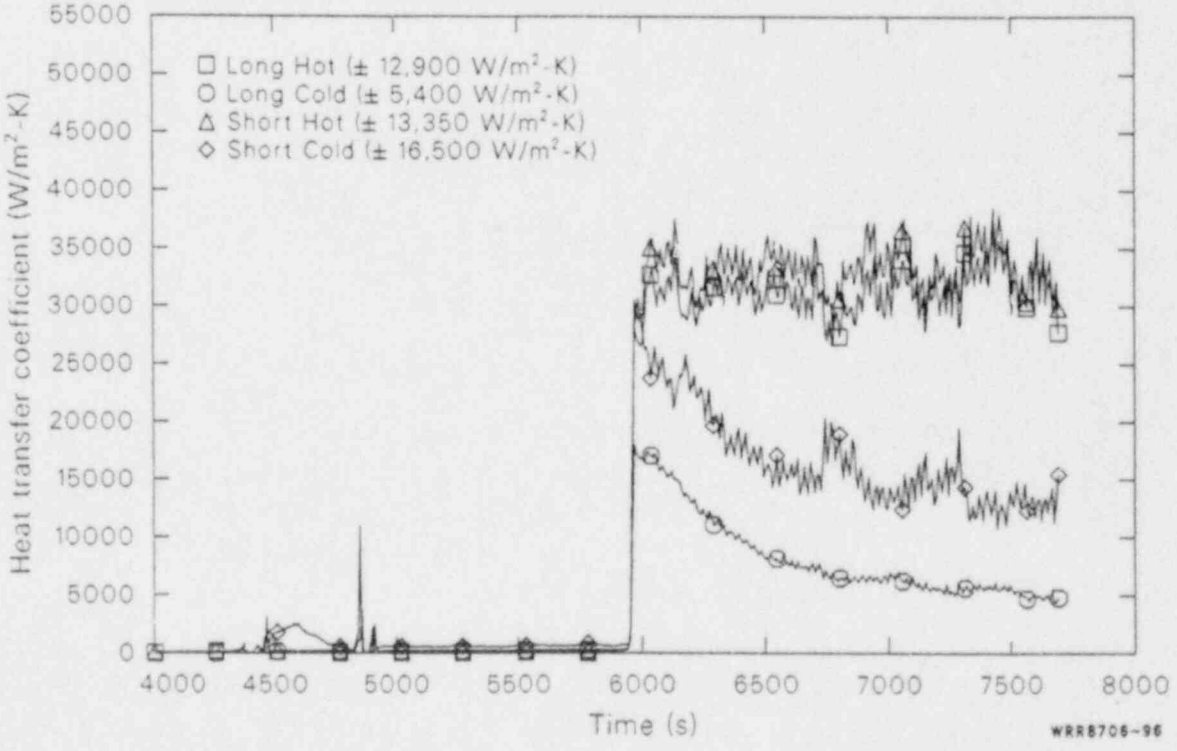

Figure 96. Affected loop steam generator secondary convective heat transfer coefficients at the 404 cm elevation during the voided secondary refill phase of 50% FWLB experiment S-FS-11 (4000 to 8000 s).

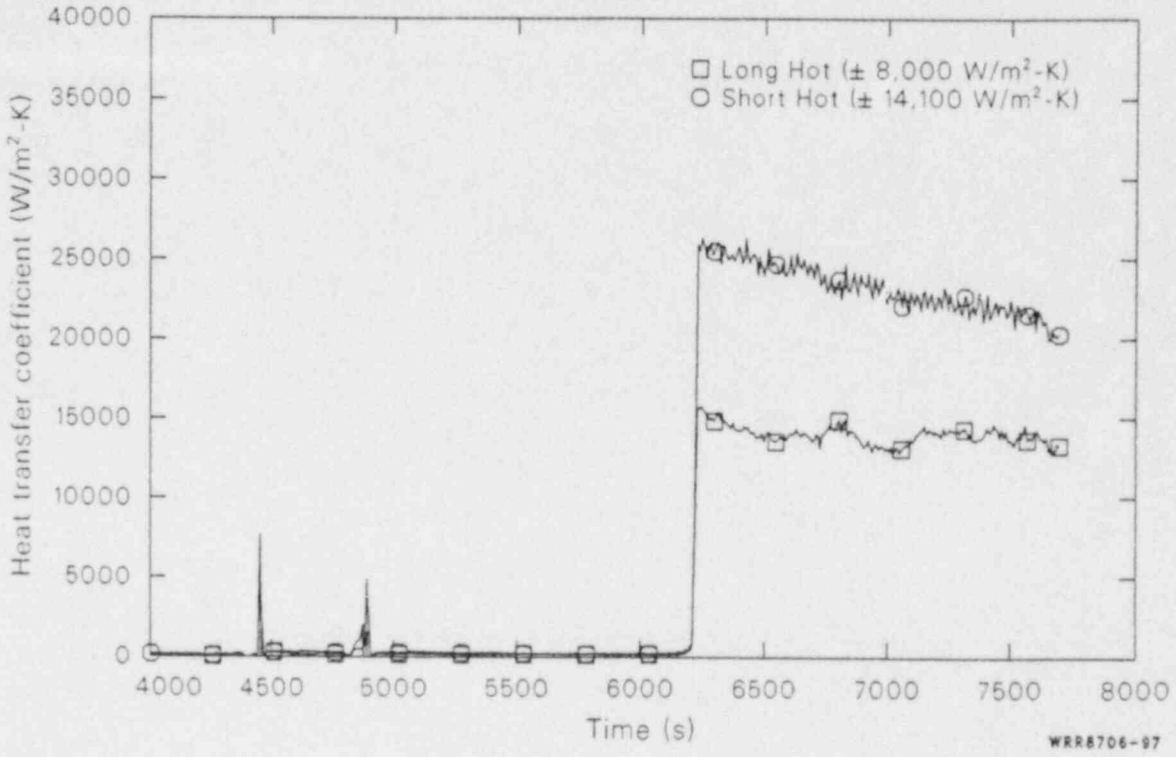

Figure 97. Affected loop steam generator secondary convective heat transfer coefficients at the 556 cm elevation during the voided secondary refill phase of 50% FWLB experiment S-FS-11 (4000 to 8000 s).

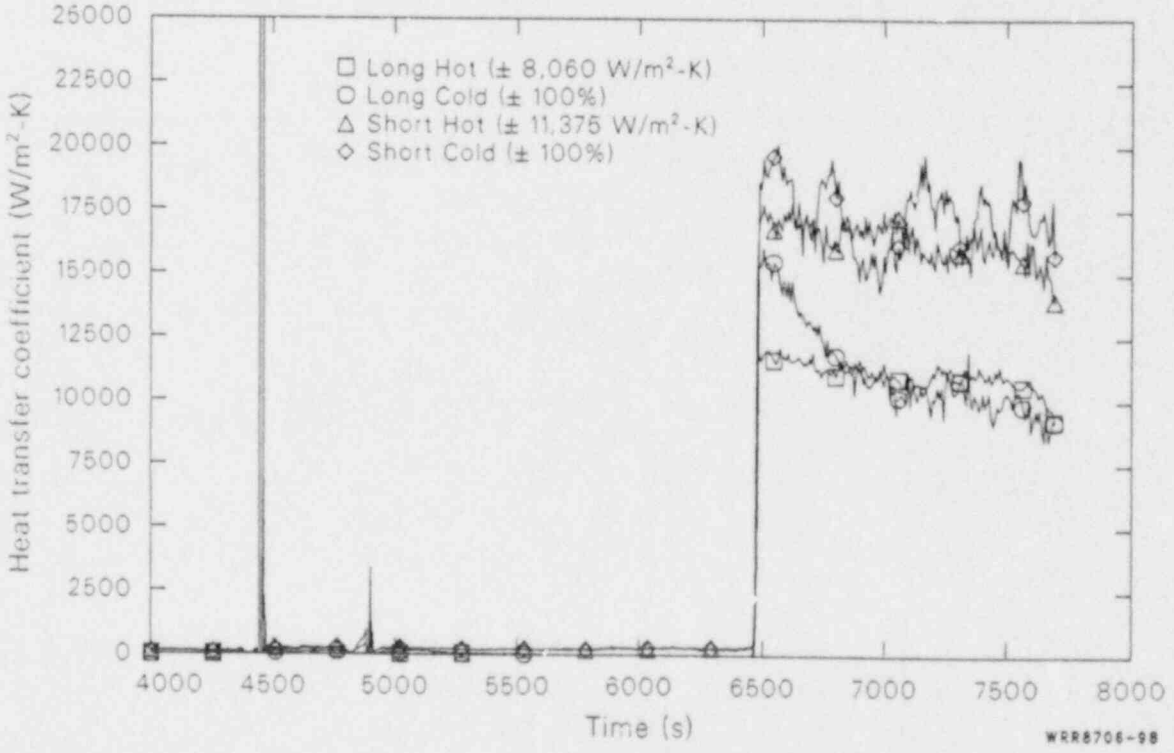

Figure 98. Affected loop steam generator secondary convective heat transfer coefficients at the 709 cm elevation during the voided secondary refill phase of 50% FWLB experiment S-FS-11 (4000 to 8000 s).

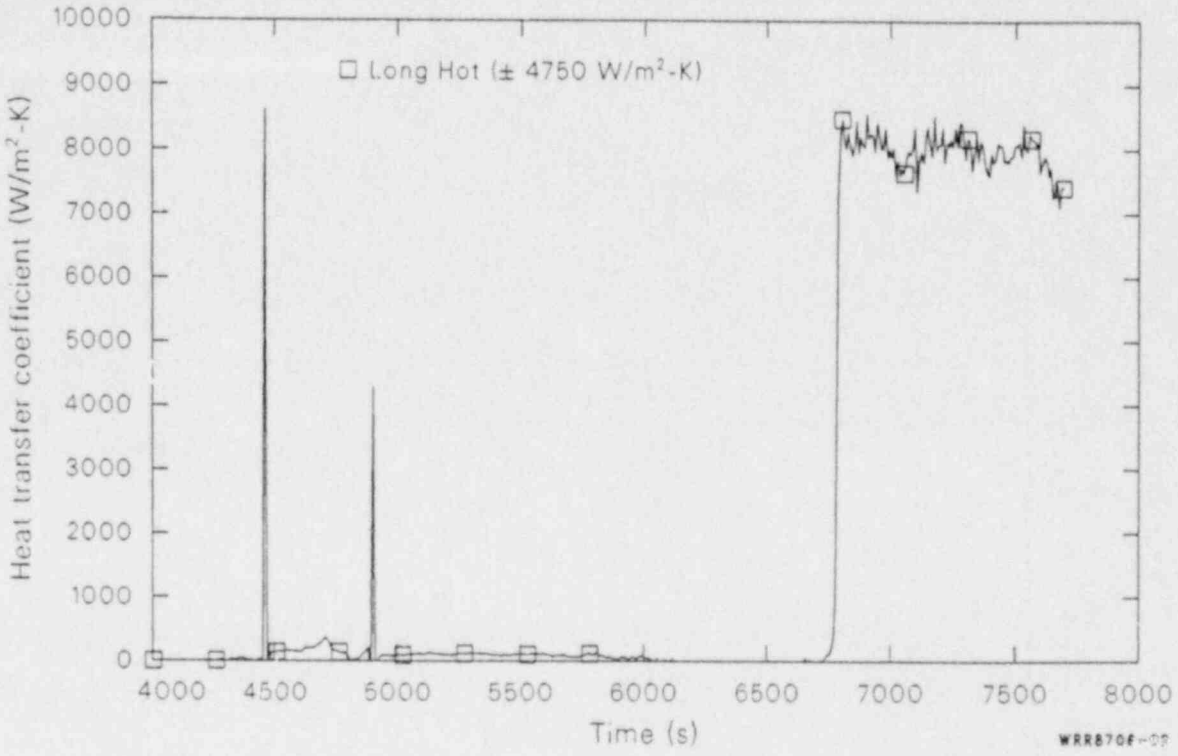

Figure 99. Affected loop steam generator secondary convective heat transfer coefficient at the 886 cm elevation during the voided secondary refill phase of 50% FWLB experiment S-FS-11 (4000 to 8000 s).

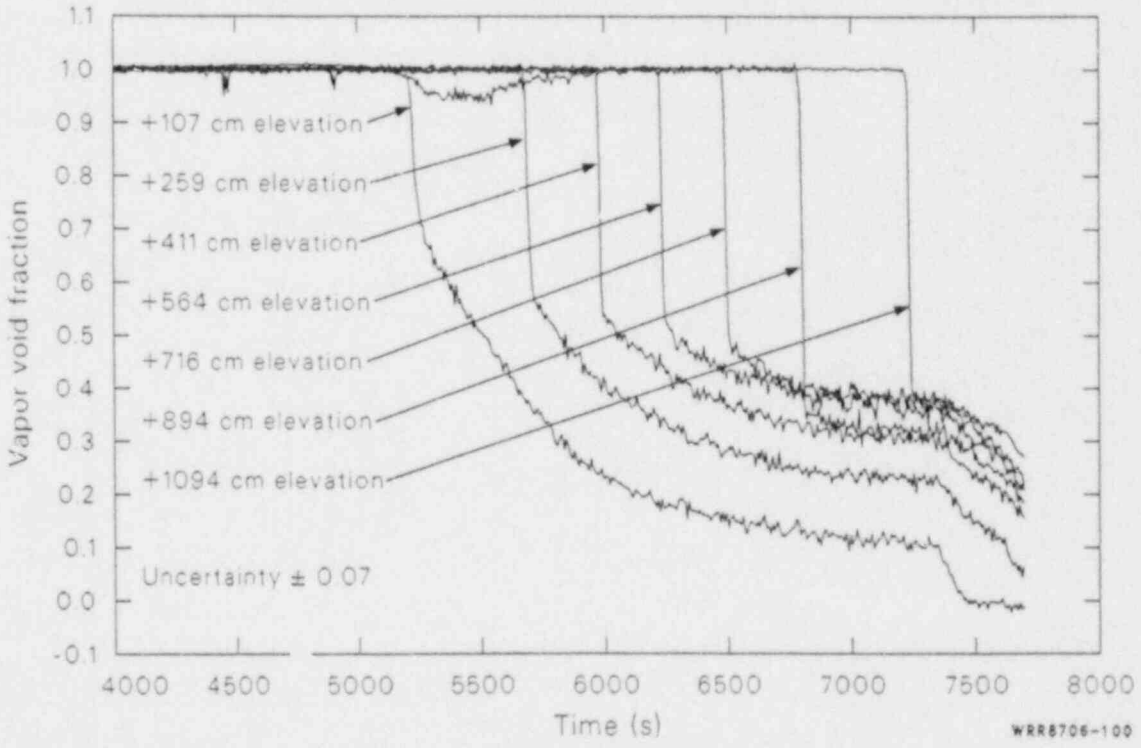

Figure 100. Affected loop steam generator tube bundle vapor-void fractions during the voided secondary refill phase of 50% FWLB experiment S-FS-11 (4000 to 8000 s).

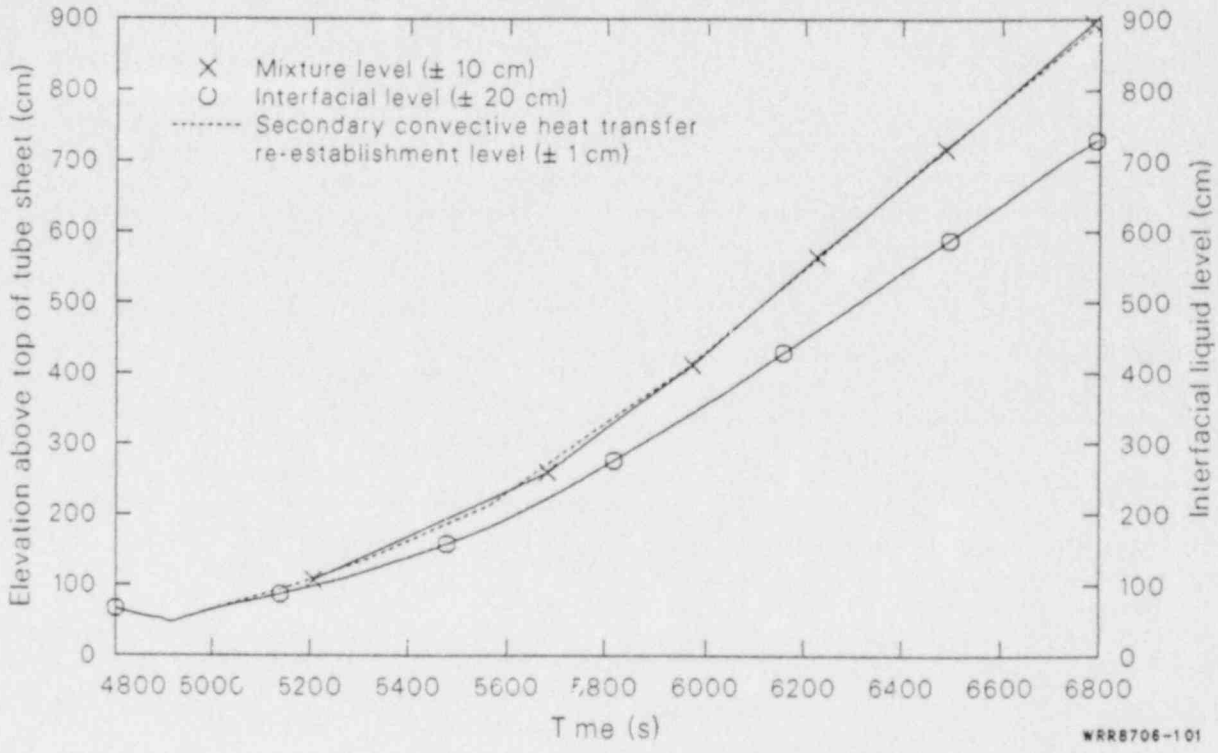

Figure 101. Affected loop steam generator tube bundle mixture level, secondary convective heat transfer re-establishment level, and interfacial liquid level during the voided secondary refill phase of 50% FWLB experiment S-FS-11 (4800 to 6800 s).

based on the timing of the initiation of the local vapor-void fraction reduction from 1.0 for each elevation) reaches that elevation. Thus, because of the relatively low heat flux and the relatively low initial wall temperatures, there is no precursory cooling such as occurs in a PWR core during reflood. The voided secondary refill heat-transfer response is more characteristic of a rewet type of mechanism where the re-initiation of convective heat transfer is dependent upon the existence of some liquid.

The affected loop steam generator secondary response to the voided secondary refill operations can be envisioned as a gradually increasing *pool* of two-phase mixture in the tube-bundle region. The progression of the level for the re-initiation of the local convective heat transfer is identical to the progression of the two-phase mixture level. The two-phase mixture level precedes the measured interfacial liquid level, with the magnitude of the level difference dependent upon the amount of voiding present in the two-phase mixture. The greater the amount of voiding, the greater the difference in the mixture and interfacial liquid levels. This is the reason for the gradual divergence of the mixture and interfacial levels shown in Figure 101.

While the affected loop steam generator secondary response can be envisioned as a gradually increasing *pool* of two-phase mixture, the nature of the response of the measured secondary convective heat transfer coefficients does not agree with that predicted by existing boiling heat transfer correlations (References 20 through 24). The measured secondary convective heat transfer coefficients decrease with decreasing void fraction, while existing correlations either have no void fraction dependency or produce the opposite trend with regard to void fraction. This difference in the secondary convective heat transfer coefficient predicted and measured trends is the same as that discussed earlier for full-power conditions.

The Semiscale Type III affected loop steam generator heat transfer data points out a definite deficiency in current boiling heat transfer correlations for predicting secondary convective heat transfer coefficients. It is very probable that the correlation deficiencies are due to the fact that the correlations were developed from data for flow inside of a heated tube, not for flow around heated tubes in a tube bundle. Vapor present inside of a heated tube can blanket the tube inside wall, limiting the area for liquid contact with the wall and reducing the

local convective heat transfer coefficient, as predicted by the existing correlations. However, vapor present around the outside of a tube bundle can produce a turbulent mixing and *pumping* action, which can increase both the liquid and the vapor cooling efficiency, thereby increasing the local convective heat transfer coefficient (as observed in the Semiscale data).

Primary System Response to Voided Secondary Refill Operations. The primary system response to the voided secondary refill operations is characterized as a very gradual cooldown and depressurization. The major change in the primary response during this phase was in response to re-initiation of the affected loop steam generator primary-to-secondary heat transfer and the primary coolant pump restart.

The re-initiation of the affected loop steam generator primary energy removal initially cooled the primary substantially as the affected loop steam generator primary energy removal combined with the unaffected loop steam generator primary energy removal to cool the primary fluid. Following termination of the unaffected loop steam generator auxiliary feedwater injection, the affected loop steam generator primary energy removal increased to the level of the unaugmented core power (Figure 102). The primary system then entered a phase of nearly constant average fluid temperature with very gradual cooling and depressurization.

Restarting the affected loop primary coolant pump caused the hot leg temperatures to decrease, while the cold leg temperatures increased (Figure 89). This was due to the increased flow rate through the loops and the core reducing the magnitude of the resultant fluid temperature rise for the same amount of heat transfer. The reduced unaffected loop hot leg temperature produced an increased primary subcooled margin (Figure 91), which aided in maintaining stable operating conditions. The voided secondary refill operations were very effective in maintaining stable conditions in the system.

Comparisons of Voided Secondary Refill Responses. With the exception of the affected loop steam generator auxiliary feedwater mass flow rate, the specified operations for the voided secondary refill phase of tests S-FS-7 and S-FS-11 were the same. The basic response of the system to the voided secondary refill operations was the same for both tests with the differences primarily in the timing of events and the magnitudes of the affected loop steam generator heat transfer parameters. Figures containing the pertinent parameters for the overall system response (the same parameters as those presented in the overall system response subsection for test S-FS-11), for test S-FS-7 may be found in Appendix D (Figures D-33 through D-39).

The voided secondary refill operations were specified to be initiated at the end of the stabilization phase for both tests. The refill operations were initiated by closing the affected loop steam generator bottom main feedwater line break valve (isolating the break) and re-initiating the affected loop steam generator auxiliary feedwater flow. This occurred at 6204 s for test S-FS-7 and 4100 s for test S-FS-11, with the auxiliary feedwater flow at a scaled degraded flow rate (0.004 kg/s) for test S-FS-7 and the scaled typical flow rate (0.016 kg/s) for test S-FS-11. For both tests, the initiation of the increase in the secondary level was delayed until the break assembly and feedwater line piping were refilled. The primary-to-secondary heat transfer was then re-initiated as the liquid supplied to the tube-bundle region was heated by the primary fluid. For both tests, the basic response to the re-initiation of the affected loop steam generator primary energy removal was the same. The primary coolant pumps had to be restarted and the unaffected loop steam generator auxiliary feedwater flow was terminated for both tests. The main differences in the overall response were: the unaffected loop steam generator ADV had to be cycled once during test S-FS-7; both primary coolant pumps were operated for test S-FS-7; and the affected loop steam generator primary energy removal and more stabilization operations were required due to the greater length of time involved in refilling the affected loop steam generator. Also, test S-FS-7 was terminated at 20,000 s due to data acquisition time limitations with the affected loop steam generator secondary level below 1036 cm. While more operations were required for test S-FS-7, the basic responses were the same for both tests.

The secondary convective heat transfer coefficients for test S-FS-7 (Figures 103 through 109) showed the same characteristic response to the voided secondary refill as those for test S-FS-11. They exhibited a step change increase as saturated steam contacted the U-tube wall outside surface, followed by a gradual reduction as the local vapor-void fraction (Figure 110) decreased. The magnitudes of the secondary convective heat transfer coefficients were, however, much lower than for test S-FS-11. Similar to test S-FS-11, re-initiation of the local secondary convective heat transfer at each elevation did not occur until the tube bundle mixture level reached that

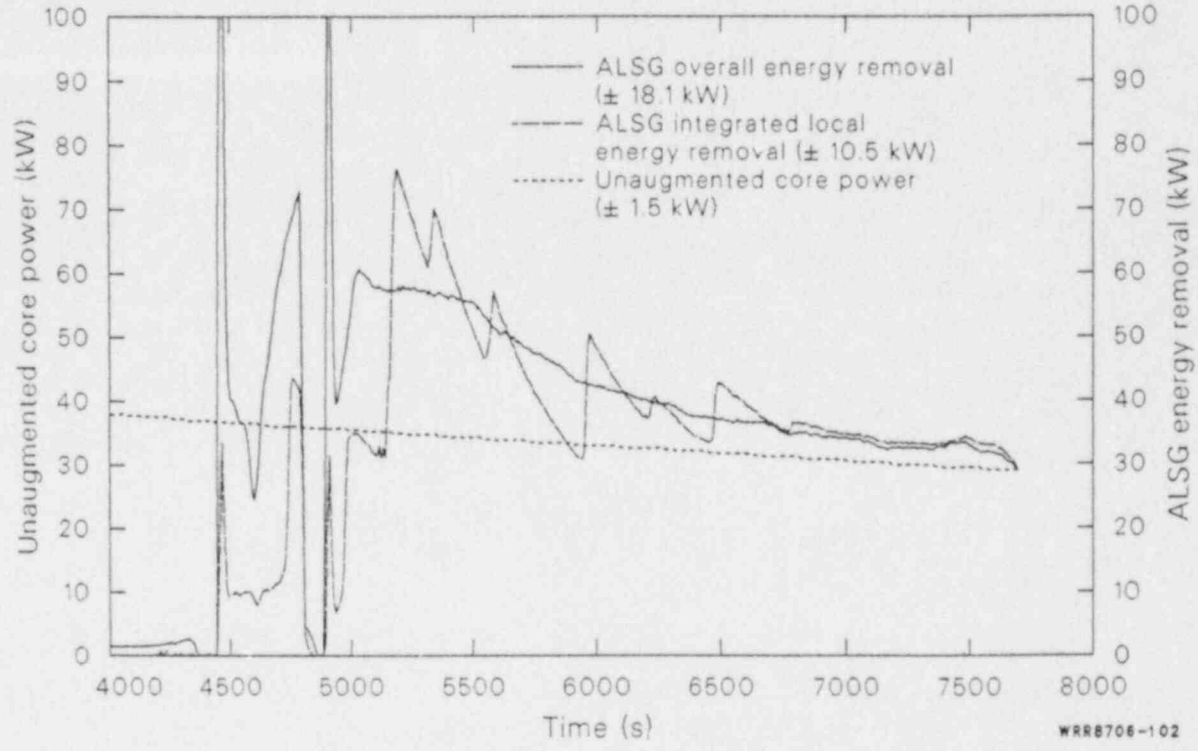

Figure 102. Affected loop steam generator primary-to-secondary heat transfer and core power during the voided secondary refill phase of 50% FWLB experiment S-FS-11 (4000 to 8000 s).

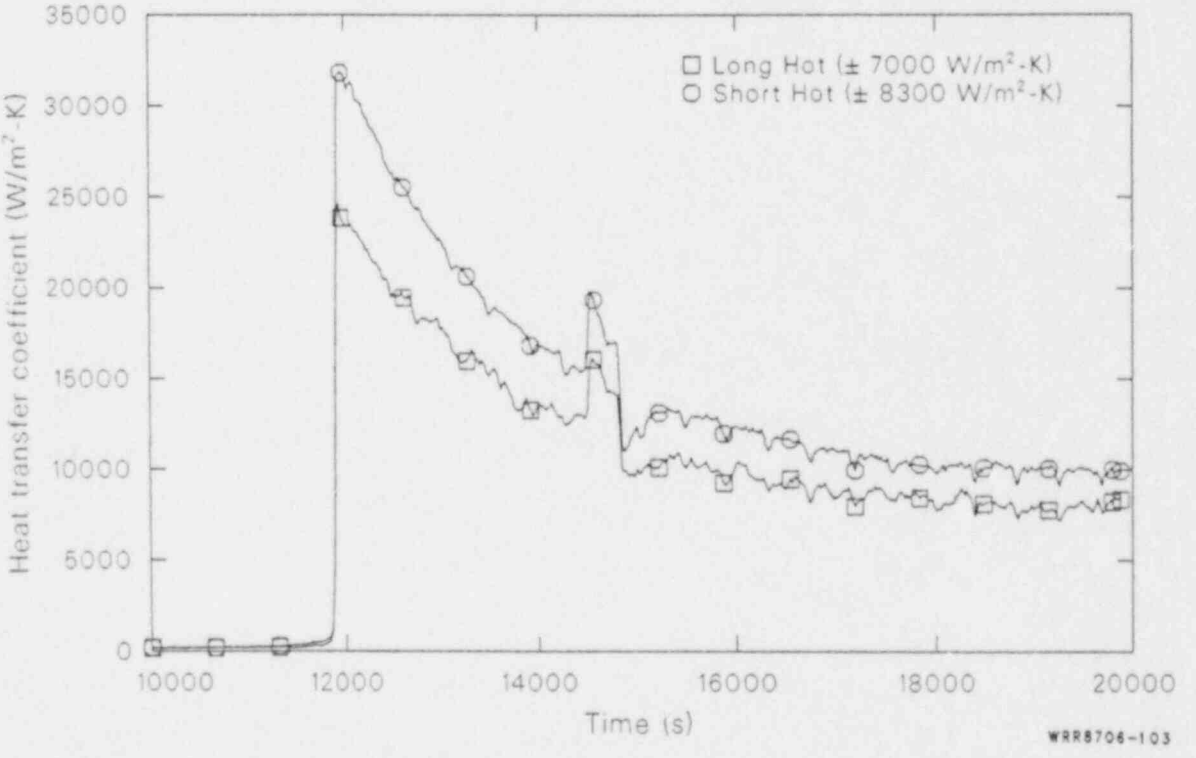

Figure 103. Affected loop steam generator secondary convective heat transfer coefficients at the 61 cm elevation during the voided secondary refill phase of 14.3% FWLB experiment S-FS-7 (10,000 to 20,000 s).

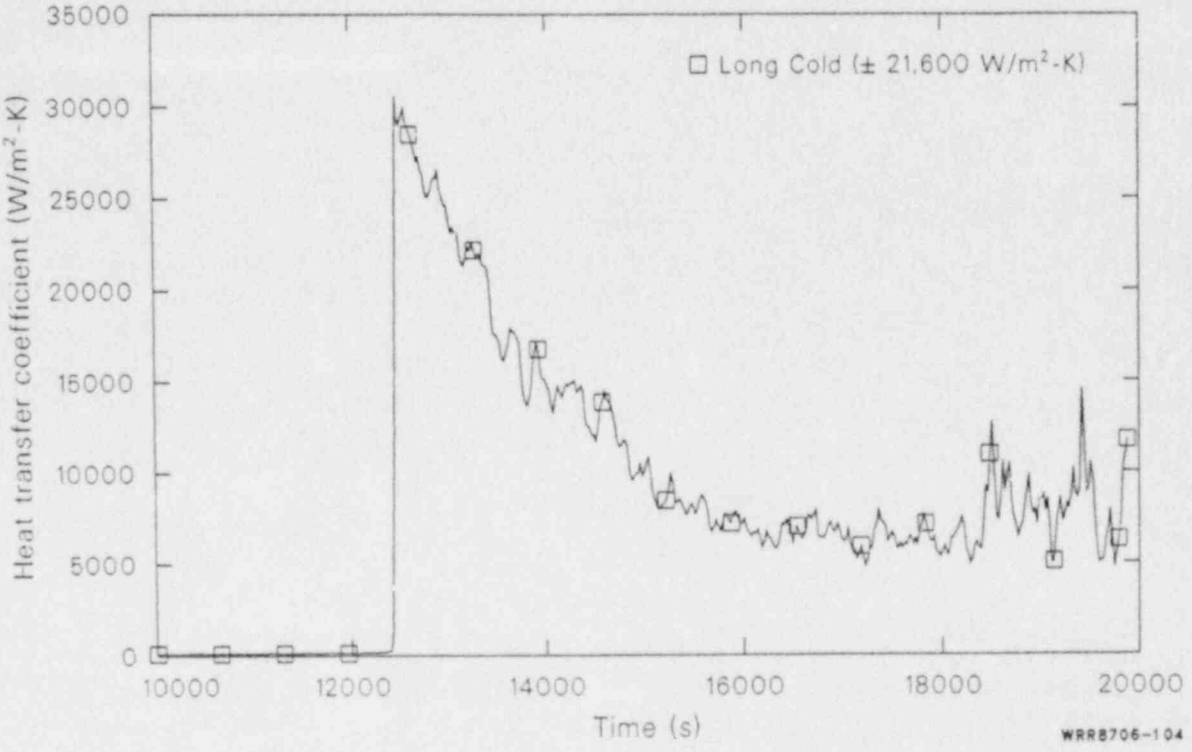

Figure 104. Affected loop steam generator secondary convective heat transfer coefficients at the 99 cm elevation during the voided secondary refill phase of 14.3% FWLB experiment S-FS-7 (10,000 to 20,000 s).

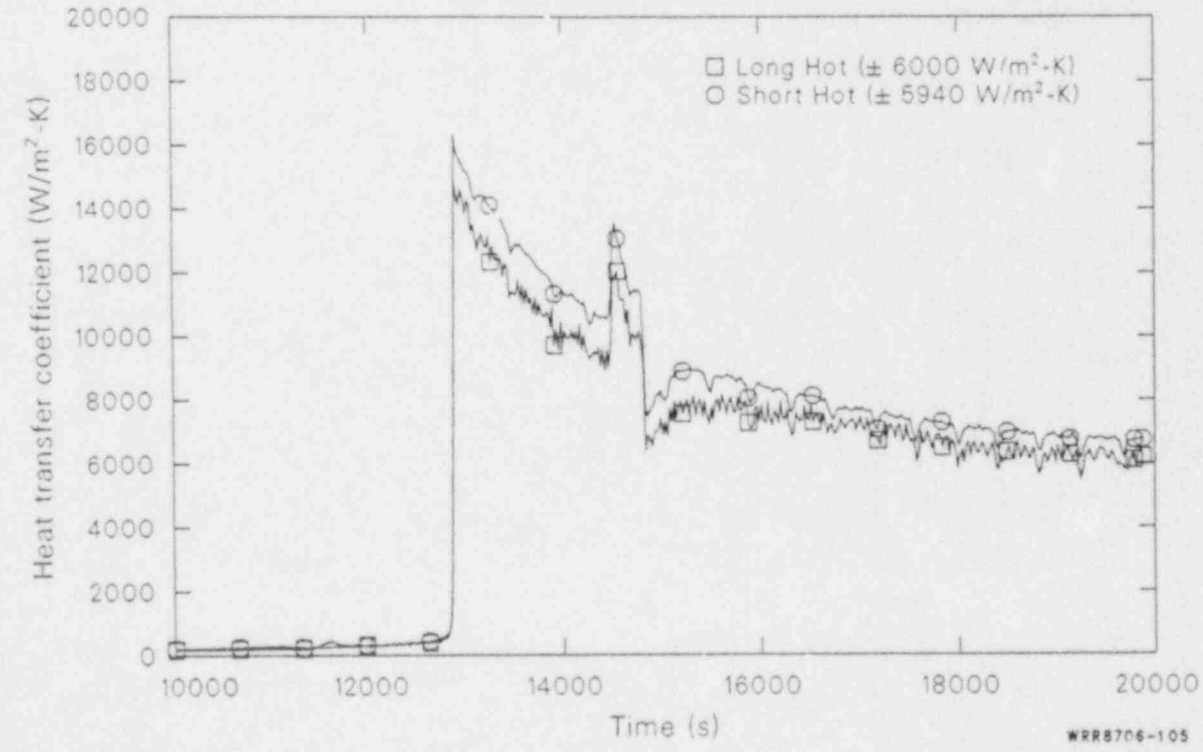

Figure 105. Affected loop steam generator secondary convective heat transfer coefficients at the 137 cm elevation during the voided secondary refill phase of 14.3% FWLB experiment S-FS-7 (10,000 to 20,000 s).

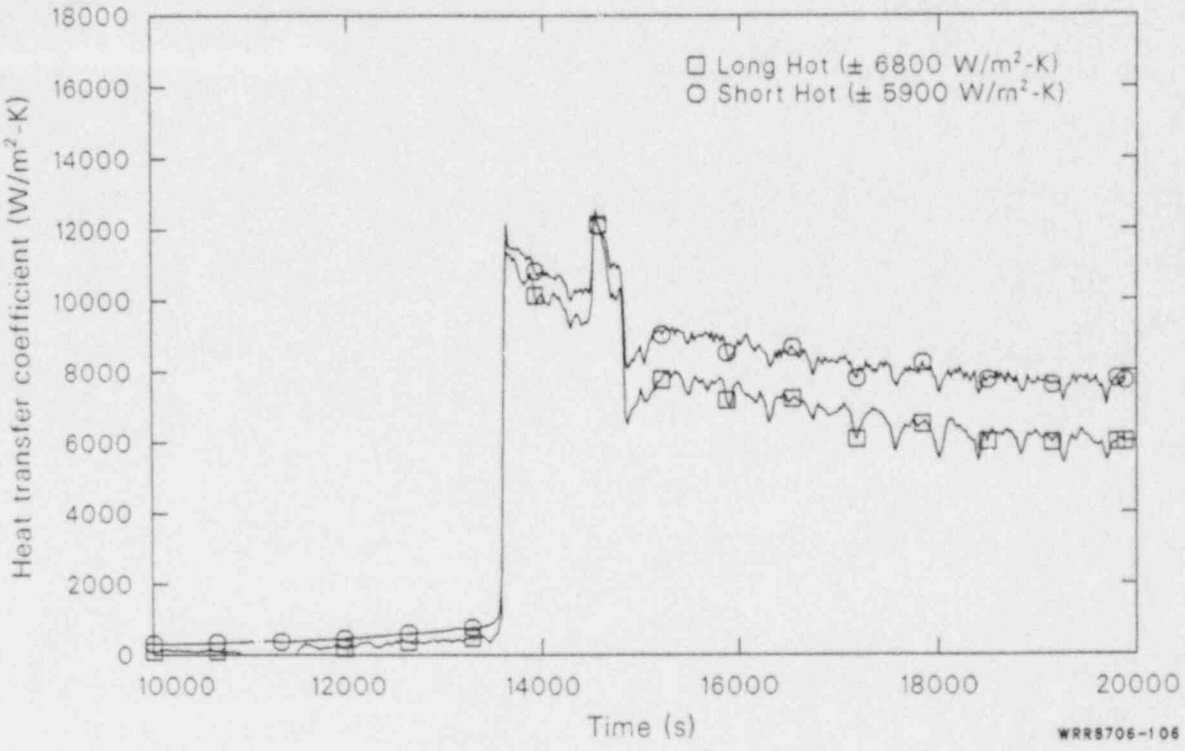

Figure 106. Affected loop steam generator secondary convective heat transfer coefficients at the 213 cm elevation during the voided secondary refill phase of 14.3% FWLB experiment S-FS-7 (10,000 to 20,000 s).

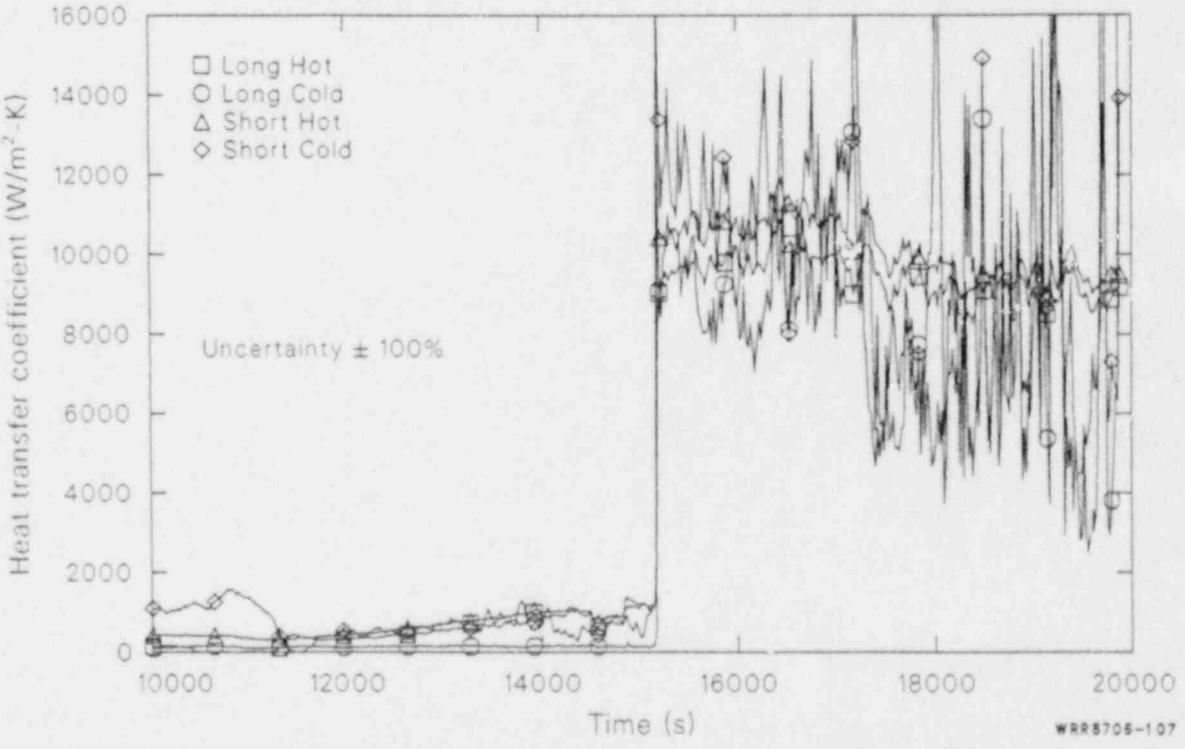

Figure 107. Affected loop steam generator secondary convective heat transfer coefficients at the 404 cm elevation during the voided secondary refill phase of 14.3% FWLB experiment S-FS-7 (10,000 to 20,000 s).

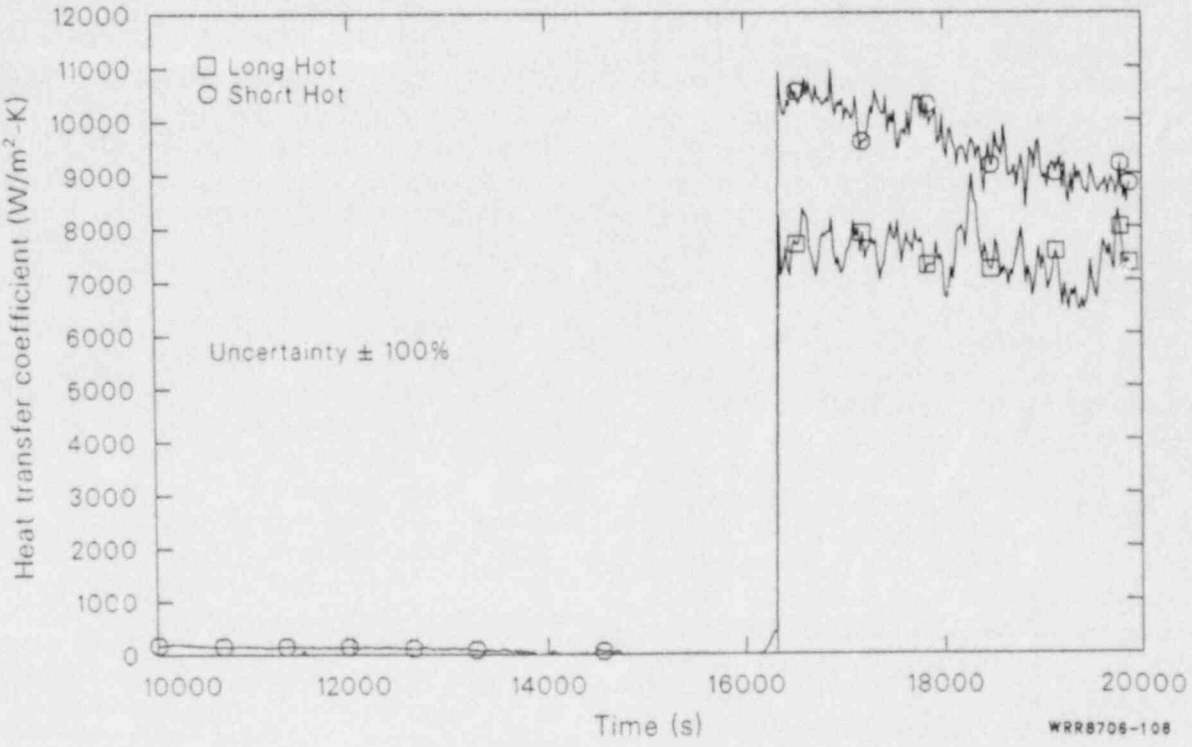

Figure 108. Affected loop steam generator secondary convective heat transfer coefficients at the 556 cm elevation during the voided secondary refill phase of 14.3% FWLB experiment S-FS-7 (10,000 to 20,000 s).

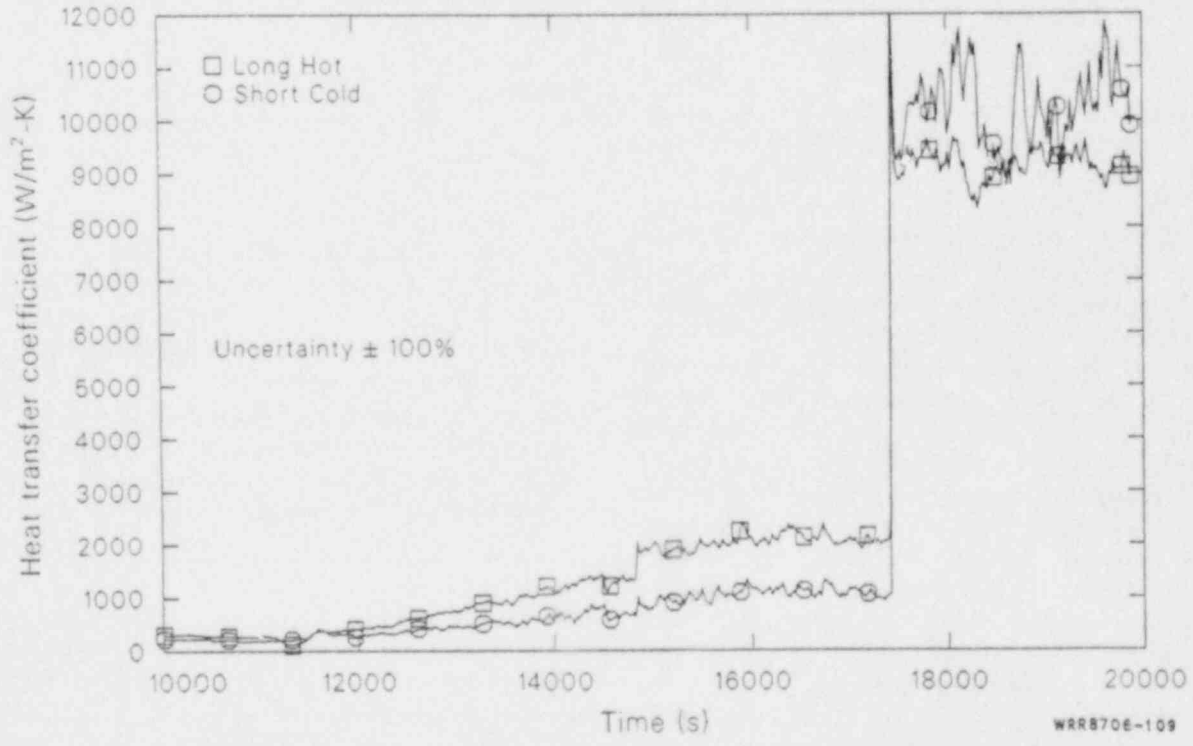

Figure 109. Affected loop steam generator secondary convective heat transfer coefficients at the 709 cm elevation during the voided secondary refill phase of 14.3% FWLB experiment S-FS-7 (10,000 to 20,000 s).

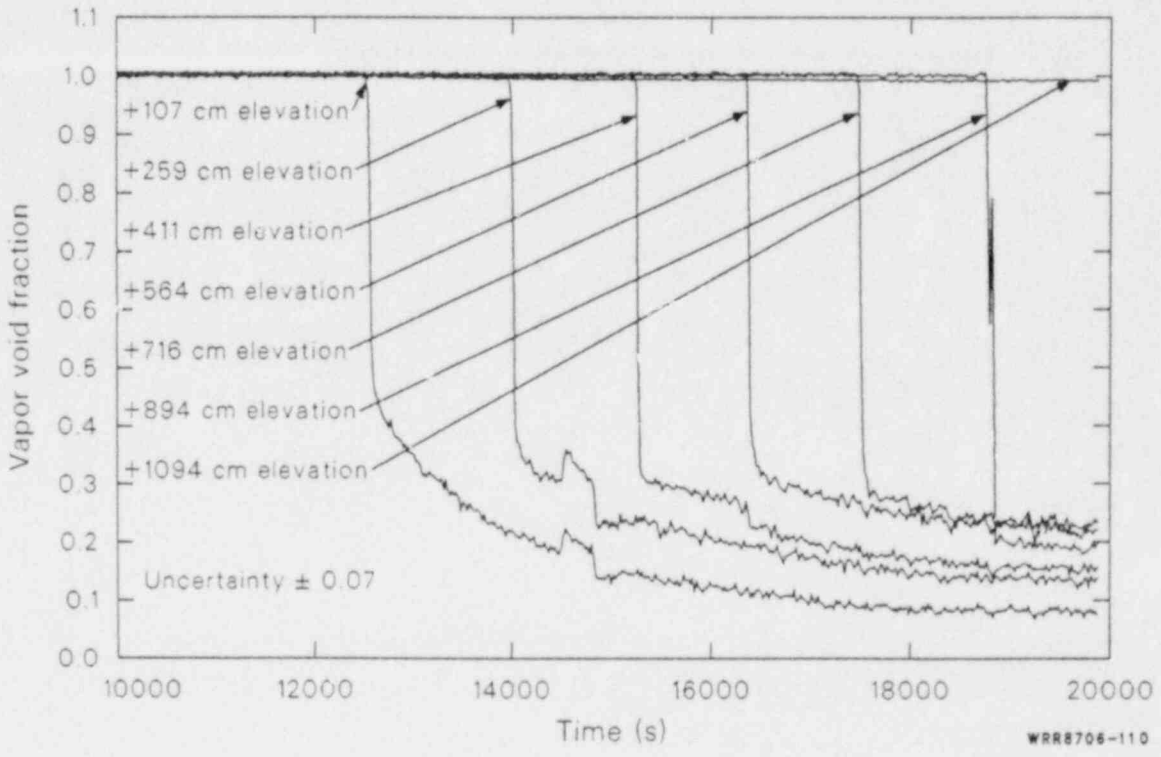

Figure 110. Affected loop steam generator tube bundle vapor-void fractions during the voided secondary refill phase of 14.3% FWLB experiment S-FS-7 (10,000 to 20,000 s).

elevation. The voided secondary refill heat transfer response was more characteristic of a rewet type of mechanism for both test.

For both tests, the affected loop steam generator secondary response to the voided secondary refill operations can be envisioned as a gradually increasing *pool* of two-phase mixture in the tube-bundle region. The progression of the level for the re-initiation of the local convective heat transfer is identical to the progression of the two-phase mixture level. The two-phase mixture level precedes the measured interfacial liquid level, with the magnitude of the level difference dependent upon the amount of voiding present in the two-phase mixture. The greater the amount of voiding, the greater the difference in the mixture and interfacial liquid levels, as shown in Figure 111.

The measured local secondary convective heat transfer coefficients for both tests exhibited the same trend of decreasing local heat transfer coefficient with decreasing local vapor-void fraction. This trend is directly the opposite of that predicted by existing correlations and further supports the conclusion that the existing correlations are not sufficient for predicting tube bundle exterior convective boiling heat transfer coefficients.

For both tests, the primary system response to the voided secondary refill operations is characterized as a very gradual cooldown and depressurization. The major change in the primary response during this phase of the tests was in the response to re-initiation of the affected loop steam generator primary-to-secondary heat transfer and the primary coolant pump restart.

The re-initiation of the affected loop steam generator primary energy removal in both tests initially cooled the primary substantially as the affected loop steam generator primary energy removal combined with the unaffected loop steam generator primary energy removal to cool the primary fluid. Following termination of the unaffected loop steam generator auxiliary feedwater injection, the affected loop steam generator primary energy removal increased to the level of the unaugmented core power (Figures 102 and 112). The primary system then entered a phase of nearly constant average fluid temperature with very gradual cooling and depressurization.

Restarting the affected loop primary coolant pump caused the hot leg temperatures to decrease, while the cold leg temperatures increased for both tests. The reduced unaffected loop hot leg temperature produced an increased primary subcooled

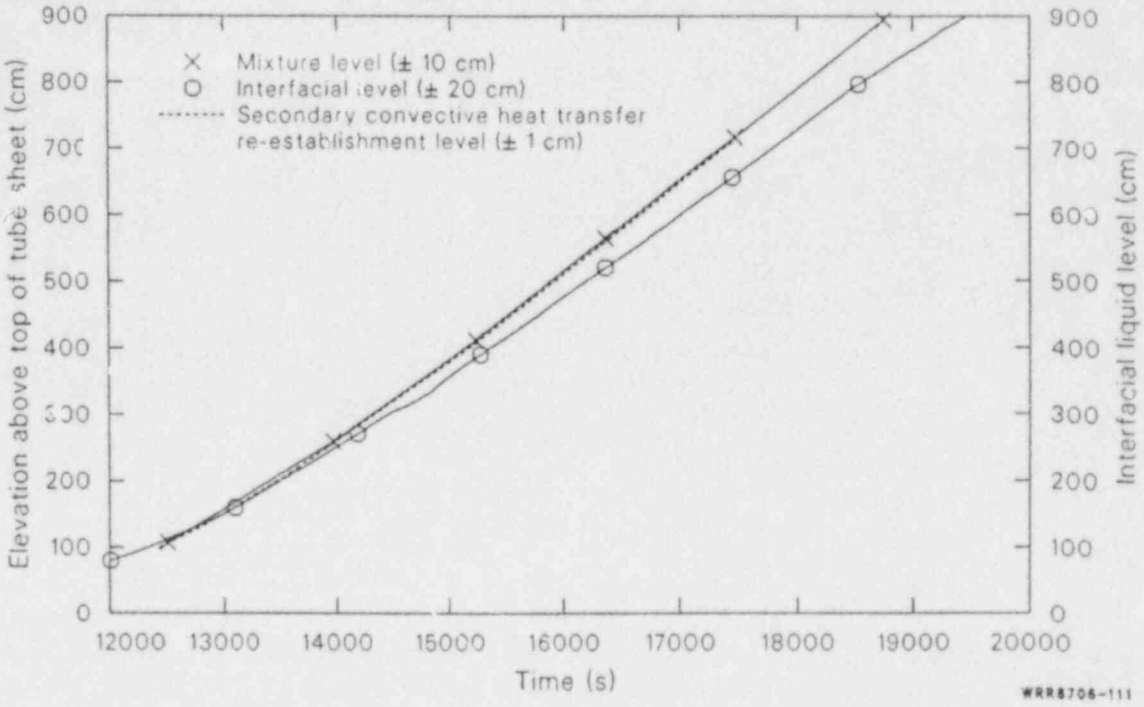

Figure 111. Affected loop steam generator tube bundle mixture level, secondary convective heat transfer re-establishment level, and interfacial liquid level during the voided secondary refill phase of 14.3% FWLB experiment S-FS-7 (12,000 to 19,500 s).

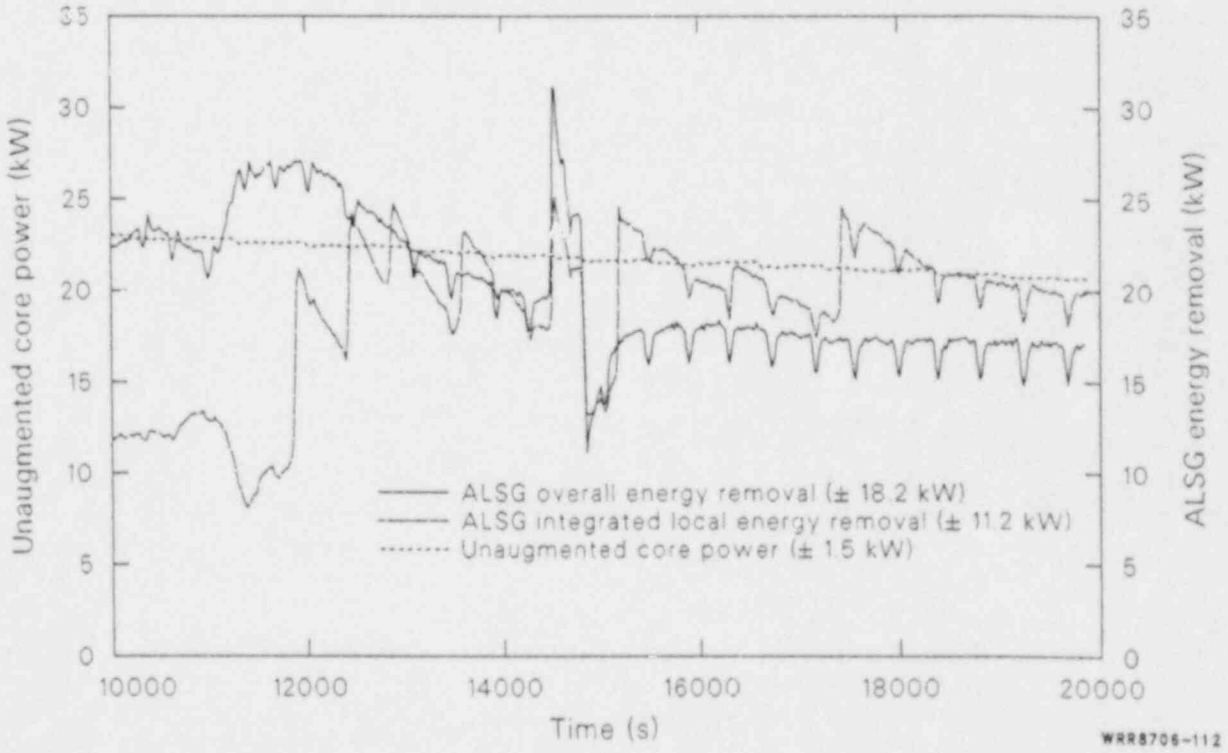

Figure 112. Affected loop steam generator primary-to-secondary heat transfer and core power during the voided secondary refill phase of 14.3% FWLB experiment S-FS-7 (10,000 to 20,000 s).

margin, which aided in maintaining stable operating conditions. The voided secondary refill operations were very effective in maintaining stable conditions in the system for both tests.

Relevance to Bottom Main Feedwater Line Break Issues

One of the objectives behind performing these bottom main feedwater line break experiments was to provide data to assist the USNRC in addressing the various concerns regarding these kinds of events. The major concerns being: the peak primary system pressure; the relative effects, conservatisms or applicability of several FSAR calculation assumptions; and the effectiveness of EOP-specified recovery procedures for recovering and cooling down the plant. This section contains a discussion of these major concerns, taking into account the results of these experiments. The implications of the experimental results relative to FSAR assumption concerns are discussed first. This is followed by a discussion of the implications of the experimental results relative to the peak primary system pressure predicted for a full-scale PWR plant. Finally, the implications that the experimental results provide regarding the effectiveness of the EOP-specified recovery procedures for recovering and cooling down the plant are discussed.

Final Safety Analysis Report Assumption Conservatisms. As discussed in the *Historical Background* section, due to the limited data base on steam generator bottom main feedwater line breaks, a large number of assumptions and simplifications are made when performing transient calculations for FSARs. Because the calculations performed for the C-E System 80 FSAR predicted a peak primary system pressure in excess of 110% of the system design pressure, questions were raised regarding the degree of conservatism inherent in the calculations. While the vendor considered the calculations to be highly conservative, such a large number of assumptions and simplifications were utilized that the degree of conservatism inherent in the calculations was unknown. The intent of this subsection is to provide some insight into the effects of the major assumptions and simplifications utilized for the FSAR calculations on the transient severity, based on the results of these bottom main feedwater line break experiments. In this manner, the degree of conservatism inherent in the FSAR calculations may be partially addressed. However, the final determination of the degree of conservatism inherent in the FSAR calculations will require comparisons of the FSAR-calculated parameters to best-estimate parameters calculated using a code that has been assessed and verified against these experimental results. The assumptions and simplifications addressed in this report are limited to: the assumed degradation in heat transfer with the reduction in liquid inventory; assumed break flow state; assumed main steam line check valve failure; assumed loss of offsite power at SCRAM; and response of the secondary liquid level differential pressure measurements and their utilization for reactor trip signals. For these discussions, assumptions which maximize the primary pressurization but do not emulate the actual response exhibited by the experimental data are considered to be conservative.

The assumption made for the C-E System 80 FSAR Appendix 15B bottom main feedwater line break calculations regarding the reduction of heat transfer with liquid inventory (i.e., 100% heat transfer until the liquid inventory is depleted followed by a step change reduction in the heat transfer to 0%) is not conservative for the Semiscale Type III steam generator. The assumed heat transfer degradation actually closely emulates the measured secondary convective heat transfer response to the loss of liquid inventory. The measured secondary convective heat transfer coefficients actually increase with increasing void fraction until the void fraction reaches 1.0. Then, they rapidly decrease to zero. Thus, the primary-to-secondary heat transfer remains high until the tube-bundle region is devoid of liquid. The heat transfer parameters in the Type III steam generator were measured for heat fluxes, mass fluxes, secondary fluid conditions, pressures, and temperature profiles typical of a full-scale inverted U-tube steam generator (including the C-E System 80 steam generator). Therefore, the measured heat transfer phenomena are representative of the phenomena that occur in the full-scale steam generator.

The strong dependency of the secondary convective heat transfer on the tube bundle liquid inventory emphasizes the need to accurately predict the secondary fluid hydraulic response to the bottom main feedwater line break. Preservation of the secondary fluid hydraulic response in the Semiscale Type III steam generator was provided by designing the steam generator components to: preserve the full-power operating condition characteristics (circulation ratio, fluid velocities, fluid densities, fluid temperatures, fluid pressures);

and, produce the same relative frictional pressure drop (percentage of the total flow circuit frictional pressure drop) that occurs in the corresponding component in the full-scale steam generator. The measured full-power operating conditions for the Type III steam generator (see Appendix C) are representative of those for a C-E System 80 steam generator. It is believed that the component relative pressure drops are representative of those for the C-E System 80 steam generator. However, a lack of information from C-E has precluded determining the accuracy of the simulation. One notable difference between the Semiscale Type III and the C-E System 80 steam generators is in the lower tube-bundle section. The C-E System 80 steam generator has a plate installed that separates the cold side tube-bundle region from the hot side tube-bundle region for approximately the bottom one-third of the tube bundle height. This is not simulated in the Semiscale Type III steam generator. The effects of this difference are not known at this time but are believed to be minimal. Ultimately, accurate modeling of the C-E System 80 steam generator secondary fluid system components, accurate calculation of the break flow, and accurate calculation of the secondary convective heat transfer coefficient transient response (based on the Type III steam generator data) will provide quantification of the effects of any differences. While questions exist with regard to the accuracy of the simulation of the secondary fluid hydraulic response, the transient secondary fluid hydraulic response for the Type III steam generator was sufficiently representative to preserve the secondary convective heat transfer phenomena and provide data to allow determination of the *best estimate* heat transfer response to a bottom main feedwater line break accident. The measured heat transfer parameters are applicable to the full-scale steam generator.

The assumptions made for the C-E System 80 FSAR Appendix 15B bottom main feedwater line break calculations regarding the break flow state (i.e., that saturated liquid was discharged until no liquid remained at which time saturated steam was discharged), and the break flow modeling (i.e., frictionless critical flow was calculated using the Henry-Fauske correlation[31]) severely distorted the effects of the break size on the transient response. The combined effect of these assumptions produced calculated break flows and timings of events for the 14.3% break case calculation, which more closely emulate the 100% break size experimental results. This is because the measured break flow did not consist of only saturated liquid and saturated steam flow, but exhibited a transition through the full range of conditions (i.e., subcooled liquid, to saturated liquid, to two-phase fluid, to saturated steam), and the magnitude of the measured break flow was significantly smaller than that predicted by the frictionless critical flow Henry-Fauske correlation (a combination known to significantly overpredict the magnitude of critical flows). The break flow assumptions preclude accurate simulation of the secondary component fluid hydraulic responses because they control the draining of the secondary. They also distorted the results of the break size sensitivity analysis performed for the FSAR because the secondary responses calculated for the 14.3% break size case are actually more representative of that expected for a 100% break. Thus, the FSAR assumptions regarding break flow severely distorted the effect of the break size on the system response. Such assumptions provide no real benefit to the FSAR analysis and would preclude accurate *best-estimate* calculations.

The failed affected steam generator main steam line check valve assumption utilized for the C-E System 80 FSAR Appendix 15B bottom main feedwater line break calculations was not a conservative assumption based on the results of the Semiscale Mod-2C experiments. The intersecondary communication that occurs, due to the failure, produces increased steam flow from the unaffected steam generator, which increases or maintains its primary energy removal, thereby reducing the effect of losing the affected loop steam generator heat sink. While the substantial loss of secondary fluid inventory from the unaffected steam generator is of concern, the time required for this to occur is prohibitive (a fact that is not evident in the C-E FSAR calculations due to the accelerated timing of events caused by the break flow modeling), and operator identification and intervention is expected to occur before the inventory loss would be sufficient to significantly effect the energy removal capability of the steam generator. The assumed main steam line check valve failure is, therefore, not considered to be conservative based on the results of the Semiscale Mod-2C experimental results.

The C-E System 80 FSAR Appendix 15B bottom main feedwater line break calculation assumption regarding the loss of offsite power at SCRAM is conservative based on the results of the Semiscale Mod-2C experiments. The loss of offsite power caused loop flow reductions, which reduced the cooling of the primary fluid system by the unaffected loop steam generator following SCRAM. This left the primary fluid system at a higher energy state following SCRAM, which in turn provided more restrictive conditions from which plant recovery had to be initiated.

Additionally, the continued loss of offsite power provided limiting conditions and capabilities for recovering the plant. From this point of view, the loss of offsite power assumption can be considered to be conservative.

The expected responses of the secondary liquid level differential pressure measurements during a bottom main feedwater line break accident vary depending on the downcomer fluid hydraulic response and the differential pressure measurement tap connection orientation. With the positive side of the differential pressure transducer connected to the higher elevation tap, the frictional pressure drop due to downflow through the downcomer produces indicated liquid levels that are lower than the actual level. Thus, during the transient as the downcomer liquid inventory is depleted, if the downcomer flow remains at its steady-state value or increases, then the indicated liquid level then will decrease at a rate consistent with or greater than the liquid inventory depletion rate. This kind of response would produce either *best-estimate*, or nonconservative, results with regard to generating reactor trip signals. If, however, the differential pressure transducer is connected in the opposite manner (i.e., the negative side connected to the higher elevation tap), the frictional pressure drop due to downflow through the downcomer then produces an indicated liquid level that is higher than the actual liquid level. For this case, as the downcomer liquid inventory is depleted during the transient, if the downcomer flow remains at its steady state-value or increases, the indicated liquid level then will decrease at a rate consistent with or less than the liquid inventory depletion rate. This kind of response would produce either *best-estimate*, or conservative, results with regard to generating reactor trip signals. For this discussion, conservative means relative to the expected *best-estimate* responses. However, from the standpoint of the overall transient severity, the most conservative assumption with regard to reactor trip generating signals continues to be the high pressurizer pressure trip SCRAM set point. The configurational and fluid hydraulic dependencies of the downcomer liquid level measurements makes them suspect for conservative assumption candidates but it is conceivable that they would produce earlier system SCRAM initiation and thus be nonconservative.

Maximum Primary Pressure. The major concern with regard to a bottom main feedwater line break accident in a C-E System 80 plant is the maximum primary pressure resulting from the loss of one-half of the plants heat sink combined with the relatively large pressurizer surge line hydraulic resistance. While direct extrapolation of the Semiscale Mod-2C results to those expected for a C-E System 80 plant is not adequate to fully answer this concern, the Semiscale results can be utilized to provide some indication of the actual pressures that might be expected.

A simple lumped-parameter analysis was performed that modeled the primary fluid system, excluding the pressurizer, as one volume with the pressurizer surge line hydraulic resistance restricting the flow into a second volume that modeled the pressurizer. By modeling: the primary fluid system as one volume initially at the energy state associated with the initial condition average fluid properties; the pressurizer as another volume initially at the specified initial conditions; and using the normalized primary energy balance from the experiments (adjusted to account for the fact that the Semiscale Type III steam generator represents only one-half of the relative heat sink of a C-E steam generator), with the C-E initial condition power to perform an integrated primary energy addition and mass transfer analysis, peak primary pressures were estimated for the C-E System 80 plant for the three different break size cases.

The estimated peak primary pressures (Table 1) represent pressures near, but not quite at, 110% of the design pressure limit. Additional consideration must be given to the scaling distortions in Semiscale associated with metal mass effects,[19,32] and the possible differences in the secondary fluid hydraulic responses associated with possible steam generator design differences. However, the relative proximity to the 110% design pressure limit shows the need to perform *best-estimate* calculations with a thermal-hydraulic computer code, which has been assessed against and verified for the results of these experiments.

Emergency Operating Procedures. The major concern with regard to system recovery from a bottom main feedwater line break accident is the effectiveness of the recovery operations specified in the plant Emergency Operating Procedures in recovering and maintaining control of the plant. Due to inherent scaling distortions (such as atypical metal mass to volume ratios, heat loss/heat loss mitigation, and timing distortions) (References 19, 32), and facility limitations, the results of these experiments are not a precise replication of full-scale PWR response. However, the experiments provided thermal-hydraulic behavior sufficiently representative of full-scale PWR behavior

Table 1. Peak primary pressures predicted for C-E system 80 plant based on extrapolation of Semiscale MOD-2C data

Bottom Main Feedwater Line Break Size (%)	Peak Predicted C-E System 80 Pressure (MPa)	Peak Predicted Pressure (percent of design pressure)
100	18.07	105
50	18.23	106
14.3	18.26	106

to preserve important phenomena and allow quantification of the effectiveness of the EOP-specified operations in recovering the system from a bottom main feedwater line break accident.

The automatic actions performed by the plant safety systems (i.e., SCRAM, SI initiation, and MSIV closure) were effective in mitigating the consequences of the bottom main feedwater line break accident. The automatic actions left the Semiscale Mod-2C system in a quasi-stable condition, which aided in the stabilization and recovery of the system.

The stabilization operations performed following operator identification of the transient (i.e., SI termination, pressurizer internal heater operations, normal charging/letdown operations, and unaffected loop steam generator steam and feed operations) were effective in stabilizing the system at conditions that would permit a natural circulation cooldown and depressurization to begin. While it was not necessary to steam the unaffected loop steam generator to achieve stable operating conditions, based on the success of steaming operations in later phases of the tests, such an operation would not be expected to create any difficulties for the operators. The limiting factor in achieving stable conditions was the recovery of the unaffected loop steam generator secondary liquid inventory to a level that would ensure adequate cooling capability and level control during the natural circulation cooldown.

The primary fluid system natural circulation cooldown and depressurization operations performed following system stabilization in test S-FS-6 (i.e., pressurizer auxiliary spray operations, pressurizer internal heater operations, normal charging/letdown operations, and unaffected loop steam generator steam and feed operations with stairstep reductions in the secondary pressure) were very effective in cooling down and depressurizing the primary fluid system in a controlled manner.

For a normal natural circulation cooldown and depressurization, the EOPs specify an operating boundary for the primary fluid system pressure as a function of time into the transient, which is based on the vessel upper head heat loss. This is designed to avoid the system pressure reaching the saturation pressure associated with the upper head metal temperature by matching the depressurization rate to the upper head metal cooling rate; the intent being to avoid the formation of a vessel upper head void. During the initial phase of the cooldown and depressurization, the system pressure was maintained above the specified minimum for that point in time in a normal cooldown. No upper head voiding was observed to occur during this phase of the cooldown.

The second phase of the natural circulation cooldown and depressurization involved depressurizing the primary fluid system at a rate that provided a minimum unaffected loop hot leg fluid subcooled margin of 11.1 K, as specified in the EOPs for a rapid natural circulation cooldown and depressurization. This phase of the cooldown proceeded with continued control of the recovery, but with the vessel upper head fluid subcooled margin constantly decreasing. The subcooled margin eventually reached ≤ 2 K with no upper head voiding indicated after 600 s at that point. At this point, in the interest of time, a deviation from the rapid natural circulation cooldown and depressurization EOP-specified operations was taken. The system was purposely depressurized to force the formation of a void in the vessel upper head. However, had the rapid natural circulation cooldown and depressurization EOP-specified operations been continued, it is very likely that eventual upper head voiding would have occurred.

Subsequent operations were performed to force vessel upper head void formations and collapse the

voids using two different methods of upper head void collapse. The first upper head void was collapsed using the *fill and drain* method of vessel upper head void collapse, as outlined in the EOPs. The second upper head void was collapsed using the *pump restart* method of vessel upper head void collapse, also as outlined in the EOPs. Both methods proved effective in collapsing the vessel upper head void; however, an important observation was made with regard to determining final upper head void collapse. For both methods, the pressurizer liquid level started to increase before the upper head void was completely collapsed. This shows the importance of monitoring the rate of the pressurizer liquid level increase to ensure that it matches that expected for the normal charging flow rate as a means of determining final upper head void collapse. The major differences noted for the two methods of upper head void collapse were in the rate of the void collapse and the amount of cooling provided for the upper head fluid and metal. The *fill and drain* method resulted in a more rapid collapse of the vessel upper head void. However, the *pump restart* method resulted in more cooling of the vessel upper head fluid and metal. Thus, a recurrence of the vessel upper head voiding would happen more readily following the *fill and drain* void collapse than following the *pump restart* void collapse. It is, therefore, conceivable that the cooldown and depressurization could continue at a more rapid rate using the *pump restart* method of upper head void collapse.

The voided secondary refill operations performed following the stabilization phases of tests S-FS-7 and S-FS-11 verified the effectiveness of the operations for maintaining stable conditions while recovering the inventory in a voided steam generator. Refilling the voided secondary provides a significant source of primary energy removal, ensures an adequate cooling source for the primary, and produces no major challenges to maintaining stable system conditions.

The EOP-specified operations were very effective in maintaining control of the Semiscale Mod-2C system during these experiments. Scale effects (atypical metal mass to fluid volume ratio, and heat loss/heat loss mitigation) had little effect on the system response.

The atypically large metal mass to fluid volume ratio had little effect because the system stabilized at temperatures very close to the initial condition temperatures, and during the course of the transient, the change in system temperatures was very gradual. If anything, the atypically large metal mass provided an additional energy source that slowed the system cooldown and depressurization, providing conservative system recovery responses.

The heat loss/heat loss mitigation had little effect because most of the primary fluid system remained subcooled for the largest portion of the transients (the vessel upper head and the pressurizer were the only components that saturated), making the external heaters very effective in mitigating the heat loss. The largest heat loss effect was observed in the pressurizer surge line where the pressurizer insurge fluid was cooled due to the heat loss. This greater subcooling of the pressurizer surge line liquid provided greater cooling of the pressurizer fluid following each normal charging driven insurge. The net result was a slight increase in the rate of the primary depressurization during the recovery operations. This would tend to make the system response slightly nonconservative relative to a full-scale PWR plant.

The metal mass and heat loss scale effects on the system response were minimal. In addition, the effects offset each other such that the overall system response should be a reasonable indicator of the general response expected for a full-scale PWR plant. In any case, the atypically large metal mass to fluid volume ratio and the system heat loss/heat loss mitigation have been well characterized and can be modeled. Hence, the data is useful for the thermal-hydraulic code verification required before utilizing the code to predict full-scale PWR plant response.

CONCLUSIONS

The following conclusions have been drawn based on analyses of the experimental data from the Semiscale Mod-2C Feedwater and Steam Line Break Experiment (S-FS) series feedwater line break experiments:

1. A simplistic, lumped-parameter extrapolation of Semiscale Mod-2C experimental results to those expected for a C-E System 80 plant indicates substantial pressurization of the C-E System for all three break sizes. While the predicted pressures do not exceed 110% of the system design pressure, their relative proximity to the 110% pressure limit provides substantial evidence in support of the need to perform *best-estimate* calculations with a code verified against this experimental data.
2. The C-E FSAR assumption of 100% heat transfer until the liquid inventory is depleted followed by a step change reduction in the heat transfer to 0% is not conservative. The assumption actually emulates the convective heat transfer that occurs in the tube-bundle region. The local secondary convective heat transfer coefficients increase with increasing local void fraction until liquid deficiencies occur, at which point the local heat transfer coefficients degrade instantaneously to zero.
3. Accurate *best-estimate* calculations of the primary-to-secondary heat transfer transient response for these kinds of accidents will require improvements in the boiling heat transfer correlations used in current thermal-hydraulic computer codes. The measured local secondary convective heat transfer coefficients show a trend in the dependency on the local vapor-void fraction, which is exactly the opposite of the trend predicted by the Chen boiling heat transfer correlation used in current thermal-hydraulic computer codes.
4. The bottom main feedwater line break experimental results were essentially insensitive to the break size. The affected loop steam generator secondary fluid hydraulic response showed a slight sensitivity to break size, which had a limited effect on the heat transfer degradation versus total secondary mass characteristics. However, the peak primary pressures that occurred were essentially the same for all three break sizes. The mass loss from the unaffected loop steam generator secondary, past the failed main steam line check valve to the affected loop steam generator secondary, increases as the break size decreases, as expected.
5. Excellent comparison between the results for the two 100% break experiments (S-FS-6 and S-FS-6B) prove the validity and repeatability of the results.
6. The automatic actions (SCRAM, SI initiation, and MSIV closure) performed by the safety systems were effective in mitigating the consequences of the bottom main feedwater line break accident in the Semiscale experiments. The actions left the system in a quasi-stable condition, which minimized the amount of operator intervention required to stabilize the plant.
7. The EOP-specified stabilization operations (affected loop steam generator auxiliary feedwater injection and SI termination, pressurizer internal heater operation, normal charging/letdown operation, and unaffected loop steam generator steam and feed operation) were effective in stabilizing the Semiscale Mod-2C system at conditions that permit initiation of a natural circulation cooldown and depressurization.
8. The EOP-specified normal natural circulation cooldown and depressurization operations (pressurizer auxiliary spray operation, pressurizer internal heater operation, normal charging/letdown operation, and unaffected loop steam generator steam and feed operation with stair-step secondary pressure reductions) were effective in maintaining a controlled cooldown and depressurization of the Semiscale Mod-2C system. No vessel upper head voiding occurred while the system pressure was maintained within the pressure versus time envelope specified in the EOPs.
9. The EOP-specified rapid natural circulation cooldown and depressurization operations (the same operations as for the normal cooldown, but without the pressure versus time envelope restriction) were effective in

maintaining a rapid controlled cooldown and depressurization of the Semiscale Mod-2C system. Due to time restraints, vessel upper head voiding was forced to occur in Semiscale before it had occurred during the natural course of the rapid cooldown. However, the trend of constantly decreasing vessel upper head fluid subcooled margin indicates that upper head voiding would have occurred eventually.

10. The *fill and drain* (normal charging and pressurizer internal heater operations) and *pump restart* (primary coolant pump restart operations) methods of vessel upper head void collapse were both effective in collapsing the upper head void. The results for both methods show that the rate of the pressurizer liquid level increase should be used as an indication of final vessel upper head void collapse; not just the fact that the level is increasing. The *fill and drain* method collapsed the upper head void faster. However, the *pump restart* method provided more cooling of the upper head fluid and metal, leaving the system in a condition that would permit greater primary depressurization before upper head voiding would reoccur.
11. Refilling the affected loop steam generator secondary with auxiliary feedwater proved to be a very effective method of providing increased primary energy removal while maintaining stable system conditions. The measured response exhibits significant heat transfer with minimal mass. The effect of the different auxiliary feedwater injection rates on the overall response was minimal and limited primarily to extending the time required to refill the secondary.
12. The measured local secondary convective heat transfer coefficients for both voided secondary refills exhibited the same basic trends with regard to the local vapor-void fraction as was observed during the heat transfer degradation phase of the experiments. The local heat transfer coefficients exhibited a step change increase from zero to a maximum when the secondary *mixture* level (the two-phase level determined from the densitometers) reached the elevation of the local measurements, providing liquid for cooling. The heat transfer coefficients then decreased as the local vapor-void fraction decreased. Here again, the measured trend is exactly the opposite of that predicted by existing boiling heat transfer correlations. The lower auxiliary feedwater injection rate at the lower core power levels produced smaller secondary convective heat transfer coefficient magnitudes.
13. The voided secondary refill data is representative of the phenomena occurring in an either partially of fully voided secondary undergoing refill with auxiliary feedwater. The data is, therefore, useful for a number of possible transient conditions wherein a secondary is voided and refilled with auxiliary feedwater, such as a loss of feedwater transient or the unaffected loop steam generator refill following MSIV closure during these experiments.
14. The assumed heat transfer degradation for the C-E FSAR calculations is not conservative. Therefore, *best-estimate* calculations should be performed with the measured heat transfer phenomena appropriately incorporated into the code. The strong dependency of the secondary convective heat transfer on the tube bundle liquid inventory also emphasizes the need to accurately predict the secondary fluid hydraulic response to the bottom main feedwater line break.
15. The break flow assumptions (i.e., saturated liquid discharge until no liquid remains, and frictionless critical flow as calculated using the Henry-Fauske correlation) severely distorted the effects of the break size on the transient response. They preclude accurate simulation of the secondary component fluid hydraulic responses because they control the draining of the secondary. They also distorted the results of the break size sensitivity analysis performed for the FSAR because the secondary responses calculated for the 14.3% break size case are actually more representative of that expected for a 100% break. These assumptions provide no real benefit to the FSAR analysis and would preclude accurate *best-estimate* calculations.
16. The failed affected steam generator main steam line check valve assumption utilized for the C-E FSAR calculations is not conservative. Further analysis without the steam line check valve failure assumption is warranted. The nonconservatism associated with the increased steam flow from the unaffected loop steam generator more

than offsets the conservatism associated with the loss of unaffected loop steam generator secondary mass. The increased steam flow increases or maintains the unaffected loop steam generator primary energy removal, thereby reducing the effect of the loss of the affected loop heat sink on the primary energy addition and pressurization. While substantial loss of the unaffected loop steam generator secondary fluid inventory is of concern, the time required for this to occur is prohibitive and operator intervention is expected to occur before the inventory loss would be sufficient to significantly effect the energy removal capability of the steam generator.

17. The assumed loss of offsite power at SCRAM utilized for the C-E FSAR calculations is conservative. The resulting loop flow reductions reduce the cooling of the primary fluid system by the unaffected loop steam generator following SCRAM. This leaves the system in a higher energy state and provides more restrictive conditions at plant recovery initiation. Also, the continued loss of offsite power provides limiting conditions and capabilities for recovering the plant.
18. Downcomer liquid level response dependencies on the measurement configuration and the secondary fluid hydraulic response makes them suspect for conservative assumption trip-generating candidates. It is conceivable that they would produce earlier system SCRAM initiation and thus be nonconservative for FSAR calculations. However, with appropriate consideration of the differential pressure measurement configuration and accurate modeling and calculation of the secondary fluid hydraulic responses, they could prove to be the actual trip signal generators for *best-estimate* calculations.
19. The data obtained during these bottom main feedwater line break experiments satisfy the stated objectives for the experiments. The data are of sufficient detail and quality to allow verification of thermal-hydraulic computer codes for bottom main feedwater line break accident, system stabilization, system cooldown and depressurization, vessel upper head void collapse, and voided secondary refill calculations. The analyses of the experiment results has provided invaluable insight into the phenomena and driving mechanisms evidenced in the experiments and applicable to full-scale PWR plants.

RECOMMENDATIONS

During the course of analyzing the results of these experiments, a number of deficiencies were identified in the current methods of computer code simulations for these transients. These deficiencies need to be corrected before an accurate estimate of the actual full-scale plant response (an accurate *best-estimate* calculation) can be obtained.

Foremost in the deficiencies is the existing correlations for predicting secondary convective heat transfer coefficients. The Semiscale Type III steam generator measured local secondary convective heat transfer coefficient dependency on the local vapor-void fraction exhibits a trend that is exactly the opposite of that predicted by the existing boiling heat transfer correlations. This is believed to be due to the fact that existing correlations were developed based on data for flow inside a single heated tube, not for flow around internally heated tube bundles. Inside of an externally heated tube, increasing vapor-void fractions can result in the vapor *blanketing* the tube inside wall, limiting the area for liquid-to-wall contact, and reducing the liquid cooling effect, thereby reducing the convective heat transfer coefficient, as predicted by the existing correlations. Outside of an internally heated tube bundle, increasing vapor-void fractions can result in turbulent mixing and *pumping* of the liquid to the outside tube wall, resulting in enhanced liquid and vapor cooling effects and increased secondary convective heat transfer coefficients, as measured in the Type III steam generator.

Improvements in the secondary convective heat transfer calculation methodology will be required for thermal-hydraulic computer codes to accurately calculate the actual primary-to-secondary transient heat transfer because the secondary convective heat transfer controls the onset of heat transfer degradation and heat transfer re-initiation. This will require either modifying existing, or developing new, boiling convective heat transfer correlations based on the Semiscale Type III steam generator heat transfer data.

A second deficiency exists in the FSAR calculation assumptions and calculation simplifications. The Semiscale Mod-2C bottom main feedwater line break experiment results show that the assumed affected loop steam generator heat transfer degradation with loss of inventory and the assumed affected steam generator main steam line check valve failure are not conservative assumptions. In addition, the simplifications and assumptions applied to the break flow calculations preclude accurate calculation of the secondary component fluid hydraulic responses (necessary to accurately simulate the heat transfer degradation), and severely distort the effects of break size on the system response. This negates the results of the break size sensitivity study performed for the C-E System 80 FSAR.

Future bottom main feedwater line break calculations for FSARs should not assume the heat transfer degradation with liquid inventory assumption used for the C-E System 80 FSAR to be conservative. Additionally, the failed main steam line check valve assumption should not be used because it actually yields nonconservative results in this application. Finally, the break flow assumptions and simplifications should be replaced with a *best-estimate* method because they provide no real benefit to the FSAR analysis and actually distort the simulation for either FSAR or *best-estimate* calculations.

Best-estimate bottom main feedwater line break calculations should only be performed after the thermal-hydraulic computer code used for the calculations has been verified against this experimental data. In addition, care should be taken in modeling the secondary fluid hydraulic system, the break flow should be calculated using a *best-estimate* method, the failed main steam line check valve assumption should not be used, and consideration may be given to utilizing the secondary liquid level obtained from the downcomer differential pressure as a possible trip-generating signal, if the measurement configuration and secondary fluid component hydraulic response can be accurately simulated.

Finally, recent problems encountered in calculating the unaffected loop steam generator heat transfer following MSIV closure during TRAC-PF1 simulations of these experiments,[33] and in calculating the isolated secondary refill responses during TRAC-PF1 simulations of Semiscale Mod-2C Small Break LOCA without HPIS Test S-NH-3[34] may be resolved by assessing the code against the voided secondary refill data obtained during these experiments. The phenomena occurring in the affected loop steam generator during the voided secondary refill phase of these experiments are similar to the phenomena occurring in the unaffected loop steam generator following MSIV closure. They are also similar to the phenomena occurring

in the secondaries following secondary isolation during Test S-NH-3. Assessing the TRAC-PF1 code against the voided secondary refill data should provide invaluable insight into the probable cause of the problems encountered in the recent simulations.

REFERENCES

1. T. J. Boucher and J. R. Wolf, *Experiment Operating Specification for the Semiscaie Mod-2C Feedwater and Steam line Break Experiment Series*, EGG-SEMI-6625, May 1984.

2. T. J. Boucher and W. A. Owca, *Appendix S-FS-6 and S-FS-7 of the Experiment Operating Specification for the Semiscale Mod-2C Feedwater and Steam Line Break Experiment Series*, EGG-SEMI-6871, May 1985.

3. T. J. Boucher and D. G. Hall, *Quick Look Report for Semiscale Mod-2C Test S-FS-6*, EGG-SEMI-7022, September 1985.

4. D. G. Hall, *Quick Look Report for Semiscale Mod-2C Test S-FS-7*, EGG-RTH-7072, October 1985.

5. T. J. Boucher and W. A. Owca, *Appendix S-FS-11 of the Experiment Operating Specification for the Semiscale Mod-2C Feedwater and Steam Line Break Experiment Series*, EGG-SEMI-6909, June 1985.

6. M. P. Plessinger, *Quick Look Report for Semiscale Mod-2C Test S-FS-11*, EGG-RTH-7103, November 1985.

7. A. Goldberg and R. D. Streit, R. G. Scott, *Evaluation of Cracking in Feedwater Piping Adjacent to the Steam Generators in Nine Pressurized Water Reactor Plants*, NUREG/CR-1603, October 1980.

8. "The USNRC Calendar," Volume II, Number 6, February 4, 1983, p. 4.

9. U.S. Nuclear Regulatory Commission, USNRC Unusual Occurrence Report, Reportable Event Number 07140, December 1986.

10. CESSAR-80, *Final Safety Analysis Report*, Appendix 15, Combustion Engineering Company.

11. St. Lucie No. 2 Nuclear Plant, *Final Safety Analysis Report*, Appendix 15, Florida Power and Light Company.

12. Waterford Unit No. 3 Nuclear Plant, *Final Safety Analysis Report*, Appendix 15, Louisiana Power and Light Company.

13. Palo Verde Nuclear Plant, *Final Safety Analysis Report*, Appendix 15, Arizona Public Service Company.

14. R. J. Mattson (USNRC Memorandum) to O. E. Bassett "Additional Semiscale and RELAP5 Needs for DSI", January 11, 1982.

15. D. J. Shimeck, *Experiment Operating Specification for Semiscale Mod-2A Steam and Feedwater Line Break Series*, EGG-SEMI-5830, March 1982.

16. G. R. Berglund and L. J. Martinez, D. J. Shimeck, *Quick Look Report for Semiscale Mod-2A Feedwater Line Break Tests S-SF-1, S-SF-2, and S-SF-3*, EGG-SEMI-5940, July 1982.

17. M. Y. Young et. al., *Prototypical Steam Generator (MB-2) Transient Testing Program*, NUREG/CR-3661, EPRI-NP-3494, WCAP-10475, March 1984.

18. E. Klingler, *The Semiscale Mod-2C Feedwater and Steam Line Break Configuration Report for Experiments S-FS-1, S-FS-2, S-FS-6, S-FS-6B, S-FS-7, and S-FS-11*, EGG-RTH-7445, October 1986.

19. T. K. Larsen and J. L. Anderson, D. J. Shimeck, *Scaling Criteria and Assessment of Semiscale Mod-3 Scaling for Small Break Loss-of-Coolant Transient*, EGG-SEMI-5121, March 1980.

20. W. A. Jens and P. A. Lottes, *Analysis of Heat Transfer, Burnout, Pressure Drop and Density Data for High Pressure Water*, USAEC Report ANL-4627, U.S. Atomic Energy Commission, 1951.

21. M. R. S. Thom, W. M. Walker, T. A. Fallon, G. F. S. Reising, "Boiling in Subcooled Water During Flow in Tubes and Annuli," *Proc. Inst. Mech. Eng.*, 3C180, 1966.

22. C. E. Dengler, J. N. Addoms, "Heat Transfer Mechanism for Vaporization of Water in a Vertical Tube," *Chem. Eng. Prog. Ser.*, *52*, 18, 1956, p. 95.

23. J. A. R. Bennett, J. G. Collier, A. R. C. Pratt, J. D. Thornton, "Heat Transfer in Two-Phase Gas-Liquid Systems, Part I: Steam Water Mixtures in the Liquid-Dispersed Region in an Annulus," *Trans. Inst. Chem. Eng.* (London), 1961, p. 39.

24. J. C. Chen, *A Correlation for Boiling Heat Transfer to Saturated Fluids in Convective Flow*, ASME preprint 63-HT-34, American Society of Mechanical Engineers, 1963.

25. V. H. Ransom et. al., *RELAP5/MOD-2 Code Manual*, EGG-SAAM-6377, April 1984.

26. *TRAC-PF1/MOD1: An Advanced Best-Estimate Computer Program for Pressurized Water Reactor Thermal-Hydraulics Analysis*, NUREG/CR-3858 (LA-10157-MS), July 1985.

27. T. J. Boucher and R. A. Dimenna, *Semiscale Mod-2A Intermediate Break Test Series - Test Results Comparison*, NUREG/CR-3126, EGG-2238, January 1983.

28. Waterford Unit 3 Nuclear Plant, "Emergency Operating Procedures," Louisiana Power and Light Company.

29. St. Lucie Unit 2 Nuclear Plant, "Emergency Operating Procedures," Florida Power and Light Company.

30. Guy G. Loomis, *Results of the Semiscale MOD-2B Steam Generator Tube Rupture Test Series*, NUREG/CR-4073, EGG-2363, January 1985.

31. R. E. Henry and H. K. Fauske, "The Two-Phase Critical Flow of One-Component Mixtures in Nozzles, Orifices, and Short Tubes, *Journal of Heat Transfer*, Transactions of the ASME, May 1971.

32. K. G. Condie et. al., *Evaluation of Integral Continuing Experimental Capability (CEC) Concepts for Light Water Reactor Research - PWR Scaling Concepts*, NUREG/CR-4824, EGG-2494, February 1987.

33. D. G. Hall and J. C. Watkins, *An Evaluation of TRAC-PF1/MOD1 Computer Code Performance During Posttest Simulations of Semiscale Mod-2C Feedwater Line Break Transients*, NUREG/CR-4802, EGG-2486, January 1987.

34. W. E. Driskell and C. M. Kullberg, *An Analysis of the Semiscale Mod-2C S-NH-3 Test Using the TRAC-PF-1 Computer Program*, NUREG/CR-4845, EGG-2496, March 1987.

APPENDIX A

DETAILED SYSTEM DESCRIPTION AND EXPERIMENTAL PROCEDURE

CONTENTS

SYSTEM DESCRIPTION A-3

Fluid System Configuration A-3

Measurement System Configuration A-10

EXPERIMENTAL PROCEDURE A-11

REFERENCES A-15

FIGURES

A-1. The Semiscale Mod-2C facility as configured for the FS series feedwater line break experiments A-4

A-2. The Semiscale Mod-2C pressure vessel A-5

A-3. The Semiscale Type III affected loop steam generator configuration A-6

A-4. The Semiscale Type III affected loop steam generator steam dome/separator configuration A-9

TABLES

A-1. Comparison of Westinghouse Model 51 steam generator design values, scaled design values, and Semiscale Type III affected loop steam generator design values A-8

A-2. Initial conditions for feedwater line break experiments in the S-FS test series A-12

A-3. Timing of events for the blowdown phase of the S-FS series feedwater line break experiments A-13

APPENDIX A

DETAILED SYSTEM DESCRIPTION AND EXPERIMENTAL PROCEDURE

SYSTEM DESCRIPTION

The Semiscale test facility consists of; fluid systems (pipes, pumps, vessel, heat exchangers, etc.), control systems (power to core, pumps, valves, and instrument air and control signals), and an experimental measurement system (transducers, amplifiers, digital data system) necessary to integral steam line and feedwater line break experiments. These are described in detail in Reference A-1. The fluid systems and the experimental measurement system will be summarily described here.

Fluid System Configuration

The Semiscale Mod-2C fluid system configured for the FS series feedwater line break tests is shown in Figure A-1. The Mod-2C system consists of the Mod-2B system with several modifications. A new *Type III* affected loop steam generator, new main steam line and feedwater line break assemblies, break effluent catch tanks, and refined steam generator control systems have been incorporated into the system for this test series. A letdown line has been added to provide better control of primary system inventory. The primary fluid system is a 2500 psi, 650°F 1-1/2 to 3 in. Schedule 160 stainless steel system. It consists of an unaffected loop and an affected loop, the former representing three of the four loops in a pressurized water reactor (PWR). Thus, flow rates and equipment sizes are in the ratio of 3:1 for the two loops. The pressurizer is connected by a surge line to the unaffected loop hot leg. Scaled emergency core coolant from an accumulator and high or low pressure injection system pumps are routed to the loop cold legs. The secondary fluid system consists of an unaffected loop steam generator and an affected loop steam generator, the former representing three of the four steam generators in a PWR. Feedwater was supplied to the lower downcomer of the two steam generators from a heated tank and the steam was routed through control valves to the atmosphere, i.e., an open loop secondary coolant system was used. Auxiliary feedwater was routed to the upper downcomer of both steam generators at approximately the top U-tube bend elevation.

In Semiscale, the annular downcomer of the PWR vessel is replaced with an external pipe to permit extensive instrumenting of both the core and downcomer regions. These are shown in Figure A-2. Most of the fluid system components are full height, including the core that consists of a 5 x 5 array of electrically heated 3.66-m long rods that simulate the fuel rods in a 15 x 15-type PWR core. The number of turns per inch of the electrical heated coil is varied along the rod length to give the staircase approximation of a cosine axial heat flux shape. Total core power is nominally 2 MW.

The upper head, upper plenum, and core flow bypass arrangement in the Semiscale reactor vessel simulates a Westinghouse inverted top hat, upper-head internals package design.

The steam generators incorporate 7/8-in. OD Inconel inverted U-tubes; six in the unaffected loop generator, and two in the affected loop unit. The tube lengths cover the range found in a PWR generator. Two tubes in each generator are supplied with small diameter Inconel sheathed thermocouples brazed to the tubes, which provide primary and secondary coolant temperatures and tube wall temperature at various elevations in the upflow and downflow legs. Note that the major portion of the unaffected loop steam generator secondary flow area/volume is taken up by filler pieces in order to obtain the approximately correct secondary side liquid volume and velocity.

Assessment of computer code capabilities to predict secondary side transient response requires accurate measurement of important parameters, such as local primary-to-secondary heat transfer and fluid condition data and component mass inventories. The Type III affected loop steam generator design incorporates a downcomer that is external to the tube bundle and riser sections (Figure A-3). In this manner, component mass inventory and fluid property, including density/void fraction, information were obtained. The design also entails a steam dome with separator equipment that provides steam exit qualities of approximately 90% during full-power steady-state operations.

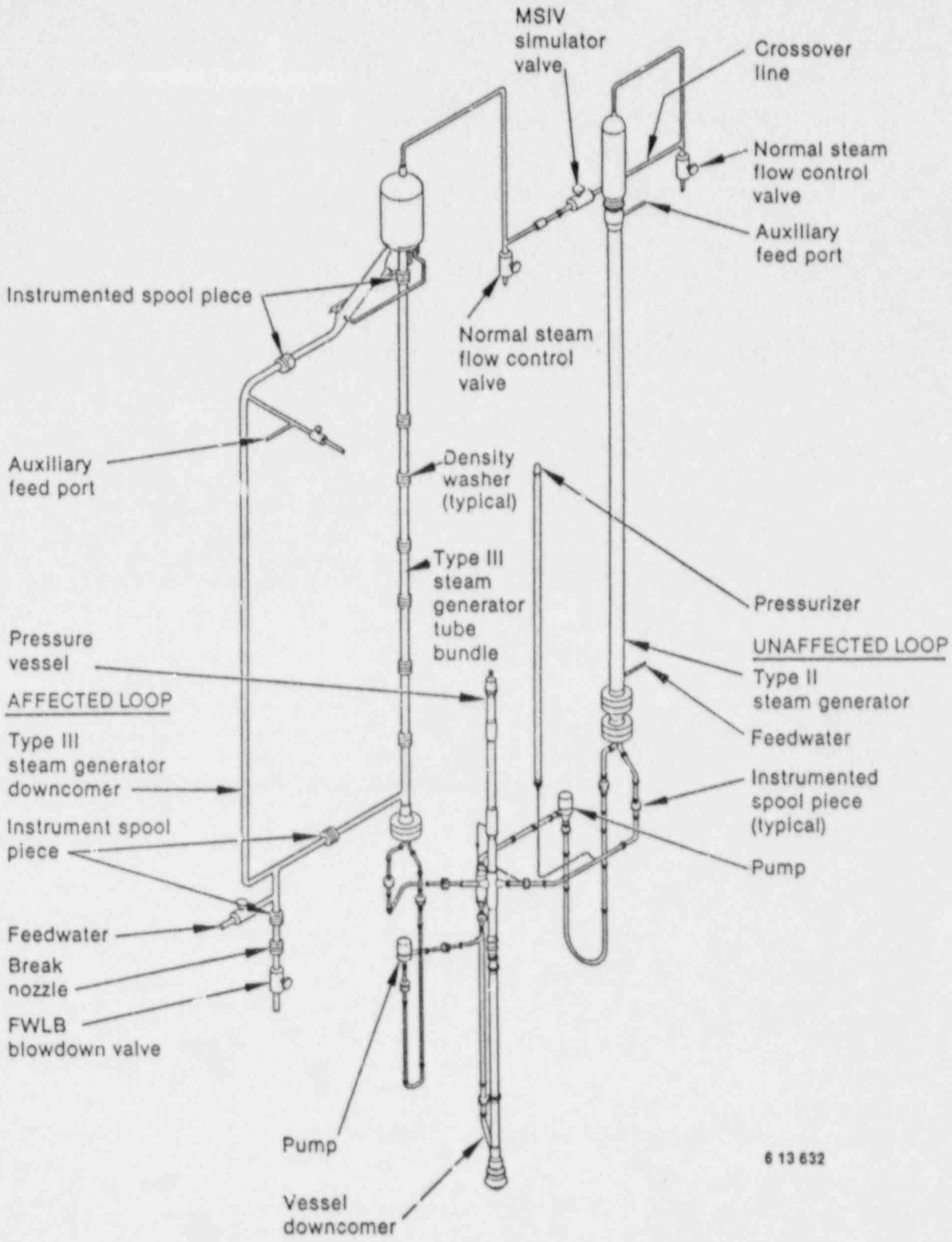

Figure A-1. The Semiscale Mod-2C facility as configured for the FS series feedwater line break experiments.

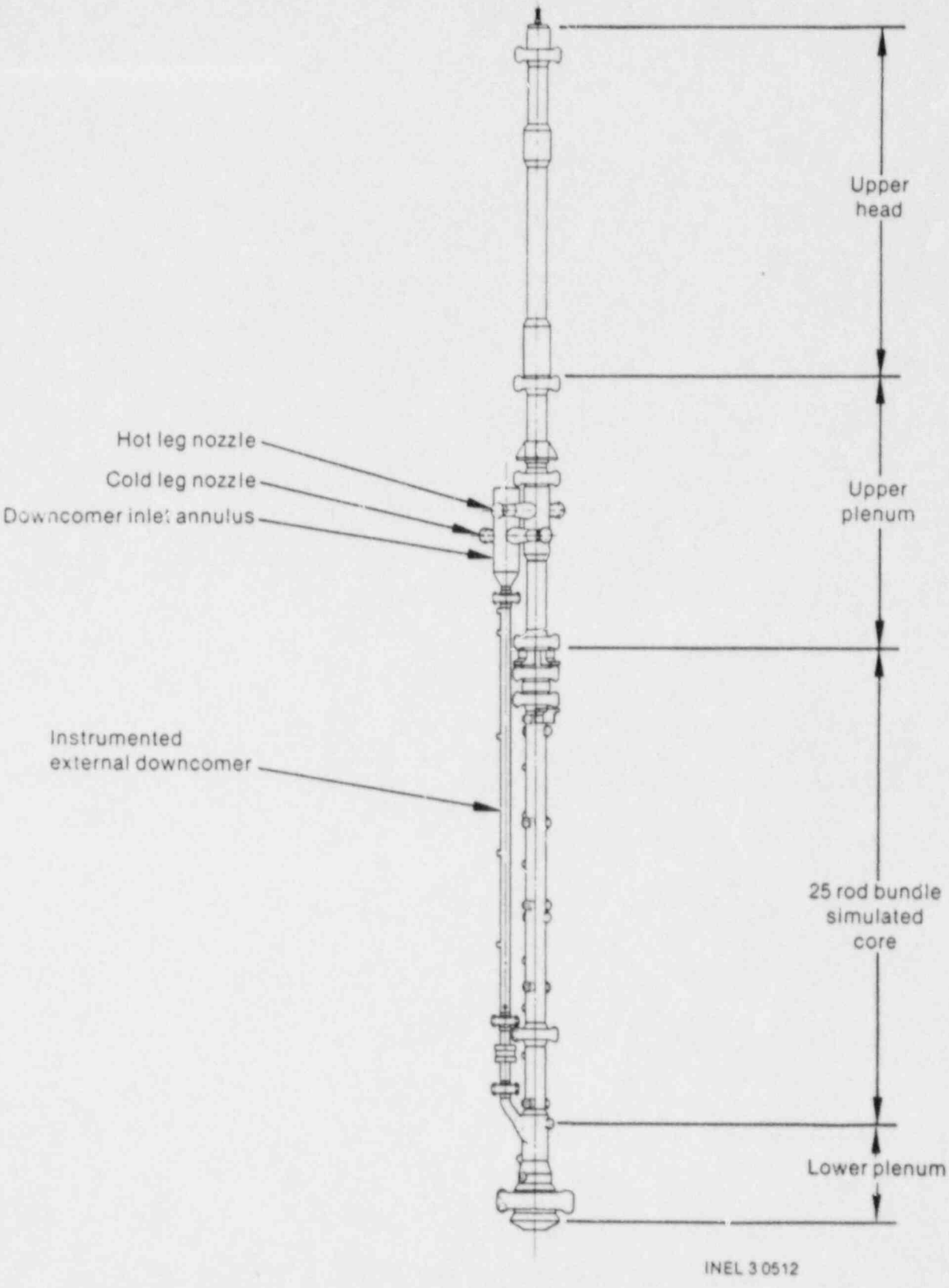

Figure A-2. The Semiscale Mod-2C pressure vessel.

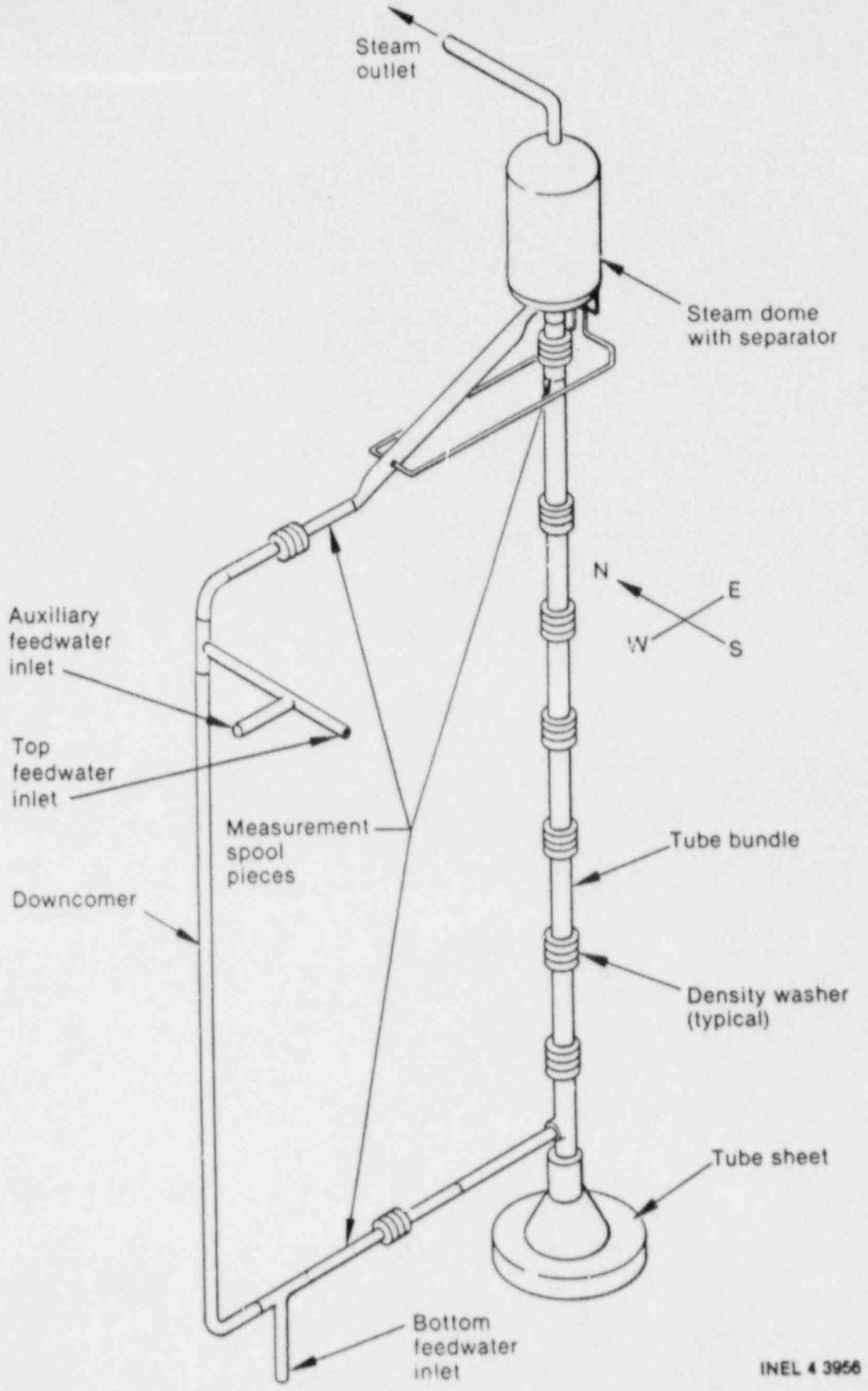

Figure A-3. The Semiscale Type III affected loop steam generator configuration.

Component flow area, volumes, lengths, and pressure drops were sized to simulate a Westinghouse Model 51 steam generator. Table A-1 contains both the scaled and reference values for the more important performance parameters and components of the Type III affected loop generator. The tube bundle contains two 7/8-in. OD Inconel inverted U-tubes with a tube thickness of 0.065 in. to allow for more reliable temperature measurements than were possible with an 0.049 in. tube wall. Design calculations indicate little difference in either heat transfer or flooding characteristics for the 0.065 in. wall tube as opposed to the 0.049 in. tube wall used in a Westinghouse Model 51 steam generator. The tubes are configured with a *square* pitch similar to a Model 51 steam generator and simulate a long and a short tube in the prototype. Tube heights were selected to maintain symmetry with the unaffected loop steam generator. A portion of the tube bundle secondary flow area and volume is taken up by two instruments tubes. However, filler tubes were not necessary to obtain the correct secondary side liquid volume and velocity. Tube bundle support baffle plates were sized to produce approximately the correct frictional pressure drop.

The downcomer flow area and volume were sized to obtain approximately the correct liquid volume and velocity while producing approximately the correct frictional pressure drop. Either top or bottom feedwater injection, and break simulation, can be accommodated with the new downcomer design.

The steam dome/separator, shown in Figure A-4, was designed to simulate the behavior of the corresponding component in a Westinghouse Model 51 steam generator. Similar to the Westinghouse Model 51 steam generator component, separation of the liquid from the steam occurs in three stages. The two-phase mixture exiting the riser section is deflected into the steam dome wall where some of the liquid is separated from the mixture, flows down the wall, and is transferred to the downcomer through a connecting line. The remaining mixture continues up through the dome to the secondary separator with some gravity-separated liquid falling back down to the bottom of the dome and mixing with the liquid separated by the deflector at the first stage (*primary* separator). The *secondary* separator, or third stage of separation, accepts the remaining two-phase mixture and imparts a centripetal motion upon it. The resulting separated liquid then flows down through the connecting lines to the downcomer. This final stage of separation produces steam dome exit qualities of approximately 90% for full-power conditions.

Failure of the check valve in the main steam line of the affected loop steam generator during a feedwater line break event results in flow from the unaffected to the affected loop steam generator before MSIV closure. To simulate this communication, a line was connected to the unaffected and affected loop steam generator main steam lines upstream of the normal steam flow control valves. This connecting *crossover* line provided scaled flow resistances, flow rates, and flow restriction as well as flow measurement. Simulation of the MSIV closure was realized by closing a valve in this line.

The bottom feedwater line break assembly for the affected loop steam generator consisted of a break flow nozzle and instrumentation to measure single-phase and two-phase break mass flows as well as fluid density, pressure, and temperature. The break nozzle was interchangeable to allow simulation of a wide range of break sizes. Information on the nozzle geometry for each test is contained in the EOS Appendixes [A-2, A-3] and Reference A-1. The break assembly was physically located in a tee from the affected loop steam generator lower downcomer horizontal section. To provide a history of mass exiting from the system, the break flow was routed to a tank where it was collected in a liquid pool and measured. For steady-state operations, the bottom feedwater line was located upstream of the break assembly. Transient initiation was realized via rapid (nominally 1 s) closure of the isolation valve in the bottom main feedwater line at the same time that the valve in the line to the collecting tank was rapidly (nominally 1 s) opened.

Letdown simulation in the Semiscale system consisted of a valved line connected to the unaffected loop cold leg. A flow control valve in the Semiscale letdown simulation line provided a letdown flow rate of 0.01081 kg/s for fluid conditions typical of the cold leg fluid at initial conditions.

Heat loss makeup in the Semiscale system was accomplished by using external heaters distributed fairly uniformly throughout the Semiscale system. These heaters are controlled by six separate power supplies including: vessel, hot legs, cold legs, unaffected loop pump suction, affected loop pump suction, and pressurizer. The total power provided by these heaters is about 44 kW (excluding the pressurizer). An additional 22 kW of heat loss makeup was provided by augmenting core power throughout the core power decay portion of the transient. Control of the heaters was as follows: If the maximum allowable temperature (755 K) was reached on the inside surface of the pipe insulation, external power to that component was reduced by half. If the temperature trip limit continued to be exceeded, power to that component was terminated. For the vessel upper head external heater bank, the control procedure followed was for the operator to

Table A-1. Comparison of Westinghouse Model 51 steam generator design values, scaled design values, and Semiscale Type III affected loop steam generator design values

Steam Generator Description	Flow Area in Constant Area Region of Downcomer (m^2)	Flow Area in Constant Area Region of Tube Bundle (m^2)	Elevation[a] of U-tubes (m)	Elevation[a] of Riser (m)	Elevation[a] Downcomer (m)	Total Secondary Volume Below Top of U-tubes (m^3)	Total Secondary Volume Below Top of Riser (24 Inches Above Top U-tube) (m^3)	Total Secondary Volume Below Top of Downcomer (m^3)	Relative Pressure Drop (Percentage of Total Flow Circuit Pressure Drop)		
									Downcomer (%)	Tube Bundle (%)	Primary Separator (%)
Westinghouse Model 51 steam generator values	0.658	5.100	10.59	11.21	13.91	65.5	73.7	112.2	24	26	50
Westinghouse Model 51 steam generator volume scaled[b] values	0.000386	0.002990	10.59	11.21	13.91	0.0384	0.0432	0.0658	24	26	50
Semiscale Type III affected loop steam generator values	0.000965	0.003039	9.93	10.54	11.31	0.0439	0.0502	0.0712	20	23	57[c]

a. Relative to top of tube sheet.

b. Volume scaling factor is 1705.5.

c. Obtained by orificing top of riser.

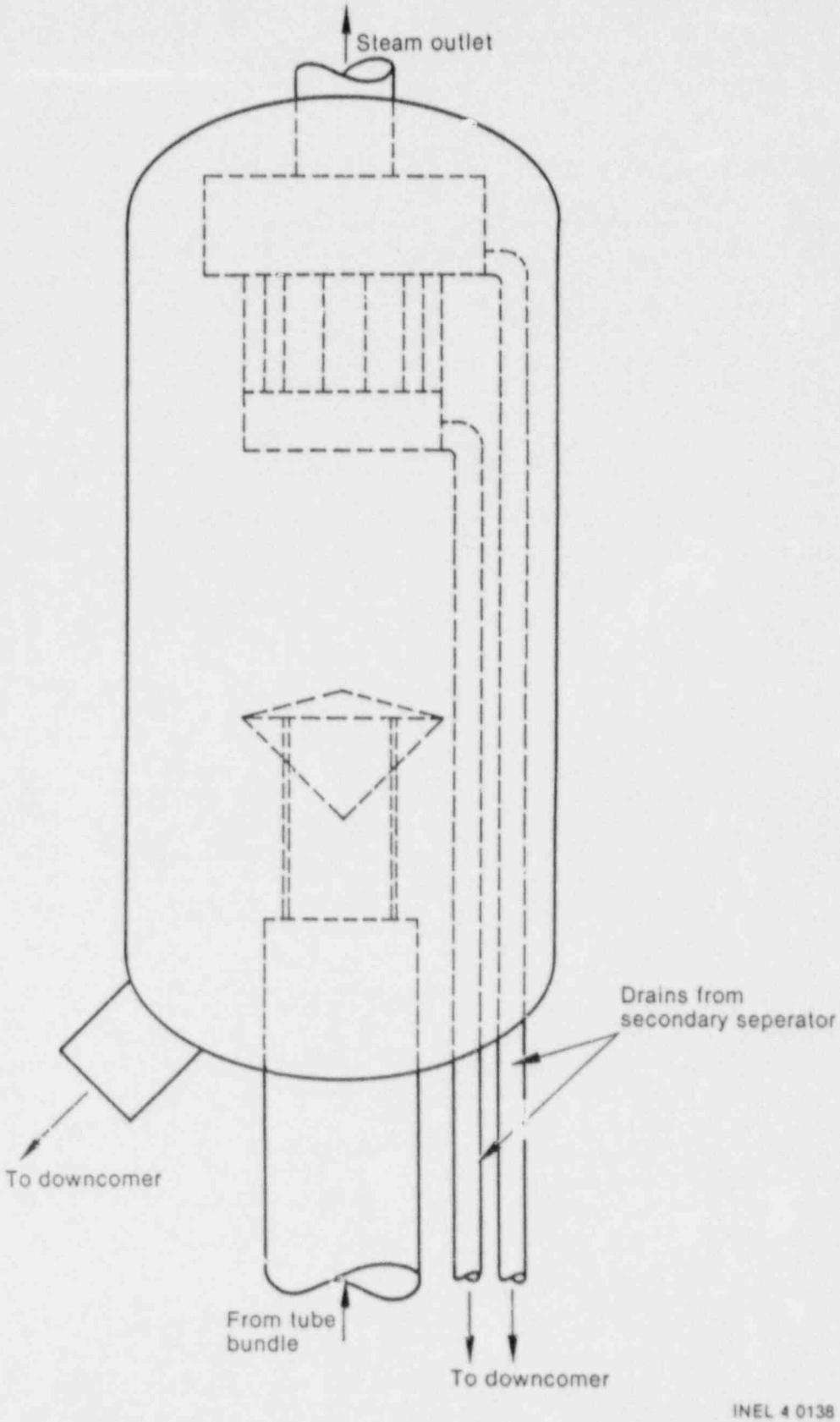

Figure A-4. The Semiscale Type III affected loop steam generator steam dome/separator configuration.

turn off the bank at the start of the countdown (t-120 s). Then at 35 s into the transient, the operator started an automatic timer, which cycled the bank on for 30 s and off for 155 s. This produced approximately the scaled integrated energy loss due to upper head heat loss. In addition, when the upper head liquid level decreased to <356 cm, the operator turned off the bank until the level recovered to ≥ 356 cm, at which time the automatic on/off cycling was reinitiated.

Pressurizer internal heater simulation in the Semiscale system for these tests consisted of using the system pressurizer warm-up heaters. These heaters were controlled manually, supplying 6.99 kW to three of the six warm-up heater rods. The internal heaters were operated in an on/off mode to maintain primary system subcooling.

Measurement System Configuration

The measurement system consists of primary and secondary system measurement hardware and the software utilized for measurement manipulation and recording. The general hardware configuration is discussed in the following text. Description of the measurements made for each feedwater line break test in the series are given in the Appendix for that test.[A-2,A-3]

Experiment instrumentation transducers include thermocouples; resistance temperature detectors; absolute and differential pressure cells; full-flow turbine rotors, each with one or two external magnetic or R.F. blade sensors to measure bidirectional flow; full-flow drag screens, each with one deflection sensor; multiple beam densitometer detectors with radioactive sources; and orifice plates or nozzles with differential pressure cells (for unidirectional flow of single-phase fluids).

The approximately 350 instruments along with further detailed information regarding the particular configuration for each test of the series were documented in the final instrumentation log sheet (Reference A-1). Measurements were chosen to provide information on fluid conditions at key points throughout the primary, secondary, and support systems. A number of measurements were included to provide redundancy so that instrument failures were accommodated without compromising the test objectives. Included in the secondary measurements category were special measurements involving instrumentation development.

New measurement system capabilities were provided for the FS series to allow for more accurate assessment of secondary transient phenomena. The changes included measurement of global, local, and component data for the new Type III affected loop steam generator and break flow measurements expected to allow break effluent characterization.

The measurements on the Type III affected loop steam generator for the FS series provided thermal-hydraulic data about the steam generator during steady-state and transient conditions. The measured data can be grouped into three categories: global, local, and component data. The global data were used to determine the overall mass and energy balances for the affected loop steam generator. Because performing these mass and energy balance calculations requires knowledge of the input, output, and storage terms for the steam generator, the break flow measurement, (discussed later), can be considered as part of the global data measurement category. The local data are utilized to determine local heat transfer coefficients and fluid conditions and as such include the local fluid and material states (primary fluid, U-tube outside wall, secondary fluid temperature triplets and densities) as well as local mass flow rates (secondary mass flow rates and U-tube primary mass flow rates). Data on the mass and energy transfer rates between, and the mass distribution and fluid states within, components of the new Type III affected loop steam generator, component data, were used to analyze the interaction of the components during secondary transients. Determination of break flow conditions was provided by two-phase mass flow measurements upstream of the break nozzle.

EXPERIMENTAL PROCEDURE

As a general procedure before initiation of the transient, the primary system was filled with demineralized water and vented to ensure a liquid-full system. Instrumentation was calibrated and zeroed as necessary. The primary system was heated to initial conditions using core power and pumped flow, and pressurized using the pressurizer internal heaters to draw a steam bubble. The steam generators, after being heat soaked, dissipated the core power to atmosphere by steaming. The Semiscale initial conditions (Table A-2) were typical of, or scaled from, the Combustion Engineering (C-E) System 80 FSAR Appendix 15B[A-4] feedwater line break calculation initial conditions with the exception of the primary pressure, which was specified to emulate the typical C-E System 80 plant normal pressure to SCRAM pressure set point operating margin.

During the period of primary system heating, a procedure was performed to acquire data to allow for normalization of the Type III affected loop steam generator temperature triplets. The procedure involved bringing the primary-to-secondary heat transfer through zero (i.e., gradually reversing the direction of energy transfer) for three different absolute temperatures. By determining the difference between the triplet temperatures at the point of no heat transfer (i.e., where the temperature difference should be zero) the correction required to match the triplets to the average temperature were determined. By performing the procedure for three different absolute temperatures, three different correction versus temperature points were obtained for each temperature measurement. The three correction versus temperature points were then curve fit to obtain a linear correction versus temperature function for each temperature measurement. The linear correction functions were then applied to the temperature measurements to obtain the normalized temperature triplet data. Normalization substantially reduces the uncertainty of the measured temperature difference between the three triplet thermocouples.

The transient was initiated at time zero (t = 0 s) by opening the valve in the break assembly in the affected loop steam generator. The simulated bottom main feedwater line break, in conjunction with the simulated affected loop steam generator main steam line check valve failure, produced pressure reductions and inventory losses in both steam generator secondaries and rapid pressurization of the primary system. The primary and secondary pressure responses caused signals to be generated, which triggered automatic responses[a] by various systems. The reactor and turbine trip (SCRAM) signal was generated by a high pressurizer pressure of 15.86 MPa and triggered: closure of the normal steam flow control valves (turbine stops valve simulators) with a 4 s valve closure time simulated; and core power decay with a 3.2 s delay to simulate transducer response and rod drip times. Loss of offsite power was assumed to occur at SCRAM producing primary coolant pump coastdowns (with a 2 s delay to simulate transformer decay time) and delaying the availability of safety injection and auxiliary feedwater flows by 25 s (the time required to start the diesel generators that power the pumps). The MSIV closure action (with a 4 s valve closure time simulated) and the auxiliary feedwater and HPIS initiation (SIS) actions were triggered by a low affected loop steam generator steam dome pressure of 4.47 MPa. The completion of these automatic actions and operator identification of the event (assumed to require a minimum of 600 s) represented the end of the blowdown phase of the test. The timing of events for the blowdown phase of the tests are contained in Table A-3.

Various recovery operations were performed for Tests S-FS-6, S-FS-7, and S-FS-11 based on the guidance provided by Emergency Operating Procedures.[A-5,A-6] The recovery procedures for Test S-FS-6 were specified to simulate the expected operator actions in response to a feedwater line break and to provide data on two methods of upper head void collapse. The recovery procedures for Test S-FS-6 consisted of: (a) stabilizing the plant at specified pressures, temperatures, and levels, using normal charging/letdown operation, pressurizer heater operation, and an unaffected loop steam generator steam and feed operation; and (b) performing a natural circulation cooldown and depressurization (including operations to investigate a *fill and drain* method and a pump restart method of upper head void collapse) using pressurizer auxiliary spray operation, pressurizer heater operation, normal charging/letdown operation, an unaffected loop steam generator steam and feed operation, and a primary coolant pump restart operation.

The recovery procedures for Tests S-FS-7 and S-FS-11 were specified to simulate the early operator actions in response to a feedwater line break and

a. The automatic events were specified to simulate those used for the C-E System 80 FSAR calculations.

Table A-2. Initial conditions for the feedwater line break experiments in the S-FS test series

Parameters	S-FS-6	S-FS-6B	S-FS-11	S-FS-7
Pressurizer pressure	14.94 MPa	15.01 MPa	15.03 MPa	14.98 MPa
Core power[a]	2.18 MW	2.17 MW	2.18 MW	2.18 MW
Core ΔT	36.3 K	36.9 K	36.7 K	36.9 K
Pressurizer liquid level, [collapsed liquid level relative to zero reference elevation (bottom of pressurizer)]	482 cm	477 cm	484 cm	488 cm
Cold leg fluid loop-to-loop temperature difference (absolute)	4.4 K	3.9 K	4.5 K	4.2 K
Cold leg fluid temperature (nominal)	569 K	569 K	568 K	569 K
Primary flow rates (nominal)				
Unaffected loop cold leg	9.6 L/s	9.5 L/s	9.4 L/s	9.3 L/s
Affected loop cold leg	3.2 L/s	3.2 L/s	3.3 L/s	3.2 L/s
Initial bypass flow (% of total loop flow)	2.35%	2.40%	2.36%	2.32%
Steam generator secondary pressures				
Unaffected loop	6.29 MPa	6.28 MPa	6.27 MPa	6.23 MPa
Affected loop	6.26 MPa	6.26 MPa	6.23 MPa	6.21 MPa
Steam generator secondary side masses				
Unaffected loop	108 kg	120 kg	103 kg	117 kg
Affected loop	26.0 kg	25.0 kg	26.0 kg	28.8 kg
Affected loop steam generator circulation ratio	4.54	4.60	4.50	4.34
Steam generator feedwater flow rates (nominal)				
Unaffected loop	0.88 kg/s	0.90 kg/s	0.86 kg/s	0.89 kg/s
Affected loop	0.25 kg/s	0.26 kg/s	0.24 kg/s	0.27 kg/s
Steam generator feedwater temperatures (nominal)				
Unaffected	485 K	488 K	485 K	484 K
Affected	483 K	485 K	481 K	480 K

Table A-2. (continued)

Parameters	S-FS-6	S-FS-6B	S-FS-11	S-FS-7
Pretest measured leakage				
Primary	0.0016 kg/s	0.0023 kg/s	0.0019 kg/s	0.0019 kg/s
Affected loop secondary	0.00014 kg/s	0.00009 kg/s	0.00014 kg/s	0.00014 kg/s

a. Core power augmentation of 22 kW was applied only during the core power decay following SCRAM.

Table A-3. Timing of events for the blowdown phase of the S-FS series feedwater line break experiments

Event	Specified Time (s)	Test S-FS-6 (s)	Test S-FS-6B (s)	Test S-FS-7 (s)	Test S-FS-11 (s)
Transient initiation	0.0	0.0	0.0	0.0	0.0
Affected loop MFLB blowdown valve fully open	1	1	1	1	1
Main feedwater isolation valves closed					
Unaffected loop	1	1	1	1	1
Affected loop	1	1	1	1	1
Pressurizer pressure = 15.86 MPa	$T = T_{SCRAM}$	23.5	22.0	46.3	23
Unaffected and affected loop pump begin coastdown	$T = T_{SCRAM} + 2$	23.5	24.2	48	25
Core power decay initiated	$T = T_{SCRAM} + 3.2$	26.0	24.6	49	26.5
Unaffected and affected loop steam generator main steam flow control valves fully closed	$T = T_{SCRAM} + 4$	26.5	24.4	49	26.5
Vessel upper head external heater bank starts on/off cycling	35.0	40	38	38	38
Power to both pumps tripped	$T = T_{SCRAM} + 38.0$	61.8	60.2	85	61
Affected loop steam generator steam dome pressure = 4.47 MPa	$T = T_{SIS}$	101	99	919	209
Auxiliary feedwater flow initiated; HPIS flow available	$T \geq T_{SIS}$ and $T \geq T_{SCRAM} + 25$	102	AL: 99.6 UL: 300	920	211
Crossover line valve (MSIV) closed	$T = T_{SIS} + 4$	105	103	923	214
Operator identification of transient (blowdown over)	$T \geq 600$ and $T \geq T_{SIS} + 4$	600	600	923	600

to provide data on voided secondary refills at two different refill rates. The recovery procedures for Tests S-FS-7 and S-FS-11 consisted of: (a) stabilizing the plant as was done for Test S-FS-6, and (b) isolating the break and refilling the affected loop steam generator secondary with auxiliary feedwater while maintaining the stable conditions attained earlier in the test. The specific requirements for these recovery procedures were outlined in References A-2, A-3, A-7 through A-9.

REFERENCES

A-1. E. Klingler, *The Semiscale Mod-2C Feedwater and Steam Line Break Configuration Report for Experiments S-FS-1, S-FS-2, S-FS-6, S-FS-6B, S-FS-7, and S-FS-11*, EGG-RTH-7445, October 1986.

A-2. T. J. Boucher and W. A. Owca, *Appendix S-FS-6 & 7 of the Experiment Operating Specification for the Semiscale Mod-2C Feedwater and Steam Line Break Experiment Series* EGG-SEMI-6871, May 1985.

A-3. T. J. Boucher and W. A. Owca, *Appendix S-FS-11 of the Experiment Operating Specification for the Semiscale Mod-2C Feedwater and Steam Line Break Experiment Series*, EGG-SEMI-6909, June 1985.

A-4. CESSAR-80, *Final Safety Analysis Report*, Appendix 15, Combustion Engineering Company.

A-5. Waterford Unit 3 Nuclear Plant, *Emergency Operating Procedures*, Louisiana Power and Light Company.

A-6. St. Lucie Unit 2 Nuclear Plant, *Emergency Operating Procedures*, Florida Power and Light Company.

A-7. T. J. Boucher and D. G. Hall, *Quick Look Report for Semiscale Mod-2C Test S-FS-6*, EGG-SEMI-7022, September 1985.

A-8. D. G. Hall, *Quick Look Report for Semiscale Mod-2C Test S-FS-7*, EGG-RTH-7072, October 1985.

A-9. M. P. Plessinger, *Quick Look Report for Semiscale Mod-2C Test S-FS-11*, EGG-RTH-7103, November 1985.

APPENDIX B

REPEATABILITY OF RESULTS (S-FS-6/S-FS-6B COMPARISONS)

APPENDIX B

REPEATABILITY OF RESULTS (S-FS-6/S-FS-6B COMPARISONS)

CONTENTS

INTRODUCTION B-5

COMPARISON OF RESULTS B-6

CONCLUSIONS B-16

FIGURES

B-1. Comparisons of affected and unaffected loop steam generator secondary pressures during the blowdown phases of 100% FWLB experiments S-FS-6 and S-FS-6B B-7

B-2. Comparisons of measured break mass flow rates during the blowdown phases of 100% FWLB experiments S-FS-6 and S-FS-6B B-7

B-3. Comparisons of break fluid densities during the blowdown phases of 100% FWLB experiments S-FS-6 and S-FS-6B B-8

B-4. Comparisons of affected loop steam generator upper downcomer mass flow rates during the blowdown phases of 100% FWLB experiments S-FS-6 and S-FS-6B B-8

B-5. Comparisons of affected loop steam generator riser and steam mass flow rates during the blowdown phases of 100% FWLB experiments S-FS-6 and S-FS-6B B-9

B-6. Comparisons of riser orifice frictional pressure drops (indicative of flow direction) during the blowdown phases of 100% FWLB experiments S-FS-6 and S-FS-6B B-9

B-7. Comparisons of affected loop steam generator lower downcomer to lower tube bundle differential pressure (indicative of flow direction) for the blowdown phase of 100% FWLB experiments S-FS-6 and S-FS-6B B-10

B-8. Comparisons of intersecondary mass flow rates through the crossover line during the blowdown phases of 100% FWLB B-15 experiments S-FS-6 and S-FS-6B B-10

B-9. Comparisons of affected loop steam generator overall downcomer and tube bundle interfacial liquid levels during the blowdown phases of 100% FWLB experiments S-FS-6 and S-FS-6B B-11

B-10. Comparisons of unaffected loop steam generator overall downcomer and tube bundle collapsed liquid levels and auxiliary feedwater mass flow rates during the blowdown phases of 100% FWLB experiments S-FS-6 and S-FS-6B B-11

B-11. Comparisons of affected and unaffected loop steam generator secondary fluid mass inventories during the blowdown phases of 100% FWLB experiments S-FS-6 and S-FS-6B B-12

B-12. Comparisons of affected and unaffected loop steam generator primary-to-secondary heat transfer and primary energy addition during the blowdown phases of 100% FWLB experiments S-FS-6 and S-FS-6B B-12

B-13. Affected loop steam generator tube bundle secondary fluid vapor void fractions during the blowdown phase of 100% FWLB experiment S-FS-6 ..... B-13

B-14. Affected loop steam generator tube bundle secondary fluid vapor void fractions during the blowdown phase of 100% FWLB experiment S-FS-6B B-13

B-15. Comparisons of pressurizer and loop cold leg pressures during the blowdown phases of 100% FWLB experiments S-FS-6 and S-FS-6B B-14

B-16. Comparisons of pressurizer overall collapsed liquid levels during the blowdown phases of 100% FWLB experiments S-FS-6 and S-FS-6B B-14

B-17. Comparisons of affected and unaffected loop hot and cold leg fluid temperatures during the blowdown phases of 100% FWLB experiments S-FS-6 and S-FS-6B B-15

B-18. Comparisons of average primary fluid temperatures during the blowdown phases of 100% FWLB experiments S-FS-6 and S-FS-6B B-15

APPENDIX B

REPEATABILITY OF RESULTS (S-FS-6/S-FS-6B COMPARISONS)

INTRODUCTION

Analysis of the affected loop steam generator temperature triplet normalization data taken before 100% bottom main feedwater line break experiment S-FS-6 showed that the data was not adequate for obtaining normalized heat transfer data. Because of the importance of the local heat transfer data to understanding and utilizing of the bottom main feedwater line break experimental results, it was deemed necessary to repeat the blowdown phase of the 100% break experiment to obtain the local heat transfer data. Experiment S-FS-6B was, therefore, performed as a repeat of the first 600 s of experiment S-FS-6 in order to obtain the local heat transfer data not obtained during experiment S-FS-6. The initial conditions and sequence of events for experiment S-FS-6B were the same as those for experiment S-FS-6 (see Tables A-2 and A-3).

Comparisons of the results for the two experiments are presented in this appendix as a means of assessing the appropriateness of intermingling the data from the two experiments and verifying the repeatability of results.

COMPARISON OF RESULTS

The excellent comparison of the results of experiments S-FS-6 and S-FS-6B is readily evident in the excellent agreement of the data in the included figures. The secondary thermal-hydraulic responses (Figures B-1 through B-14) and the primary thermal-hydraulic responses (Figures B-15 through B-18) are almost identical for the two experiments. The minor differences observed in the data are due to the slight difference in the initial conditions and the delayed initiation (about 200 s late) of the unaffected loop steam generator auxiliary feedwater injection during experiment S-FS-6B. The secondary and primary responses exhibit identical phenomena throughout the entire blowdown. The effect of the slight differences is most apparent at the end of the blowdown phase and is minimal (within the measurement uncertainty in most cases). The observed difference in the riser mass flow rate is due to a problem with the drag screen measurement device for experiment S-FS-6B. The flow reversal exhibited in the measured riser mass flow rate for experiment S-FS-6 is the actual response for both tests (as evidenced by the negative frictional pressure drop across the orifice in the riser for both experiments). The observed differences in the unaffected loop steam generator secondary pressure, liquid level, and primary energy removal response are due to the slight difference in the initial mass and the delayed auxiliary feedwater initiation for experiment S-FS-6B. The observed difference in the initial pressurizer and loop cold leg pressure responses is due to the simulated pressurizer code safety [safety relief valve (SRV)] cycling during experiment S-FS-6B, but not during experiment S-FS-6. This is due to the fact that the actual SRV opening set point pressure was slightly higher than, but within the specified tolerance of, the desired set point for experiment S-FS-6; and slightly lower than, but within the specified tolerance of, the desired set point for experiment S-FS-6B. The other minor differences in the primary system response are due primarily to the slight difference in the unaffected loop steam generator secondary response. The experimental results show excellent comparison, verifying both the validity of intermingling the data from the two experiments and the repeatability of results.

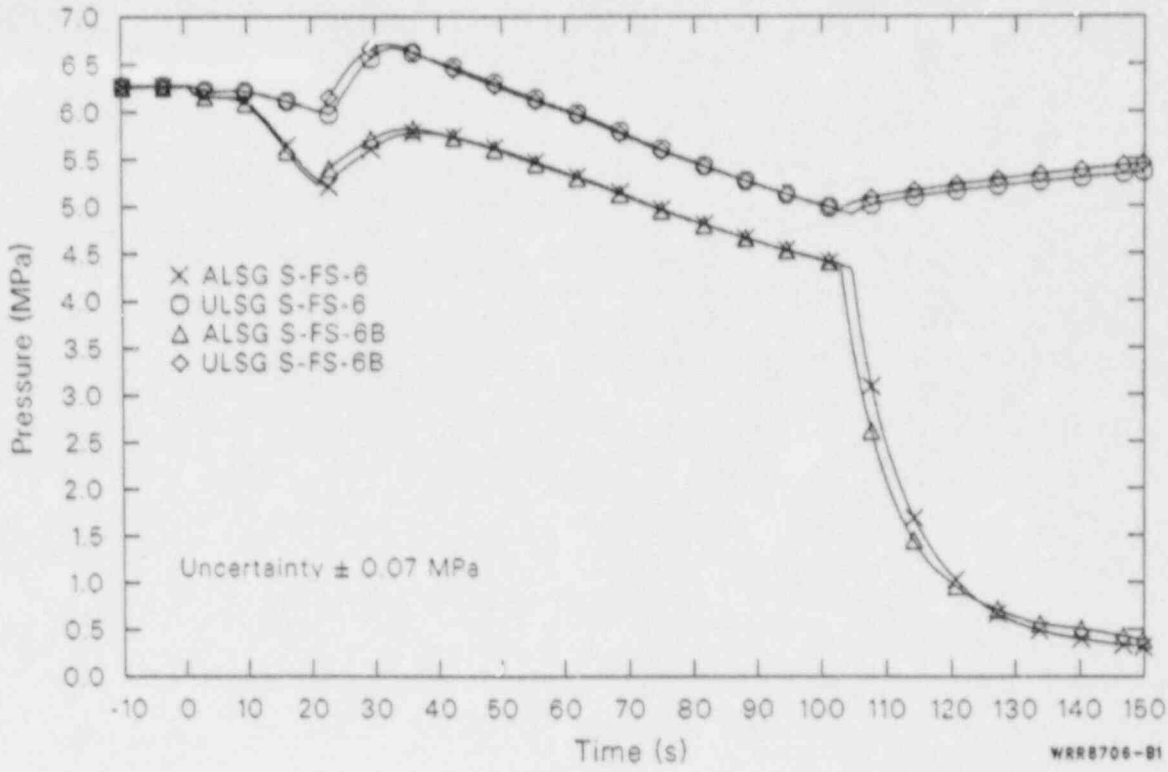

Figure B-1. Comparisons of affected and unaffected loop steam generator secondary pressures during the blowdown phases of 100% FWLB experiments S-FS-6 and S-FS-6B.

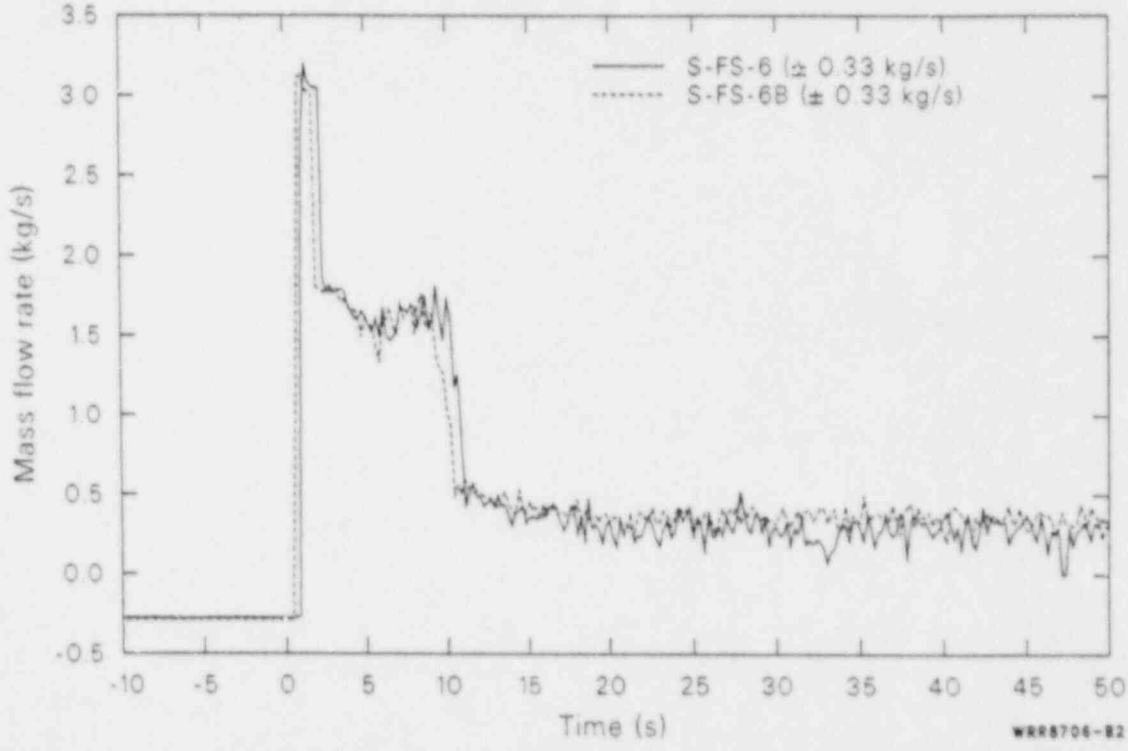

Figure B-2. Comparisons of measured break mass flow rates during the blowdown phases of 100% FWLB experiments S-FS-6 and S-FS-6B.

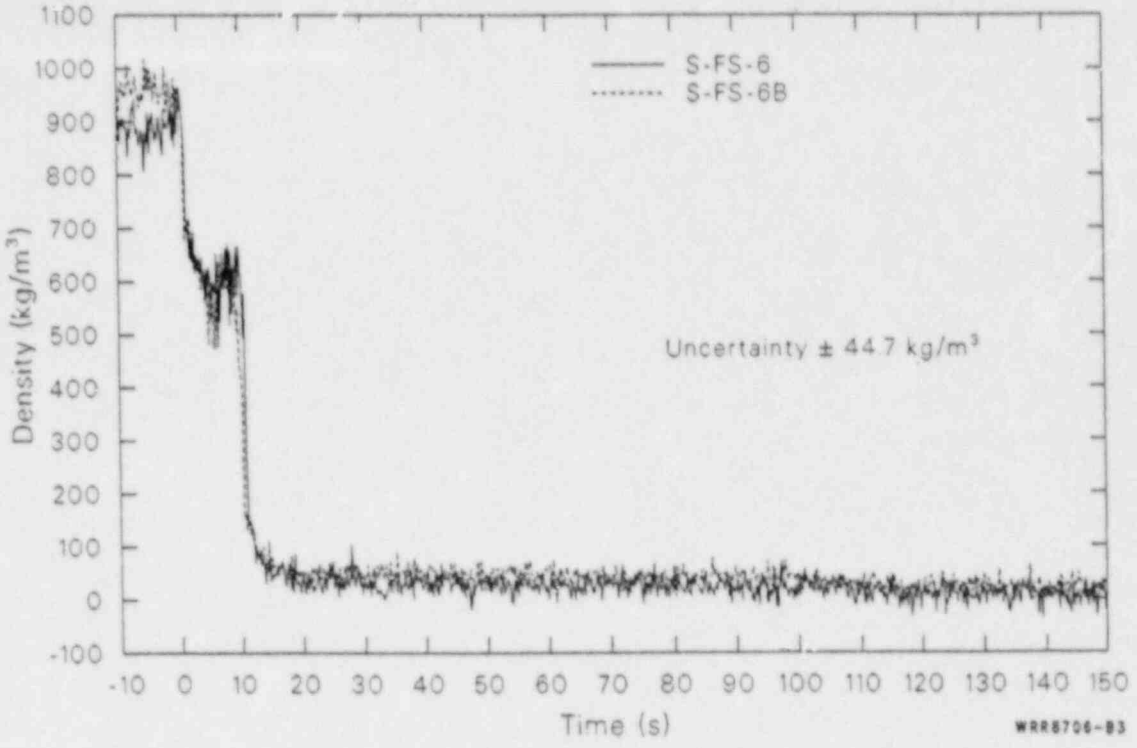

Figure B-3. Comparisons of break fluid densities during the blowdown phases of 100% FWLB experiments S-FS-6 and S-FS-6B.

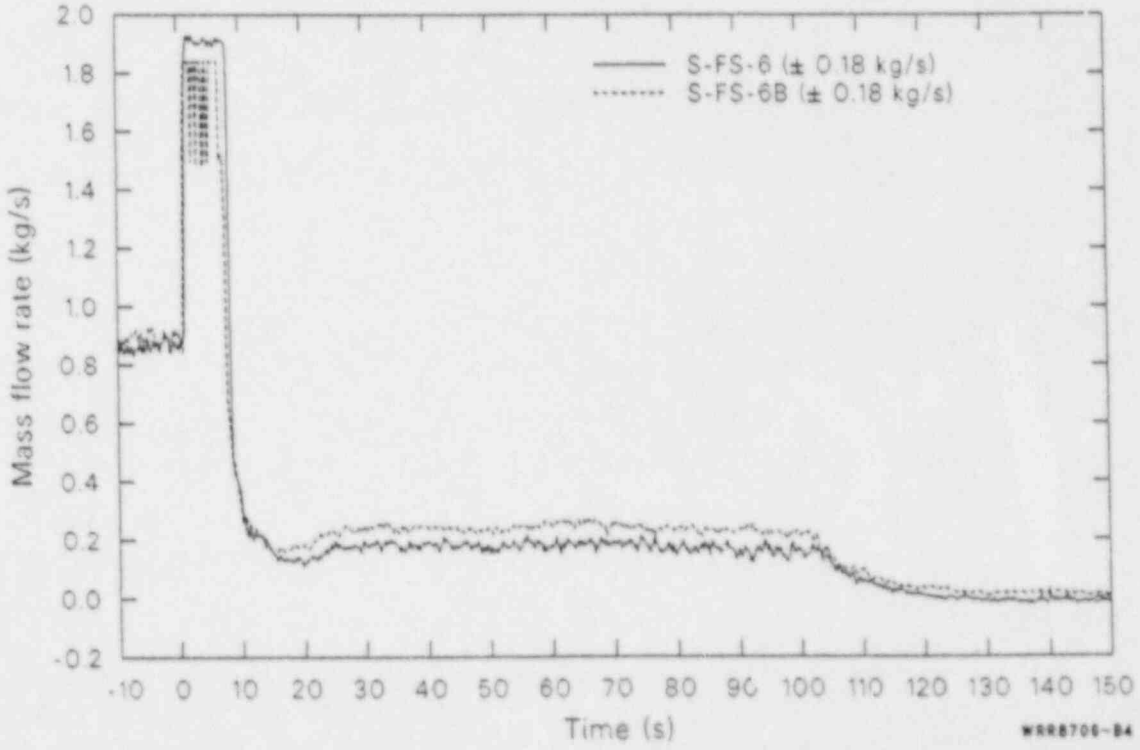

Figure B-4. Comparisons of affected loop steam generator upper downcomer mass flow rates during the blowdown phases of 100% FWLB experiments S-FS-6 and S-FS-6B.

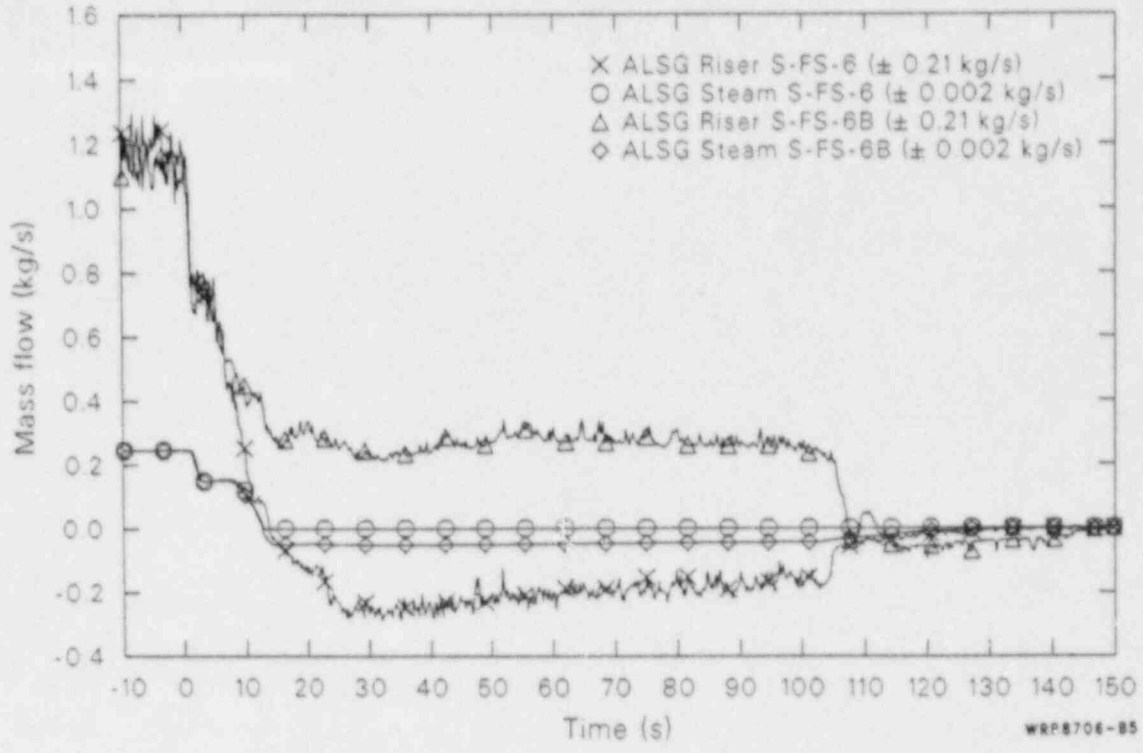

Figure B-5. Comparisons of affected loop steam generator riser and steam mass flow rates during the blowdown phases of 100% FWLB experiments S-FS-6 and S-FS-6B.

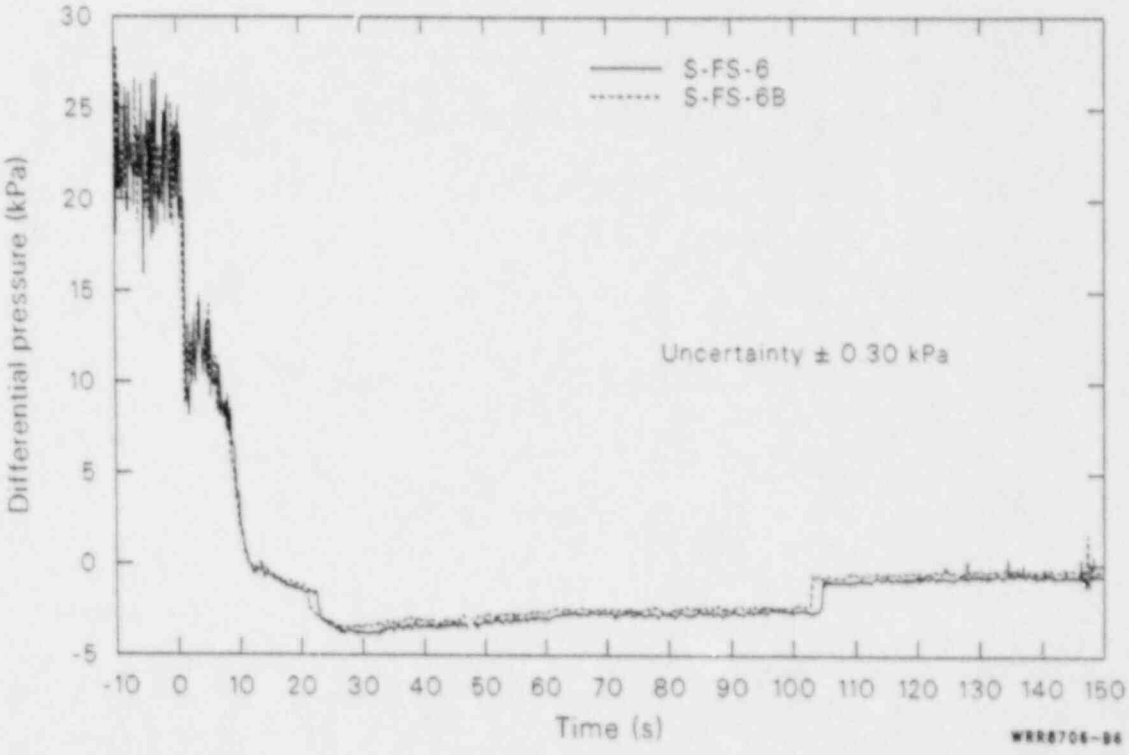

Figure B-6. Comparisons of riser orifice frictional pressure drops (indicative of flow direction) during the blowdown phases of 100% FWLB experiments S-FS-6 and S-FS-6B.

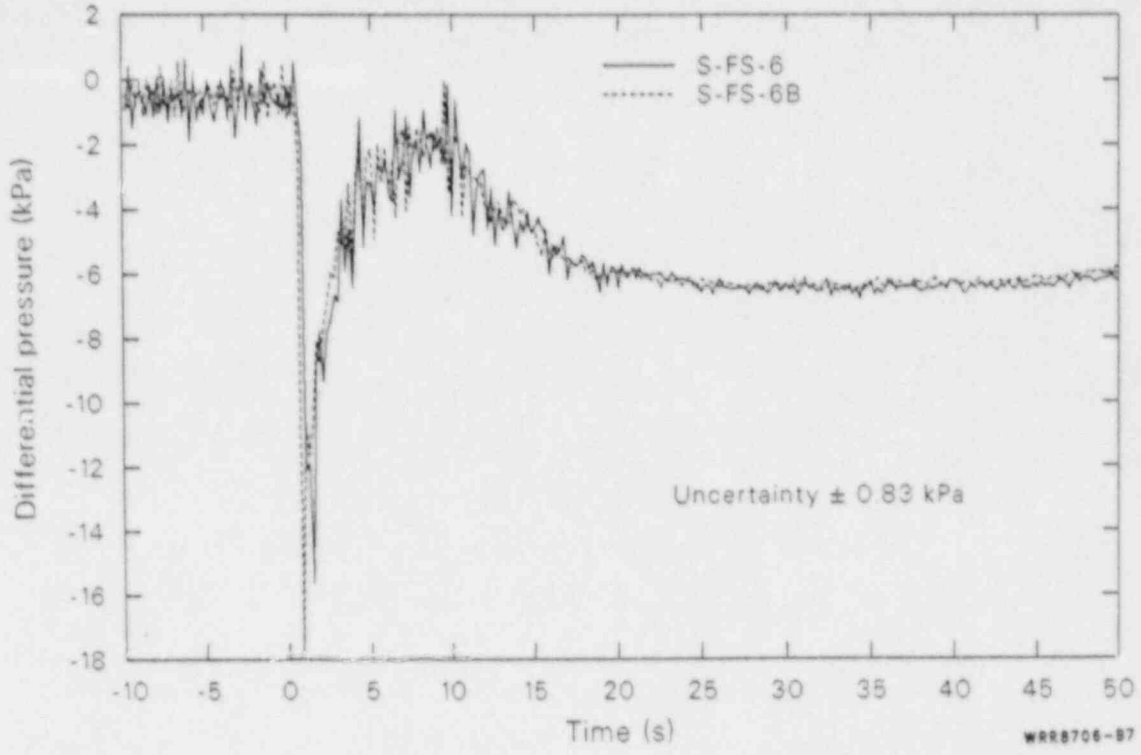

Figure B-7. Comparisons of affected loop steam generator lower downcomer to lower tube bundle differential pressure (indicative of flow direction) for the blowdown phase of 100% FWLB experiments S-FS-6 and S-FS-6B.

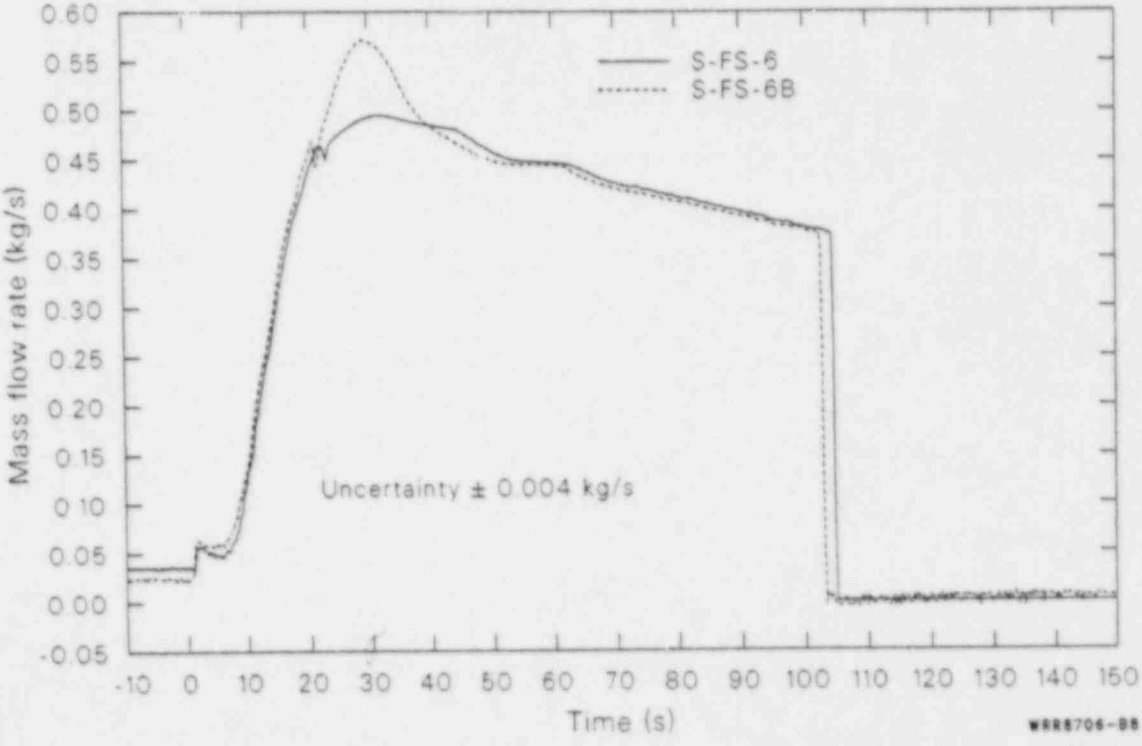

Figure B-8. Comparisons of intersecondary mass flow rates through the crossover line during the blowdown phases of 100% FWLB experiments S-FS-6 and S-FS-6B.

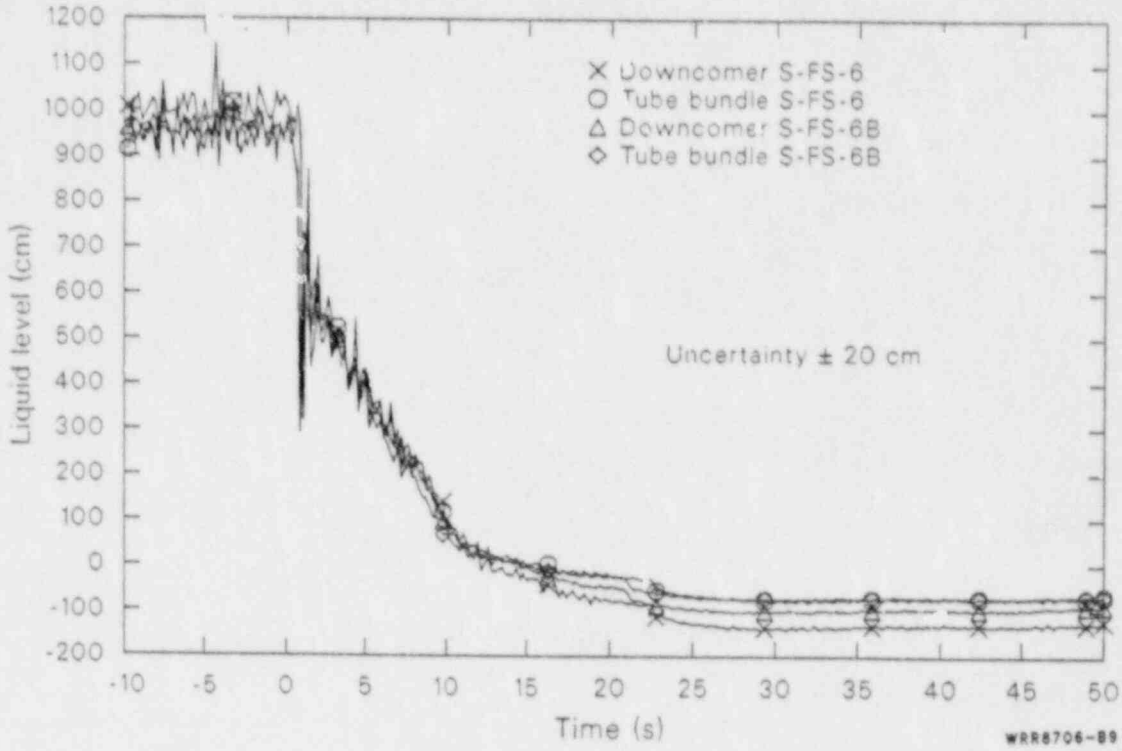

Figure B-9. Comparisons of affected loop steam generator overall downcomer and tube bundle interfacial liquid levels during the blowdown phases of 100% FWLB experiments S-FS-6 and S-FS-6B.

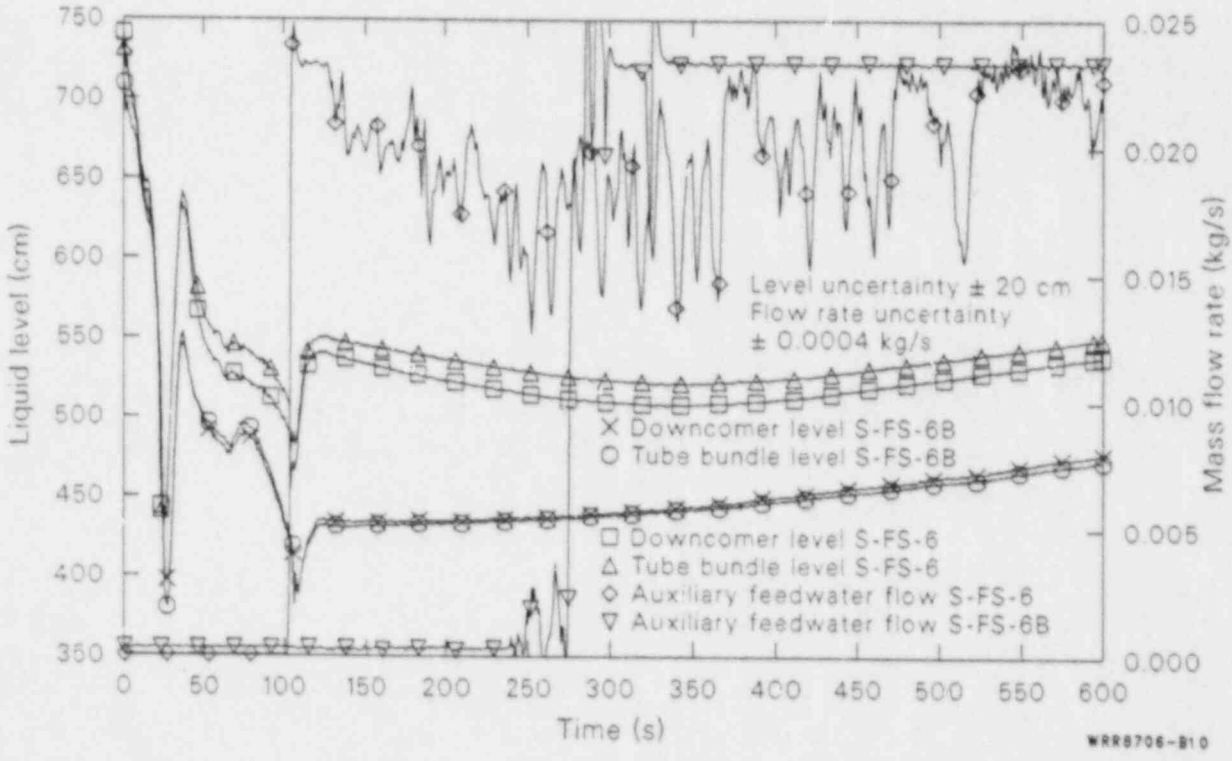

Figure B-10. Comparisons of unaffected loop steam generator overall downcomer and tube bundle collapsed liquid levels and auxiliary feedwater mass flow rates during the blowdown phases of 100% FWLB experiments S-FS-6 and S-FS-6B.

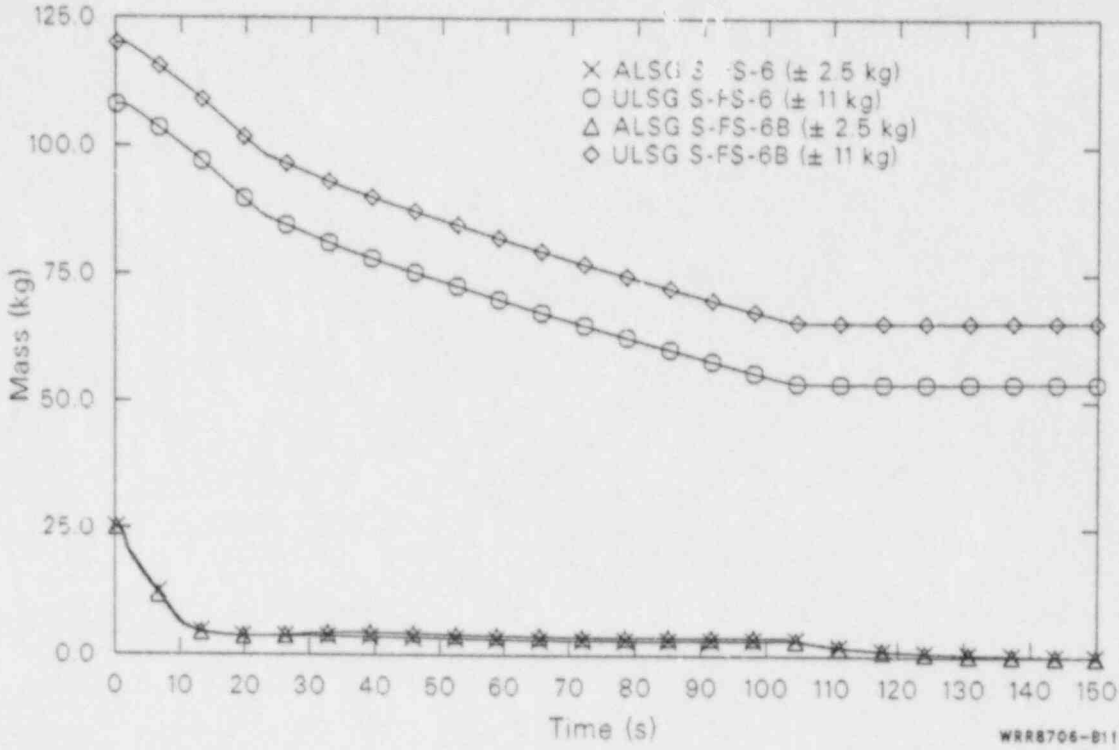

Figure B-11. Comparisons of affected and unaffected loop steam generator secondary fluid mass inventories during the blowdown phases of 100% FWLB experiments S-FS-6 and S-FS-6B.

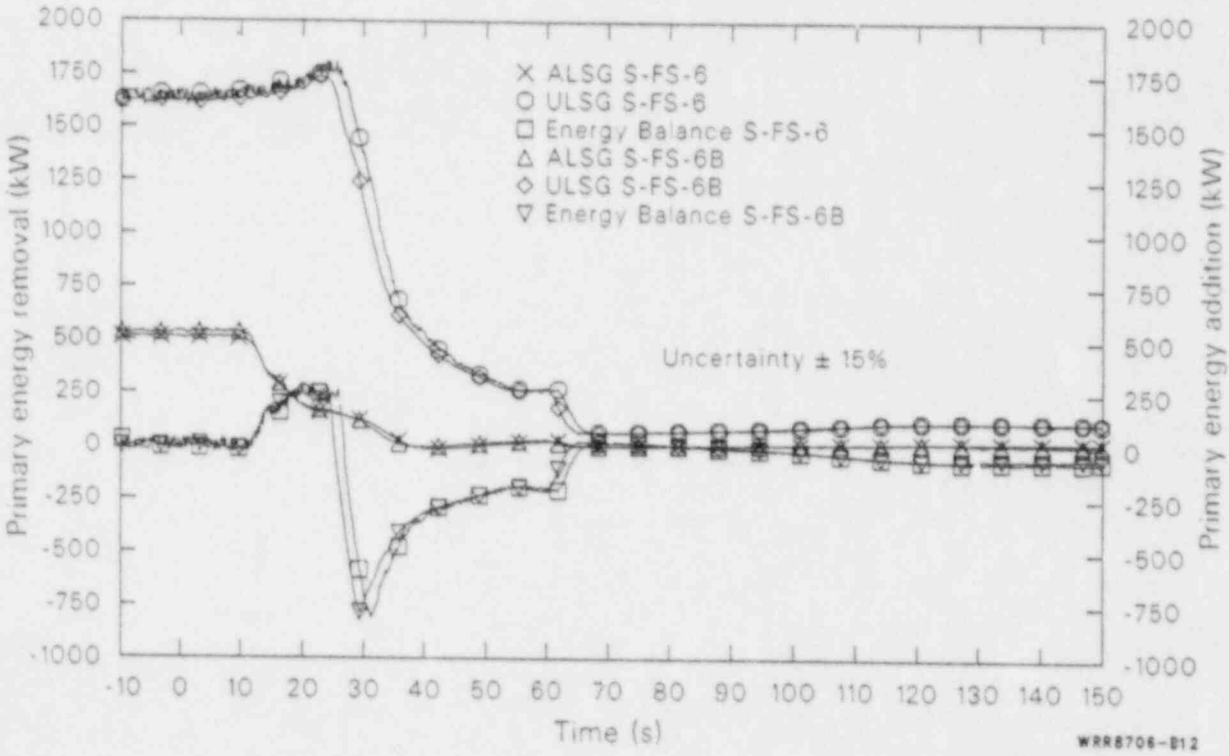

Figure B-12. Comparisons of affected and unaffected loop steam generator primary-to-secondary heat transfer and primary energy addition during the blowdown phases of 100% FWLB experiments S-FS-6 and S-FS-6B.

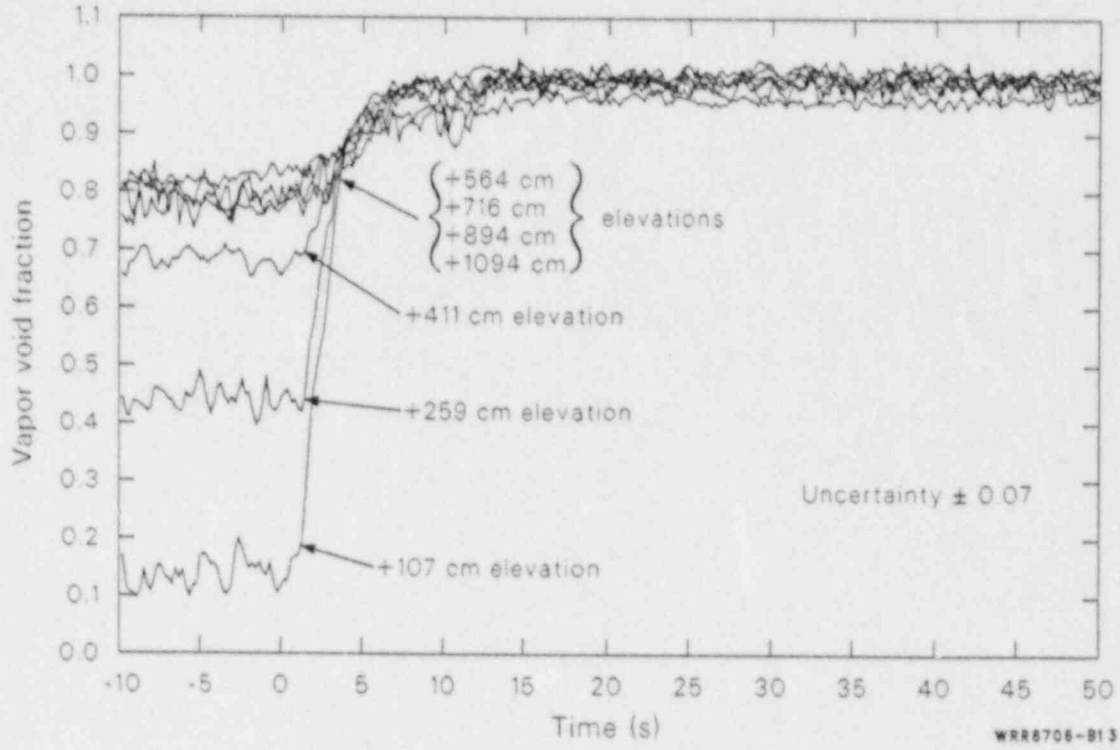

Figure B-13. Affected loop steam generator tube bundle secondary fluid vapor void fractions during the blowdown phase of 100% FWLB experiment S-FS-6

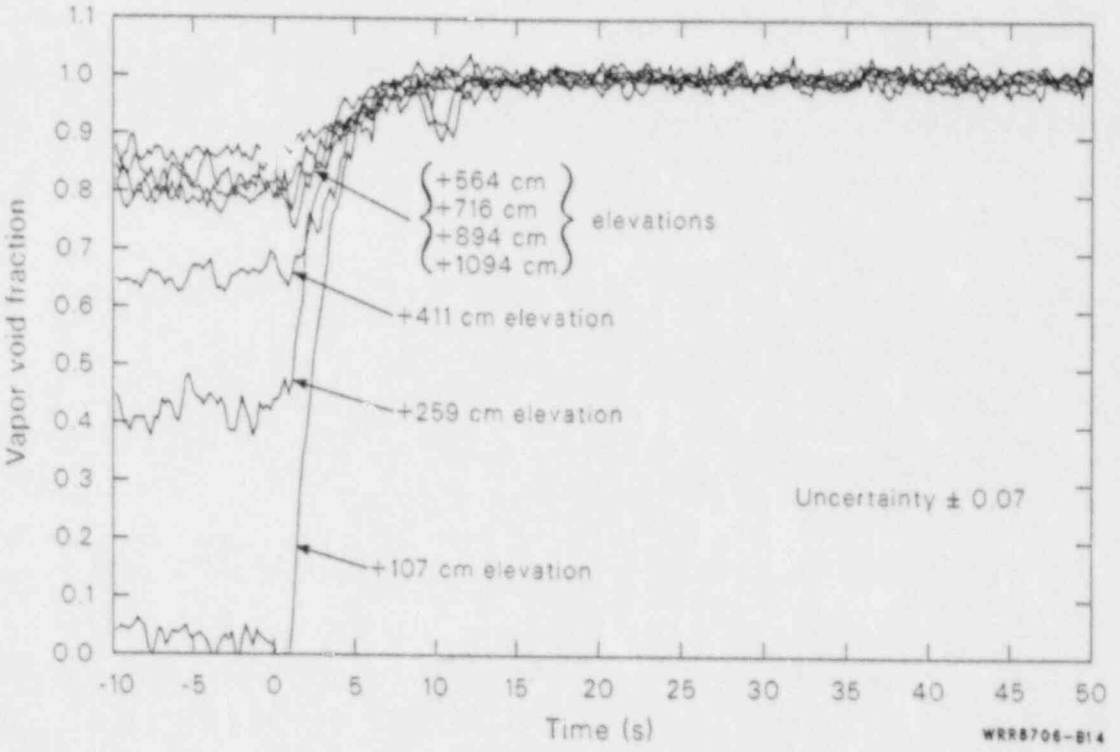

Figure B-14. Affected loop steam generator tube bundle secondary fluid vapor void fractions during the blowdown phase of 100% FWLB experiment S-FS-6B.

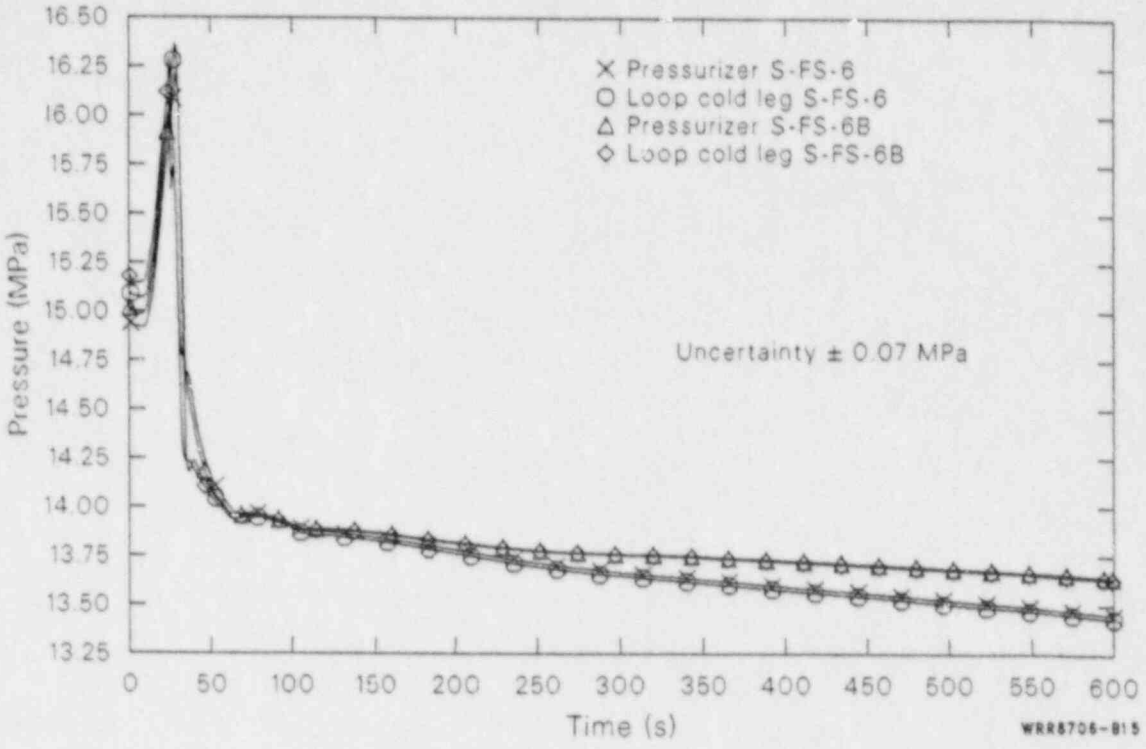

Figure B-15. Comparisons of pressurizer and loop cold leg pressures during the blowdown phases of 100% FWLB experiments S-FS-6 and S-FS-6B.

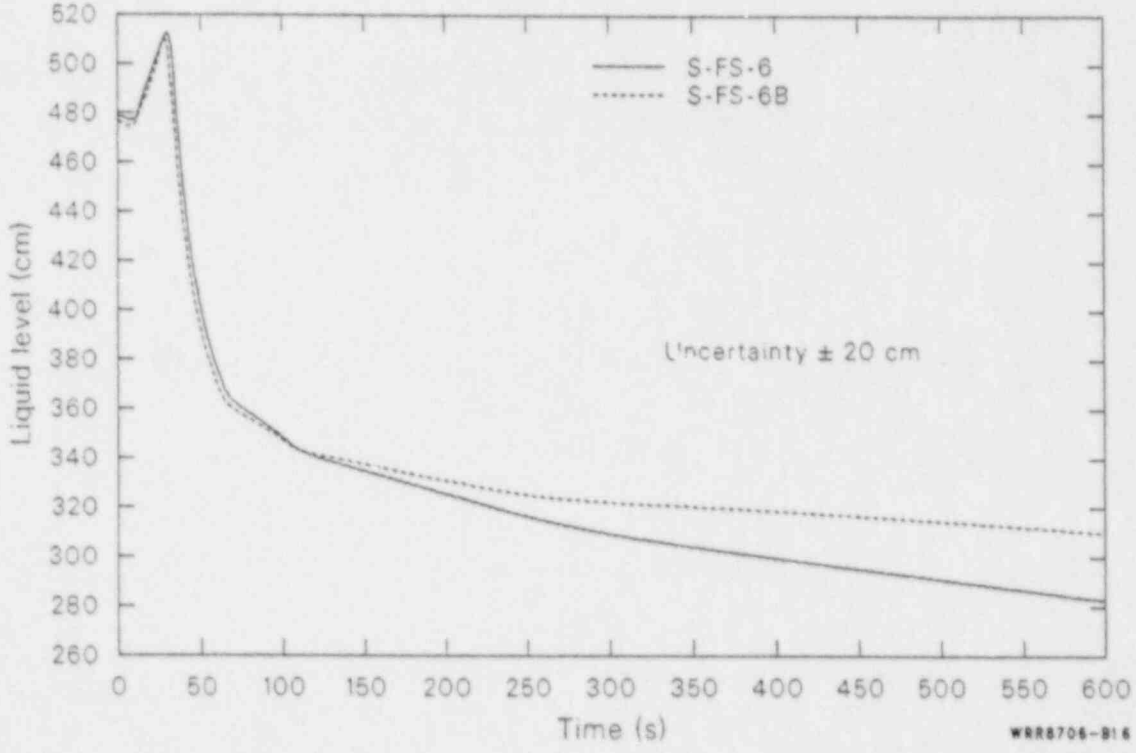

Figure B-16. Comparisons of pressurizer overall collapsed liquid levels during the blowdown phases of 100% FWLB experiments S-FS-6 and S-FS-6B.

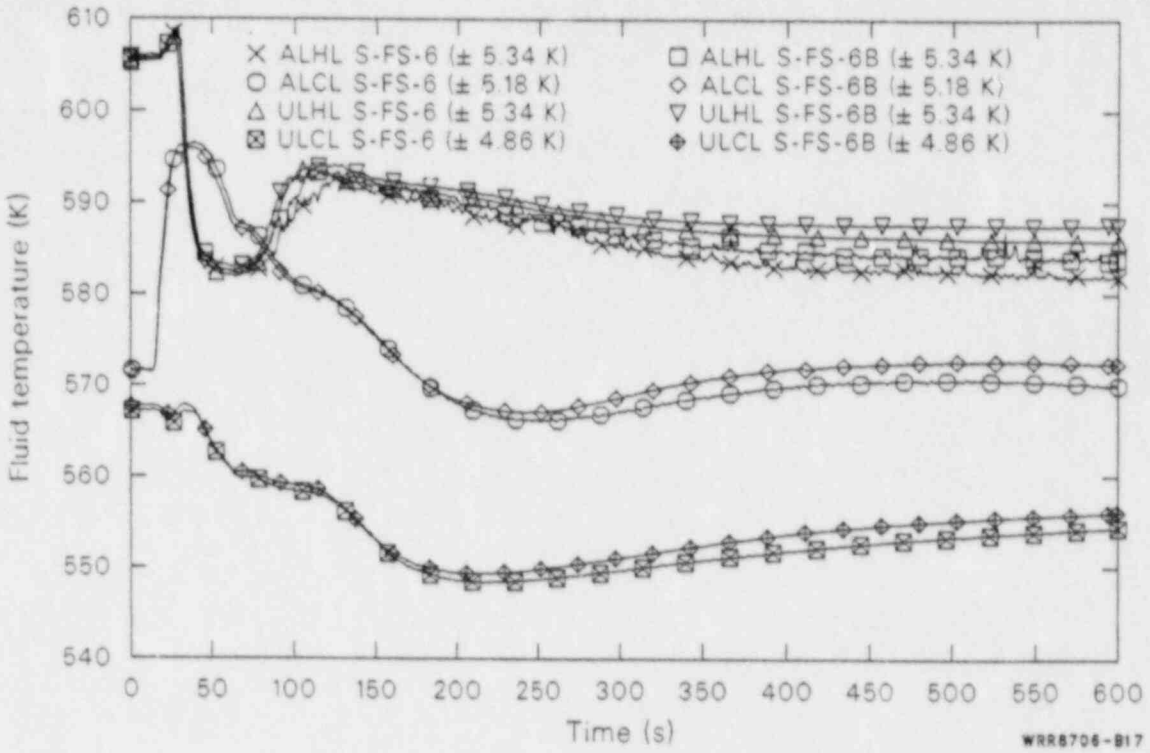

Figure B-17. Comparisons of affected and unaffected loop hot and cold leg fluid temperatures during the blowdown phases of 100% FWLB experiments S-FS-6 and S-FS-6B.

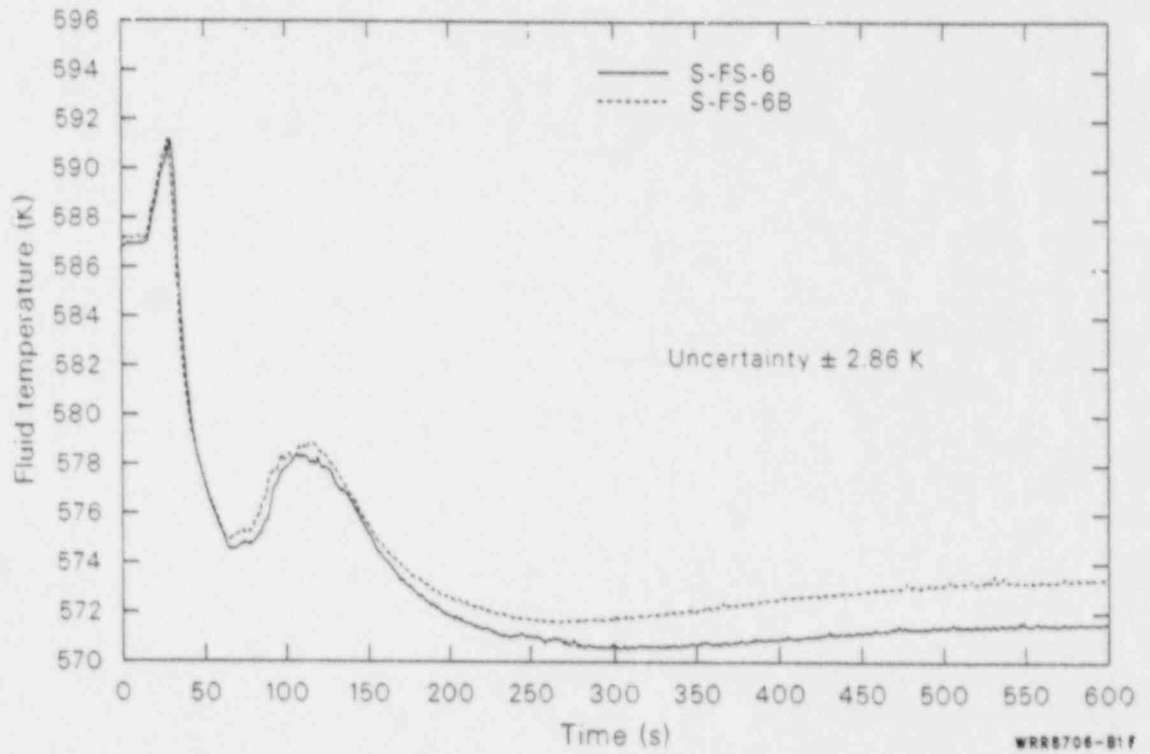

Figure B-18. Comparisons of average primary fluid temperatures during the blowdown phases of 100% FWLB experiments S-FS-6 and S-FS-6B.

CONCLUSIONS

The excellent comparison of the results of experiments S-FS-6 and S-FS-6B verifies both the validity of intermingling the data from the two experiments and the repeatability of the results. The very minor differences observed are due to slight differences in the initial conditions and delayed unaffected loop steam generator auxiliary feedwater initiation during experiment S-FS-6B.

APPENDIX C

STEADY-STATE RESULTS

APPENDIX C

STEADY-STATE RESULTS

CONTENTS

INTRODUCTION C-5

STEADY-STATE SECONDARY THERMAL-HYDRAULIC CHARACTERISTICS C-6

REFERENCES C-16

FIGURES

C-1. Affected loop steam generator average full-power, steady- state secondary fluid subcooled margin versus elevation above the top of the tube sheet for FWLB experiments S-FS-6B, S-FS-11, and S-FS-7 ..... C-7

C-2. Affected loop steam generator average full-power, steady-state U-tube outside wall heat fluxes versus length along the tube (from inlet to outlet plenum) for the long and short tubes for FWLB experiments S-FS-6B, S-FS-11, and S-FS-7 ..... C-9

C-3. Affected loop steam generator average full-power, steady-state U-tube outside wall integrated heat fluxes versus length along the tube (inlet to outlet plenum) for the long and short tubes for FWLB experiments S-FS-6B, S-FS-11, and S-FS-7 ..... C-9

C-4. Affected loop steam generator average full-power, steady-state long tube hot and cold side secondary convective heat transfer coefficients versus elevation above the top of the tube sheet for FWLB experiments S-FS-6B, S-FS-11, and S-FS-7 ..... C-10

C-5. Affected loop steam generator average full-power, steady-state short tube hot and cold side secondary convective heat transfer coefficients versus elevation above the top of the tube sheet for FWLB experiments S-FS-6B, S-FS-11, and S-FS-7 ..... C-10

C-6. Affected loop steam generator full-power, steady-state long tube hot side U-tube outside wall-to-secondary fluid temperature differences versus elevation above the top of the tube sheet for FWLB experiments S-FS-6B, S-FS-11, and S-FS-7 ..... C-11

C-7. Affected loop steam generator full-power, steady-state long tube cold side U-tube outside wall-to-secondary fluid temperature differences versus elevation above the top of the tube sheet for FWLB experiments S-FS-6B, S-FS-11, and S-FS-7 ..... C-11

C-8. Affected loop steam generator full-power, steady-state short tube hot side U-tube outside wall-to-secondary fluid temperature differences versus elevation above the top of the tube sheet for FWLB experiments S-FS-6B, S-FS-11, and S-FS-7 ..... C-12

C-9. Affected loop steam generator full-power, steady-state short tube cold side U-tube outside wall-to-secondary fluid temperature differences versus elevation above the top of the tube sheet for FWLB experiments S-FS-6B, S-FS-11, and S-FS-7 ..... C-12

C-10. Affected loop steam generator average full-power, steady-state tube-bundle region secondary cross-sectional average vapor-void fractions versus elevation above the top of the tube sheet for FWLB experiments S-FS-6B, S-FS-11, and S-FS-7 ..... C-13

C-11. Affected loop steam generator average full-power, steady-state tube-bundle region secondary fluid homogeneous and estimated (based on the primary-to-secondary energy addition in a portion of the tube bundle) flow qualities versus elevation above the top of the tube sheet averaged for FWLB experiments S-FS-6B, S-FS-11, and S-FS-7 ..... C-14

C-12. Affected loop steam generator average full-power, steady-state tube-bundle region secondary fluid estimated (based on the estimated flow quality and the measured vapor-void fraction) slip ratio versus elevation above the top of the tube sheet averaged for FWLB experiments S-FS-6B, S FS-11, and S-FS-7 ..... C-14

TABLES

C-1. Measured conditions used for determining correlation predicted secondary heat transfer coefficients for the long tube hot side at several elevations C-15

C-2. Measured and correlation predicted secondary heat-transfer coefficients for the long tube hot side at several elevations C-15

APPENDIX C

STEADY-STATE RESULTS

INTRODUCTION

Understanding and calculating the affected loop steam generator secondary fluid system thermal-hydraulic response to a bottom main feedwater line break requires consideration of the tube-bundle region secondary fluid thermal-hydraulic response. The transient thermal-hydraulic response may be understood more clearly after considering the thermal-hydraulic conditions that exist in the secondary fluid system at steady-state, full-power conditions.

STEADY-STATE SECONDARY THERMAL-HYDRAULIC CHARACTERISTICS

The basic steady-state, full-power secondary fluid thermal-hydraulics consist of complex two-phase natural circulation flow and forced convection heat transfer mechanisms. The secondary fluid two-phase natural circulation is driven by liquid head difference between the downcomer and the tube bundle, the boiling in the tube-bundle region, addition of subcooled liquid in the lower downcomer, and extraction of steam in the steam dome. The intercomponent flow consists of two-phase flow in the tube-bundle region, with separated steam exiting the steam dome and liquid being recirculated down the downcomer. Subcooled liquid is added in the lower downcomer to replace the mass of steam removed in the steam dome. The downcomer downflow (about 0.82 kg/s), tube bundle upflow (about 1.09 kg/s), and steam and feedwater flows (about 0.27 kg/s each), result in a mass balance for all of the secondary components. The secondary fluid thermal characteristics consist of: feedwater entering the lower downcomer and producing slightly subcooled liquid at the entrance to the tube bundle; forced convection nucleate boiling heat transfer in the tube-bundle region; two-phase mixture exiting the tube bundle; and, vapor generated in the tube-bundle region exiting the steam generator as high quality steam. The energy addition from the primary fluid system, removal of feedwater subcooling (Figure C-1), boiling in the tube bundle, and high quality steam flow out of the secondary result in an energy balance for the secondary fluid system.

The local heat flux and secondary heat transfer coefficients were determined from the measured tube volumetric flow rate, primary fluid pressure and temperature, tube outside wall temperature, and secondary fluid temperature. For the case of steady-state heat transfer, a simple energy balance for the tube inner and outer surfaces results in two equations and three unknowns. A correlation such as Dittus-Boelter or Colburn can be used in conjunction with the measured tube fluid properties and flow rate to obtain the primary fluid convective heat transfer coefficient. The two equations can then be solved for the two remaining unknowns. However, to allow for accurate calculations of transient heat transfer a calculation technique that includes energy storage terms was necessary. The technique used[C-1] involves a one-dimensional finite difference numerical scheme applicable to a slab, cylinder or sphere.

The tube wall is modeled as a series of finite difference nodes with a finite volume surrounding each node. The integral conservation of heat equation is applied to a general shaped one-dimensional solid. Separate energy balances are performed for the portion of the volume element to the left and right of an interior node with: no volumetric heat generation, the heat flux vector approximated by Fourier's law of heat conduction, and a backward difference approximation used for time. The energy balances are then combined to get the conservation of energy equation for the volume element. The resulting conservation equation for the interior volume element is then rearranged resulting in an equation with the current values of three nodal temperatures T_{i-1}, T_i, and T_{i+1} unknown and the associated current value of the thermal conductivities and volumetric heat capacities between the nodes unknown. Modeling the wall with N nodes, N-2 equations can be written for the interior nodes with, neglecting for now the temperature dependency of the thermal conductivities and volumetric heat capacities, N-1 unknowns (the temperature at node N is measured). For the left hand boundary at node 1, an energy balance for the volume element to the right of the node is again performed with the conduction at the left boundary equated to the primary convective heat transfer. This produces a total of N-1 equations and N unknowns. For the right hand boundary at node N, an energy balance for the volume element to the left of the node is performed with the conduction at the right boundary equated to the secondary convective heat transfer. This yields N equations and N + 1 unknowns. Now, using the Dittus-Boelter and Colburn correlations to determine the primary convective heat transfer coefficient will result in N equations with N unknowns (T_1, T_2, . . . , T_{n-1}, h_{sf}), where T_1 through T_{n-1} is the current value of the temperature at nodes 1 through N-1, and h_{sf} is the secondary convective heat transfer coefficient.

The solution technique involves using iteration on the primary convective heat transfer coefficient and the current thermal conductivities and volumetric heat capacities, with Gaussian elimination solution of the set of N equations. A simple steady-state energy balance technique is used to determine the value of the unknowns for the first few steady-state data points.

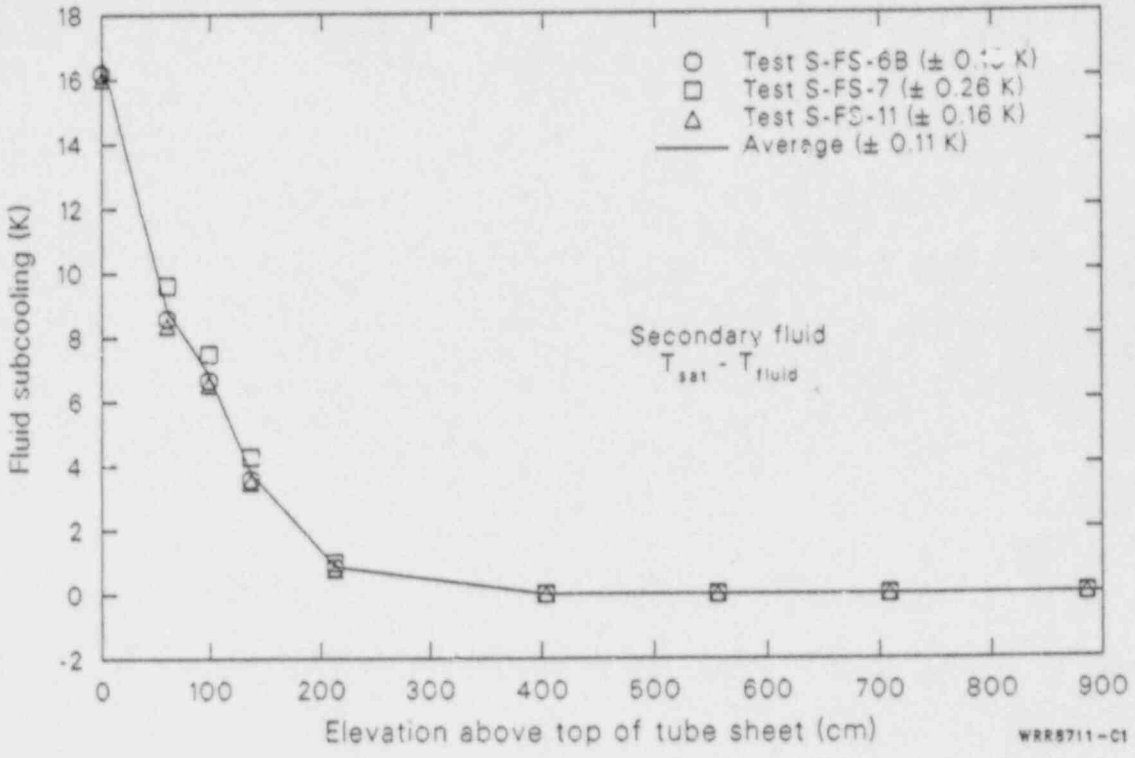

Figure C-1. Affected loop steam generator average full-power, steady- state secondary fluid subcooled margin versus elevation above the top of the tube sheet for FWLB experiments S-FS-6B, S-FS-11, and S-FS-7.

The thermal conductivity and volumetric heat capacity current values are initially set to the value from the previous time step. The primary convective heat transfer coefficient is initially calculated using the Dittus-Boelter correlation. The unknown temperatures and h_{sf} are solved for using Gaussian elimination and the inside wall and primary fluid temperatures are averaged to determine a film temperature. The film temperature is then used with the Colburn correlation to determine a new primary convective heat transfer coefficient, and a new inside wall temperature. The iteration on h_{sf} continues until the calculated inside wall temperature is changing by less than 0.02 K (an order of magnitude less than the differential temperature measurement uncertainty). The program then calculates the outside wall heat flux and uses the new calculated temperatures to determine new current thermal conductivities and volumetric heat capacities. New nodal temperatures are then calculated with iteration on h_{pf}. A new outside wall heat flux is then calculated and compared to the old value. The procedure is repeated until the calculated outside wall heat flux is changing by less than one-tenth of one percent. The calculated temperatures, h_{pf}, h_{sf}, the inside and outside wall heat fluxes and the current thermal conductivity and volumetric heat capacity values are saved and the calculation for the next time step is initiated.

During steady-state, full-power operating conditions, there is a dependency of local heat flux, secondary convective heat transfer coefficient, void fraction, and flow quality on the location in the tube bundle. The Semiscale Type III affected loop steam generator accurately simulates the operating conditions of inverted U-tube steam generators. Therefore, the measured distributions are an invaluable indicator of the accuracy of current analytical methods of predicting local heat transfer and fluid property conditions in an inverted U-tube steam generator tube bundle at steady-state, full-power operating conditions. The steady-state, full-power local heat flux distributions are discussed first. This is followed by a discussion of the steady-state, full-power secondary convective heat transfer coefficient distribution, along with the void fraction, flow quality, and slip-ratio distributions.

The tube outside wall local heat flux was determined for each measurement location in the tube bundle. The average steady-state, full-power local heat flux was then obtained for each location by averaging the data over the steady-state, full-power

operating time span. This procedure was performed for all three sets of data (Experiments S-FS-6B, S-FS-11, and S-FS-7). The average heat fluxes were then plotted versus their location along the tube (from inlet to outlet plenum) for both the long and the short tube. As shown in Figure C-2, the three sets of data are in excellent agreement. Significant variation in the local heat flux with location along the tube is apparent for both tubes. Comparisons of the long and short tube heat flux averaged distributions shows similar trends for both tubes. The lower heat flux values observed for the long tube are caused by less flow through the long tube because of its greater hydraulic flow resistance.

Some measure of the accuracy of the calculated heat fluxes can be obtained by integrating the heat flux per unit length of tube over the length of the tube (Figure C-3). The sum of the long and short tube integrated heat flux per unit length should equal the steam generator steady-state full-power operating load. The integrated heat flux per unit length for the long and short tube was found to be 531 ± 15 kW. The average steam generator steady-state, full-power operating load was 533 ± 25 kW. Thus, the integrated local heat flux per unit length is in excellent agreement with the full-power operating load.

The average steady-state, full-power local secondary heat transfer coefficients were obtained for each measurement location, for each experiment, in the same manner as the local heat fluxes. The average secondary heat transfer coefficients for both tubes were then plotted versus their elevation above the top of the tube sheet (Figures C-4 and C-5). For the most part, the three sets of data are in excellent agreement. Significant variation in the local secondary heat transfer coefficient with both elevation and U-tube outside wall-to-secondary fluid temperature difference (Figures C-6 through C-9) is apparent for both tubes. Comparisons of the long and short tube hot and cold side secondary heat transfer coefficient averaged distributions show, with the exception of the long tube hot side 556 cm elevation data point, similar trends for both tubes. The reduction in the secondary heat transfer coefficient at the long tube hot side 886 cm elevation is due to the increased flow area (reduced mass flux) at this elevation. While the reduced heat transfer coefficient at the long tube hot side 556 cm elevation to be an anomoly, the repeatability of the data supports its validity. Insight into the probable cause of the local heat transfer coefficient reduction may be gained from a consideration of the local fluid hydraulic characteristics.

Some insight into the phenomena driving the measured distributions can be obtained by observing the measured cross-sectional average void distribution. The average steady-state, full-power cross-sectional average vapor-void fractions were obtained for each density measurement location, for each experiment, in the same manner as the local heat fluxes. The average void fractions versus their elevation above the top of the tube sheet were plotted. As shown in Figure C-10, the three sets of data are in excellent agreement. As expected, significant variation in the vapor-void fraction with elevation is apparent. The inflection point observed at the 564 cm elevation is believed to be caused by a flow regime transition occurring near the 564 cm elevation.

Further insight into the phenomena driving the measured distributions can be obtained by observing the estimated and homogeneous flow quality distributions. The estimated flow quality was obtained at elevations corresponding to the void measurement elevations by integrating the heat flux per unit length of tube over the length of tube contained between the elevations, and determining the amount of steam generation that would result from the total amount of energy added to that portion of the tube bundle. The homogeneous flow quality was obtained from the measured void fraction. The estimated and homogeneous flow qualities were then plotted versus their elevation above the top of the tube sheet. Comparisons of the flow qualities (Figure C-11) show reasonable agreement between the estimated and the homogeneous flow qualities up to the 556 cm measurement elevation. Above the 556 cm elevation, the homogeneous flow quality deviates significantly from the estimated flow quality. The observed differences in the flow qualities indicates that the liquid and vapor velocities differ throughout the majority of the tube bundle with slip ratios as shown in Figure C-12. The onset of boiling is calculated to occur at approximately the 150 cm elevation. Below this elevation the slip ratio is, by definition, 1.0. At higher elevations the slip ratio shows a fairly constant trend up to the 556 cm elevation. The reduction in the slip ratio at this elevation is believed to be caused by flow perturbation or possibly a transition to a new flow regime. Above the 556 cm elevation the slip ratio increases with increasing elevation up to the elevation of the top of the long tube. Above the top tube, the flow conditions remain essentially constant. The maximum slip ratio (approximately 1.6) occurs at about the elevation of the top of the long tube. This information should prove to be

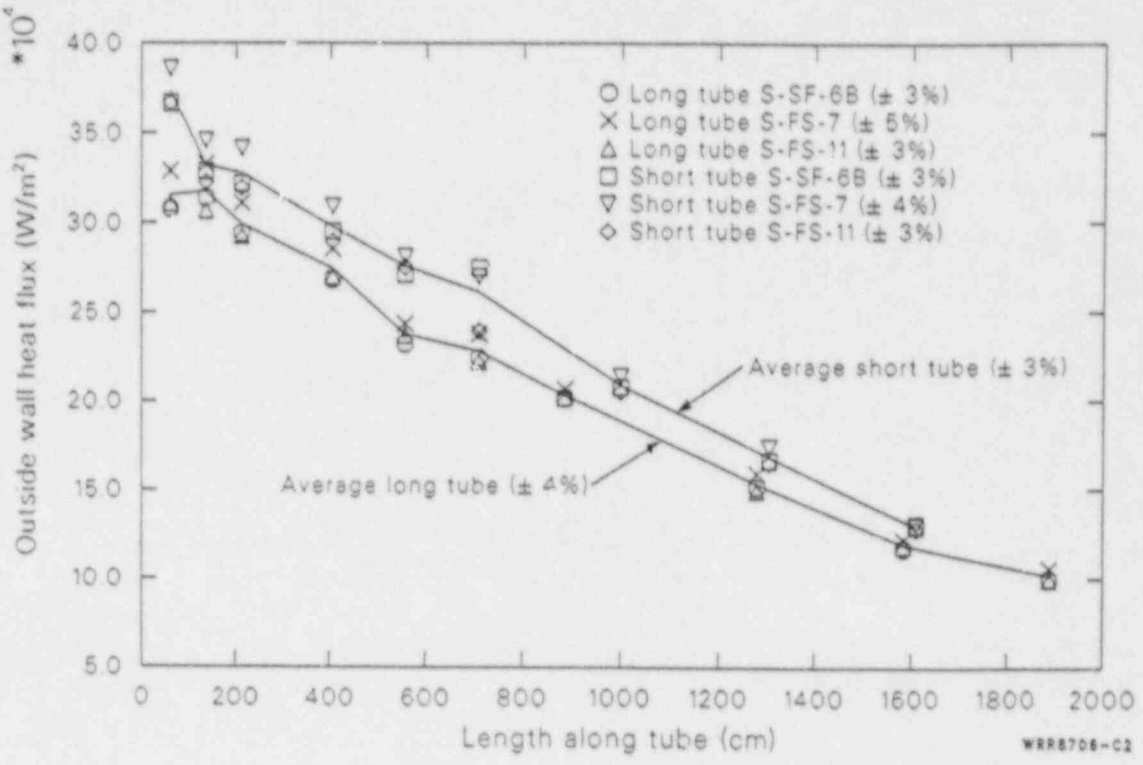

Figure C-2. Affected loop steam generator average full-power, steady-state U-tube outside wall heat fluxes versus length along the tube (from inlet to outlet plenum) for the long and short tubes for FWLB experiments S-FS-6B, S-FS-11, and S-FS-7.

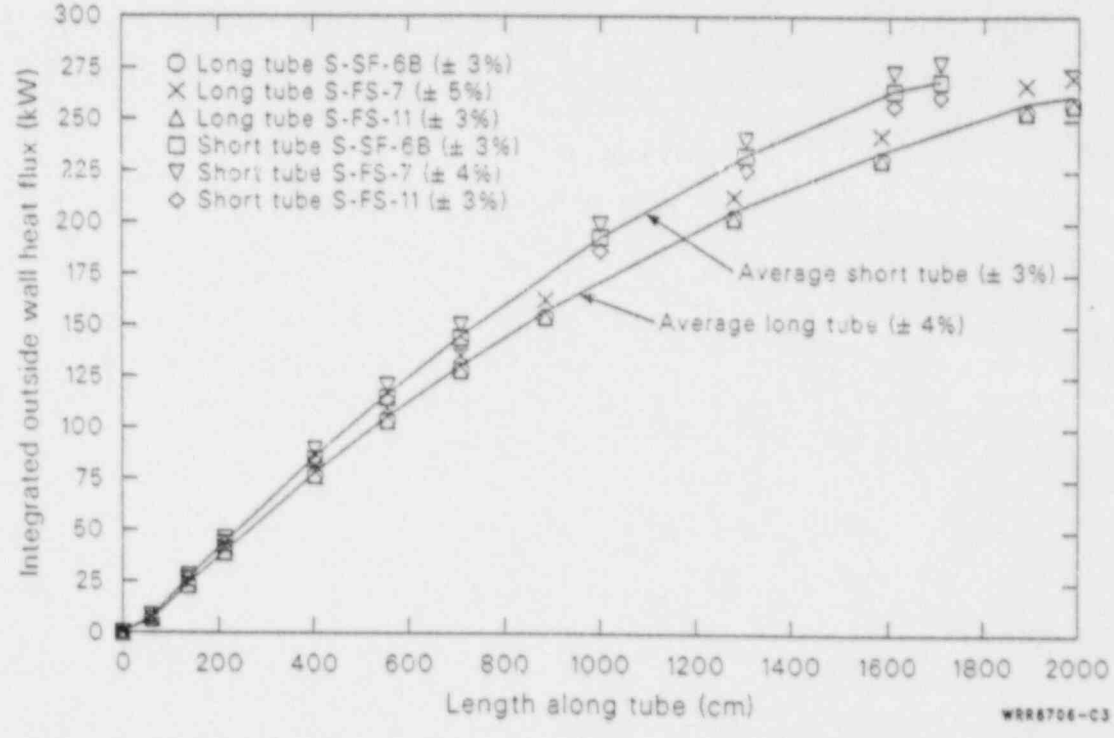

Figure C-3. Affected loop steam generator average full-power, steady-state U-tube outside wall integrated heat fluxes versus length along the tube (inlet to outlet plenum) for the long and short tubes for FWLB experiments S-FS-6B, S-FS-11, and S-FS-7.

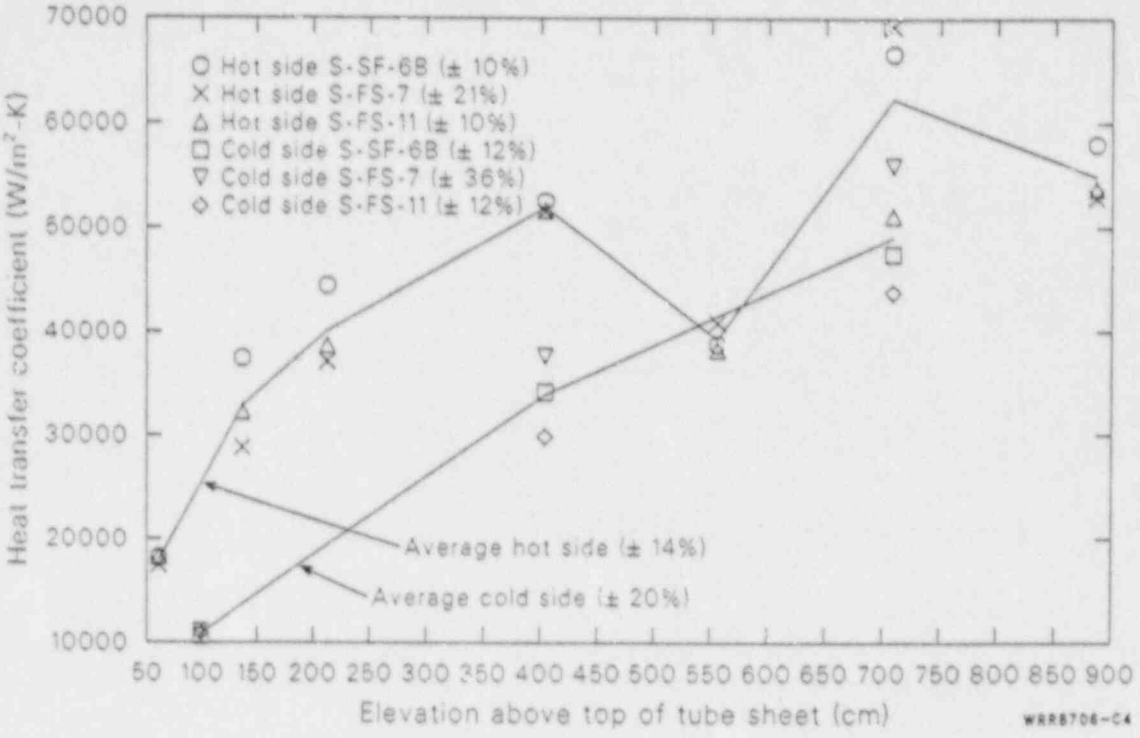

Figure C-4. Affected loop steam generator average full-power, steady-state long tube hot and cold side secondary convective heat transfer coefficients versus elevation above the top of the tube sheet for FWLB experiments S-FS-6B, S-FS-11, and S-FS-7.

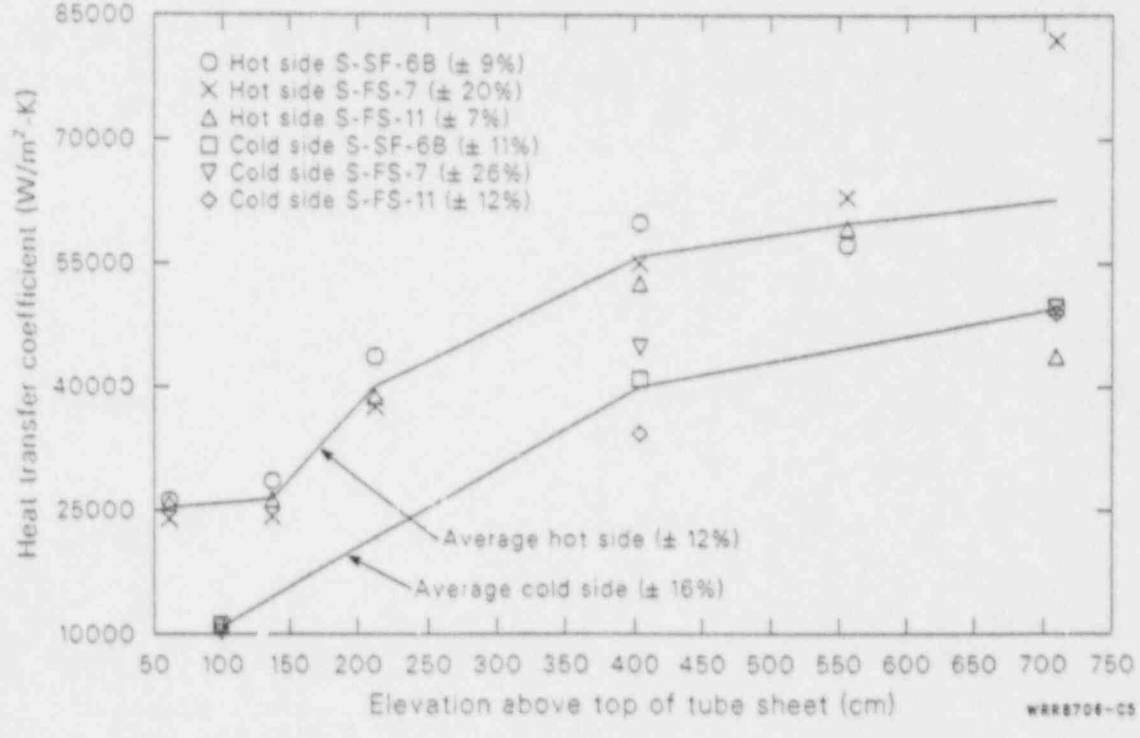

Figure C-5. Affected loop steam generator average full-power, steady-state short tube hot and cold side secondary convective heat transfer coefficients versus elevation above the top of the tube sheet for FWLB experiments S-FS-6B, S-FS-11, and S-FS-7.

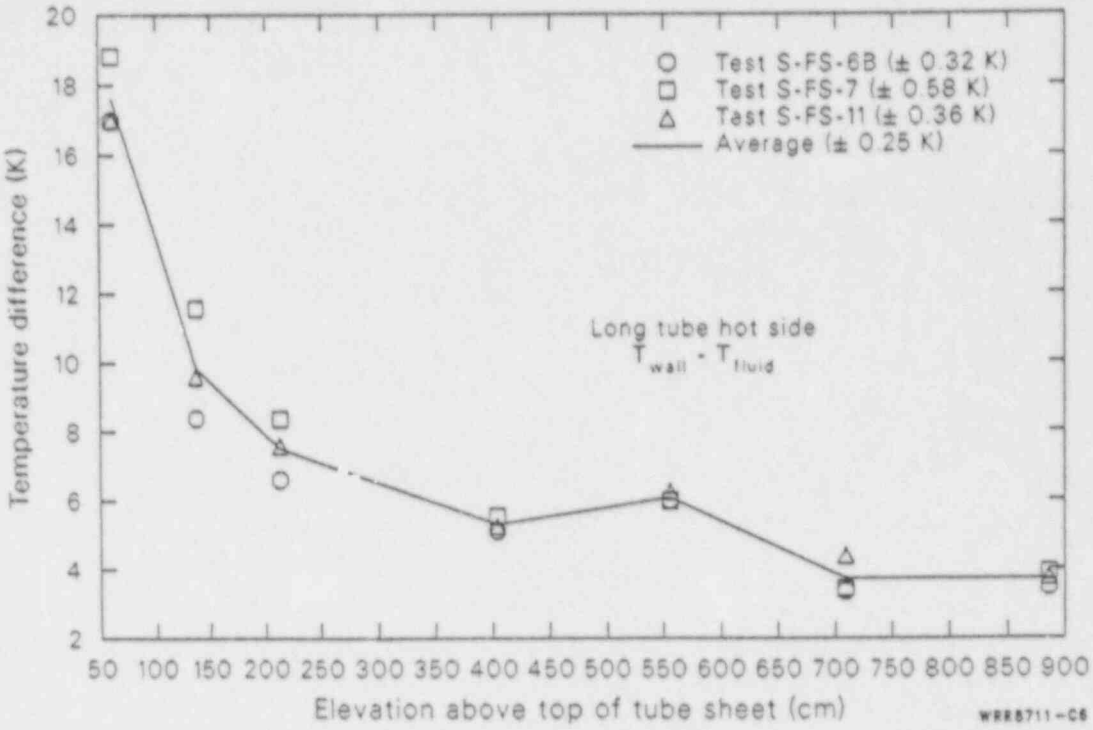

Figure C-6. Affected loop steam generator full-power, steady-state long tube hot side U-tube outside wall-to-secondary fluid temperature differences versus elevation above the top of the tube sheet for FWLB experiments S-FS-6B, S-FS-11, and S-FS-7.

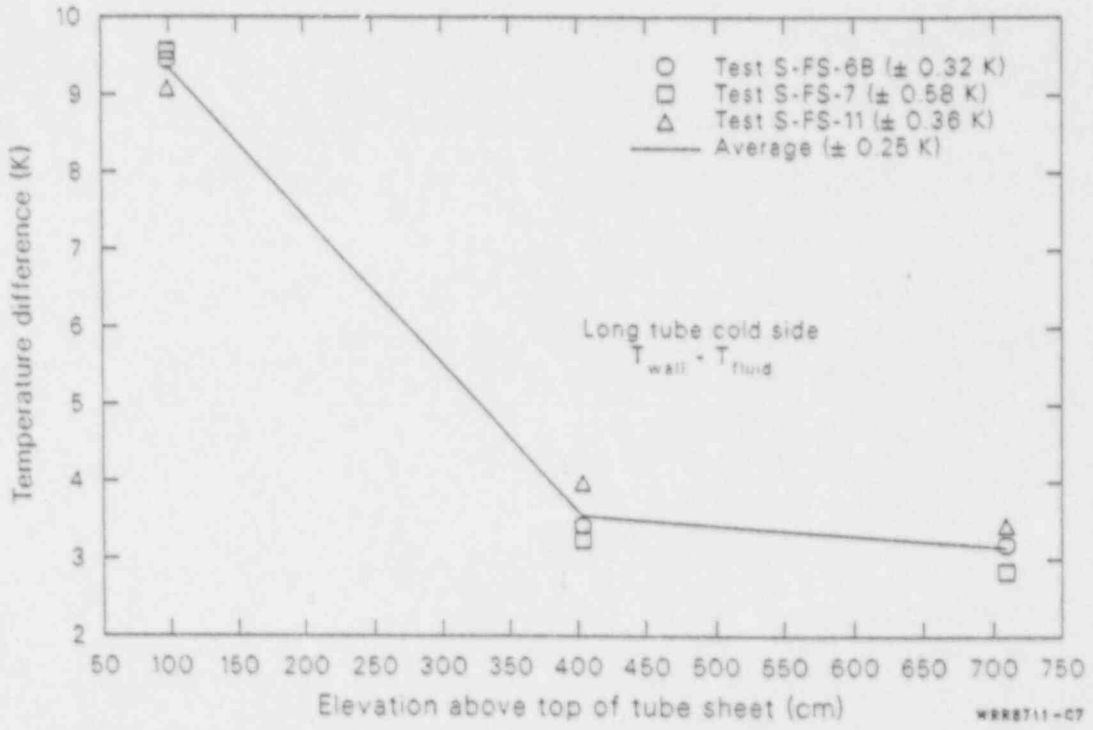

Figure C-7. Affected loop steam generator full-power, steady-state long tube cold side U-tube outside wall-to-secondary fluid temperature differences versus elevation above the top of the tube sheet for FWLB experiments S-FS-6B, S-FS-11, and S-FS-7.

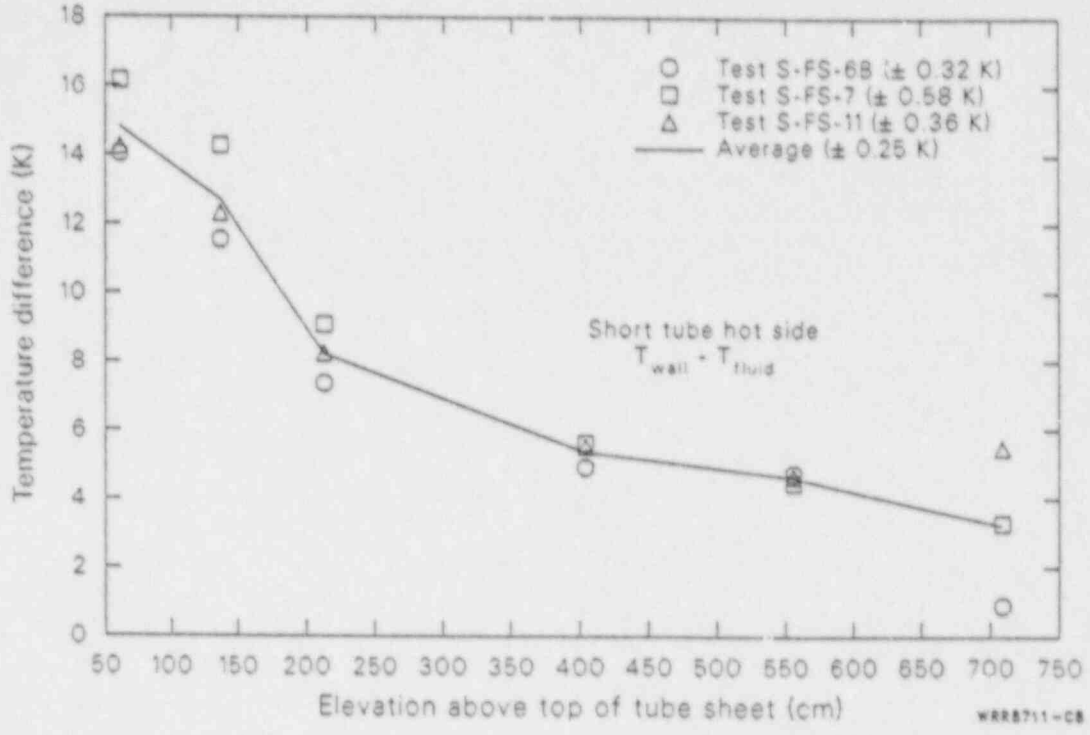

Figure C-8. Affected loop steam generator full-power, steady-state short tube hot side U-tube outside wall-to-secondary fluid temperature differences versus elevation above the top of the tube sheet for FWLB experiments S-FS-6B, S-FS-11, and S-FS-7.

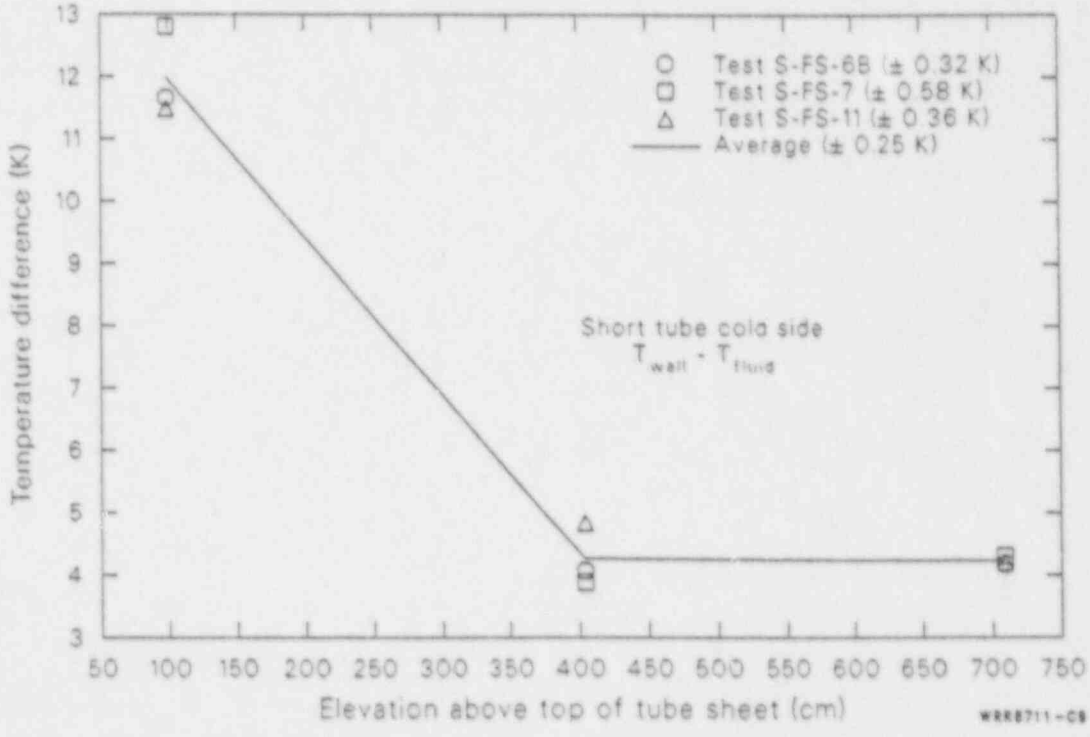

Figure C-9. Affected loop steam generator full-power, steady-state short tube cold side U-tube outside wall-to-secondary fluid temperature differences versus elevation above the top of the tube sheet for FWLB experiments S-FS-6B, S-FS-11, and S-FS-7.

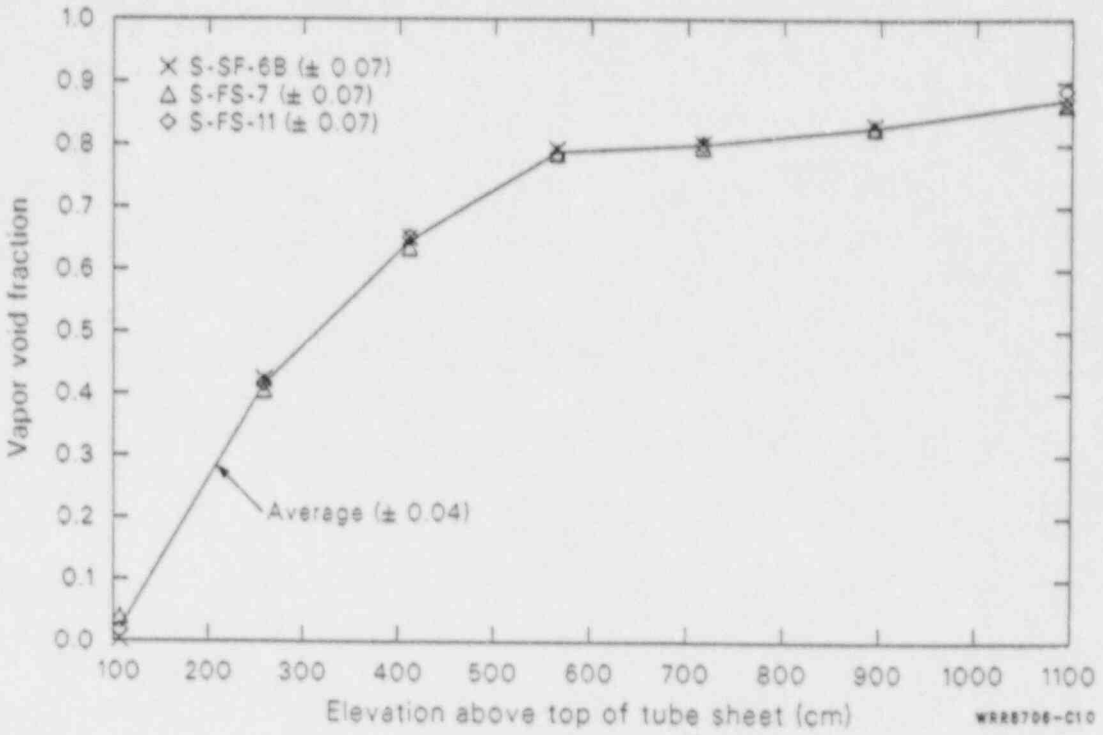

Figure C-10. Affected loop steam generator average full-power, steady-state tube-bundle region secondary cross-sectional average vapor-void fractions versus elevation above the top of the tube sheet for FWLB experiments S-FS-6B, S-FS-11, and S-FS-7.

invaluable for analyzing analytical calculations of this data.

The fluid hydraulic characteristics provide a valuable clue to the possible cause of the reduced local secondary convective heat transfer coefficient for the long tube hot side at the 556 cm elevation. The cross-sectional average void fraction, estimated, and homogeneous flow quality, and slip ratio distributions indicates that a flow perturbation or possibly a flow regime transition occurs near the 556 cm elevation. This may result in multidimensional effects wherein the local flow at the long tube hot side measurement station is significantly decreased while the local flow at the short tube hot side measurement station is not. Such a condition would result in a reduced local secondary convective heat transfer coefficient for the long tube hot side measurement station, but not for the short tube hot side measurement station.

The nature of the secondary convective heat transfer coefficient profile indicates the existence of forced convection nucleate boiling as well as forced convection vaporization heat transfer as discussed in References C-2 and C-3. A brief comparison was made of the measured secondary heat transfer coefficients at several elevations for the long tube hot side to those predicted (for the measured conditions listed in Table C-1) by the Thom[C-4] forced convection nucleate boiling heat transfer correlation, the Bennett[C-2] forced convection vaporization heat transfer correlation and the Chen[C-3] combined nucleate boiling/vaporization forced convection heat transfer correlation currently used in thermal-hydraulic computer codes. This comparison (Table C-2) points out that the Thom and Chen correlations predict the wrong trends in the heat transfer coefficient distribution. The Semiscale Type III steam generator measured local secondary convective heat transfer coefficient dependency on the local vapor-void fraction exhibits a trend that is exactly the opposite of that predicted by the Thom and Chen boiling heat transfer correlations. This is believed to be due to the fact that these correlations were developed based on data for flow inside a single heated tube, not for flow around internally heated tube bundles. Inside of an externally heated tube, increasing vapor-void fractions can result in the vapor *blanketing* the tube inside wall, limiting the area for liquid to wall contact, and reducing the liquid cooling effect, thereby reducing the convective heat transfer coefficient, as predicted by the existing correlations. Outside of an

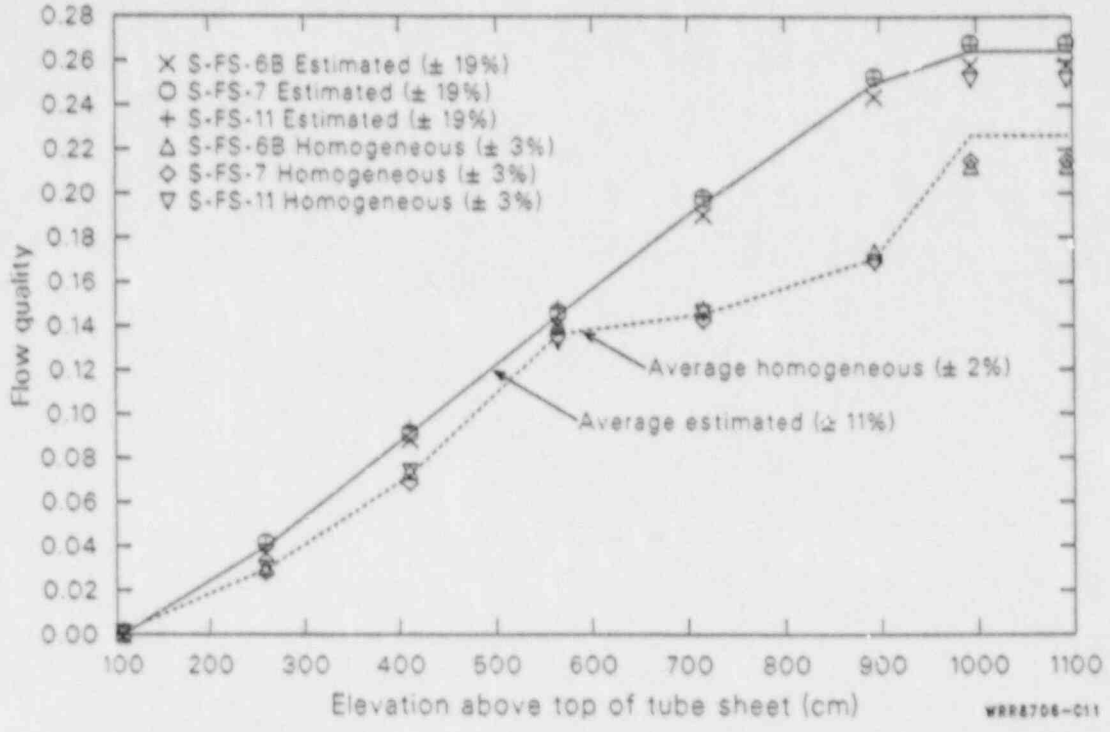

Figure C-11. Affected loop steam generator average full-power, steady-state tube-bundle region secondary fluid homogeneous and estimated (based on the primary-to-secondary energy addition in a portion of the tube bundle) flow qualities versus elevation above the top of the tube sheet averaged for FWLB experiments S-FS-6B, S-FS-11, and S-FS-7.

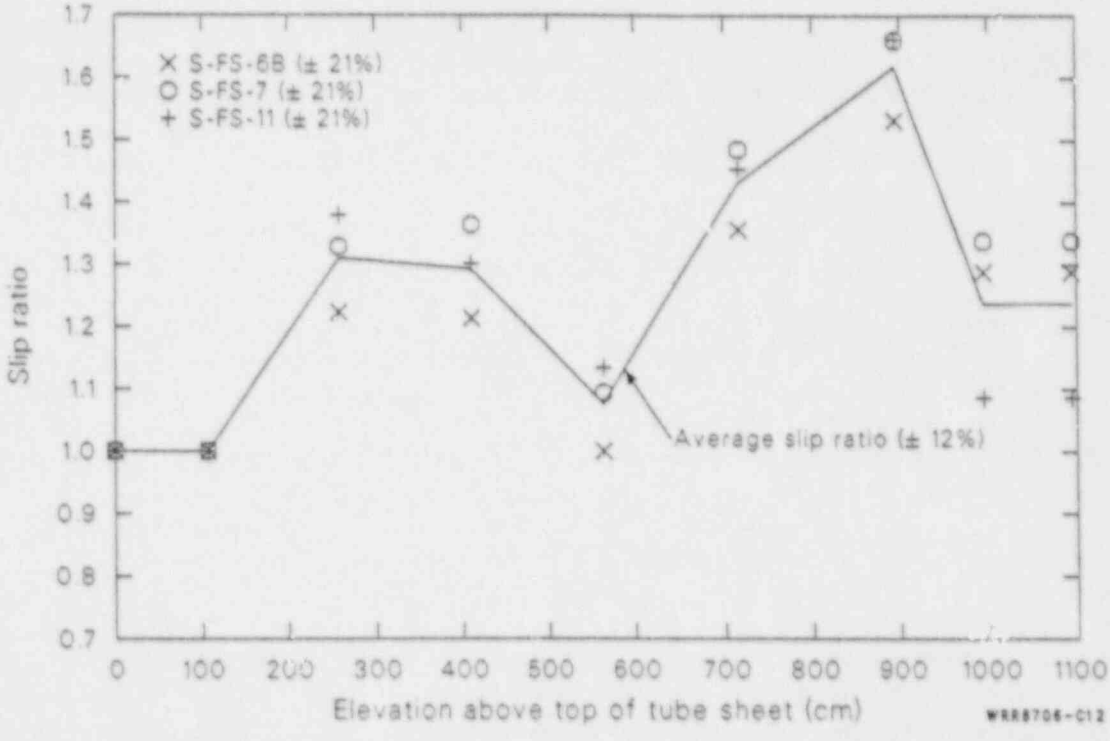

Figure C-12. Affected loop steam generator average full-power, steady-state tube-bundle region secondary fluid estimated (based on the estimated flow quality and the measured vapor-void fraction) slip ratio versus elevation above the top of the tube sheet averaged for FWLB experiments S-FS-6B, S-FS-11, and S-FS-7.

Table C-1. Measured conditions used for determining correlation predicted secondary heat transfer coefficients for the long tube hot side at several elevations

Elevation (cm)	Heated Diameter (m)	Mass Flux (kg/m^2-5)	$T_{Wall} - T_{Sat}$ (K)	$T_{Wall} - T_{Fluid}$ (K)	Vapor Void Fraction	Flow Quality	Saturation Pressure (MPa)	Outside Wall Heat Flux (W/m^2)
61	.043983	356.02	17.60	8.75	0.00	.0000	6.302	315,737
137	.043983	356.02	9.85	6.07	0.02	.0000	6.296	317,795
213	.043983	356.02	7.52	6.66	0.28	.0224	6.291	299,188
404	.043983	356.02	5.29	5.29	0.63	.0921	6.280	274,440
556	.043983	356.02	6.06	6.06	0.78	.1535	6.273	237,530
709	.043983	356.02	3.72	3.72	0.80	.2091	6.267	227,966
886	.111532	280.78	3.71	3.71	0.82	.2676	6.260	203,315

Table C-2. Measured and correlation predicted secondary heat transfer coefficients for the long tube hot side at several elevations

Elevation (cm)	Measured[a] (W/m^2-K)	Thom[a] (W/m^2-K)	Bennet[a] (W/m^2-K)	Chen[a] (W/m^2-K)
61	17,974	40,872	0[b,c]	20,779[c]
137	32,875	28,316	0[b,c]	15,768[c]
213	40,103	31,045	3,693	16,321
404	51,915	24,619	9,293	12,787
556	39,260	28,157	12,738	14,427
709	62,346	17,258	15,443	13,703
886	54,887	17,184	12,218	10,801

a. Secondary heat transfer coefficients.

b. Zero values due to zero flow qualities at these elevations.

c. Flow quality is below the stated range of applicability for this correlation.

internally heated tube bundle, increasing vapor-void fractions can result in turbulent mixing and *pumping* of the liquid to the outside tube wall, resulting in enhanced liquid and vapor cooling effects and increased secondary convective heat transfer coefficients, as measured in the Type III steam generator. The Bennett boiling heat transfer correlation predicts the correct trend in heat transfer coefficient with vapor void fraction. However, the predicted values are significantly smaller than those measured. This is believed to be due to the fact that the Bennett correlation was developed based on data for flow inside an annulus, not for flow around internally heated tube bundles.

REFERENCES

C-1. T. J. Boucher, "Steady-State Heat Transfer in an Inverted U-Tube Steam Generator," *Proceeding of the 1986 ASME Winter Annual Meeting, 86-WA/NE-6, December 7-12, 1986.*

C-2. J. A. R. Bennett, J. G. Collier, A. R. C. Pratt, J. D. Thornton, "Heat Transfer in Two-Phase Gas-Liquid Systems, Part I: Steam Water Mixtures in the Liquid-Dispersed Region in an Annulus," *Trans. Inst. Chem. Eng.* (London), 1961, pg. 39.

C-3. J. C. Chen, "A Correlation for Boiling Heat Transfer to Saturated Fluids in Convective Flow," ASME preprint 63-HT-34, American Society of Mechanical Engineers, 1963.

C-4. M. R. S. Thom, W. M. Walker, T. A. Fallon, G. F. S. Reising, "Boiling in Subcooled Water During Flow in Tubes and Annuli," *Proc. Inst. Mech., Eng.*, 3C18\ , 1966.

APPENDIX D

ADDITIONAL INFORMATIVE DATA

APPENDIX D

ADDITIONAL INFORMATIVE DATA

CONTENTS

FIGURES

D-1. Affected loop steam generator tube-bundle secondary fluid vapor-void fractions during the blowdown phase of 14.3% FWLB experiment S-FS-7 (-10 to 50 s) D-5

D-2. Affected loop steam generator tube-bundle secondary fluid vapor-void fractions during the blowdown phase of 50% FWLB experiment S-FS-11 (-10 to 50 s) D-6

D-3. Affected loop steam generator secondary convective heat transfer coefficients at the 61-cm elevation during the blowdown phase of 14.3% FWLB experiment S-FS-7 (-10 to 50 s) D-6

D-4. Affected loop steam generator secondary convective heat transfer coefficients at the 99-cm elevation during the blowdown phase of 14.3% FWLB experiment S-FS-7 (-10 to 50 s) D-7

D-5. Affected loop steam generator secondary convective heat transfer coefficients at the 137-cm elevation during the blowdown phase of 14.3% FWLB experiment S-FS-7 (-10 to 50 s) D-7

D-6. Affected loop steam generator secondary convective heat transfer coefficients at the 213-cm elevation during the blowdown phase of 14.3% FWLB experiment S-FS-7 (-10 to 50 s) D-8

D-7. Affected loop steam generator secondary convective heat transfer coefficients at the 404-cm elevation during the blowdown phase of 14.3% FWLB experiment S-FS-7 (-10 to 50 s) D-8

D-8. Affected loop steam generator secondary convective heat transfer coefficients at the 556-cm elevation during the blowdown phase of 14.3% FWLB experiment S-FS-7 (-10 to 50 s) D-9

D-9. Affected loop steam generator secondary convective heat transfer coefficients at the 709-cm elevation during the blowdown phase of 14.3% FWLB experiment S-FS-7 (-10 to 50 s) D-9

D-10. Affected loop steam generator secondary convective heat transfer coefficient at the 886-cm elevation during the blowdown phase of 14.3% FWLB experiment S-FS-7 (-10 to 50 s) D-10

D-11. Affected loop steam generator secondary convective heat transfer coefficients at the 61-cm elevation during the blowdown phase of 50% FWLB experiment S-FS-11 (-10 to 50 s) D-10

D-12. Affected loop steam generator secondary convective heat transfer coefficients at the 99-cm elevation during the blowdown phase of 50% FWLB experiment S-FS-11 (-10 to 50 s) D-11

D-13. Affected loop steam generator secondary convective heat transfer coefficients at the 137-cm elevation during the blowdown phase of 50% FWLB experiment S-FS-11 (-10 to 50 s) D-11

D-14. Affected loop steam generator secondary convective heat transfer coefficients at the 213-cm elevation during the blowdown phase of 50% FWLB experiment S-FS-11 (-10 to 50 s) D-12

D-15. Affected loop steam generator secondary convective heat transfer coefficients at the 404-cm elevation during the blowdown phase of 50% FWLB experiment S-FS-11 (-10 to 50 s) D-12

D-16. Affected loop steam generator secondary convective heat transfer coefficients at the 556-cm elevation during the blowdown phase of 50% FWLB experiment S-FS-11 (-10 to 50 s) D-13

D-17. Affected loop steam generator secondary convective heat transfer coefficients at the 709-cm elevation during the blowdown phase of 50% FWLB experiment S-FS-11 (-10 to 50 s) D-13

D-18. Affected loop steam generator secondary convective heat transfer coefficient at the 886-cm elevation during the blowdown phase of 50% FWLB experiment S-FS-11 (-10 to 50 s) D-14

D-19. Unaffected loop steam generator auxiliary feedwater mass flow rate and downcomer and riser overall collapsed liquid levels during the stabilization phase of 14.3% FWLB experiment S-FS-7 (500 to 6000 s) D-14

D-20. Primary hot leg and vessel upper head fluid subcooled margins and pressurizer internal heater power during the stabilization phase of 14.3% FWLB experiment S-FS-7 (500 to 6000 s) D-15

D-21. Pressurizer pressure and overall collapsed liquid level during the stabilization phase of 14.3% FWLB experiment S-FS-7 (500 to 6000 s) D-15

D-22. Unaffected loop steam generator secondary pressure during the stabilization phase of 14.3% FWLB experiment S-FS-7 (500 to 6000 s) D-16

D-23. Affected and unaffected loop hot and cold leg and average primary fluid temperatures during the stabilization phase of 14.3% FWLB experiment S-FS-7 (500 to 6000 s) D-16

D-24. Affected and unaffected loop normal charging mass flow rates during the stabilization phase of 14.3% FWLB experiment S-FS-7 (500 to 6000 s) D-17

D-25. Unaffected loop hot leg, pressurizer surge line inlet and outlet, pressurizer, and pressurizer saturation fluid temperatures during the stabilization phase of 14.3% FWLB experiment S-FS-7(500 to 6000 s) D-17

D-26. Unaffected loop steam generator auxiliary feedwater mass flow rate and downcomer and riser overall collapsed liquid levels during the stabilization phase of 50% FWLB experiment S-FS-11 (600 to 4100 s) D-18

D-27. Primary hot leg and vessel upper head fluid subcooled margins and pressurizer internal heater power during the stabilization phase of 50% FWLB experiment S-FS-11 (600 to 4100 s) D-18

D-28. Pressurizer pressure and overall collapsed liquid level during the stabilization phase of 50% FWLB experiment S-FS-11 (600 to 4100 s) D-19

D-29. Unaffected loop steam generator secondary pressure during the stabilization phase of 50% FWLB experiment S-FS-11 (600 to 4100 s) D-19

D-30. Affected and unaffected loop hot and cold leg and average primary fluid temperatures during the stabilization phase of 50% FWLB experiment S-FS-11 (600 to 4100 s) D-20

D-31. Affected and unaffected loop normal charging mass flow rates during the stabilization phase of 50% FWLB experiment S-FS-11 (600 to 4100 s) D-20

D-32. Unaffected loop hot leg, pressurizer surge line inlet, pressurizer, and pressurizer saturation fluid temperatures during the stabilization phase of 50% FWLB experiment S-FS-11 (600 to 4100 s) D-21

D-33. Affected loop steam generator downcomer and tube bundle overall outlet, collapsed liquid levels and auxiliary feedwater mass flow rate during the voided secondary refill phase of 14.3% FWLB experiment S-FS-7 (6000 to 20,000 s) D-21

D-34. Unaffected loop steam generator downcomer and tube bundle overall collapsed liquid levels and auxiliary feedwater mass flow rate during the voided secondary refill phase of 14.3% FWLB experiment S-FS-7 (6000 to 20,000 s) D-22

D-35. Pressurizer pressure, affected and unaffected loop steam generator secondary pressures, and unaffected loop steam generator atmospheric dump valve mass flow rate during the voided secondary refill phase of 14.3% FWLB experiment S-FS-7 (6000 to 20,000 s) D-22

D-36. Affected and unaffected loop pump speeds, affected and unaffected loop cold leg volumetric flow rates, and affected loop steam generator long and short tube outlet volumetric flow rates during the voided secondary refill phase of 14.3% FWLB experiment S-FS-7 (6000 to 20,000 s) D-23

D-37. Affected and unaffected loop hot and cold leg, and average primary fluid temperatures during the voided secondary refill phase of 14.3% FWLB experiment S-FS-7 (6000 to 20,000 s) D-23

D-38. Pressurizer collapsed liquid level and total normal charging mass flow rate during the voided secondary refill phase of 14.3% FWLB experiment S-FS-7 (6000 to 20,000 s) D-24

D-39. Unaffected loop hot leg fluid subcooled margin and pressurizer internal heater power during the voided secondary refill phase of 14.3% FWLB experiment S-FS-7 (6000 to 20,000 s) D-24

APPENDIX D

ADDITIONAL INFORMATIVE DATA

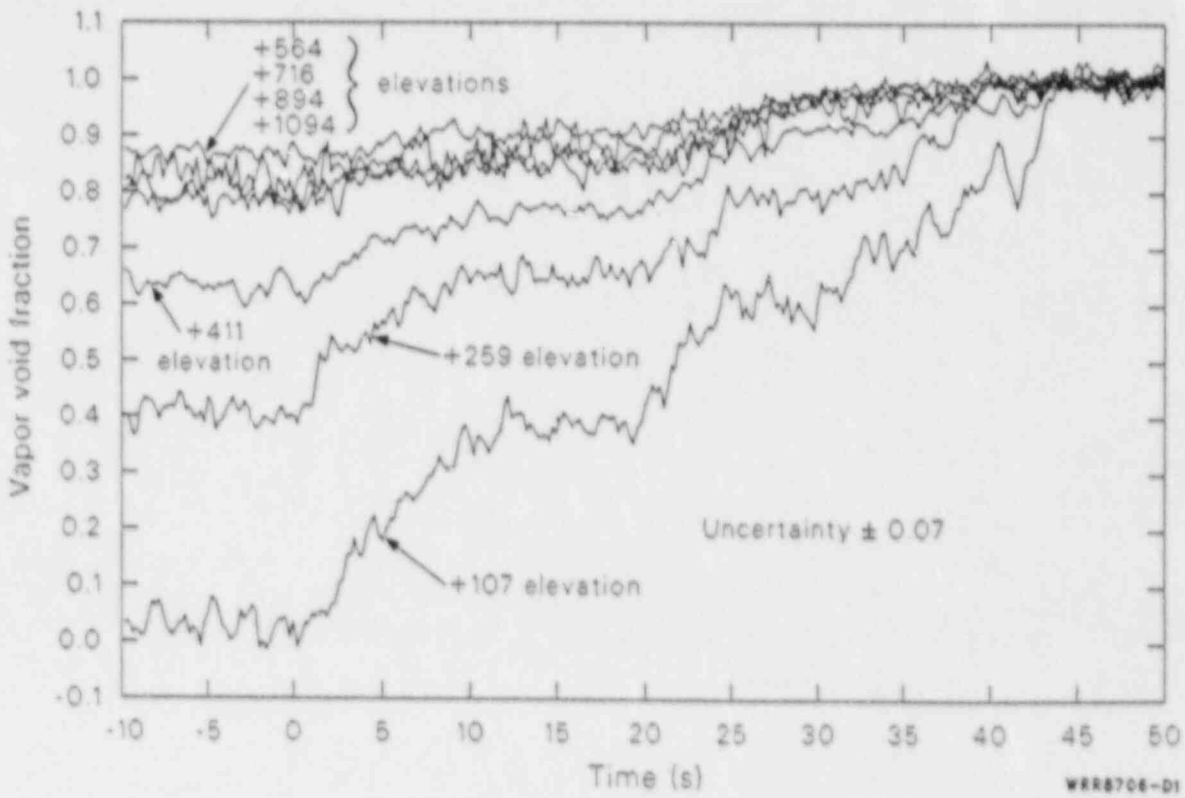

Figure D-1. Affected loop steam generator tube-bundle secondary fluid vapor-void fractions during the blowdown phase of 14.3% FWLB experiment S-FS-7 (-10 to 50 s).

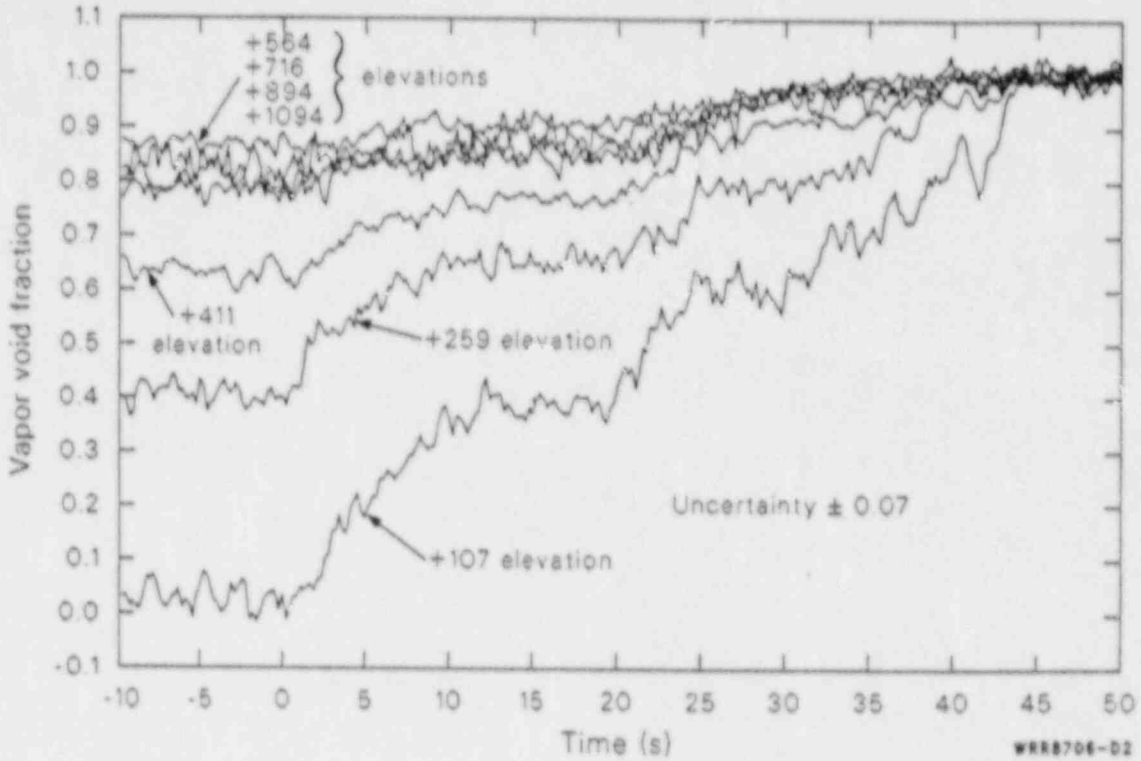

Figure D-2. Affected loop steam generator tube-bundle secondary fluid vapor-void fractions during the blowdown phase of 50% FWLB experiment S-FS-11 (-10 to 50 s).

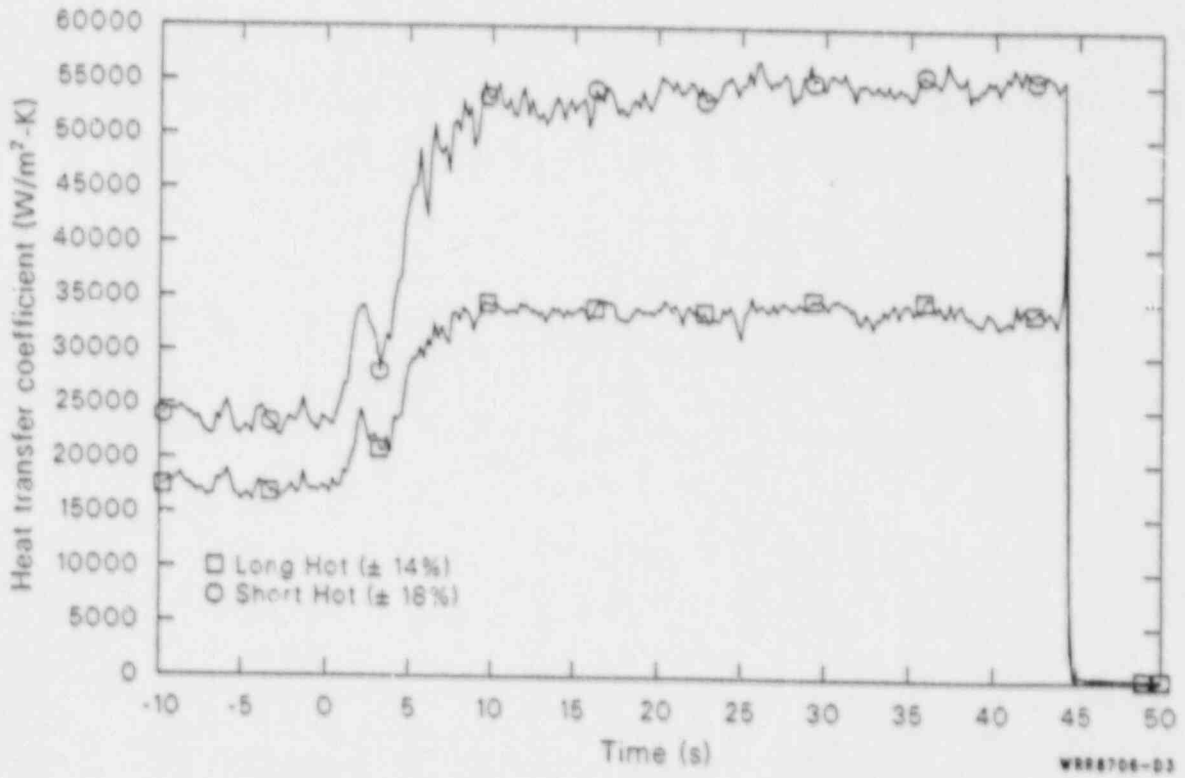

Figure D-3. Affected loop steam generator secondary convective heat transfer coefficients at the 61-cm elevation during the blowdown phase of 14.3% FWLB experiment S-FS-7 (-10 to 50 s).

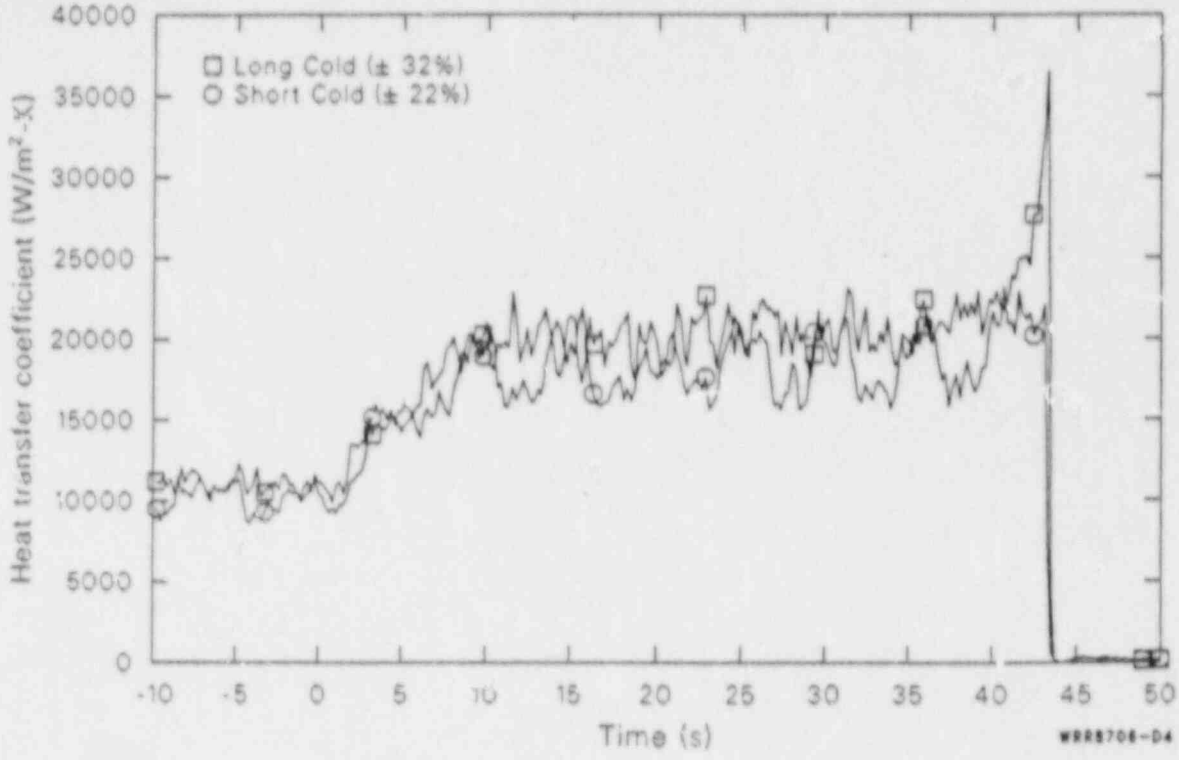

Figure D-4. Affected loop steam generator secondary convective heat transfer coefficients at the 99-cm elevation during the blowdown phase of 14.3% FWLB experiment S-FS-7 (-10 to 50 s).

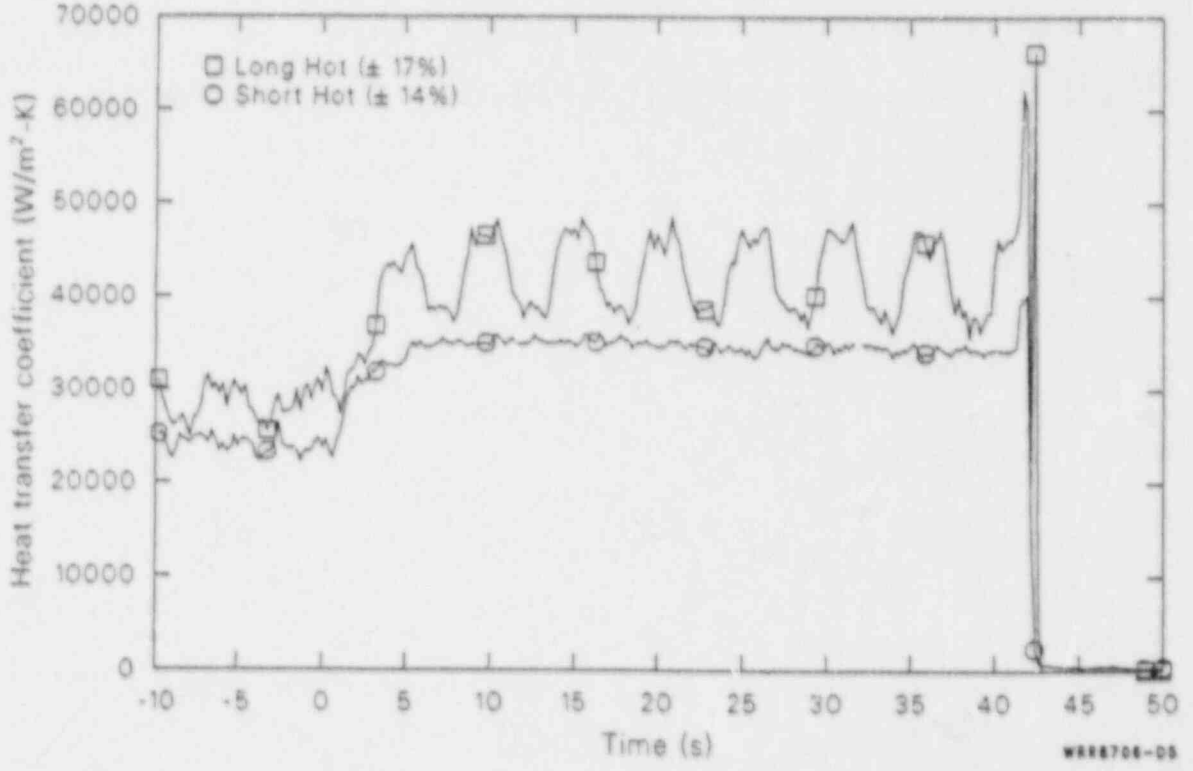

Figure D-5. Affected loop steam generator secondary convective heat transfer coefficients at the 137-cm elevation during the blowdown phase of 14.3% FWLB experiment S-FS-7 (-10 to 50 s).

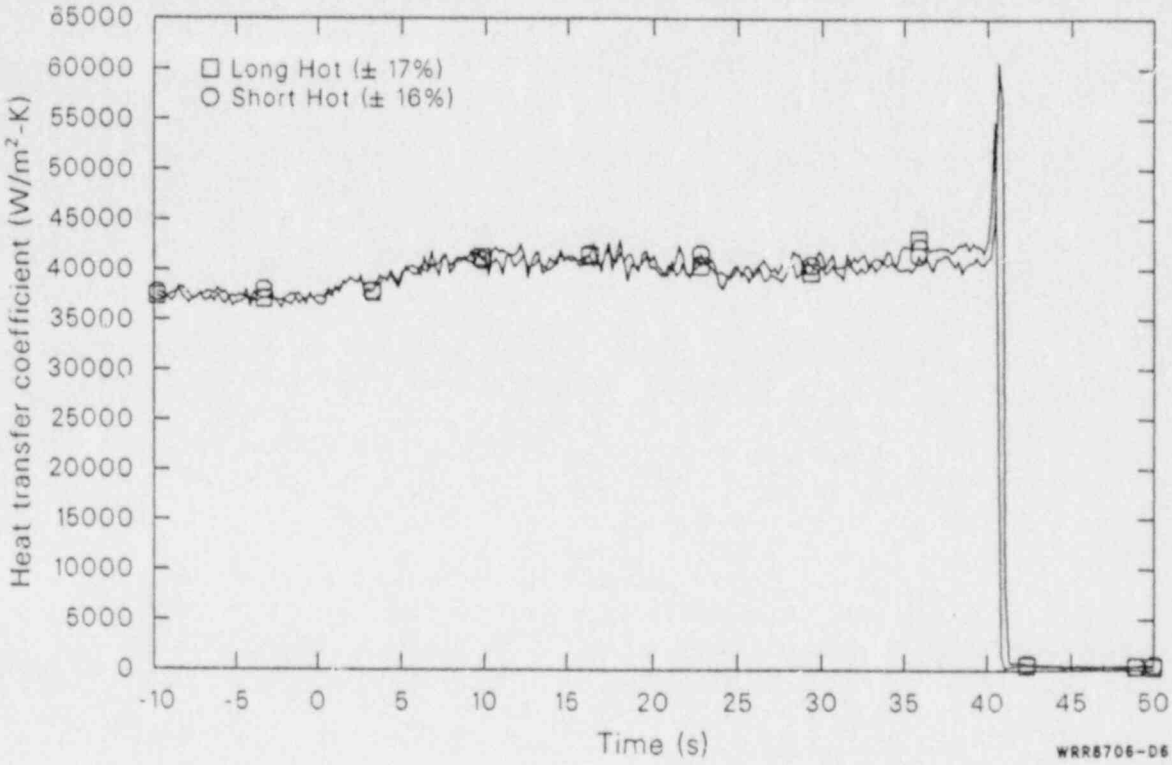

Figure D-6. Affected loop steam generator secondary convective heat transfer coefficients at the 213-cm elevation during the blowdown phase of 14.3% FWLB experiment S-FS-7 (-10 to 50 s).

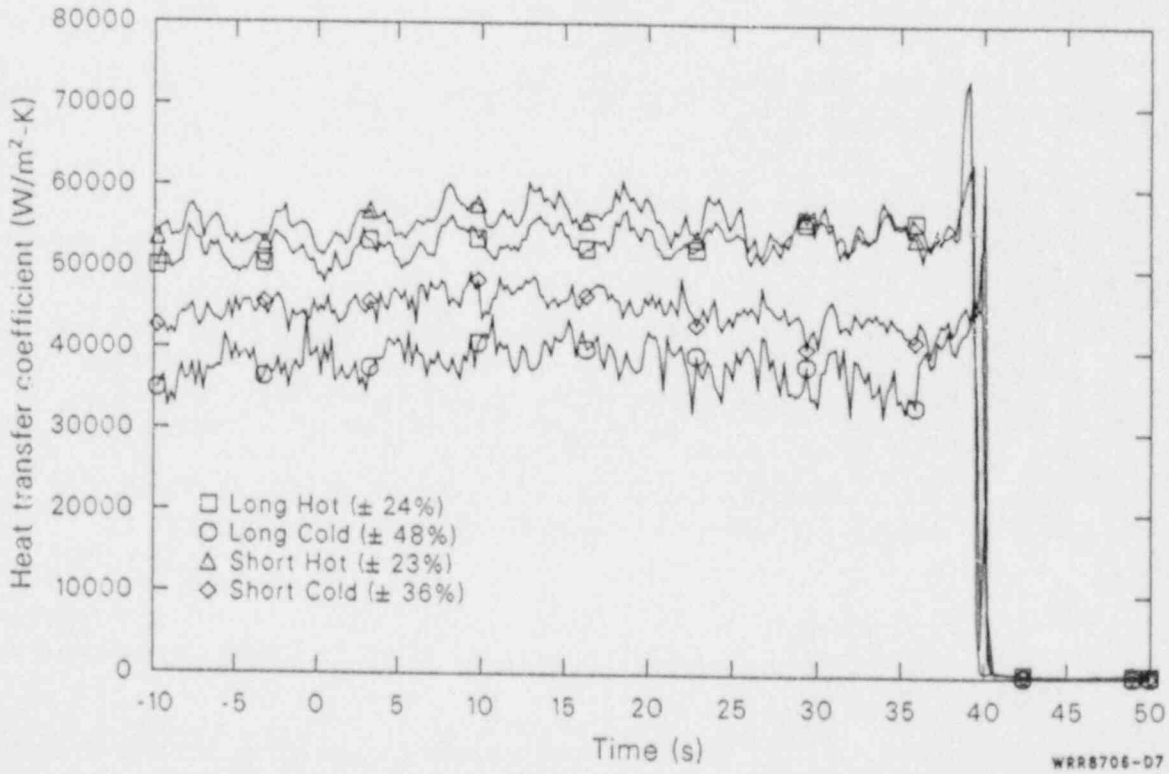

Figure D-7. Affected loop steam generator secondary convective heat transfer coefficients at the 404-cm elevation during the blowdown phase of 14.3% FWLB experiment S-FS-7 (-10 to 50 s).

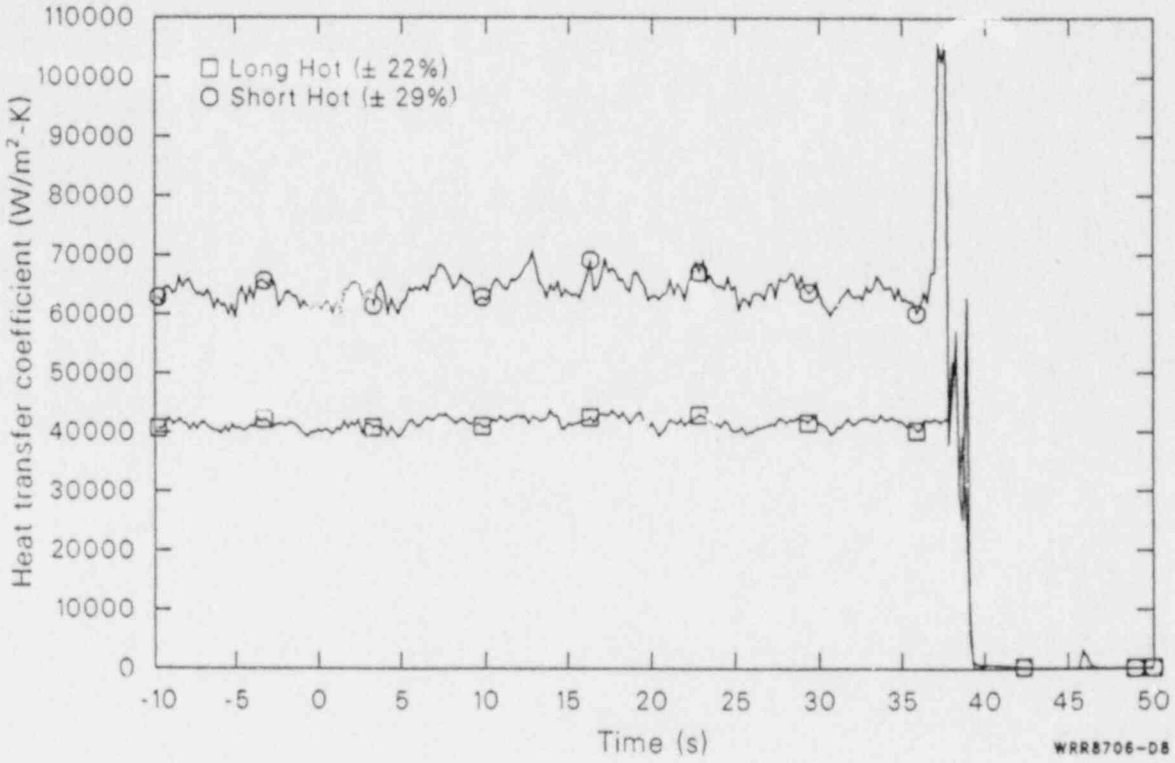

Figure D-8. Affected loop steam generator secondary convective heat transfer coefficients at the 556-cm elevation during the blowdown phase of 14.3% FWLB experiment S-FS-7 (-10 to 50 s).

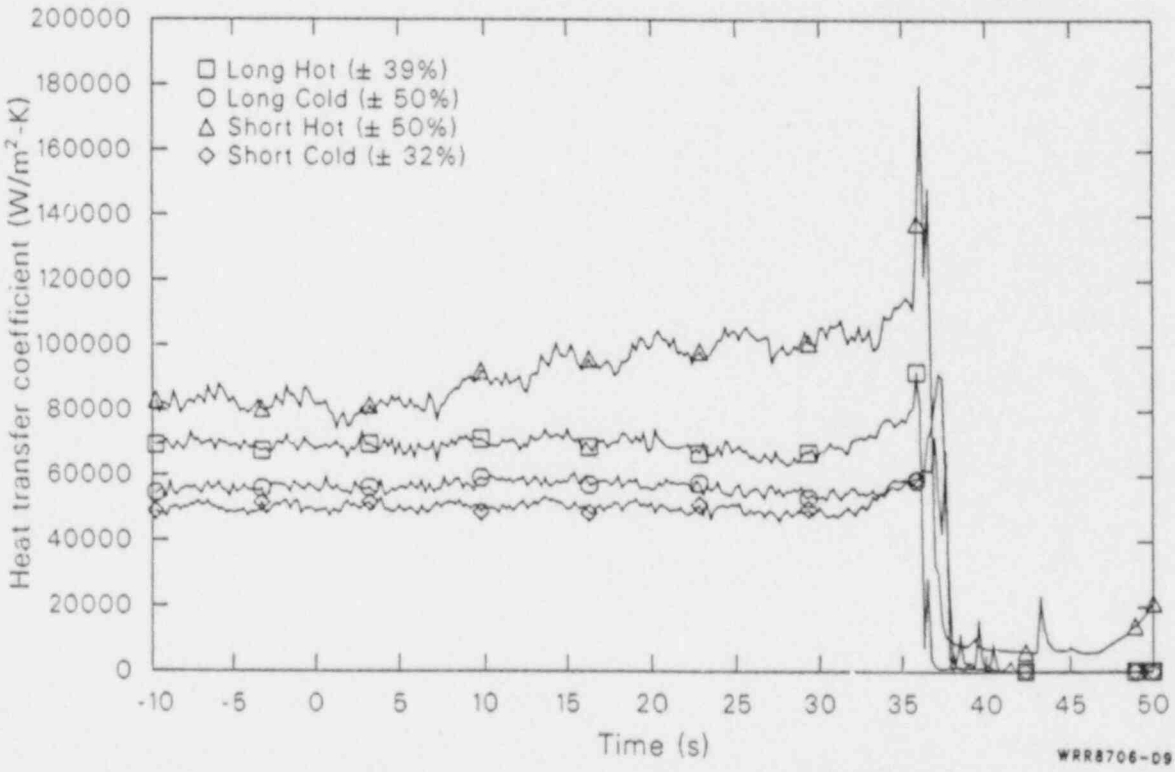

Figure D-9. Affected loop steam generator secondary convective heat transfer coefficients at the 709-cm elevation during the blowdown phase of 14.3% FWLB experiment S-FS-7 (-10 to 50 s).

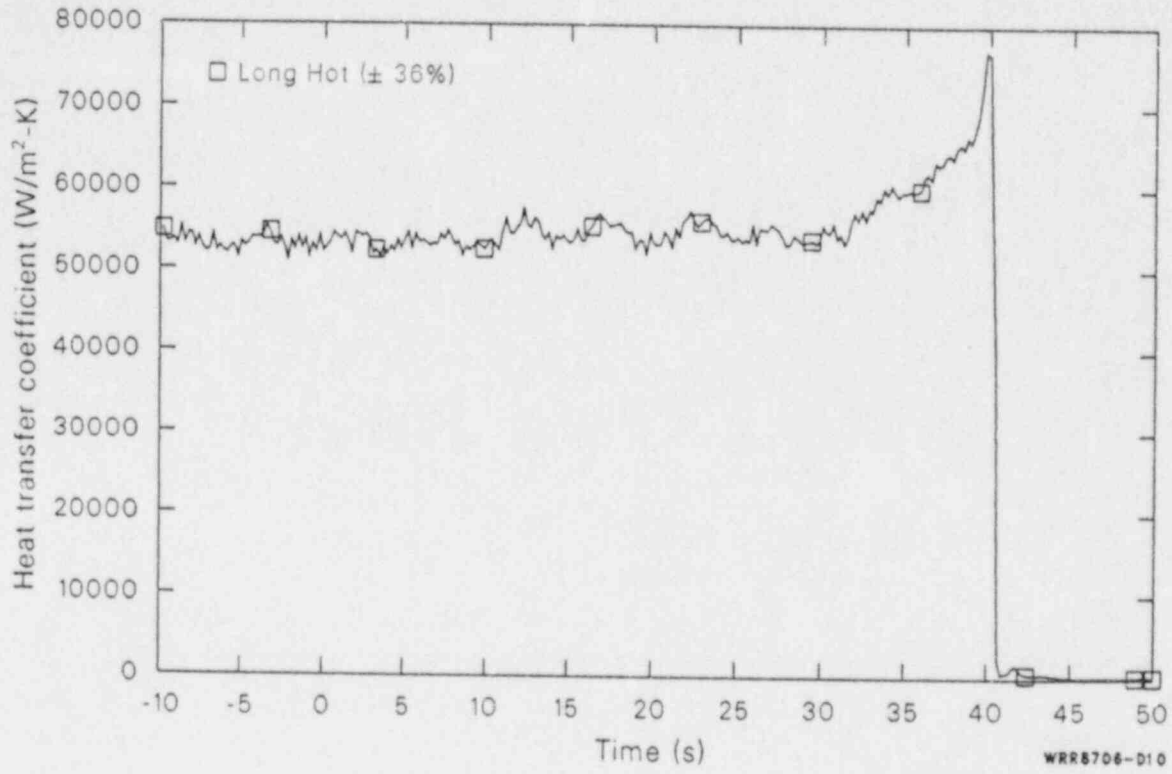

Figure D-10. Affected loop steam generator secondary convective heat transfer coefficient at the 886-cm elevation during the blowdown phase of 14.3% FWLB experiment S-FS-7 (-10 to 50 s).

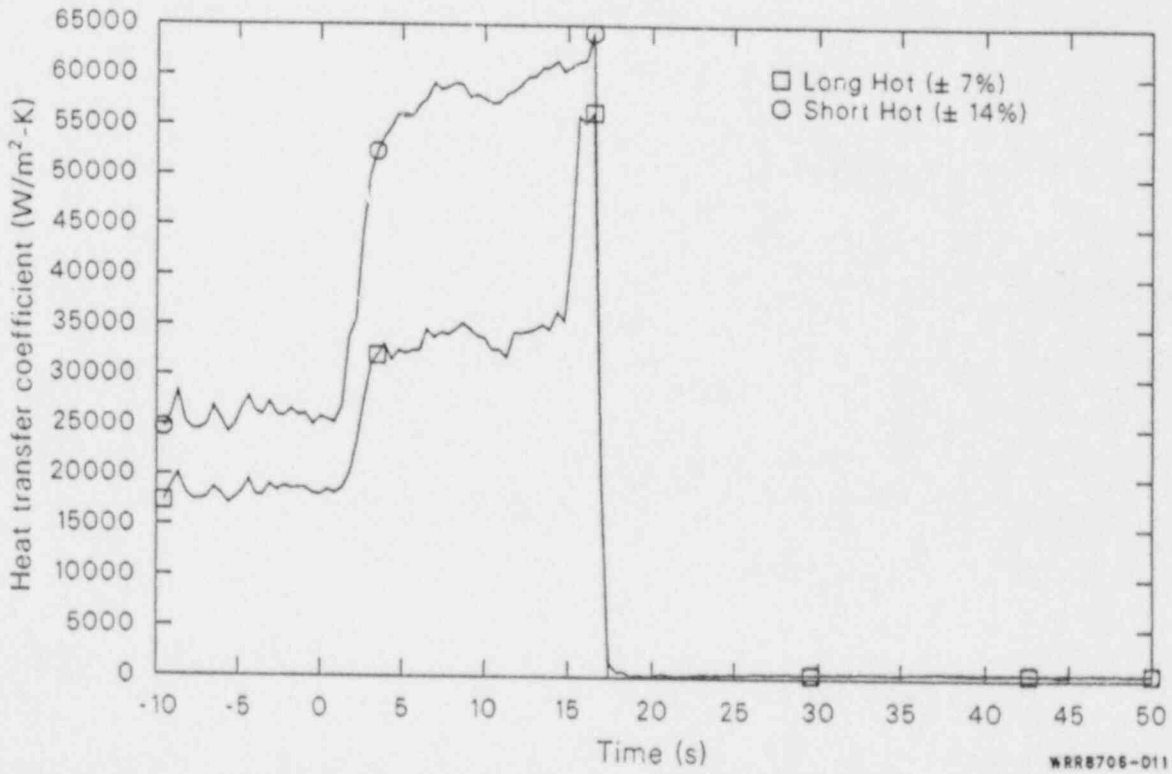

Figure D-11. Affected loop steam generator secondary convective heat transfer coefficients at the 61-cm elevation during the blowdown phase of 50% FWLB experiment S-FS-11 (-10 to 50 s).

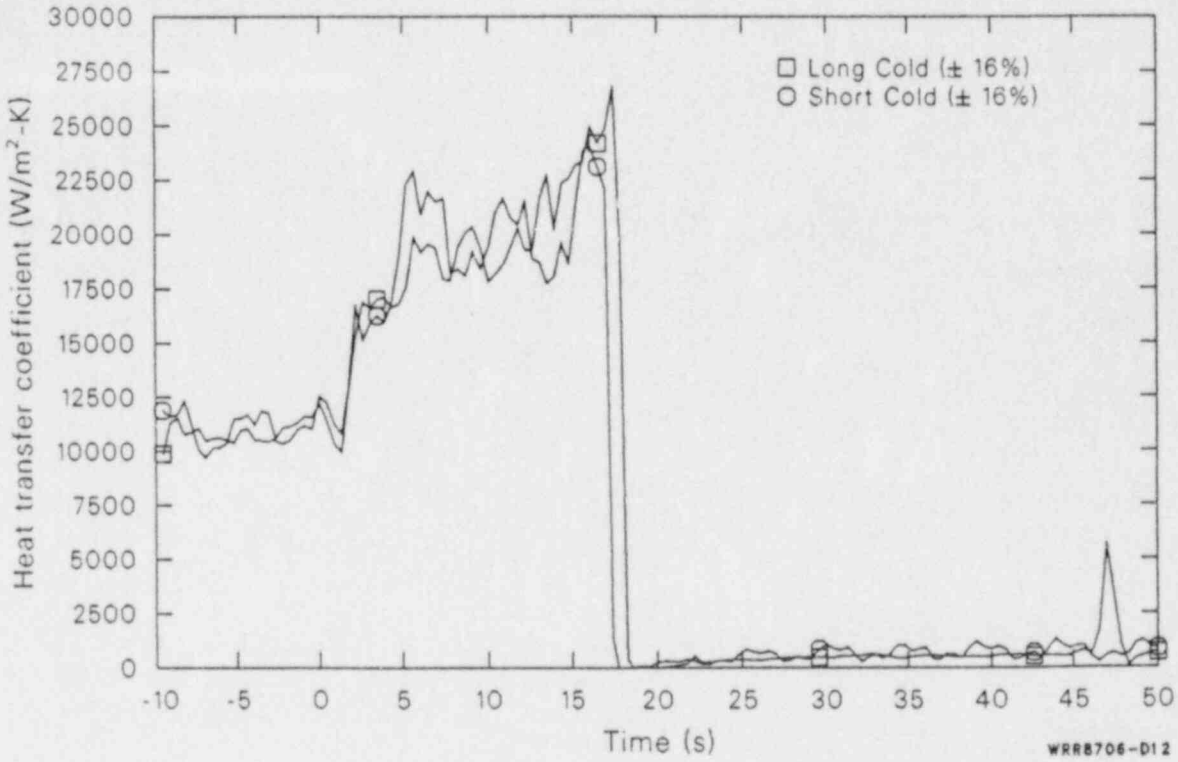

Figure D-12. Affected loop steam generator secondary convective heat transfer coefficients at the 99-cm elevation during the blowdown phase of 50% FWLB experiment S-FS-11 (-10 to 50 s).

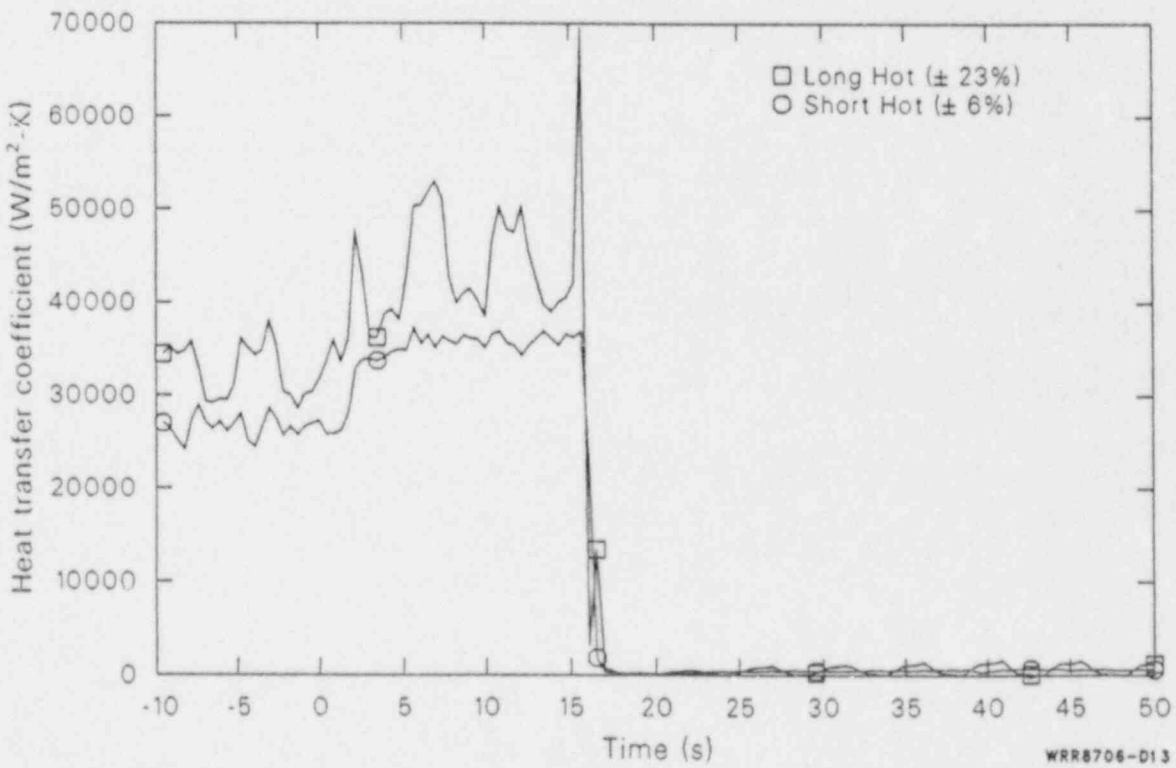

Figure D-13. Affected loop steam generator secondary convective heat transfer coefficients at the 137-cm elevation during the blowdown phase of 50% FWLB experiment S-FS-11 (-10 to 50 s).

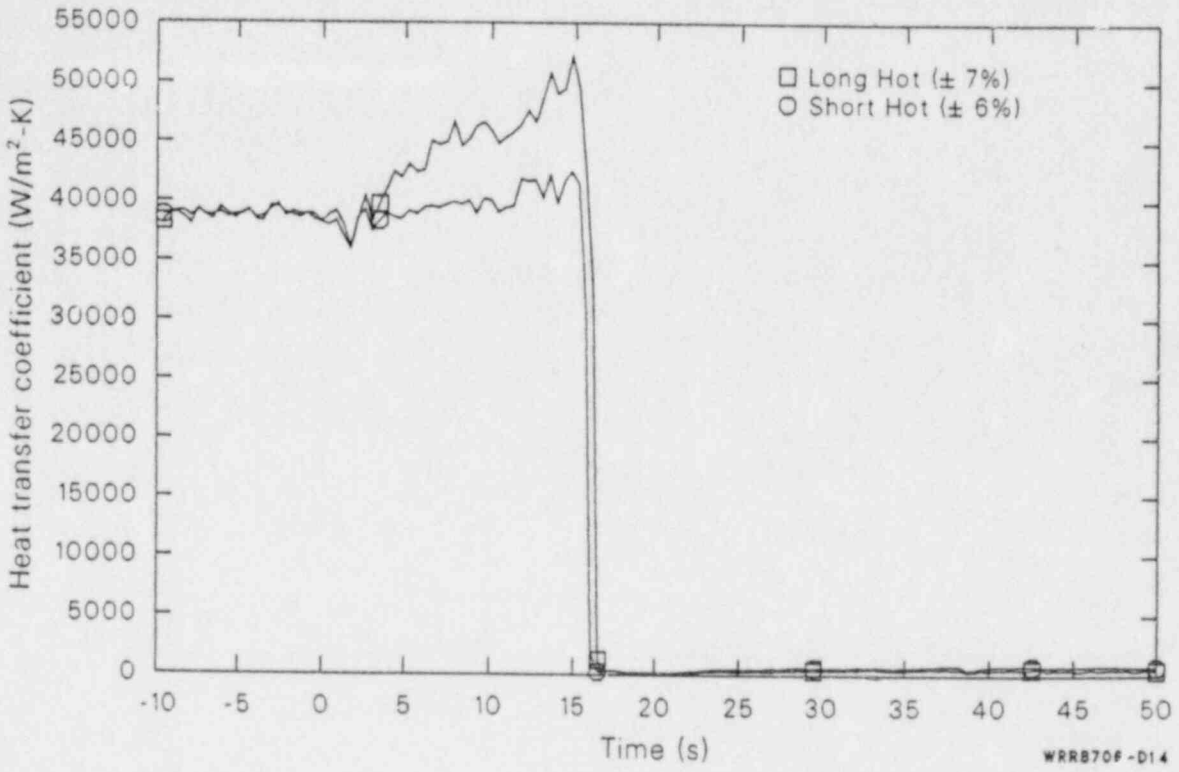

Figure D-14. Affected loop steam generator secondary convective heat transfer coefficients at the 213-cm elevation during the blowdown phase of 50% FWLB experiment S-FS-11 (-10 to 50 s).

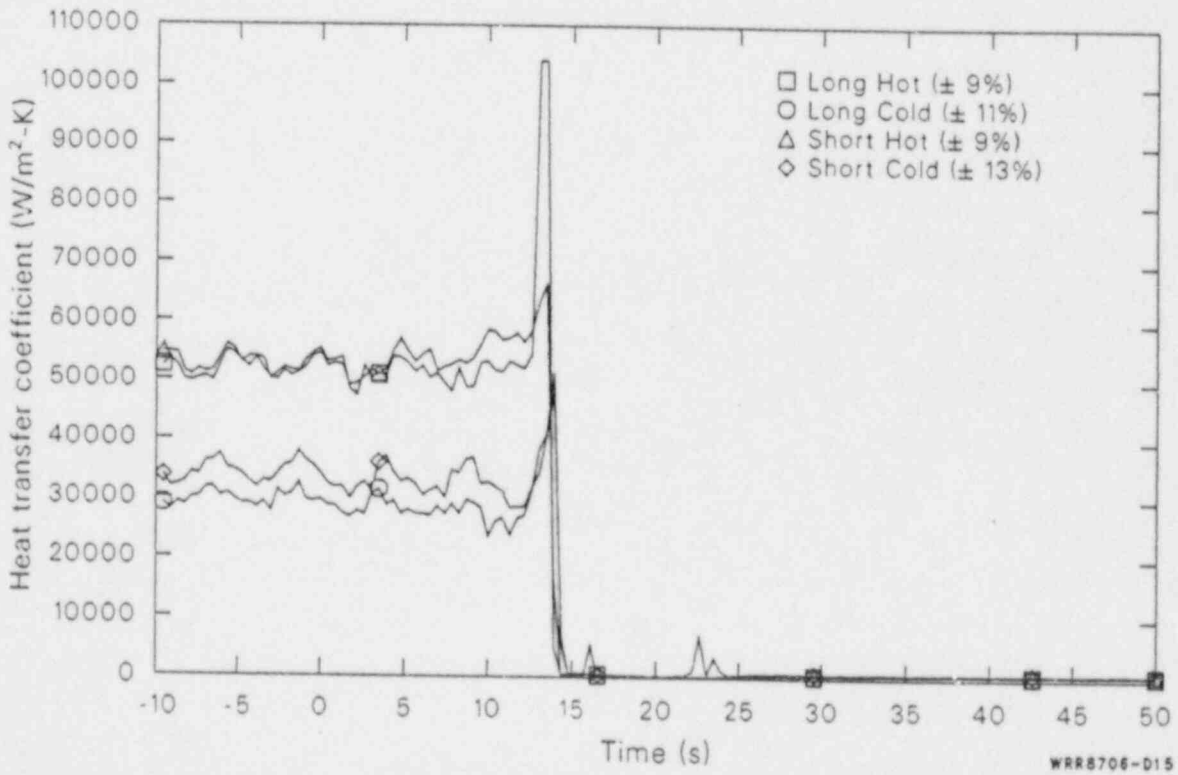

Figure D-15. Affected loop steam generator secondary convective heat transfer coefficients at the 404-cm elevation during the blowdown phase of 50% FWLB experiment S-FS-11 (-10 to 50 s).

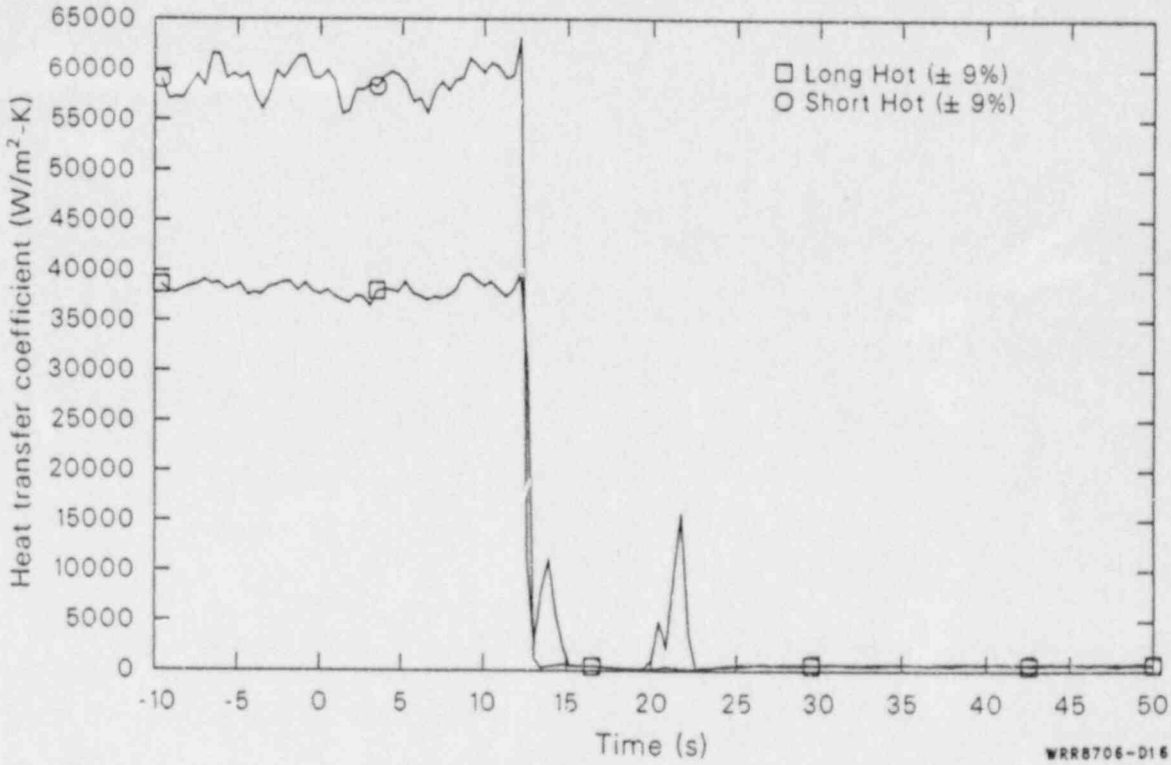

Figure D-16. Affected loop steam generator secondary convective heat transfer coefficients at the 556-cm elevation during the blowdown phase of 50% FWLB experiment S-FS-11 (-10 to 50 s).

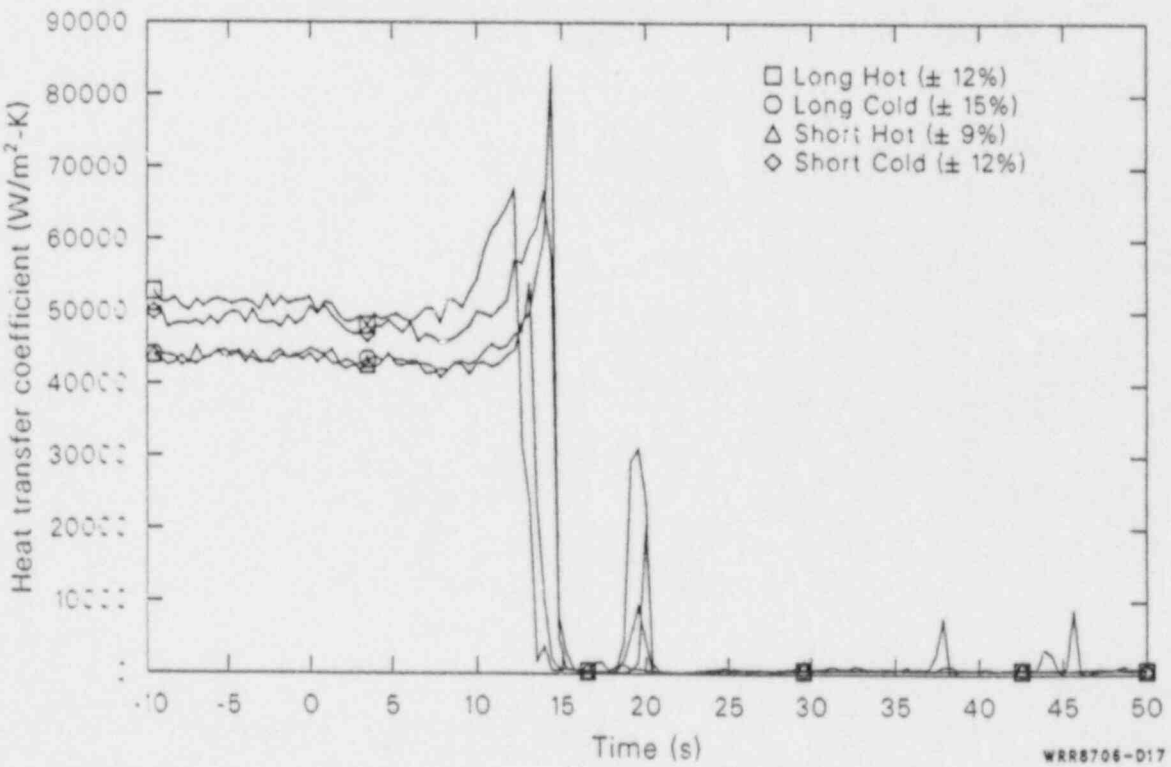

Figure D-17. Affected loop steam generator secondary convective heat transfer coefficients at the 709-cm elevation during the blowdown phase of 50% FWLB experiment S-FS-11 (-10 to 50 s).

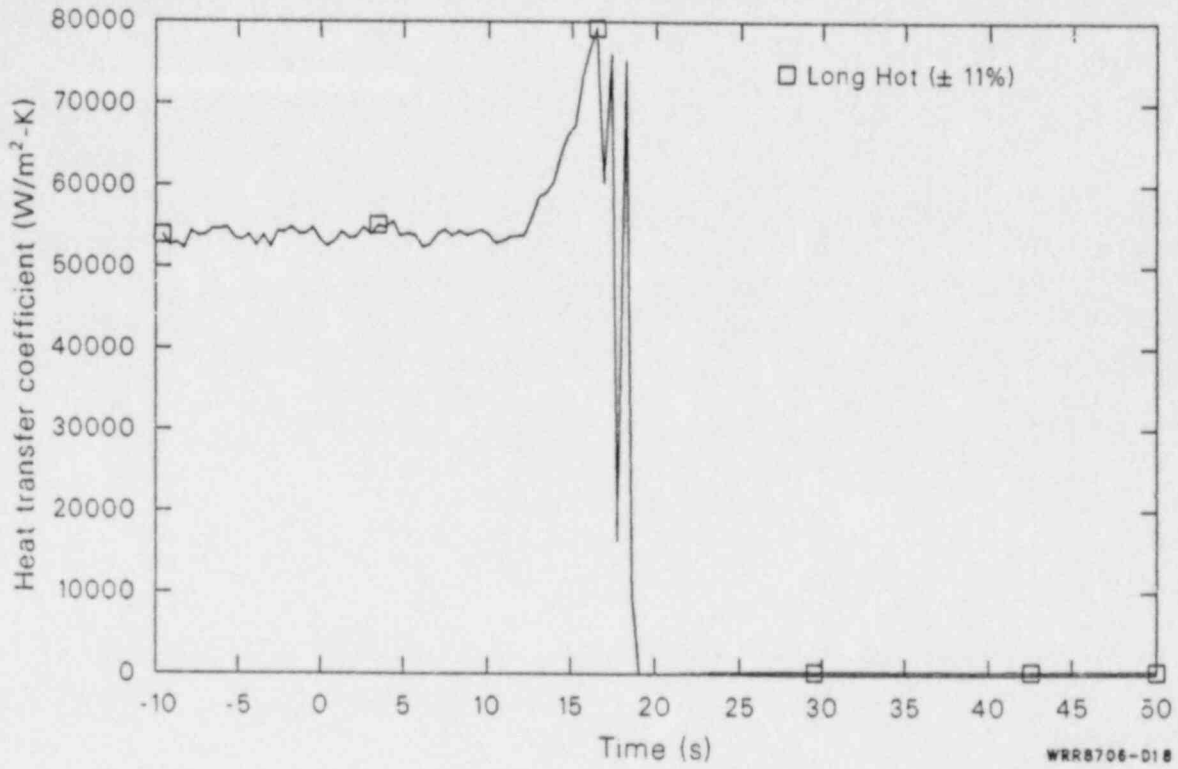

Figure D-18. Affected loop steam generator secondary convective heat transfer coefficient at the 886-cm elevation during the blowdown phase of 50% FWLB experiment S-FS-11 (-10 to 50 s).

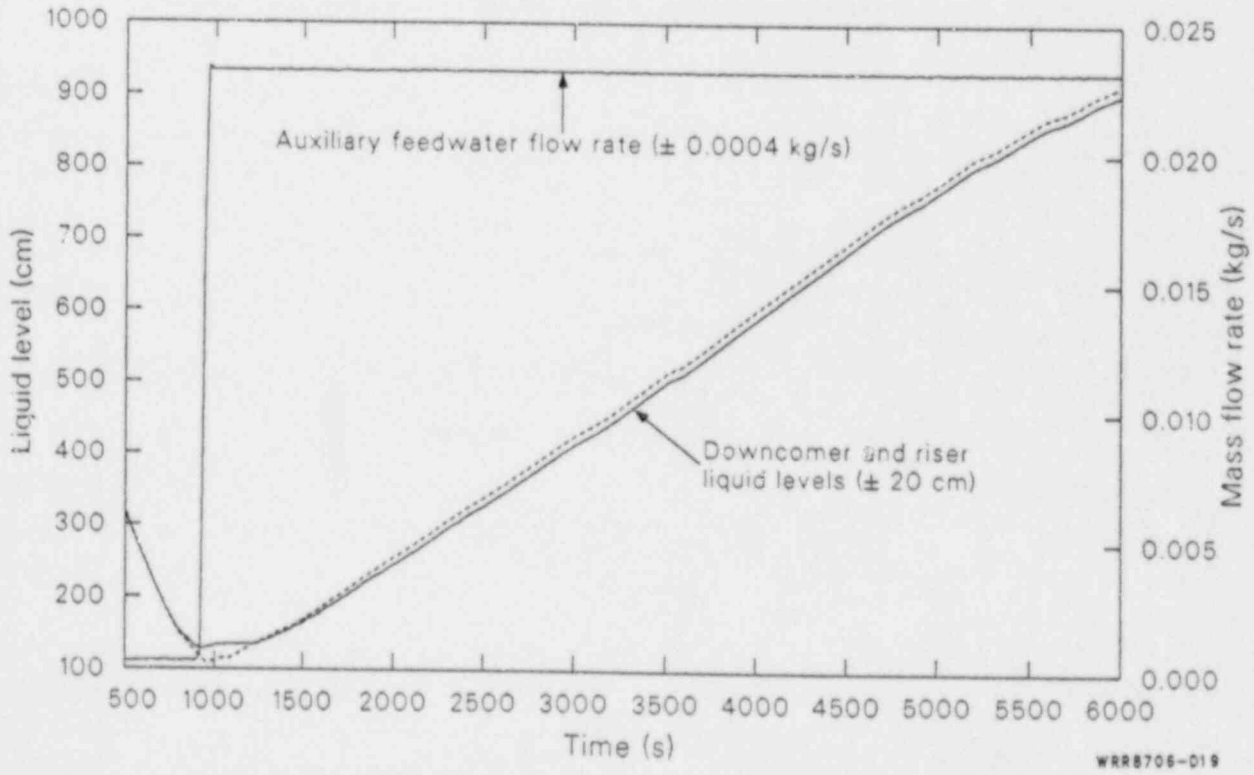

Figure D-19. Unaffected loop steam generator auxiliary feedwater mass flow rate and downcomer and riser overall collapsed liquid levels during the stabilization phase of 14.3% FWLB experiment S-FS-7 (500 to 6000 s).

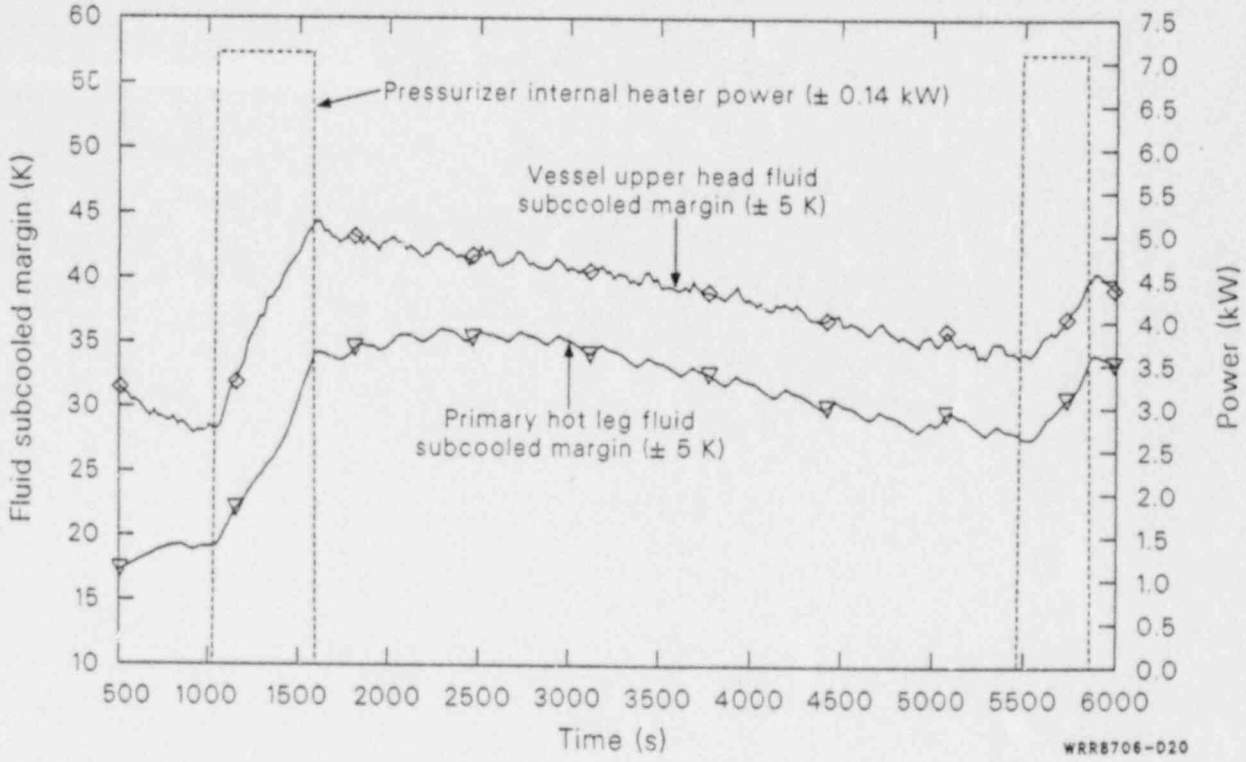

Figure D-20. Primary hot leg and vessel upper head fluid subcooled margins and pressurizer internal heater power during the stabilization phase of 14.3% FWLB experiment S-FS-7 (500 to 6000 s).

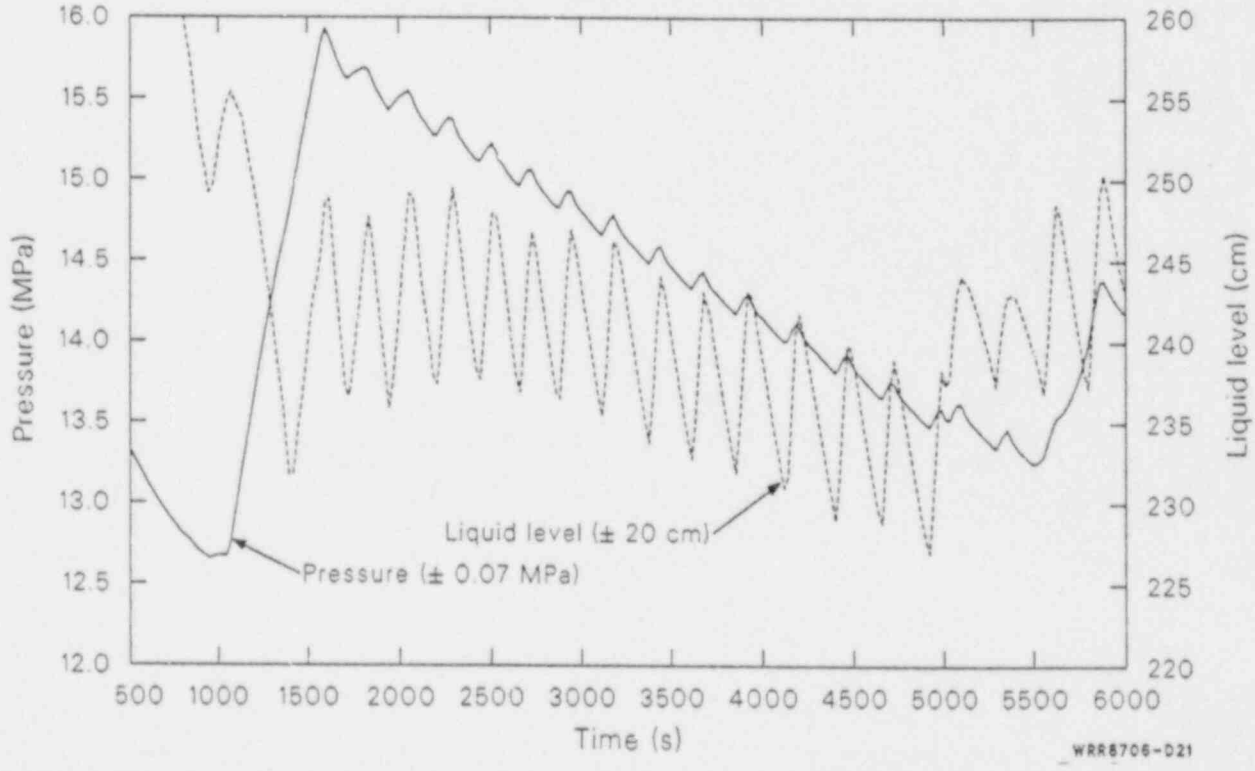

Figure D-21. Pressurizer pressure and overall collapsed liquid level during the stabilization phase of 14.3% FWLB experiment S-FS-7 (500 to 6000 s).

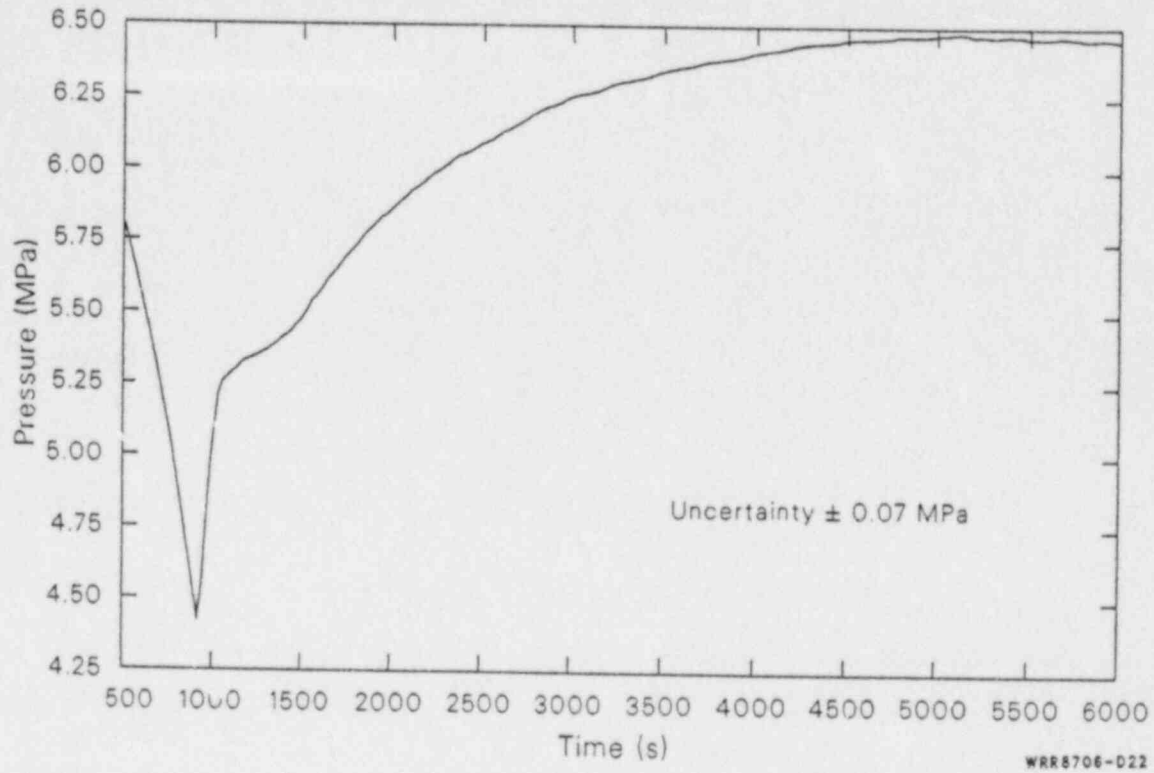

Figure D-22. Unaffected loop steam generator secondary pressure during the stabilization phase of 14.3% FWLB experiment S-FS-7 (500 to 6000 s).

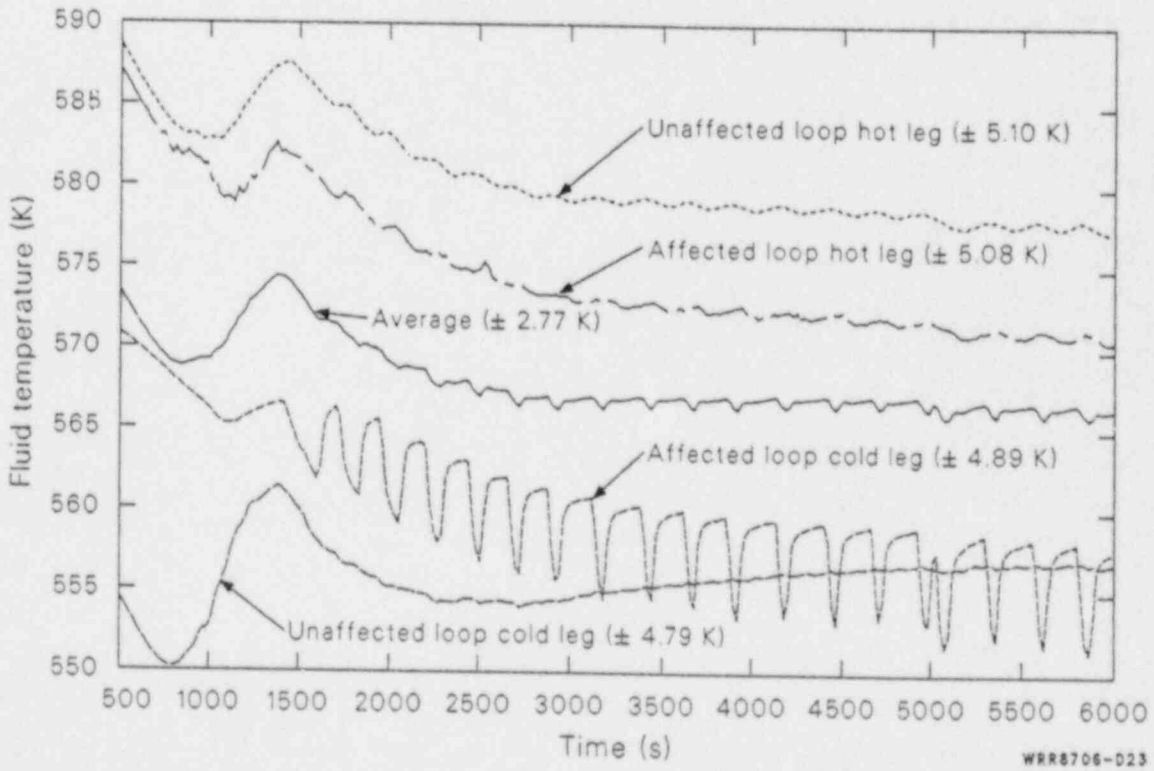

Figure D-23. Affected and unaffected loop hot and cold leg and average primary fluid temperatures during the stabilization phase of 14.3% FWLB experiment S-FS-7 (500 to 6000 s).

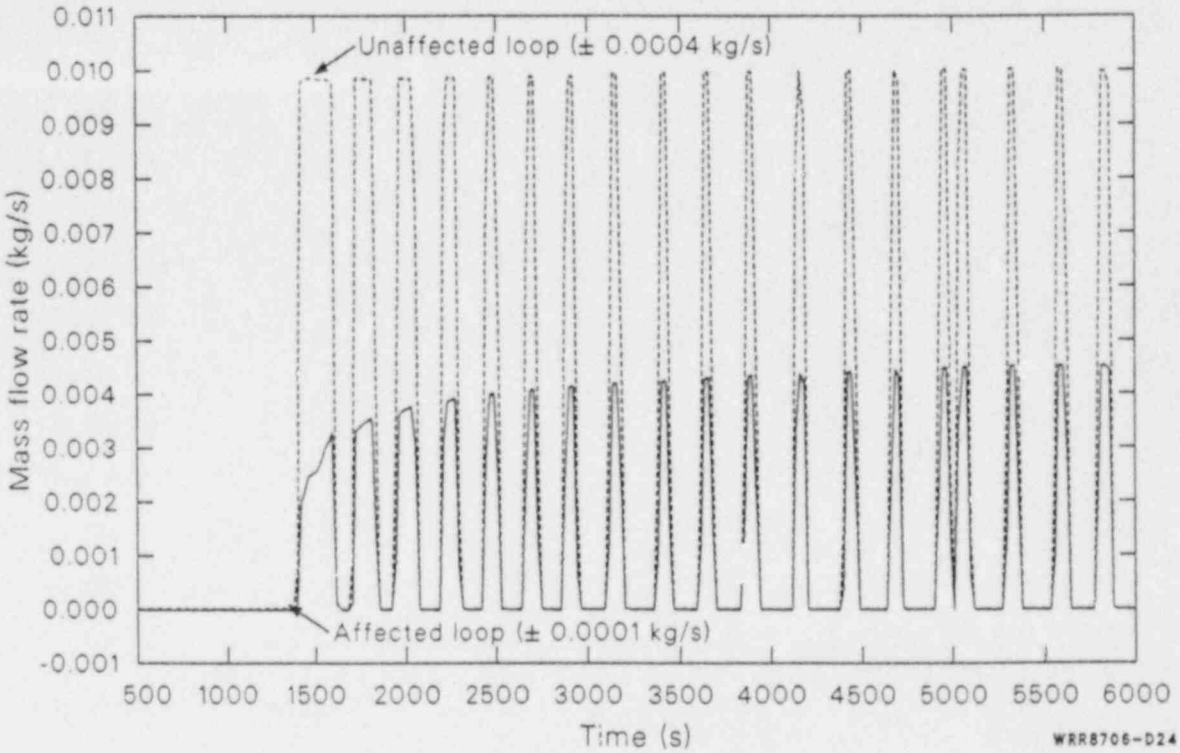

Figure D-24. Affected and unaffected loop normal charging mass flow rates during the stabilization phase of 14.3% FWLB experiment S-FS-7 (500 to 6000 s).

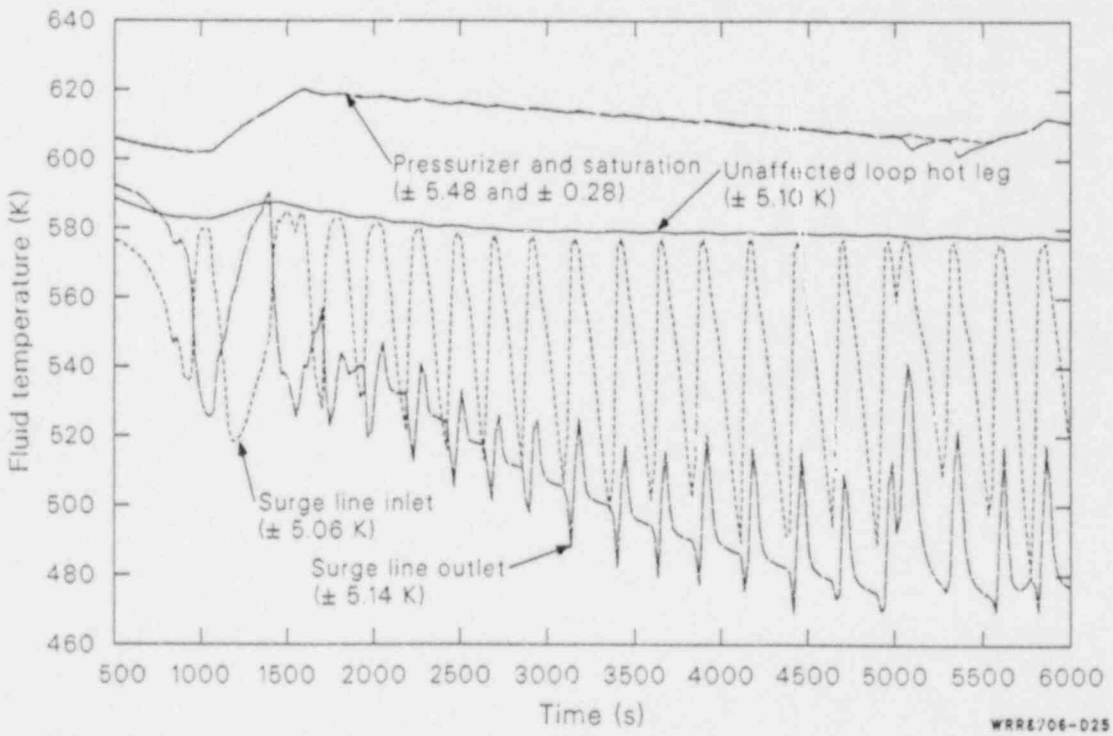

Figure D-25. Unaffected loop hot leg, pressurizer surge line inlet and outlet, pressurizer, and pressurizer saturation fluid temperatures during the stabilization phase of 14.3% FWLB experiment S-FS-7(500 to 6000 s).

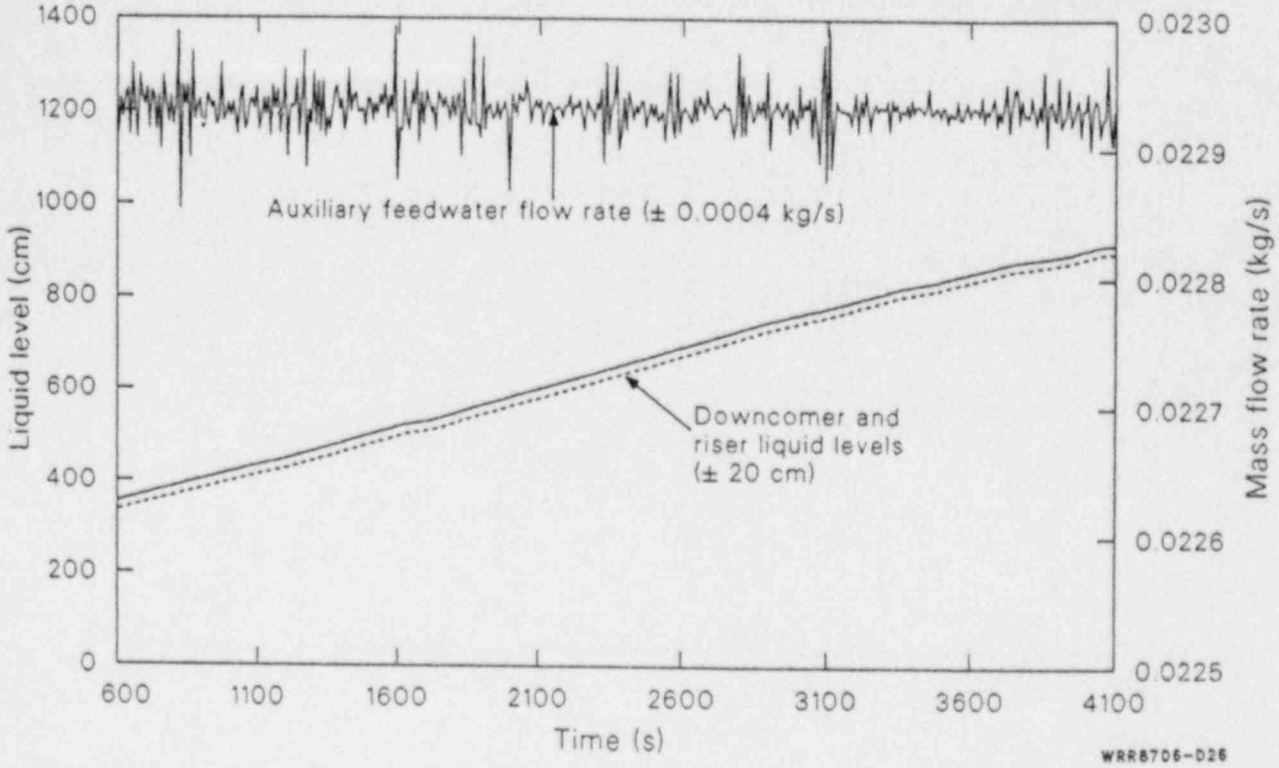

Figure D-26. Unaffected loop steam generator auxiliary feedwater mass flow rate and downcomer and riser overall collapsed liquid levels during the stabilization phase of 50% FWLB experiment S-FS-11 (600 to 4100 s).

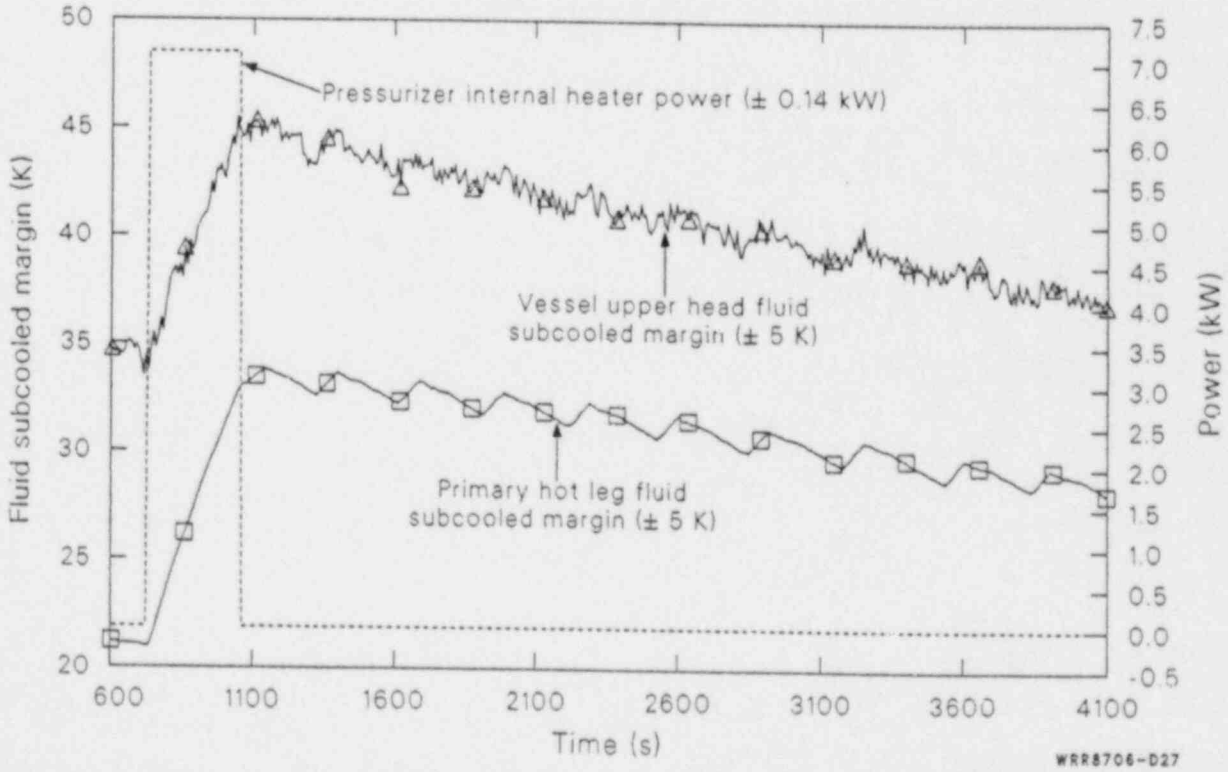

Figure D-27. Primary hot leg and vessel upper head fluid subcooled margins and pressurizer internal heater power during the stabilization phase of 50% FWLB experiment S-FS-11 (600 to 4100 s).

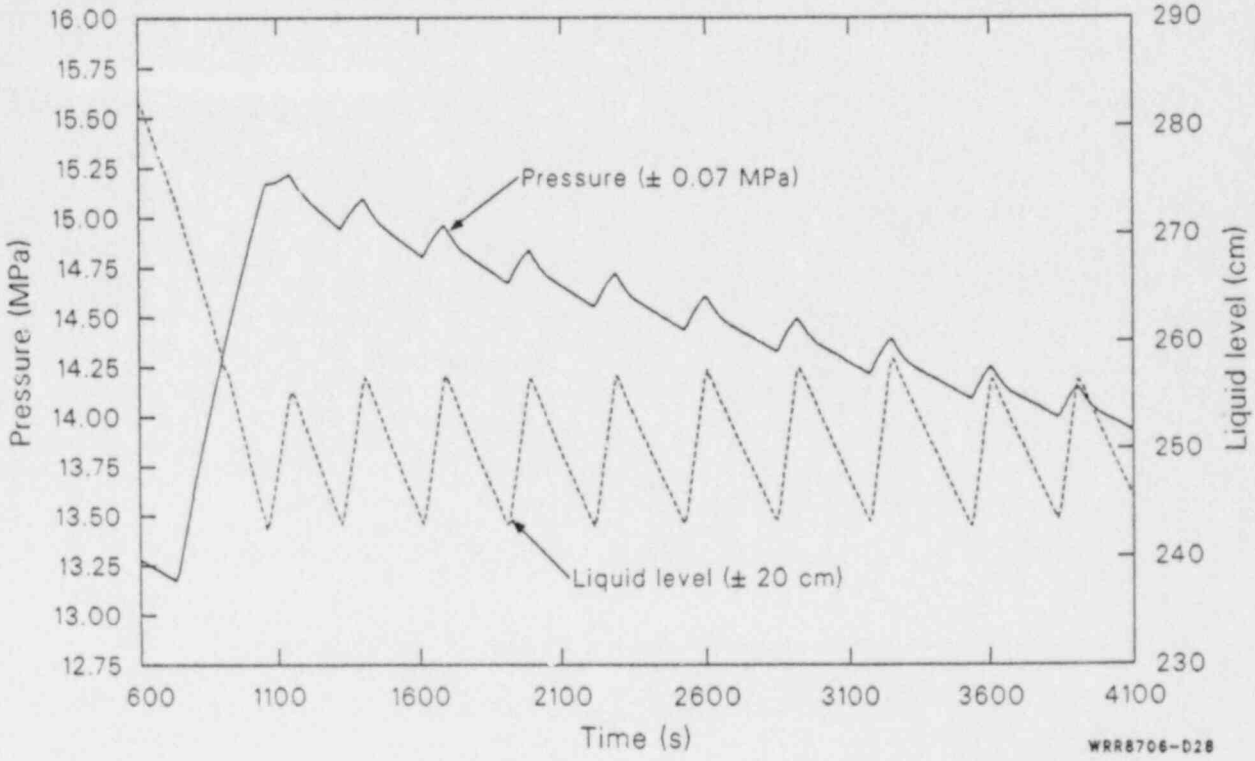

Figure D-28. Pressurizer pressure and overall collapsed liquid level during the stabilization phase of 50% FWLB experiment S-FS-11 (600 to 4100 s).

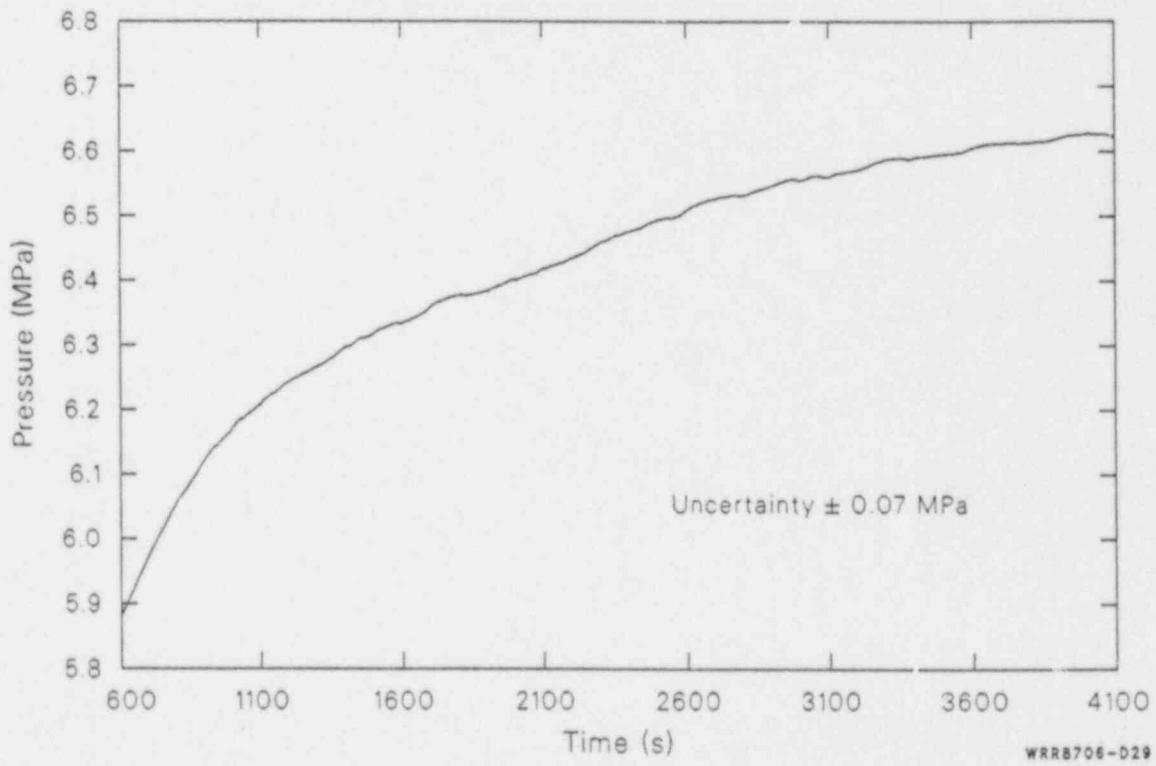

Figure D-29. Unaffected loop steam generator secondary pressure during the stabilization phase of 50% FWLB experiment S-FS-11 (600 to 4100 s).

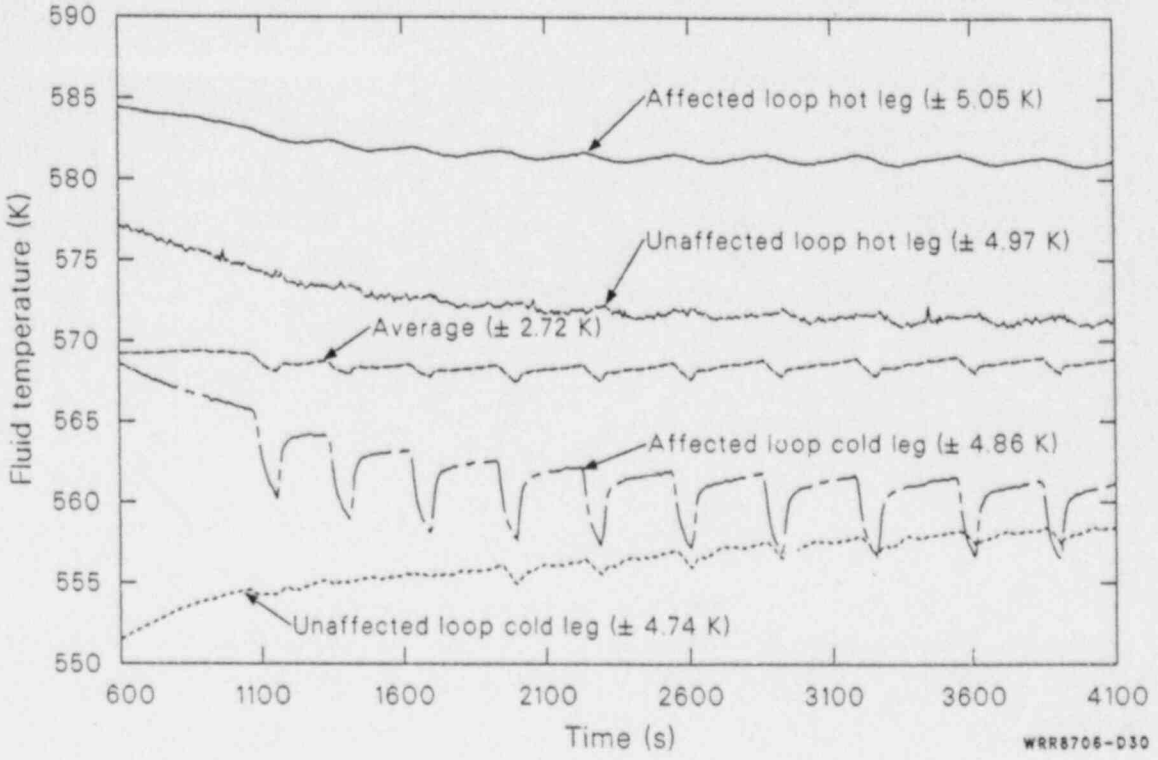

Figure D-30. Affected and unaffected loop hot and cold leg and average primary fluid temperatures during the stabilization phase of 50% FWLB experiment S-FS-11 (600 to 4100 s).

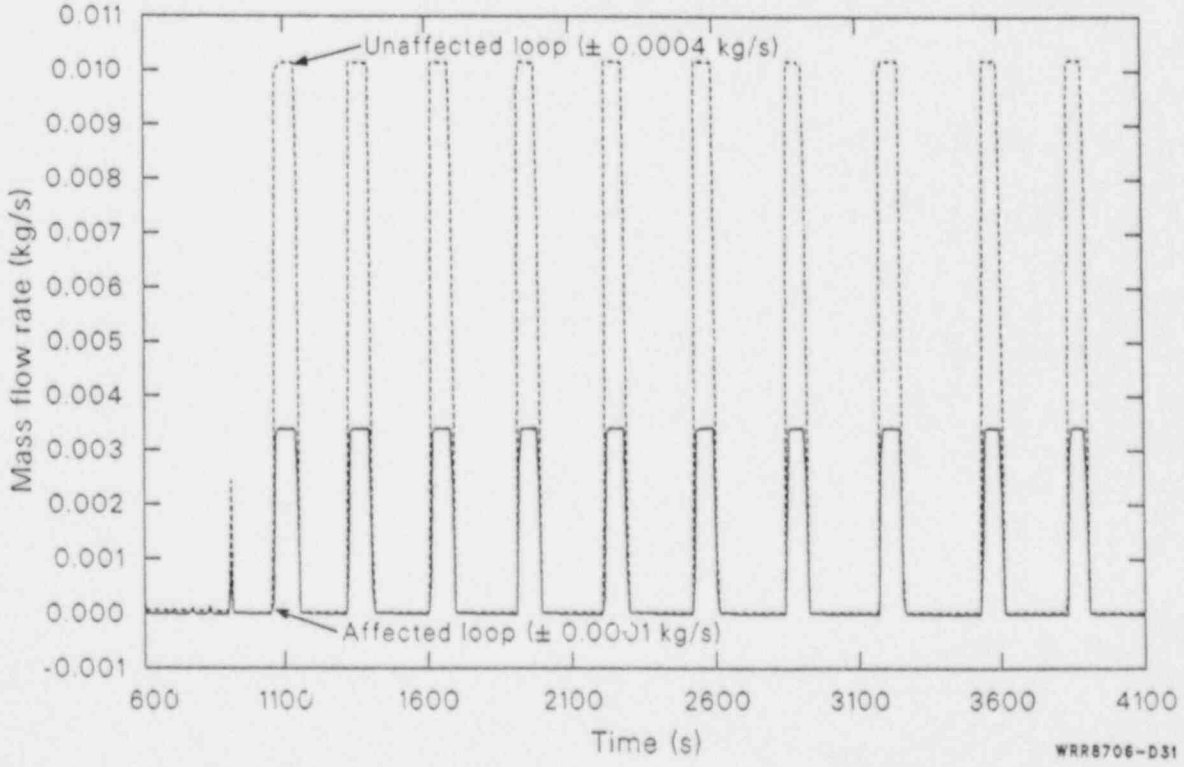

Figure D-31. Affected and unaffected loop normal charging mass flow rates during the stabilization phase of 50% FWLB experiment S-FS-11 (600 to 4100 s).

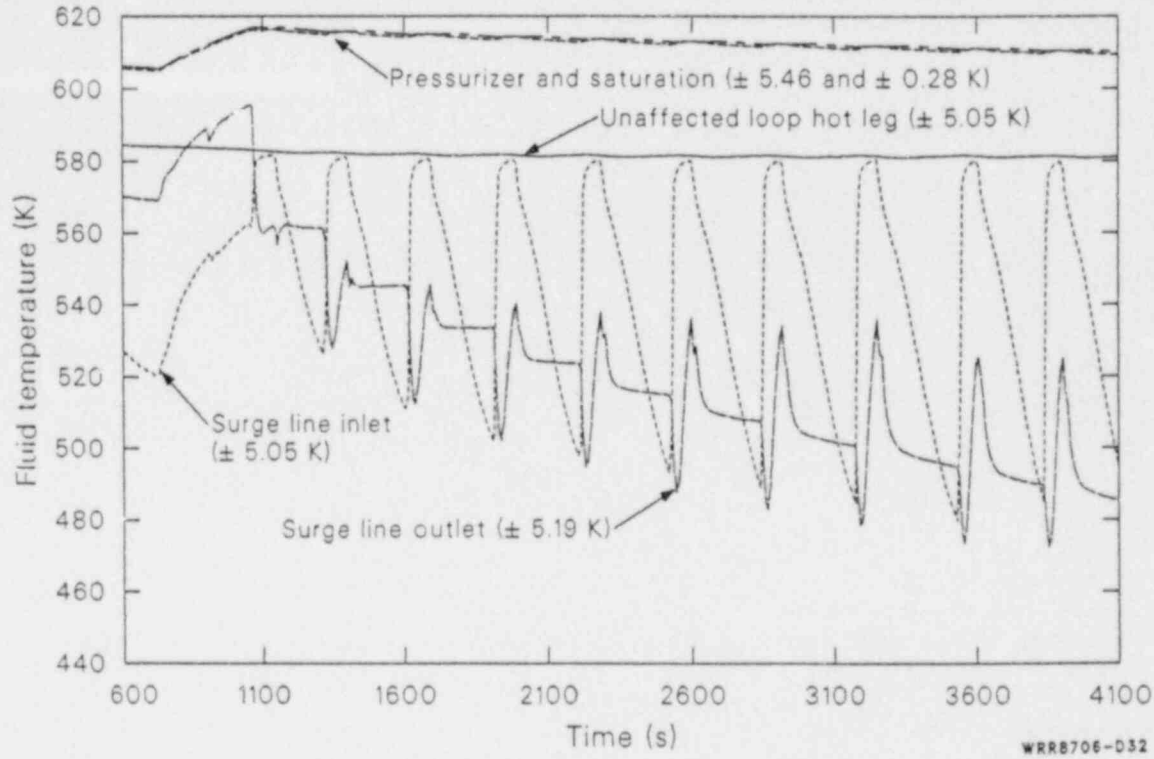

Figure D-32. Unaffected loop hot leg, pressurizer surge line inlet, pressurizer, and pressurizer saturation fluid temperatures during the stabilization phase of 50% FWLB experiment S-FS-11 (600 to 4100 s).

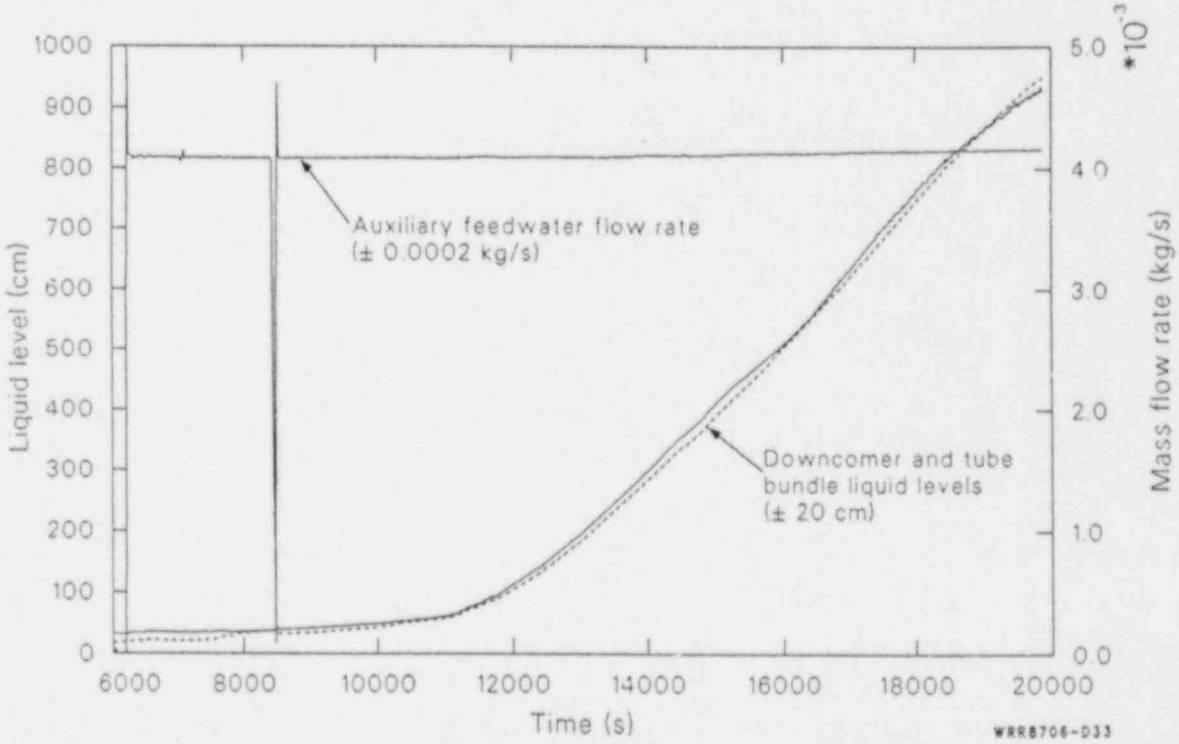

Figure D-33. Affected loop steam generator downcomer and tube bundle overall outlet, collapsed liquid levels and auxiliary feedwater mass flow rate during the voided secondary refill phase of 14.3% FWLB experiment S-FS-7 (6000 to 20,000 s).

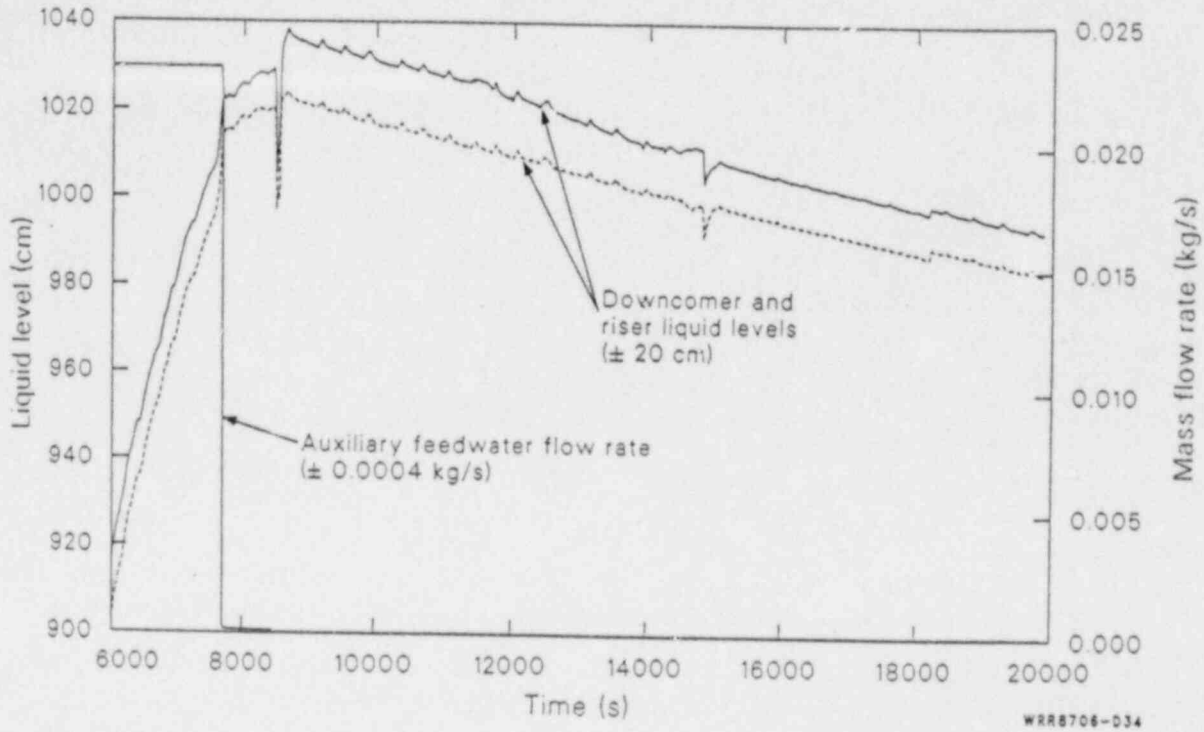

Figure D-34. Unaffected loop steam generator downcomer and tube bundle overall collapsed liquid levels and auxiliary feedwater mass flow rate during the voided secondary refill phase of 14.3% FWLB experiment S-FS-7 (6000 to 20,000 s).

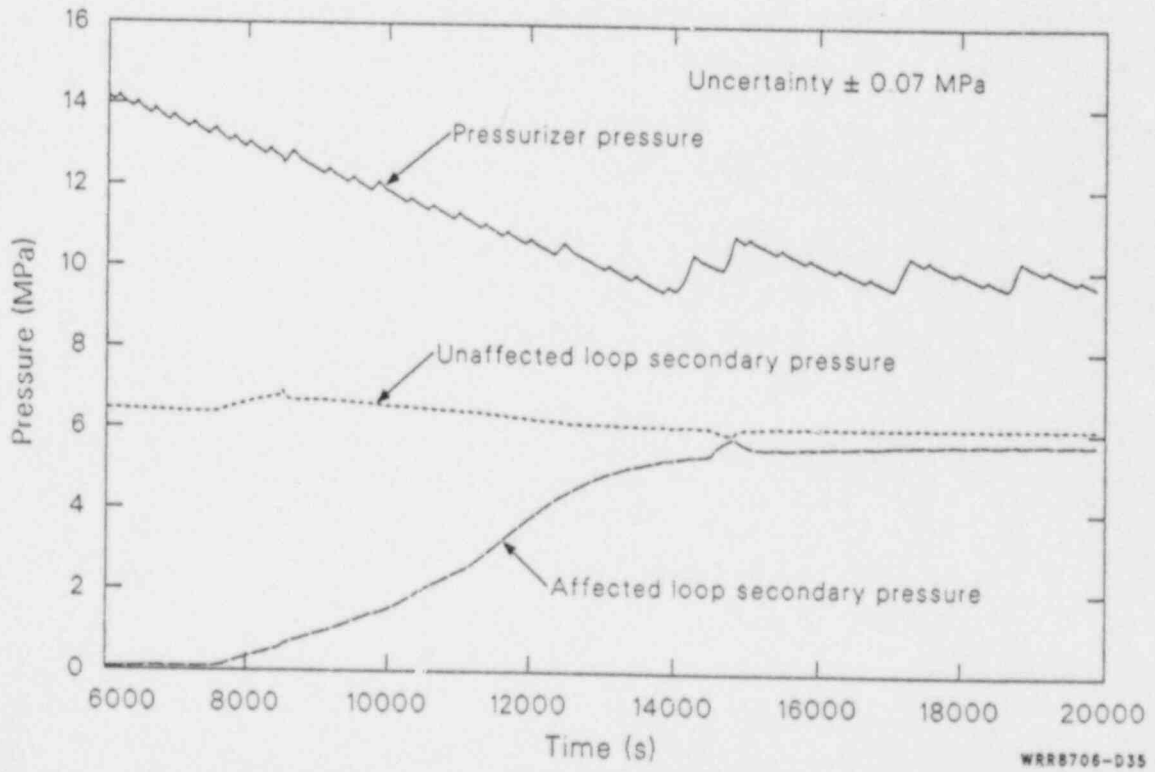

Figure D-35. Pressurizer pressure, affected and unaffected loop steam generator secondary pressures, and unaffected loop steam generator atmospheric dump valve mass flow rate during the voided secondary refill phase of 14.3% FWLB experiment S-FS-7 (6000 to 20,000 s).

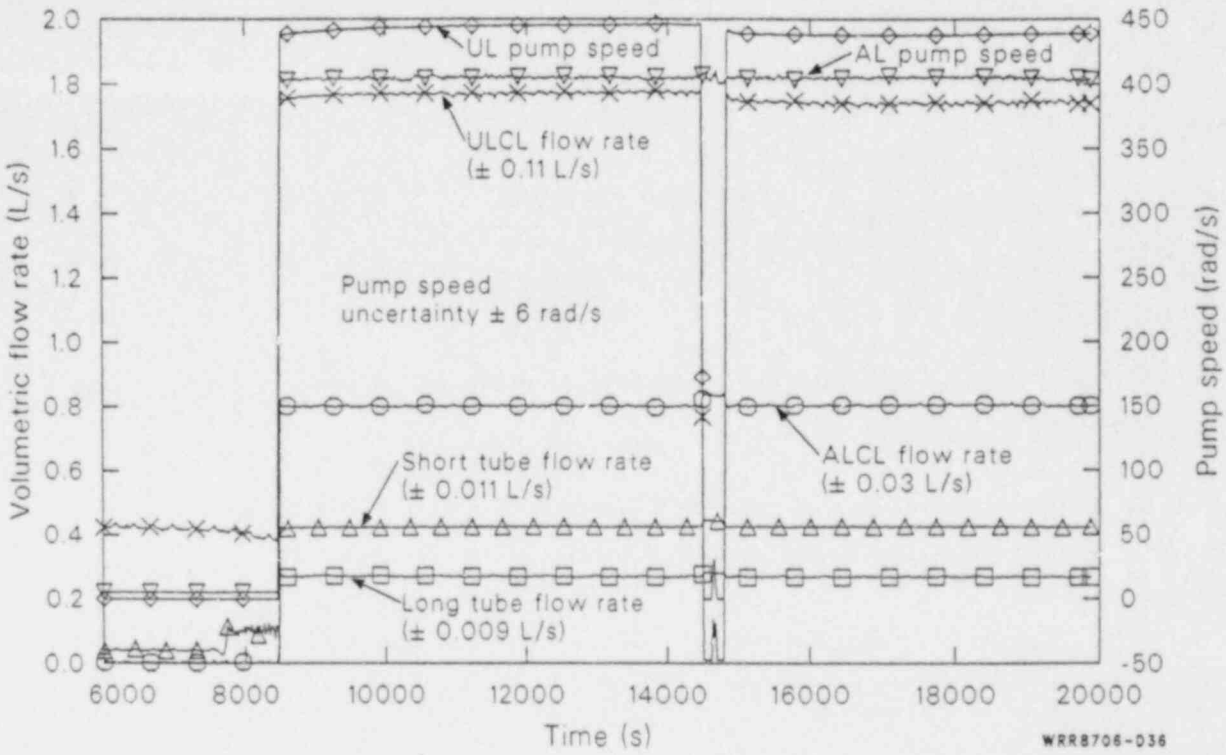

Figure D-36. Affected and unaffected loop pump speeds, affected and unaffected loop cold leg volumetric flow rates, and affected loop steam generator long and short tube outlet volumetric flow rates during the voided secondary refill phase of 14.3% FWLB experiment S-FS-7 (6000 to 20,000 s).

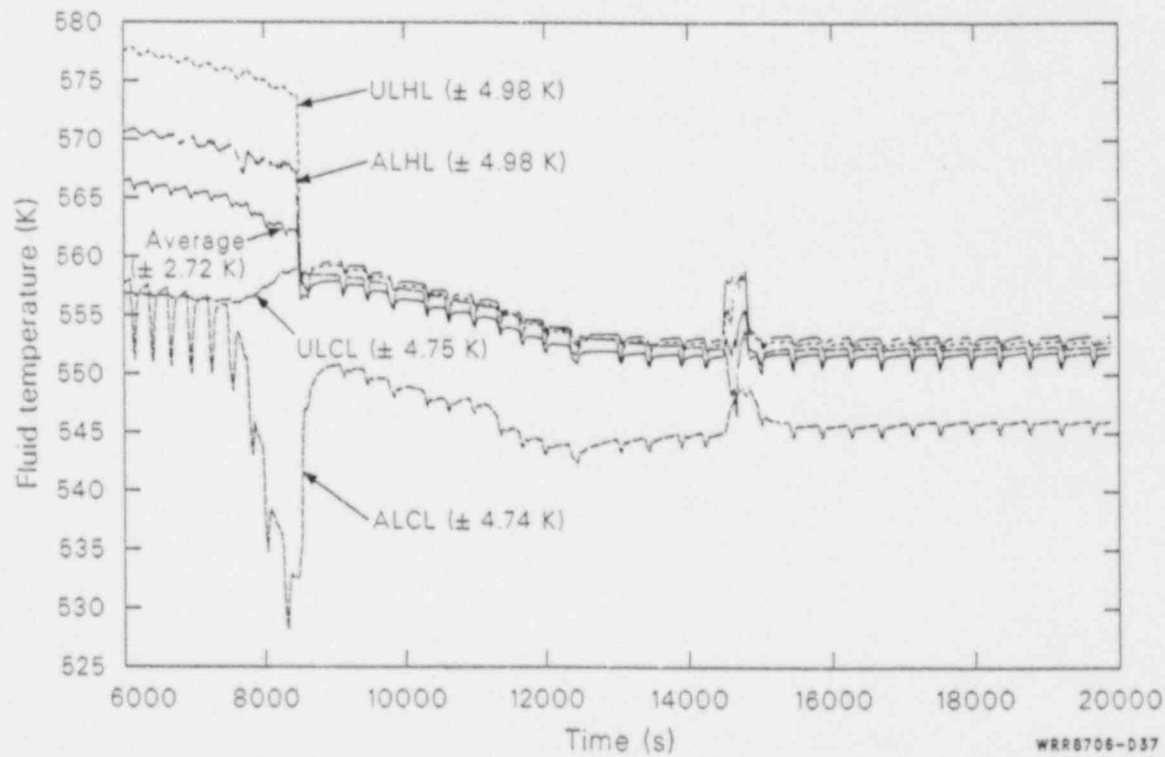

Figure D-37. Affected and unaffected loop hot and cold leg, and average primary fluid temperatures during the voided secondary refill phase of 14.3% FWLB experiment S-FS-7 (6000 to 20,000 s).

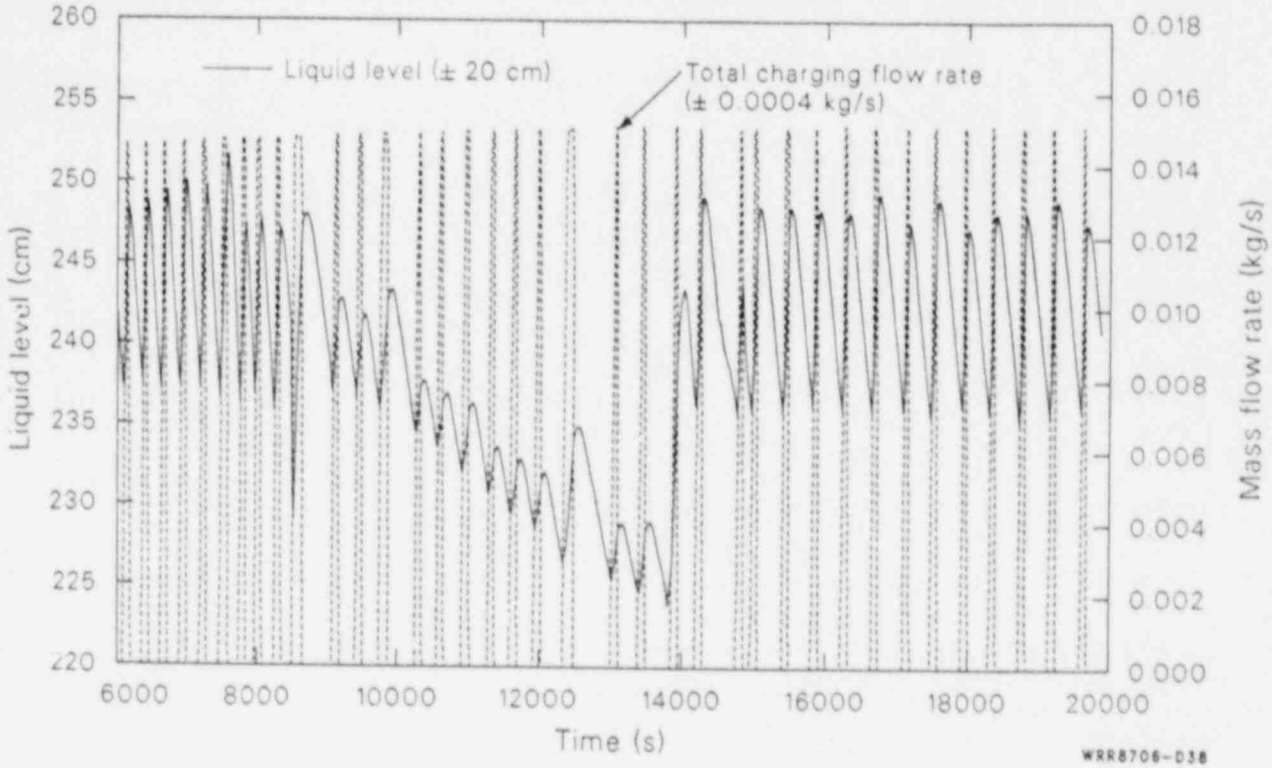

Figure D-38. Pressurizer collapsed liquid level and total normal charging mass flow rate during the voided secondary refill phase of 14.3% FWLB experiment S-FS-7 (6000 to 20,000 s).

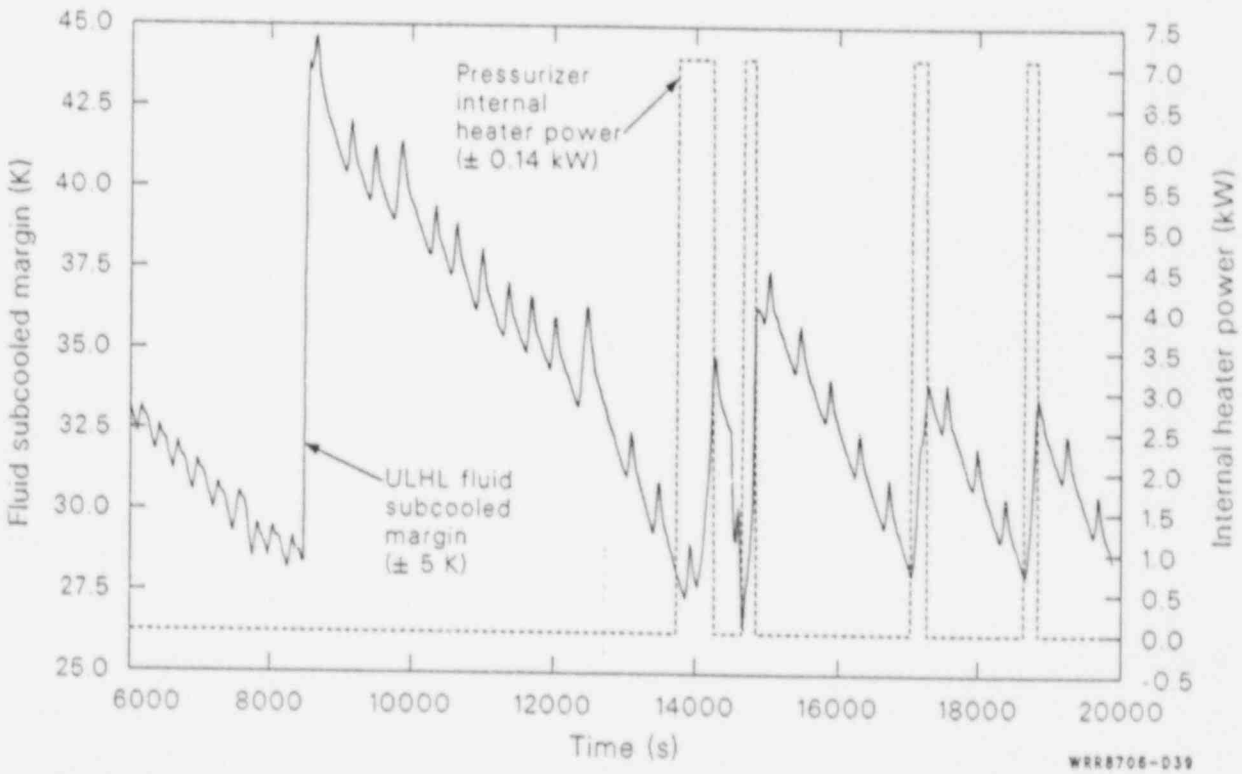

Figure D-39. Unaffected loop hot leg fluid subcooled margin and pressurizer internal heater power during the voided secondary refill phase of 14.3% FWLB experiment S-FS-7 (6000 to 20,000 s).

NRC FORM 335 (2.84) NRCM 1102 3201, 3202

U.S. NUCLEAR REGULATORY COMMISSION

BIBLIOGRAPHIC DATA SHEET

SEE INSTRUCTIONS ON THE REVERSE

1 REPORT NUMBER (Assigned by TIDC, add Vol. No., if any)
NUREG/CR-4898
EGG-2503

2 TITLE AND SUBTITLE
Results of Semiscale MOD-2C Feedwater and Steam Line Break (S-FS) Experiment Series: Bottom Main Feedwater Line Break Accident Experiments

3 LEAVE BLANK

4 DATE REPORT COMPLETED
MONTH: November YEAR: 1987

5 AUTHOR(S)
Timothy J. Boucher

6 DATE REPORT ISSUED
MONTH: February YEAR: 1988

7 PERFORMING ORGANIZATION NAME AND MAILING ADDRESS (Include Zip Code)
Idaho National Engineering Laboratory
EG&G Idaho, Inc.
Idaho Falls, ID 83415

8 PROJECT/TASK/WORK UNIT NUMBER

9 FIN OR GRANT NUMBER
A6038

10 SPONSORING ORGANIZATION NAME AND MAILING ADDRESS (Include Zip Code)
Division of Accident Evaluation
Office of Nuclear Regulatory Research
U.S. Nuclear Regulatory Commission
Washington, D.C. 20555

11a TYPE OF REPORT
Technical

b PERIOD COVERED (Inclusive dates)

12 SUPPLEMENTARY NOTES

13 ABSTRACT (200 words or less)

This report presents the results of four experiments simulating 100, 50, and 14.3% bottom main feedwater line break accidents performed at high pressure and temperature in the Semiscale Mod-2C facility. The primary and secondary thermal-hydraulic responses are characterized (including local secondary convective heat transfer) and the influence of the break size on the responses is discussed. A definite deficiency is identified in existing forced convection boiling heat transfer correlations and the conservatism of FSAR heat transfer degradation assumptions is shown to be questionable. The effectiveness of the recovery operations in maintaining control of the system is addressed, and the system response (including local secondary convective heat transfer) to voided secondary refill operations are discussed. Feedwater line break issues are discussed and conclusions are drawn based on the results of the analysis. Finally, recommendations are made for further utilization of the data and considerations for future code calculations.

14 DOCUMENT ANALYSIS a KEYWORDS/DESCRIPTORS

b IDENTIFIERS/OPEN ENDED TERMS

15 AVAILABILITY STATEMENT
Unclassified

16 SECURITY CLASSIFICATION
(This page) Unlimited
(This report) Unlimited

17 NUMBER OF PAGES

18 PRICE

EG&G Idaho
P.O. Box 1625
Idaho Falls, Idaho
83415